

e-ISSN 2586-9396



# Current Applied Science and Technology

Vol. 21 No. 4

October - December 2021

KING MONGKUT'S INSTITUTE OF TECHNOLOGY LADKRABANG

## Advisory Board

### **Prof. Dr. Suchatvee Suwansawat**

President of King Mongkut's Institute of Technology Ladkrabang, Thailand

### **Prof. Dr. Wanlop Surakamponon**

College of Advanced Manufacturing  
Innovation, King Mongkut's  
Institute of Technology Ladkrabang, Thailand  
Faculty of Engineering, King Mongkut's  
Institute of Technology Ladkrabang, Thailand

### **Prof. Dr. Monai Krairiksh**

Current Applied Science and Technology or CAST, formerly KMITL Science and Technology Journal published by King Mongkut's Institute of Technology Ladkrabang (KMITL), has been established since its inception as KMITL Science Journal in 2001. The journal has been dedicated to publishing advanced and applied knowledge in the form of high-quality research and review articles covering the main areas of Biotechnology, Environmental Science, Agricultural Technology, Food Science and other fields related to Applied Science and Technology. Special issues devoted to important topics in advanced science and technology will occasionally be published.

The journal is an open access peer-reviewed and double blinded journal using Online Journal System (OJS) publishing online academic research and review articles. Previously, articles were published in print on a regular basis (two issues per year) since 2001 and since 2010 onward the articles have been published both in print and electronic forms starting from volume 10. In 2017, the journal title has been changed from *KMITL Science and Technology Journal* to *Current Applied Science and Technology* (CAST) (e-ISSN 2586-9396) to be more identifiable to the international scientific community according to the suggestion of Thai-Journal Citation Index Centre. The journal has been published online only since volume 17(2) (July-December, 2017). In addition, the journal has attracted researchers from other countries more than 22% according to the data. Because of more demands on publication in CAST, the editorial board has decided to publish online original academic research and review articles four issues per year (January-March, April-June, July-September and October-December) from 2021 onward.

Furthermore, the advisory board and editorial board comprises honorable and well-known members from around the world in which 50% of editorial board members are from various countries like U.K., Norway, Japan, India, China, Canada, Estonia and Egypt. Only 25% of Thai editorial board members are from the publisher organization and 25% from other publisher organizations. Most of advisory and editorial board members have high H-index according to SCOPUS.

The journal is also committed to maintaining the high level of integrity in the content published and has a Conflict of Interest policy in place. The journal uses plagiarism detection software to screen the submissions. The journal has been working closely with Thai-Journal Citation Index Centre to ensure that the journal complies with international standard of SCOPUS.

**Electronic Journal Managing Editor** Asst. Prof. Dr. Vorapat Sanguanchaipaiwong  
**Assistant Managing Editors** Ms. Jermaroon Autajamsripon  
Ms. Mongkutkarn Udompongsuk  
Mr. Tanaboon Techasena

## **Current Applied Science and Technology (CAST)**

(formerly KMITL Science and Technology Journal)

### **Editor**

#### **Dusanee Thanaboripat**

King Mongkut's Institute of Technology Ladkrabang, Thailand

### **Editorial Board**

<b>Keiichi Ishihara</b>	Kyoto University, Japan
<b>Chalicheemalapalli K. Jayasankar</b>	Sri Venkateswara University, India
<b>Bjorn Kristiansen</b>	GlycaNova, Norway
<b>Hidenori Mimura</b>	Shizuoka University, Japan
<b>Yang Qian</b>	Harbin Institute of Technology, PR China
<b>Mike Matthey</b>	University of Strathclyde, UK
<b>Minoru Tanaka</b>	Tokai University, Japan
<b>Mohamed Yacout</b>	Alexandria University, Egypt
<b>He Yawen</b>	Shanghai Jiao Tong University, PR China
<b>Rajeev Bhat</b>	Estonian University of Life Sciences, Estonia
<b>Wenbiao Hu</b>	Queensland University of Technology, Australia
<b>Serge Belloncik</b>	Institut Armand- Frappier, Canada
<b>Sootawat Benjakul</b>	Prince of Songkla University, Thailand
<b>Krisana Kraisintu</b>	Krisana Kraisintu Foundation, Thailand
<b>Somboon Tanasupawat</b>	Chulalongkorn University, Thailand
<b>I-Ming Tang</b>	King Mongkut's University of Technology Thonburi, Thailand
<b>Arinthip Thamchaipenet</b>	Kasetsart University, Thailand
<b>Rattikorn Yimnirun</b>	Vidyasirimedhi Institute of Science and Technology, Thailand
<b>Anuwat Jangwanitlert</b>	King Mongkut's Institute of Technology Ladkrabang, Thailand
<b>Chamroon Laosinwattana</b>	King Mongkut's Institute of Technology Ladkrabang, Thailand
<b>Wisanu Pecharapa</b>	King Mongkut's Institute of Technology Ladkrabang, Thailand
<b>Puntani Pongsumpun</b>	King Mongkut's Institute of Technology Ladkrabang, Thailand
<b>Chanboon Sathitwiriawong</b>	King Mongkut's Institute of Technology Ladkrabang, Thailand

## CONTENTS

	Page
<b>Research Articles:</b>	
<b>Developing Agriculture Purchasing Managers' Index for Describing Taiwan's Agriculture Industry by Using Automatic Weighted <i>k</i>-means Algorithm</b>	<b>618</b>
Tzong-Ru Lee and Chien-Pang Lee	
<b>Molecular Analysis of Sergestid Shrimp <i>Acetes</i> spp. from Coastal Water of Sarawak, Malaysian Borneo Using CO1 Sequence</b>	<b>629</b>
Ruhana Hassan and Muhammad Nur Arif Othman	
<b>Medium Effect on Antagonistic Activity and Detection of Nonribosomal Peptide Synthetase Genes in Epiphytic <i>Bacillus</i> Strains</b>	<b>637</b>
Suchitra Apimeteethamrong and Chokchai Kittiwongwattana	
<b>Using Anthocyanin Extracts from Butterfly Pea as pH Indicator for Intelligent Gelatin Film and Methylcellulose Film</b>	<b>652</b>
Samart Sai-Ut Phunsiri Suthiluk, Wirongrong Tongdeesoonorn, Saroat Rawdkuen, Pimonpan Kaewprachu, Thomas Karbowiak, Frédéric Debeaufort and Pascal Degraeve	
<b>Electrical Properties of Bistable Device Based on Graphene Oxide Compositied with Polyvinylpyrrolidone Thin Films</b>	<b>662</b>
Thutiyaporn Thiawong, Potiyan Songkeaw, Korakot Onlaor and Benchapol Tunhoo	
<b>Allelopathic Effect of West Java Local Black Rice Varieties on Barnyard Grass (<i>Echinochloa crus-galli</i> (L.) Beauv.) at Germination Stage</b>	<b>673</b>
Muhamad Kadapi Denny Sobardini, Elissa Helena, Haritsa Hanindianingrum, Fachryansah Noor, Noladhi Wicaksana and Sumadi	

**Facile and Green Synthesis of Melamine-Formaldehyde@rGO Foam with Enhanced Superhydrophobicity for Oil Removal Application 686**

Natcha Jirasuttisarn and Chaval Sriwong

**Quality Improvement of Marinated Pork Stew in Retort Pouch for the Elderly 698**

Porn-tip Wiriyawattana

**Fourier Regression and ARIMAX Model for Forecasting Monthong Durian Price Index 712**

Kanittha Yimnak and Rungsarit Intaramo

**Two-sample Location Tests under Violation of the Normality and Variance Homogeneity Assumptions 721**

Mongkol Leelaphaiboon and Bumrungsak Phuenaree

**Gold Recovery from Copper-Gold Tailings by Ammoniacal Thiosulphate Leaching 735**

Kamolwich Income, Sirinat Boonpo, Thidarat Kruatian, Ponlayuth Sooksamiti<sup>1</sup> and Sukjit Kungwankunakorn

**Influence of Solvent Temperature and Type on Naphthalene Solubility for Tar Removal in a Dual Fluidized Bed Biomass Gasification Process 751**

Pimnara Tonpakdee, Janjira Hongrapipat, Vilailuck Siriwongrungron, Reinhard Rauch, Shusheng Pang, Jullapong Thaveesri, Michael Messner, Matthias Kuba and Hermann Hofbauer

**Effects of Ethylthiosulfanilate and Chromium (VI) on the State of Glutathione Antioxidant System and Oxidative Stress Marker Content in Rat Kidneys 761**

Bohdan Kotyk and Ruslana Iskra

**An Assessment of Privacy Concerns on Personal Health Information: Thailand Case Study 774**

Charnsak Srisawatsakul and Waransanang Boontarig

**Review article:**

**A Review of COVID-19: Nature of the Virus and Impact of Lockdown on Air Pollution over India and the World** 788

N.V. Krishna Prasad, P. Sasikala, S. Ramesh, M.S.S.R.K.N. Sarma, Thomaskutty Mathew, T. Anil Babu and N. Madhavi

**Instructions for Authors** I

# Developing Agriculture Purchasing Managers' Index for Describing Taiwan's Agriculture Industry by Using Automatic Weighted $k$ -means Algorithm

Tzong-Ru Lee<sup>1</sup> and Chien-Pang Lee<sup>2,3\*</sup>

<sup>1</sup>Department of Marketing, National Chung Hsing University, Taichung City, Taiwan

<sup>2</sup>Department of Maritime Information and Technology, National Kaohsiung University of Science and Technology, Kaohsiung City, Taiwan

<sup>3</sup>Master's Program in Offshore Wind Energy Engineering, National Kaohsiung University of Science and Technology, Kaohsiung City, Taiwan

Received: 7 October 2020, Revised: 21 January 2021, Accepted: 18 February 2021

## Abstract

Although the average agricultural total output is not greater than 2% of Taiwan's GDP, the Taiwan government still attaches great importance to the agriculture industry to ensure the food self-sufficiency rate. Taiwan still has no indicators to measure the status of the agriculture industry. This paper proposes an idea to develop Agriculture Purchasing Managers' Index (APMI) for Taiwan agriculture industries. To reduce the effect of some statistical assumptions and to provide more clarity and direct analysis of results, this paper proposes a novel automatic weighted  $k$ -means algorithm to develop the APMI. The results of this research suggest that four variables should be included in the APMI of the pig industry, namely "Trade amount", "Average weight per pig", "Price per pig", and "Slaughtered.". Among these, "Slaughtered" and "Trade amount" are the more important variables for developing the APMI of the pig industry. The proposed model offers three advantages: (a) it can be successfully used to construct APMI, (b) It can automatically search the weight of each variable without any human judgment in APMI, and (c) It avoids some statistical assumptions and explains the results more clearly and directly. Thus, the proposed model can be used to construct used APMI proposed in this work, and it describes the status of the agriculture industry.

**Keywords:** pig industry; trade of pigs; automatic weighted selection

DOI 10.14456/cast.2021.49

## 1. Introduction

Due to the geographical environment of Taiwan, agriculture is one of the first developed industries in Taiwan. Although the primary industry of Taiwan has changed as the technology industry in recent years, the agricultural industry is still important in Taiwan. According to the official document of the "National Accounts Yearbook" of Taiwan in Jan. 2021, the average agricultural

---

\*Corresponding author: Tel.: (+886) 7-8100888 ext. 25322  
E-mail: cplee@nkust.edu.tw

total output is about 520 billion New Taiwan dollars. That is not greater than 2% of Taiwan's GDP in recent years. Accordingly, the Taiwan government still attaches great importance to the agriculture industry to ensure the food self-sufficiency rate.

Because the agriculture industry plays a vital role in the stable operation of national economies [1, 2], many researchers focus on agriculture industry issues, especially in forecasting agricultural output [3-7]. Furthermore, there is an absence of an agricultural index to describe the macro-economic status of the market. Agricultural companies and government departments have no information except for agricultural gross domestic profit (GDP) to measure the current agriculture industry [8]. Therefore, this paper proposes the idea of developing an agriculture index to describe the agriculture industry's current status.

In the non-agriculture industry, Purchasing Managers' Index (PMI) and Non-Manufacturing (NMI) are two well-known indexes to describe industries' economic status. PMI and NMI are published by the two leading institutions, which are Markit and Institution for Supply Management (ISM). PMI is released ahead of other official indexes and is different from the measurement standards. It is used to evaluate the validity and reliability of the objective; for the reason that there are generally no "standards" of economic activity [8]. Although some countries have been releasing NMI, including the agriculture industry, NMI does not include agriculture industries in Taiwan. Even though the two indexes are not suitable to use directly for describing the status of the agriculture industry, some characteristics or features of them are suitable for us to search for the agriculture indexes.

Since 2011, PMI and NMI are published by the Chung-Hua Institution for Economic Research in Taiwan [9]. Recently, Taiwan Manufacturing PMI has been released monthly. The indicators of PMI and NMI in Taiwan include "New orders", "Production", "Employment Level", "Supplier Deliveries", "Inventory of Purchase Materials", and so on. Many researchers have mentioned five important features in PMI [10-13]: (a) Validity and Reliability; PMI is used to evaluate validity and reliability. It is not used to measure the standard of economic activity, (b) Timing; all indexes are indicators of monthly variation and are calculated as diffusion indexes. For example, new orders of this month and the last month are compared whether the orders increase, decrease or no change, (c) Timeliness; if an index is irregularly releasing schedule, it does not help reference, (d) Stability; the index must be the limits of random fluctuations or a small random component compared to the trend and cyclical components of the activity measured, (e) No Revisions; if the index is released, it is not allowed to be revised.

Because PMI and NMI indicators have not been easy to collect in Taiwan's agricultural industries, a new index has to be developed for describing Taiwan's agricultural economic status. Accordingly, the purpose of this paper is to develop the Agriculture Purchasing Managers' Index (APMI) by selecting the main agriculture indexes. Although many statistical methods are used to solve agriculture-related issues, this paper uses data mining techniques to reduce the effects of certain statistical assumptions and to provide more clarity and direct analysis of results. Since the data is suitable for unsupervised learning algorithms, this paper proposes a novel model based on a *k*-means algorithm called the automatic weighted *k*-means algorithm, to search the weight of each agricultural variables without any human judgment for developing the APMI.

There are many kinds of agricultural industries in Taiwan. This paper chooses the pig industry as an example to develop the APMI of the pig industry because the annual export value of the pig industry was at 170 billion New Taiwan dollars before 1997. However, the industry has been until recently unable to export now due to the impact of foot-and-mouth disease. Fortunately, there is no a need to vaccinate at present, and exports are expected to resume in 2020. It is conceivable that the future pig industry will become one of the primary agricultural industries in Taiwan and this is the main reason for this paper to develop the APMI of the pig industry in Taiwan.

## 2. Materials and Methods

### 2.1 Materials

This paper uses data from the pig industry in Taiwan to develop the APMI for the industry. The data were collected from the Annual Report of the Council of Agriculture, Executive Yuan (Taiwan) and included six variables, such as, “Trade amount”, “Total weight”, “Average weight per pig”, “Price per pig”, “Slaughtered”, and “Total revenue”. The meaning of the variables are described as follows:

- a. Trade amount: The number of pigs traded in a month; the unit is the number of “head”.
- b. Total weight: The total weight of pigs traded in a month; the unit is “kg/head”.
- c. Average weight per pig: The average weight of whole traded pigs in a month; the unit is “metric ton”.
- d. Price per pig: The average price per traded pig in a month; the unit is “NT\$/ton”.
- e. Slaughtered: The number of pigs slaughtered in a month; the unit is the number of “head”.
- e. Total revenue: The total revenue of traded pigs in a month; the unit is “NT 10 thousand dollars”.

### 2.2 The $k$ -means algorithm

As described in the Introduction, the characteristic of the data used for developing the APMI is that there is no direct output variable. In other words, the data lends itself to an unsupervised learning algorithms. This paper uses the  $k$ -means algorithm as the main algorithm to search the weight of each agricultural variable and to develop the APMI. The proposed model is called the automatic weighted  $k$ -means algorithm. To understand the proposed model’s main algorithm, we now introduce the relevant theory and definitions.

The  $k$ -means algorithm, which was first proposed in 1967 [14], is a well-known cluster algorithm in data mining. The main idea of the  $k$ -means algorithm is to partition  $n$  observations into  $k$  clusters in which each observation belongs to the cluster with the nearest mean [15]. Euclidean distance is usually used to measure the distance  $n$  observations belonging to  $k$  clusters. We give a simple example to explain the algorithm of the  $k$ -means. Suppose a dataset  $D=\{x_1, x_2, \dots, x_n\}$  is used to cluster to  $k$  groups. The procedure of the  $k$ -means algorithm includes four main steps.

Step 1. Randomly select  $k$  initial seeds. Subsequently, the  $k$  initial seeds are used as the centroids of the initial  $k$  clusters.

Step 2. Calculate the distance between each data point (observation) and  $k$  centroids. Subsequently, each data point (observation) is assigned to the cluster that is the smallest distance away.

Step 3. Create the new  $k$  centroids of the clusters by calculating the mean of the clusters.

Step 4. Iterate Step 2 and Step 3 until the clusters stop changing or satisfy stop conditions.

Since the Euclidean distance is usually used in the  $k$ -means algorithm, the importance of each variable is the same. However, each variable should have a different influence on different issues in the real world. Accordingly, many different weighted  $k$ -means algorithms were proposed to counter this problem [16, 17]. This paper also follows the idea to propose a novel model, which is introduced in Section 2.3, to develop the APMI

### 2.3 Methods

As described in the Introduction, this paper is concerned with the development of the APMI from the agricultural variables that are to do with the prosperity of agriculture. However, the effects of agricultural variables in the APMI vary. Thus, this paper proposes a hybrid model to counter this problem. The proposed model's main idea is based on the use of the  $k$ -means algorithm to search each variable's weight without any human judgment in the APMI. The proposed model consists of two components, data preprocessing and the automatic weighted  $k$ -means algorithm. Because the unit of each agricultural variable is different, each variable has to perform data preprocessing to reduce the effect of the unit when building the proposed model. Subsequently, this paper uses the automatic weighted  $k$ -means algorithm to automatically determine the number of clusters ( $k$ ) and each agricultural variable's weight. The proposed model's detailed procedures are shown in Figure 1 and are discussed in the following sections.

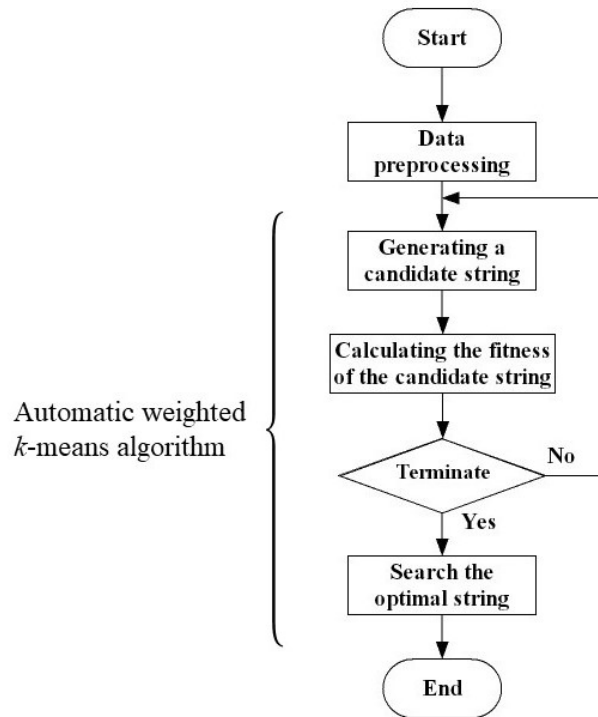


**Figure 1.** The flowchart of the proposed model

#### 2.3.1 Data preprocessing

As described in the above sections, the unit of each agricultural variable is different. For example, the unit of trade amount is “head”, and the unit of the price per pig is “NT\$/ton”. The different units would affect the proposed model's correctness, especially in calculating Euclidean distance, which is the primary measuring method in the  $k$ -means algorithm. Thus, each agricultural variable has to be preprocessed before building the proposed model. The equation of the data preprocessing is shown in Eq. (1).

$$PV_{in} = \frac{V_{in} - V_{i(n-1)}}{V_{i(n-1)}} \quad (1)$$

In Eq. (1),  $V_{in}$  and  $V_{i(n-1)}$  denote the  $i^{\text{th}}$  variable of the  $n^{\text{th}}$  month's value and the  $i^{\text{th}}$  variable of the  $(n-1)^{\text{th}}$  month's value, respectively;  $PV_{in}$  denotes the  $i^{\text{th}}$  variable of the  $n^{\text{th}}$  month's value after performing data preprocessing. Moreover, we would directly understand each agricultural variable's ratios (increase or decrease) according to the results of data preprocessing when  $PV_{in}$  is positive, which signifies that the value is greater than that of the last month.

### 2.3.2 Automatic weighted $k$ -means algorithm

The automatic weighted  $k$ -means algorithm includes three steps to automatically determine the number of clusters and each variable's weight. We then use the determined weight of each variable to develop the APMI. The details are as described in Section 2.3.2.1 to Section 2.3.2.3.

#### 2.3.2.1 Generating a candidate set of the number of clusters and the importance of variables

Generally, a set of the number of clusters and the weight of variables would affect the weighted  $k$ -means algorithms' correctness. However, determining a suitable set of the number of clusters and the weight of variables for the weighted  $k$ -means algorithms is difficult. Therefore, this paper uses a strategy that imitates chromosomes of the genetic algorithm, a popular optimization algorithm [1, 4, 18], to search for the optimal set of the number of clusters and the weight of variables.

In the strategy, we imitate chromosomes of the genetic algorithm to generate many strings as the candidate sets of the number of clusters and the weight of variables for the weighted  $k$ -means algorithms. However, the proposed model uses an integer encode method to generate a string (chromosome) for a set of the number of clusters and the weight of variables. To reduce the computing complexity, this step utilizes the importance of variables to temporarily replace the weight of variables.

A candidate string is generated in the following procedure. Firstly, a candidate string is randomly generated, and the string's structure is determined, as shown in Figure 2. Figure 2 shows that the last bit ( $g_k$ ) denotes the number of clusters and ranges from 2 to 5. The remainder bits ( $g_1$  to  $g_n$ ) denote the importance of variables and range from 0 to 10. Subsequently, a candidate string is generated based on the above strategy.

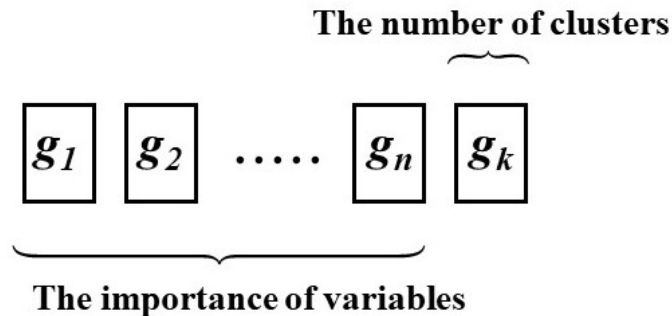


Figure 2. The structure of a candidate string

### 2.3.2.2 Generating a candidate set of the number of clusters and the importance of variables

After constructing a set of the number of clusters and the importance of variables, the importance of variables has to transform as each variable's weight format for performing Euclidean distance in the weighted  $k$ -means algorithm. Eq. (2) is used to transform each variable's importance into each variable's weight format. In Eq. (2),  $W_i$  and  $g_i$  denote the weight and the importance of the  $i^{\text{th}}$  variable, respectively. Subsequently, the algorithm of  $k$ -means according to Eq. (3) for minimizing the within-cluster sum of squares is performed. In Eq. (3),  $C_i$  denotes the  $i^{\text{th}}$  cluster;  $X_j$  denotes the  $j^{\text{th}}$  observation;  $\bar{C}_i$  denotes the mean of  $C_i$ ;  $W$  denotes the weight vector of the variables.

We next define a fitness function to measure the performance according to the characteristic of the  $k$ -means algorithm. Accordingly, Eq. (4) is defined as the proposed model's fitness function and is used to measure the performance of the proposed model. In Eq. (4), "SST" denotes the total sum of squares, and "SSB" denotes the sum of squares between clusters. According to the Eq. (4), a candidate string with higher fitness means that its performance is better than the others.

$$W_i = \frac{g_i}{\sum_{j=1}^n g_j} \quad (2)$$

$$\arg \min_C \sum_{i=1}^k \sum_{X_j \in C_i} W \|X_j - \bar{C}_i\|^2 \quad (3)$$

$$fitness = \frac{SSB}{SST} \quad (4)$$

### 2.3.2.3 Search the optimal set the number of clusters and the weight of variables

Section 2.3.2.1 and Section 2.3.2.2 are analogous to the generation of genetic algorithms. In the proposed model, Section 2.3.2.1 and Section 2.3.2.2 have to be performed many times to generate many candidate sets of the number of clusters and the weight of variables. After generating many candidate strings, we then compare the fitness value of each candidate string. The string with the best fitness value is the optimal string. Finally, the optimal string is used to determine the weights of the agricultural variables for developing the APMI.

## 3. Results and Discussion

### 3.1 Data

This paper uses the pig trade in Taiwan as an example. The monthly data, including six variables from 12/2011 to 12/2018 obtained from the Annual Report of the Council of Agriculture, Executive Yuan (Taiwan), are then collected to develop the APMI by the proposed model. Table 1 shows a part of the collected data. After collecting the data, the data have to be preprocessed using Eq. (1) before the performance of the automatic weighted  $k$ -means algorithm. The transformed results are shown in Table 2.

**Table 1.** A part of the collected data of the traded pigs in Taiwan

Year	Month	Trade amount	Total Weight	Average Weight per pig	Price per pig	Slaughtered	Total revenue
2011	Dec.	665,289	79,981.04	120.22	7,021	402,329	56,155
2012	Jan.	631,948	75,738.97	119.85	6,856	401,495	51,927
2012	Feb.	599,717	72,901.60	121.56	6,080	350,498	44,324
2012	Mar.	700,451	85,630.13	122.25	5,349	403,953	45,804
...	...	...	...	...	...	...	...
2018	Nov.	575,657	71,577.19	124.34	7,156	374,301	51,221
2018	Dec.	581,915	72,622.99	124.80	7,189	384,052	52,209

**Table 2.** A part of the collected data of the traded pigs in Taiwan after data preprocessing

Year	Month	Trade amount	Total weight	Average weight per pig	Price per pig	Slaughtered	Total revenue
2012	Jan.	-0.050	-0.053	-0.003	-0.024	-0.002	-0.075
2012	Feb.	-0.051	-0.037	0.014	-0.113	-0.127	-0.146
2012	Mar.	0.168	0.175	0.006	-0.120	0.153	0.033
...	...	...	...	...	...	...	...
2018	Nov.	-0.028	-0.018	0.010	0.006	-0.029	-0.012
2018	Dec.	0.011	0.015	0.004	0.005	0.026	0.019

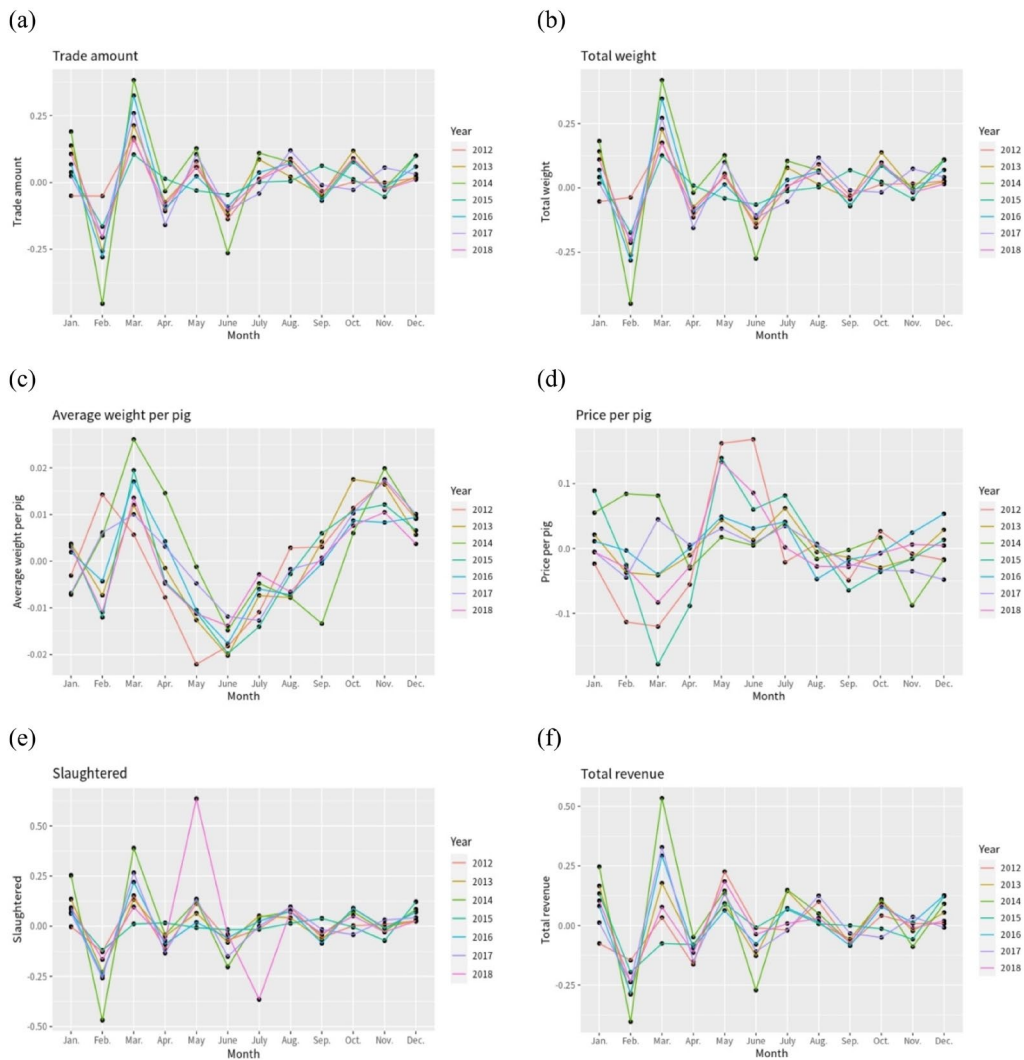
### 3.2 Descriptive statistics

Table 3 shows the descriptive statistics of variables from 12/2011 to 12/2018 after data preprocessing. Although each variable has increased slightly (mean is greater than 0), each variable's variation (SD) has significantly fluctuated apart from the average weight per pig. Subsequently, we plot line charts of each variable by month for each year to explore the trend or the variation of each variable, as shown in Figure 3. Obviously, each variable's trend in different years is almost the same except for some particular timepoints. For example, the "Trade amount" in March is greater than the "Trade amount" in February for each year; on the contrary, the fluctuation of "Slaughtered" in July 2018 is different from the other years.

To explore the trend or variation among variables, we also calculate the Pearson's correlation coefficient matrix to compare the correlation coefficient between variables, as shown in Table 4. According to Table 4, apart from the price per pig, the correlation coefficients among variables are positive. Furthermore, the correlation coefficients among some variables are close to 1. Accordingly, we only keep four variables ("Trade amount", "Average weight per pig", "Price per pig", and "Slaughtered") close the proposed model for developing the APMI.

**Table 3.** The descriptive statistics of variables after data preprocessing

	Trade amount	Total weight	Average weight per pig	Price per pig	Slaughtered	Total revenue
Min	-0.453	-0.450	-0.022	-0.179	-0.468	-0.404
Mean	0.007	0.008	0.001	0.002	0.010	0.009
SD	0.127	0.132	0.011	0.057	0.144	0.143
Median	0.0125	0.014	0.001	-0.004	0.013	0.008
Max	0.383	0.419	0.026	0.169	0.636	0.534



**Figure 3.** The variation of each variable in different years. (a) Trade amount; (b) Total weight; (c) Average weight per pig; (d) Price per pig; (e) Slaughtered; (f) Total revenue

**Table 4.** The Pearson’s correlation coefficient matrix of the variables

	<b>Trade amount</b>	<b>Total weight</b>	<b>Average weight per pig</b>	<b>Price per pig</b>	<b>Slaughtered</b>	<b>Total revenue</b>
Trade amount	1.000	0.997	0.365	-0.032	0.821	0.923
Total weight	0.997	1.000	0.436	-0.069	0.807	0.911
Average weight per pig	0.365	0.436	1.000	-0.461	0.161	0.218
Price per pig	-0.032	-0.069	-0.461	1.000	0.193	0.345
Slaughtered	0.821	0.807	0.161	0.193	1.000	0.841
Total revenue	0.923	0.911	0.218	0.345	0.841	1.000

### 3.3 Parameter setting

Three parameters have to set before performing the proposed model to construct the APMI. Firstly, the number of clusters ranges from 2 to 5 in a candidate string. Secondly, the importance of each variable ranges from 0 to 10. Finally, the number of candidate strings was set at 20,000 candidate strings. Subsequently, we use the parameter setting to perform the proposed model to generate an optimal string.

### 3.4 Stability analysis

Although the proposed model could search for an optimal string for constructing the APMI, the proposed model still had a disadvantage. Because the candidate strings of the proposed model are generated randomly, the optimal string is different when performing the proposed model at different times. To ensure the proposed model can generate a stable result, the proposed model needs to be performed 2,000 times to generate 2,000 optimal strings, which can and then be used to verify the optimal strings from the proposed model’s stability. Table 5 shows the results of the 2,000 optimal weights of variables. Table 5 shows that the mean and median of weights of variables are very close, and their SD are also less than 0.01. That is, the wights of each optimal string should be very close. According to the result, we believe that the result of the proposed model is stable. We could use the proposed model to search the optimal weights of variables for developing the APMI.

**Table 5.** The result of the optimal weights

	<b>Weights</b>			
	<b>Trade amount</b>	<b>Average weight per pig</b>	<b>Price per pig</b>	<b>Slaughtered</b>
Mean	0.334	0.201	0.086	0.379
Median	0.311	0.202	0.088	0.399
SD	0.093	0.098	0.035	0.091

### 3.5 Discussion

The average weights of variables are calculated in Section 3.3. Thus, we use the result to develop the APMI, as shown in Eq. (5):

$$APMI=(0.334X_1+0.201X_2+0.086X_3+0.379X_4)\times 100\% \quad (5)$$

where  $X_1$  denotes the “Trade amount”;  $X_2$  denotes the “Average weight per pig”;  $X_3$  denotes the “Price per pig”, and  $X_4$  denotes the “Slaughtered”.

According to Eq. (5), the “Slaughtered” and the “Trade amount” are the more important variables in the APMI of the pig industry because their weights are significantly greater than the other two variables. Among them, “Slaughtered” is the most important variable for developing the APMI of the pig industry because it has the largest weight in Eq. (5). The result is reasonable and interpretable because the “Slaughtered” and the “Trade amount” denote the pork market’s demand in Taiwan. When pigs are slaughtered immediately after the trade, it represents that the pork market’s demand is high in the month. In short, when the “Slaughtered” and the “Trade amount” of pig’s trade are increasing, the trade of pig in Taiwan is busier. Accordingly, a higher APMI denotes a higher agricultural economic environment.

## 4. Conclusions

### 4.1 Research contributions

Although the average agricultural total output is not greater than 2% of Taiwan’s GDP in recent years, the Taiwan government still attaches great importance to the agriculture industry to ensure the food self-sufficiency rate. Accordingly, many researchers are invested in agricultural research issues. Since Taiwan still has no indicators to measure the agriculture industry’s status, this paper proposes an idea to develop the APMI for the Taiwan agriculture industry.

According to the results, the APMI of the pig industry has been developed based on four variables: “Trade amount”, “Average weight per pig”, “Price per pig”, and “Slaughtered”. Among them, “Slaughtered” and “Trade amount” are the more important variables for developing the APMI of the pig industry, especially “Slaughtered”. Accordingly, we could observe the fluctuations of “Slaughtered” and “Trade amount” to judge the pig industry’s economic status.

The proposed model offers three advantages: (a) it can be successfully used to develop the APMI, (b) it can automatically search the weight of each variable without any human judgment in APMI, and (c) it is based on data mining techniques that reduce the effects of some statistical assumptions and provide more clarity and direct analysis of the results. Accordingly, the proposed model can be suggested for the development of the APMI and describes well the agriculture industry’s status.

### 4.2 Research limitations and future research

This paper’s dataset is the monthly trade of pigs in Taiwan, expressed as six variables, from 12/2011 to 12/2018, obtained from the Annual Report of the Council of Agriculture, Executive Yuan (Taiwan). As described in the Introduction, the Taiwan pig industry announced in 2019 that it was free of foot and mouth disease. Therefore, we give the following suggestions for future research: (a) Future studies should pay attention to the impact of years, especially across 2019, (b) Future studies could include more factors (variables) in the APMI and its development because the agriculture industry may be affected by more external factors, (c) Future studies should include a situation or a time point to update or reconstruct the weightings in the APMI, and (d) Future studies should use the proposed model to develop the APMI for different agriculture industries.

## References

- [1] Ou, S.-L., 2012. Forecasting agricultural output with an improved grey forecasting model based on the genetic algorithm. *Computers and Electronics in Agriculture*, 85, 33-39.
- [2] Xiong, T., Li, C., Bao, Y., Hu, Z. and Zhang, L., 2015. A combination method for interval forecasting of agricultural commodity futures prices. *Knowledge-Based Systems*, 77, 92-102.
- [3] Lee, C.-P., 2017. Reduced the risk in agriculture management for government using support vector regression with dynamic optimization parameters. *LEX LOCALIS - Journal of Local Self-Government*, 15, 243-261.
- [4] Jheng, T., Li, T. and Lee, C.-P., 2018. Using hybrid support vector regression to predict agricultural output. *Proceedings of 2018 27th Wireless and Optical Communication Conference (WOCC)*, 30 April-1 May 2018, 1-3.
- [5] Nieh, S.-C., Lin, W.-S., Hsu, Y.-H., Shieh, G.-J. and Kuo, B.-J., 2014. The effect of flowering time and distance between pollen source and recipient on maize. *GM Crops & Food*, 5, 287-295.
- [6] Higgins, A., Prestwidge, D., Stirling, D. and Yost, J., 2010. Forecasting maturity of green peas: An application of neural networks. *Computers and Electronics in Agriculture*, 70, 151-156.
- [7] Lee, C.-P., Shieh, G.-J., Yiu, T.-J. and Kuo, B.-J., 2013. The strategy to simulate the cross-pollination rate for the co-existence of genetically modified (GM) and non-GM crops by using FPSOSVR. *Chemometrics and Intelligent Laboratory Systems*, 122, 50-57.
- [8] Tien, T.-L., 2018. *The Trial Compilation of Agriculture Purchasing Managers' Index for Taiwan: The Case of Taiwanese Hog Industry*. Taichung: National Chung-Hsing University.
- [9] Chen, S.-H., 2011. *The Compilation of Purchasing Managers' Index for Taiwan*. Taipei: Chung-Hua Institution for Economic Research.
- [10] Kauffman, R.G., 1999. Indicator qualities of the NAPM report on business®. *Journal of Supply Chain Management*, 35, 29-37.
- [11] Koenig, E.F., 2002. Using the purchasing managers' index to assess the economy's strength and the likely direction of monetary policy. *Economic and Financial Policy Review*, 1(6), 1-14.
- [12] Harris, E.S., 1991. Tracking the economy with the purchasing managers' index. *Federal Reserve Bank of New York Quarterly Review*, 16(3), 61-69.
- [13] Lindsey, M.D. and Pavur, R.J., 2005. As the PMI turns: A tool for supply chain managers. *Journal of Supply Chain Management*, 41, 30-39.
- [14] MacQueen, J., 1967. Some methods for classification and analysis of multivariate observations. *Proceedings of Proceedings of the Fifth Berkeley Symposium on Mathematical Statistics and Probability*, Berkeley, California, 281-297.
- [15] Li, Y.-g. and Huang, Y.-s., 2013. Product requirements cluster analysis based on K-means. *Proceedings of 20th International Conference on Industrial Engineering and Engineering Management*, Berlin, Heidelberg, 455-461.
- [16] Thiagarajan, R., Thangavel, K. and Rathipriya, R., 2013. Recommendation of web pages using weighted K-means clustering. *International Journal of Computer Applications*, 86, 44-48.
- [17] Thangadurai, D.K., Uma, M. and Punithavalli, D.M., 2010. A study on rough clustering. *Global Journal of Computer Science and Technology*, 10(5), 55-58.
- [18] Lee, C.-P. and Lin, W.-S., 2016. Using the two-population genetic algorithm with distance-based k-nearest neighbour voting classifier for high-dimensional data. *International Journal of Data Mining and Bioinformatics*, 14, 315-331.

## Molecular Analysis of Sergestid Shrimp *Acetes* spp. from Coastal Water of Sarawak, Malaysian Borneo Using CO1 Sequence

Ruhana Hassan<sup>1,2\*</sup> and Muhammad Nur Arif Othman<sup>2</sup>

<sup>1</sup>Centre for Pre University Studies, Universiti Malaysia Sarawak, Sarawak, Malaysia

<sup>2</sup>Faculty of Resource Science and Technology, Universiti Malaysia Sarawak, Sarawak, Malaysia

Received: 2 July 2020, Revised: 8 February 2021, Accepted: 23 February 2021

### Abstract

Molecular analysis is an alternative to the conventional method of species identification. Misidentification of sergestid shrimp *Acetes* using morphological assessment data could occur due to its small size and the requirement of skilled microscope personnel. This study aims to evaluate the diversity of *Acetes* in Sarawak coastal water using mitochondrial cytochrome c oxidase 1 (CO1) gene analysis. The samples were collected from three sampling sites namely Miri, Lundu and Telaga Air, Sarawak. Based on CO1 gene analysis, two *Acetes* species were revealed, namely *Acetes erythraeus* and *A. serrulatus* with intraspecific variation of 0.20%-2.40% and 0.20%-1.19%, respectively. Besides, the diversity of this species based on geographical pattern could be observed, with two subclades of *A. erythraeus* (Miri, Sarawak and Lundu, Sarawak) and *A. serrulatus* (Telaga Air, Sarawak and west coast of Malaysia). The phylogenetic trees show that both species are reciprocally monophyletic. This finding implies that COI gene is a reliable genetic marker in species identification of *Acetes*.

**Keywords:** CO1 gene; *Acetes*; monophyletic; biodiversity

DOI 10.14456/cast.2021.50

### 1. Introduction

Molecular study involves a non-destructive method where only a small quantity of DNA sample is needed when running the analysis. It has been practiced globally to aid identification of a species, study the relationships among and within population of organisms from different regions, assess the level of genetic variability and estimate the gene flow of targeted species [1]. This technique is claimed to provide precise, timesaving, consistent and reliable information on the targeted organisms.

Cytochrome oxidase subunit 1 (CO1) gene is a widely used genetic marker due to its conserved characteristics, making it suitable for DNA barcoding exercise in animal species. Besides, this gene is highly variable among species and it has higher evolutionary rate compared to nuclear genes, making it useful to distinguish closely related species [2]. The universal LCO1490 and HCO2198 primers are commonly used to amplify CO1 region [3]. These primers have shown to be

---

\*Corresponding author: Tel.: (+60) 82582332 Fax: (+60) 82582330

E-mail: hruhana@unimas.my

successful in the amplification of CO1 gene, which helped in the identification of invertebrate species such as Echinodermata, Mollusca, Annelida, Pogonophora, Arthropoda, Nemertinea, Echiura, Sipuncula, Platyhelminthes, Tardigrada and Coelenterata [3-5]. Additionally, the primers also have been successful in species identification of shrimps and prawns [6-9].

Miri is a coastal city in the northeastern Sarawak, Malaysia, sharing the border with Brunei. The city is situated on the alluvial plain of the Miri River which then flows to the South China Sea. Miri coastal zone is made up of coral reef (Sibuti area); seagrass and beach forest ranging from Kuala Bakam to Lutong; mangrove forests found in Baram and Bakam and peat swamp areas in Senadin and Tudan. Miri coastal water is well-known for sergestid shrimp *Acetes* spp., locally known as 'Bubok' [10]. *Acetes* is the main ingredient of local menus, namely 'belacan', a fermented shrimp paste and 'cincalok', a shrimp pickle. Shrimp and its products could be sold as high as RM50 (approximately USD 12) per kilogram. The abundance of the shrimp during peak season, in between February until April every year, has provided additional income to the fishermen and local communities [11].

Recently, five out of 14 species of *Acetes* CO1 sequences are available in the database of GenBank, namely *Acetes serrulatus*, *A. sibogae*, *A. americanus*, *A. japonicus* and *A. indicus*. For *Acetes*, the species identification using morphological approach is very laborious, as it requires certain level of skill in microscope handling and is time consuming. In order to aid identification of *Acetes*, molecular approach is needed, and such data could also help to solve phylogenetic relationships among species. Therefore, the objectives of this study are (i) to develop DNA barcodes to discriminate between *Acetes* species in coastal water of Sarawak using CO1 gene, and (ii) to assess the phylogenetic relationships among *Acetes* species.

## 2. Materials and Methods

*Acetes* samples were collected from three sampling sites; Miri (LC1, N 4°30'16.7" E 113°59'13.6"), Telaga Air (LC2, N 1°45'49.5" E 109°52'00.3") and Lundu (LC3, N 1°40'38.0" E 110°12'37.9) (Figure 1), with help from local fishermen. The shrimp samples were preserved in 70% ethanol in the field, specifically for molecular analysis work, and brought back to the laboratory in the Faculty of Resource Science and Technology, Universiti Malaysia Sarawak. Prior to genetic analysis work, *Acetes* samples were identified using identification keys provided by Fischer and Bianchi [12], Amin *et al.* [13], Omori [14], Pathansali [15] and Vereshchaka *et al.* [16]. Two species were morphologically identified as *A. erythraeus* and *A. serrulatus*. A total of 14 individuals (10 samples for *A. erythraeus* and 4 samples for *A. serrulatus*) were used in molecular study (Table 1).

Total genomic DNA extraction of *Acetes* was carried out following the modified Cetyltrimethyl Ammonium Bromide (CTAB) protocol proposed by Doyle and Doyle [17]. Amplification of cytochrome oxidase subunit 1 (CO1) gene fragment was conducted using primer LCO1490 and HCO2198 designed by Folmer *et al.* [3].

PCR protocol was carried out following the method proposed by Costa *et al.* [18] in 25 µl reaction mixture containing 17.2 µl ultrapure water, 2.5 µl 10X buffer, 1.5 µl MgCl<sub>2</sub> (50mM), 0.13 µl dNTPs (25mM), 0.75 µl primer forward LCO1490 (10µM), 0.75 µl primer reverse HCO2198 (10µM), 0.2 µl Taq DNA polymerase (5U) and 2.0 µl DNA template. One negative control was included in every PCR batch. The cycle parameters consist of pre-denaturation step at 94°C for 1 min, 5 cycles of denaturation at 94°C for 30 s, annealing at 45°C for 1 min 30 s, extension at 72°C for 1 min, followed by 30 cycles of denaturation at 94°C for 30 seconds, annealing at 51°C for 1 min 30 s, extension at 72°C for 1 min and final extension at 72°C for 5 min. The PCR products were sent to Apical Scientific Sdn. Bhd. Selangor Malaysia for PCR product purification followed by single pass DNA sequencing, forward and reverse strands.

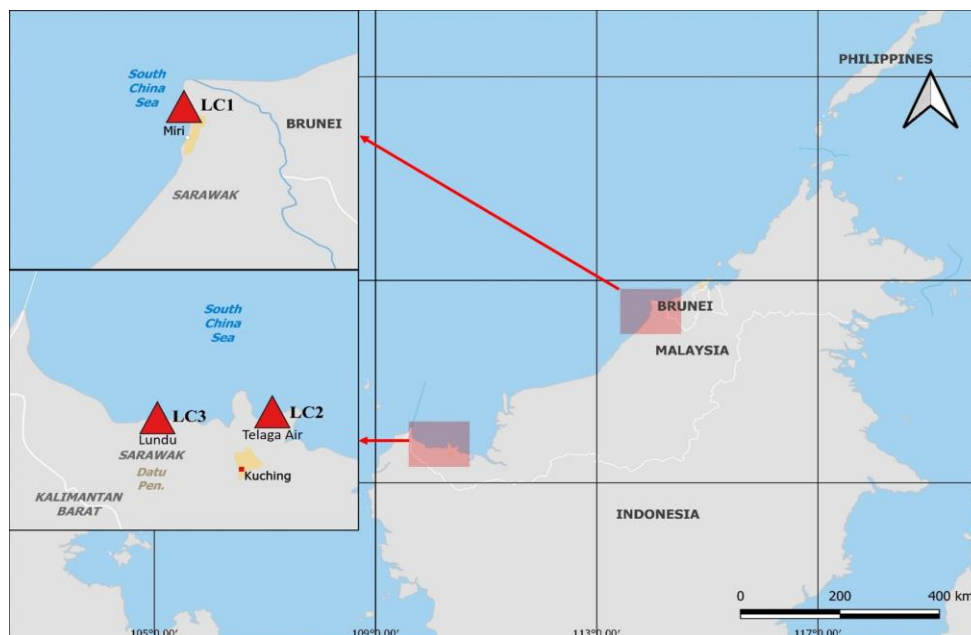


**Figure 1.** Locations of sampling sites in Sarawak coastal water as noted in red triangles; Miri (LC1); Telaga Air (LC2), Lundu (LC3)

**Table 1.** Locality, number of samples and field voucher of *Acetes* for molecular study

Species	Locality	No. of Samples	Field Voucher
<i>A. serrulatus</i>	Telaga Air, Sarawak	4	T01 – T04
<i>A. erythraeus</i>	Miri, Sarawak	6	M01 – M06
	Lundu, Sarawak	4	L01 – L04

CHROMAS software was used to display CO1 sequence results. The sequences were subjected to Basic Local Alignment Search Tool (BLAST) for sequence validation. Multiple alignments of the sequences were constructed using the CLUSTAL X program (version 1.81) and subsequently aligned with other sequences of *Acetes* from the GenBank and *Allosergestes pectinatus* was chosen as outgroup (Table 2).

**Table 2.** List of *Acetes* and other species analysed in this study

Species	Locality	Accession no.
<i>A. serrulatus</i>	Malaysia	HQ630561, HQ630562
<i>A. sibogae</i>	Malaysia	HQ630587
<i>A. aff. sibogae</i>	India	KX399434
<i>A. americanus americanus</i>	Brazil	KX196595
<i>A. japonicus</i>	Malaysia	HQ630575
<i>A. japonicus</i>	China	KF977240
<i>A. indicus</i>	Malaysia	HQ630497
<i>A. indicus</i>	India	MK784109
<i>Allosergestes pectinatus</i> (outgroup)	USA	MH572651

The phylogenetic relationship of 24 CO1 sequences were analysed using Maximum Parsimony (MP), Maximum Likelihood (ML) and Bayesian Inference (BPP) using PAUP (version 4.0). The genetic divergence was obtained using Kimura's Two Parameter Model [19]. Bayesian analysis was conducted based on the substitution model and standard phylogenetic parameters of Akaike Information Criterion (AIC) using MrBayes [20]. AIC is a mathematical method for evaluating how well a model fits the data. Modeltest 3.7 together with PAUP (Version 4.0) was used to select the suitable model for dataset [21]. Model GTR+I+G was chosen for ML and BPP analyses.

### 3. Results and Discussion

Amplification of CO1 gene was successful for six samples of *A. erythraeus* from Miri (M01, M02, M03, M04, M05, M06), four samples of *A. erythraeus* from Lundu (L01, L02, L03, L04) and four samples of *A. serrulatus* from Telaga Air (T01, T02, T03, T04). The BLAST analysis showed that sequences of T01, T02, T03 and T04 were approximately 98% similar to *A. serrulatus* (HQ630561 and HQ630562) from west coast of Malaysia. Sequences of M01, M02, M03, M04, M05, M06, L01, L02, L03 and L04 which are *A. erythraeus* based on morphological analysis show 85% similarity to *A. japonicus* (KF977240) from China (Table 3). The limited similarity of about 15% between *A. serrulatus* samples in this study with *A. japonicus* from the GenBank suggested that both are most likely from different species.

**Table 3.** Summary of BLAST results for all CO1 sequences obtained in this study

Species	Voucher no.	BLAST top hit	Accession no.	% Similarity
<i>A. serrulatus</i>	T01, T02, T03, T04	<i>A. serrulatus</i>	HQ630561, HQ630562	98
<i>A. erythraeus</i>	M01, M02, M03, M04, M05, M06	<i>A. japonicus</i>	KF977240	85
	L01, L02, L03, L04	<i>A. japonicus</i>	KF977240	85

The intraspecific variations of four samples of *A. erythraeus* from Lundu (L01, L02, L03, L04) were 0.39% - 0.99% while the intraspecific variation of six samples of *A. erythraeus* from Miri (M18, M22, M23, M26, M43, M44) were 0.00%-0.59%. The intraspecific variation of *A. erythraeus* from Lundu and Miri were 0.20%-2.40%, with variations of 1 to 12 bp out of 509 bp. The comparison of intraspecific value of *A. erythraeus* from Lundu and Miri with samples from other locality could not be done due to unavailability of *A. erythraeus* CO1 information in the GeneBank. *A. serrulatus* from Telaga Air (T01, T03, T05, T09) had intraspecific variation of 0.20%-1.19%. The intraspecific divergence between *A. serrulatus* found in Telaga Air, Sarawak and *A. serrulatus* from Malaysia (HQ630561, HQ630562) ranged from 1.80% to 2.83%. To summarise, *Acetes* sample sequences in this study that has variation between minimum value and 2.83% fall into similar species category. The results in this study are concordant with previous studies of intraspecific CO1 gene variation on crustacean studies [22, 23, 8]. For example, Quan *et al.* [23] had reported intraspecific variation of five different shrimps namely *Metapenaeus affinis*, *Metapenaeus ensis*, *Penaeus chinensis*, *Penaeus japonicus* and *Penaeus penicillatus* ranged from 0.20%-1.20%. Moreover, Udayasuriyan *et al.* [8] found that the intraspecific variation of *Macrobrachium rosenbergii* from Brazil and India ranged from 1.39% to 1.61%. Meanwhile, 13 species of *Penaeus* collected from USA, Brazil, Taiwan and Spain had intraspecific variation of 0.00% - 3.00% [22]. In

terms of interspecific variation, both *A. erythraeus* and *A. serrulatus* in this study had variation between 19.17% and 20.20%.

The phylogenetic trees of *Acetes* in Sarawak constructed using Maximum Parsimony (MP), Maximum Likelihood (ML) and Bayesian Inference (BPP) are shown in Figure 2 with agreement in the tree topologies. The phylogenetic analysis successfully revealed two major clades (clade *A. erythraeus* and clade *A. serrulatus*) and four subclades namely SC A, SC B, SC C and SC D. Both major clades agreed well with species identification of *Acetes* using the morphological approach.

All *A. erythraeus* samples in this study formed a clade with strong bootstrap values of 100% (MP), 100% (ML) and 1.00 (BPP). Detailed examination of *A. erythraeus* clade reveals two subclades in agreement with the geographical distribution of the samples. The first subclade (SC A) consists of *A. erythraeus* from Miri, Sarawak while the second subclade (SC B) is made up of *A. erythraeus* from Lundu, Sarawak. Interestingly, the phylogenetic trees revealed that single individual of *A. erythraeus* from Miri (M02) was grouped together with *A. erythraeus* from Lundu suggesting that there is a relationship between the two populations. Future work should involve more samples in order to resolve the low bootstrap values obtained in this study. In the present study, *A. erythraeus* originated from Lundu probably migrate to Miri during the southwest monsoon because of the direction of wind that causes the current flow towards the north of Sarawak, as Akhir [24] claimed that the water circulation of South China Sea is influenced by monsoon seasons. A similar result was reported by Aziz *et al.* [25] claiming that migration of *A. japonicus* from Malacca and Perak, on the west coast of Peninsular Malaysia, was observed based on RAPD results.

*A. serrulatus* samples in this study formed a single clade with strong bootstrap values of 100% (MP), 100% (ML) and 1.00 (BPP), therefore *A. serrulatus* is monophyletic. Two subclades could be observed within clade of *A. serrulatus*, based on geographical distributions. The first subclade (SC C) comprises of *A. serrulatus* from Peninsular Malaysia while the second subclade (SC D) contains *A. serrulatus* from Telaga Air, Sarawak.

The phylogenetic trees in this study indicated that CO1 gene is a good marker for the study of the geographical distribution of *Acetes* shrimp. Previous studies have shown the effectiveness of CO1 gene marker in identification of shrimps and prawns [6, 8, 9]. Bilgin *et al.* [6] revealed 12 different species of shrimps in Turkish seas using CO1 gene with the addition of a single cryptic species. Wong *et al.* [9] successfully revealed four different species of *Acetes* along the west coast of Peninsular Malaysia based on CO1 gene information. In addition, Udayasuriyan *et al.* [8] tested the efficiency of using CO1 gene to identify five species of prawns and showed positive results as being a good marker for species identification.

#### 4. Conclusions

In this study, the putative CO1 gene confirmed that the *Acetes* samples from Telaga Air, Sarawak were identified as *A. serrulatus* due to the following reasons: (i) the identification matched *A. serrulatus* from Genebank with accession no. of HQ630561 and HQ630562 (ii) low genetic variation recorded between *A. serrulatus* was obtained in this study with *A. serrulatus* from GeneBank (1.80%-2.83%) and (iii) they were grouped into one clade with *A. serrulatus* from GeneBank with high bootstrap values of 100% (NJ), 100% (MP) and 1.00 (BPP). *Acetes* samples from Miri and Lundu were identified as *A. erythraeus* because they were grouped together into one clade with high bootstrap values of 100% (NJ), 100% (MP) and 1.00 (BPP). Although no comparison could be made between *A. erythraeus* from Miri and Lundu, Sarawak with similar species from GeneBank, the taxonomy of *A. erythraeus* was resolved based on Phylogenetic Species Concept. This study supports the usage of CO1 gene as marker for DNA barcoding of Sergestid shrimp *Acetes*.

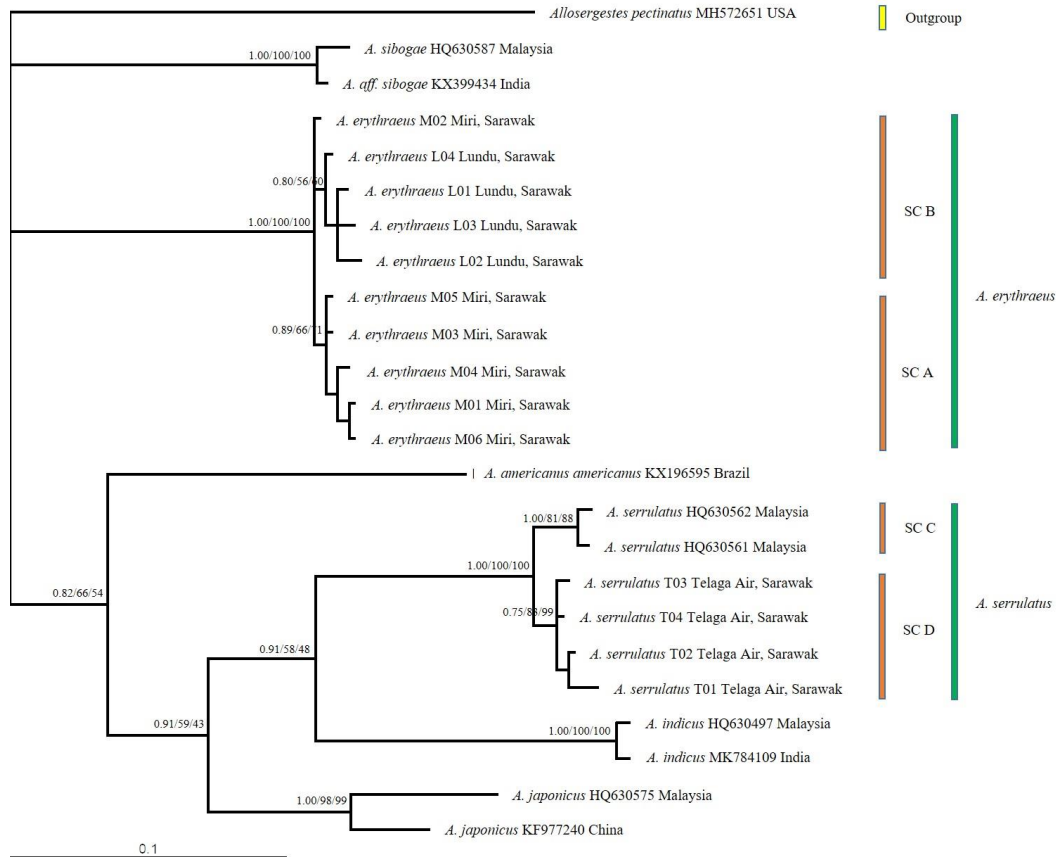


**Figure 2.** Bootstrap 50% majority rule consensus Bayesian inference tree of *A. erythraeus* and *A. serrulatus* from Miri, Telaga Air and Lundu, Sarawak with species of *Acetes* acquired from GeneBank, *Allosergestes pectinatus* as the outgroup. The values at the node represents BPP, ML (%) and MP (%)

## 5. Acknowledgements

This work is supported by UNIMAS-UMS collaboration work Grant Scheme GL/F07/UMS/06/2017. Authors would like to thank local people of Batu 1 village and UNIMAS postgraduate students for their kind assistance during sampling trips and thank to UNIMAS for laboratory facilities.

## References

- [1] Gupta, A., Bhardwaj, A., Supriya, Sharma, P., Pal, Y., Mamta and Kumar, S., 2015. Mitochondrial DNA- a tool for phylogenetic and biodiversity search in equines. *Journal of Biodiversity & Endangered Species*, S1, S1.006, <https://doi.org/10.4172/2332-2543.S1.006>
- [2] Roldán, M.I., Heras, S., Patellani, R. and Maltagliati, F., 2009. Analysis of genetic structure of the red shrimp *Aristeus antennatus* from the Western Mediterranean employing two mitochondrial regions. *Genetica*, 136, 1-4.
- [3] Folmer, O., Black, M., Hoeh, W., Lutz, R. and Vrijenhoek, R., 1994. DNA primers for amplification of mitochondrial cytochrome c oxidase subunit 1 from diverse metazoan invertebrates. *Molecular Marine Biology and Biotechnology*, 3(5), 294-299.
- [4] Maturana, C.S., Moreno, R.A., Labra, F.A., González-Wevar, C.A., Rozbaczylo, N., Carrasco, F.D. and Poulin, E., 2011. DNA barcoding of marine polychaetes species of southern Patagonian fjords. *Revista de Biología Marina y Oceanografía*, 46, 35-42.
- [5] Mikkelsen, N.T., Schander, C. and Willassen, E., 2007. Local scale DNA barcoding of bivalves (Mollusca): A case study. *Zoologica Scripta*, 36, 455-463.
- [6] Bilgin, R., Utkan, M.A., Kalkan, E., Karhan, S.U. and Bekbolet, M., 2015. DNA barcoding of twelve shrimp species (Crustacea: Decapoda) from Turkish seas reveals cryptic diversity. *Mediterranean Marine Science*, 16, 36-45.
- [7] Kundu, S., Rath, S., Tyagi, K., Chakraborty, R. and Kumar, V., 2018. Identification of penaeid shrimp from Chilika Lake through DNA barcoding. *Mitochondrial DNA Part B: Resources*, 3(1), 161-165.
- [8] Udayasuriyan, R., Bhavan, P.S., Vadivalagan, C. and Rajkumar, G., 2015. Efficiency of different COI markers in DNA barcoding of freshwater prawn species. *Journal of Entomology and Zoology Studies*, 3(3), 98-110.
- [9] Wong, B.Y., Awtar Singh, T.K.A., Khoo, G. and Ong, A.H.K., 2017. Intra- and inter-specific variation of four *Acetes* species (Crustacea: Decapoda: Sergestidae) sampled along the West Coast of Peninsular Malaysia. *Sains Malaysiana*, 46(12), 2393-2416.
- [10] Othman, M.N.A., Hassan, R. and Chen, C.A., 2020. Checklist of sergestid shrimps, *Acetes* (Decapoda: Sergestidae) from selected sites along the coastal water of Sarawak, Malaysia. *Malayan Nature Journal*, 72(1), 121-131.
- [11] Abdullah, M., 2018. *Bubuk Season is Back in Miri*. [online] Available at: <https://www.theborneopost.com/2018/03/05/bubuk-season-is-back-in-miri/>
- [12] Fischer, W. and Bianchi, G., 1984. *FAO Species Identification Sheets for Fisheries Purposes: Western Indian Ocean*. Rome: Food and Agriculture Organization of the United Nations.
- [13] Amin, S.M.N., Arshad, A., Siraj, S.S. and Bujang, J.S., 2011. Update on the species composition and distribution of sergestid shrimps (*Acetes* spp.) in Malaysian Waters. *Journal of Fisheries and Aquatic Science*, 6(7), 761-770.
- [14] Omori, M., 1975. The systematics, biogeography, and fishery of epipelagic shrimps of the Genus *Acetes* (Crustacea, Decapoda, Sergestidae). *Bulletin of the Ocean Research Institute*, 7, 1-86.
- [15] Pathansali, D., 1966. *Acetes* (Sergestidae) from the Malay Peninsula. *Bulletin of the National Museum of Singapore*, 33(18), 59-63.
- [16] Vereshchaka, A.L., Lunina, A.A. and Jørgen, O., 2016. Phylogeny and classification of the shrimp genera *Acetes*, *Peisos*, and *Sicyonella* (Sergestidae: Crustacea: Decapoda). *Zoological Journal of the Linnean Society*, 177, 353-377.
- [17] Doyle, J. J. and Doyle, J.L., 1987. A rapid DNA isolation procedure from small quantities of fresh leaf tissue. *Phytochemical Bulletin*, 19, 11-15.

- [18] Costa, F.O., DeWaard, J.R., Boutillier, J., Ratnasingham, S., Dooh, R.T., Hajibabaei, M. and Hebert, P.D.N., 2007. Biological identifications through DNA barcodes: The case of the Crustacea. *Canadian Journal of Fisheries and Aquatic Sciences*, 64, 272-295.
- [19] Kimura, M., 1980. A simple method for estimating evolutionary rates of base substitutions through comparative studies of nucleotide sequences. *Journal of Molecular Evolution*, 16, 111-120.
- [20] Ronquist, F. and Huelsenbeck, J.P., 2003. MRBAYES 3: Bayesian phylogenetic inference under mixed models. *Bioinformatics*, 19, 1572-1574.
- [21] Swofford, D.L., 2002. PAUP\*. *Phylogenetic Analysis using Parsimony (\*and Other Methods)*. Version 4. Massachusetts: Sinauer Associates.
- [22] Baldwin, J.D., Bass, A.L., Bowen, B.W. and Clark, W.H., 1998. Molecular phylogeny and biogeography of the marine shrimp penaeus. *Molecular Phylogenetics and Evolution*, 10, 399-407.
- [23] Quan, J., Zhuang, Z., Deng, J., Dai, J. and Zhang, Y.P., 2014. Phylogenetic relationships of 12 Penaeoidea shrimp species deduced from mitochondrial DNA sequences. *Biochemical Genetics*, 42, 331-345.
- [24] Akhir, M.F. 2014. Review of current circulation studies in the Southern South China Sea. *Journal of Sustainability Science & Management*, 9, 21-30.
- [25] Aziz, D., Siraj, S.S., Arshad, A., Nurul Amin, S.M. and Harmin, S.A., 2010. Population characterization of planktonic shrimp, *Acetes japonicus* (Decapoda: Sergestidae) using RAPD technique. *Journal of Biological Sciences*, 10, 355-361.

## Medium Effect on Antagonistic Activity and Detection of Nonribosomal Peptide Synthetase Genes in Epiphytic *Bacillus* Strains

Suchitra Apimeteethamrong and Chokchai Kittiwongwattana\*

Faculty of Science, King Mongkut's Institute of Technology Ladkrabang,  
Bangkok, Thailand

Received: 24 July 2020, Revised: 6 January 2021, Accepted: 26 February 2021

### Abstract

The biosynthesis of non-ribosomal peptides (NRPs) in biocontrol bacteria was one of the major antagonistic mechanisms for their application in agriculture. *Bacillus* spp. 1021, 2211 and 3210 were previously shown to inhibit mycelial growth of the leaf blast fungus *Pyricularia oryzae*. Here, we aimed to further study the antagonistic mechanism in those three strains. Cell-free supernatants obtained from bacteria grown in potato dextrose broth (PDB) exhibited a higher degree of inhibition against *P. oryzae* when compared to those obtained from nutrient broth (NB). This indicated the effect of culture media in the production of extracellular antibiotic compounds by these strains. Phylogenetic analysis of their partial 16S rRNA gene sequences indicated a close relationship between the three strains and *Bacillus siamensis* KCTC13613<sup>T</sup>, *Bacillus amyloliquefaciens* DSM7<sup>T</sup> and *Bacillus velezensis* CR-502<sup>T</sup>. Complete genome sequences of these *Bacillus* species were analyzed on the antiSMASH server to identify the presence of NRP biosynthesis gene clusters. Non-degenerate primers were designed for the detection of the core biosynthesis genes for surfactin (*srfAA*), fengycin (*fenC*) and bacillibactin (*dhbF*). All three genes were amplified in strains 1021 and 2211, while only *srfAA* and *dhbF* were detected in strain 3210. Phylogenetic analysis of the deduced amino acid sequences indicated that the sequences of strain 1021 were distinct from those of strains 2211 and 3210. This result indirectly suggests the possibility of NRP production as the antagonistic mechanism of these three strains.

**Keywords:** *Bacillus*; nonribosomal peptides; nonribosomal peptide synthetases; *Pyricularia oryzae*

DOI 10.14456/cast.2021.51

---

\*Corresponding author: Tel.: (+66) 23298400 Fax: (+66) 23298427  
E-mail: chokchai.ki@kmitl.ac.th

## 1. Introduction

Members of the genus *Bacillus* are well known for their antimicrobial activities against various groups of phytopathogens. One of the antagonistic mechanisms is the production of bioactive compounds that are collectively known as antimicrobial peptides (AMPs) [1]. These peptides consist of proteinogenic and non-proteinogenic amino acids that are linked together by peptide bonds. Based on the biosynthesis pathways, AMPs can be divided into two subgroups. The first group is ribosomally synthesized peptide antibiotics, e.g., subtilin, coagulins and entomocin [1]. The second group is known as NRPs. Members of this group, such as fengycins, lichenysins and surfactins, are synthesized non-ribosomally [1]. Several NRPs from members of the genus *Bacillus* were found to have inhibitory effects against phytopathogenic fungi. Bacillomycin D produced by *Bacillus vallismortis* ZZ185 displayed antifungal activities against *Alternaria alternata* and *Fusarium graminearum* [2]. Another study showed that iturin- and fengycin-like peptides from *Bacillus amyloliquefaciens* LBM 5006 suppressed the growth of *Aspergillus* spp. [3]. Fengycin from *Bacillus subtilis* BBG201 was implicated in the inhibition of *Botrytis cinerea* [4].

Nonribosomal peptide synthetases (NRPSs) are large enzyme complexes that biosynthesize NRPs [5]. An NRPS complex consists of multiple enzymatic modules [6]. Generally, a module contains three functionally distinctive domains including adenylation, thiolation and condensation domains. The adenylation domain acts as a gate keeper that selects a specific amino acid to be incorporated into an NRP molecule. It catalyzes two important steps. The first one is the adenylation of an amino acid using an ATP molecule. This results in the formation of aminoacyl-AMP. The second step is the transfer of the aminoacyl-AMP molecule to the pantetheine cofactor of the thiolation domain. Finally, the amino acid that is carried on the module is linked to the preceding one by the peptide bond generated by the condensation domain. Additional domains could be found on some modules [6]. For example, the thioesterase domain is present in the last module to catalyze either the release or cyclization of the NRP molecule [6]. Some modules may carry domains that modify the amino acid structure [6]. These structural and functional aspects of NRPS domains generate diverse NRPs with different biological activities. NRPSs are encoded by large gene clusters on bacterial genomes [7]. Amplification of partial NRPS gene fragments could be used as a primary indicator of NRP production. Primers are designed based on the conserved regions of NRPS genes. Antagonistic bacterial strains in major NRP-producing taxa including actinomycetes, *Bacillus* and *Pseudomonas* have been previously identified using this method [8-12]. This indicates the effectiveness of the molecular approach for identification of potential antagonistic bacteria.

Strains 1021, 2211 and 3210 were previously identified as members of the genus *Bacillus* based on approximately 900-bp 16S rRNA gene sequences [13]. The dual-culture test on potato dextrose agar (PDA) showed that the bacteria were among the strains that displayed the highest growth inhibition against *P. oryzae* mycelia [13]. However, the crude extracts, obtained from the bacterial culture in NB medium, were unable to suppress the fungus. It was surmised that the antagonistic activities may depend on the medium used for the bacterial culture [13]. Additionally, the antagonistic mechanisms of these three strains were not known. Thus, the first objective of the present work was to investigate the effect of the culture media PDB and NB on the production of antifungal compounds by these strains. The second aim was to indirectly study the antagonistic mechanism of these *Bacillus* strains. This was done by amplification and phylogenetic analysis of the partial fragments of genes coding for NRPSs, since members of the genus *Bacillus* were known to produce bioactive NRPs [4]. The results obtained from this study suggest the possible mechanisms of the antagonistic activity in *Bacillus* spp. 1021, 2211 and 3210.

## 2. Materials and Methods

### 2.1 Effects of culture media on antagonistic activities

Strains 1021, 2211 and 3210 were obtained from our previous study [13]. Single colonies grown on nutrient agar (Himedia, India) were inoculated in 50 ml tubes containing 10 ml of NB (Himedia, India) or PDB (Himedia, India). The tubes were placed on a rotary shaker at 180 rpm and incubated at 30°C for 72 h. Bacterial cultures were centrifuged at 8,000 rpm for 15 min to obtain the supernatants. The supernatants were filter-sterilized using 0.2 µm diameter filters. *Pyricularia oryzae* was grown on PDA (Himedia, India) at 30°C for 7 days and used for preparation of the mycelial plugs with a cork borer. Six *P. oryzae* mycelial plugs were submerged in 5 ml of the filter sterilized supernatants and incubated at 30°C for 48 h. Mycelial plugs incubated in sterilized distilled water were used as controls.

### 2.2 Bacterial DNA isolation

Strains 1021, 2211 and 3210 were grown in 5 ml NB at 30°C for 24 h. Total genomic DNA was isolated using a Bacterial Genomic DNA Kit (Geneaid, Taiwan), following the manufacturer's protocol. DNA concentration and purity were examined using agarose gel electrophoresis and Nanodrop spectrophotometer (Thermo Fischer Scientific, USA.).

### 2.3 Amplification and phylogenetic analysis of 16S rRNA gene sequences

16S rRNA gene fragments of strains 1021, 2211 and 3210 were amplified, using universal 41F (5'-GCTCAGATTGAACGCTGGCG-3') and 1492R (5'-TACGGYTACCTTGTTACGACTT-3') [14-15]. The amplified products were purified, using a Gel/PCR Purification Kit (Favorgen, Taiwan), and subsequently sequenced using additional universal primers 337F, 785F and 800R by Macrogen Inc. (South Korea). Partial 16S rRNA gene sequences were obtained. The pairwise alignment analysis was done on EzBioCloud [16]. Sequences of related *Bacillus* strains were obtained from the GenBank database. The multiple alignment was analyzed with the CLUSTAL W program version 1.81 [17]. After manual adjustment and correction of gaps and ambiguous nucleotides, phylogenetic trees were reconstructed using the neighbour joining [18], maximum parsimony [19] and maximum likelihood [20] methods in MEGA7 [21]. The bootstrap analysis [22], with 1,000 re-samplings, determined the confidence levels of the clusters.

### 2.4 Amplification of NRPS genes

Complete genome sequences of related *Bacillus* strains were obtained from the GenBank database. The sequences were submitted to antiSMASH version 4.0 [23] for the prediction of NRPS gene clusters. Sequences of NRPS modules were selected and subjected to blastn analysis. Sequences of high similarity levels from different *Bacillus* species were obtained from the GenBank database and aligned using the Clustal Omega program [24]. In this study, non-degenerate primers were manually designed for the amplification of the adenylation domain of *srfAA*, *fenC* and *dhbF* genes (Figure 1). Primer sequences are provided in Table 1. The primers were used for amplification of the target genes from the genomic DNA of strains 1021, 2211 and 3210. The thermal cycles for amplification were: 94°C for 3 min; 40 cycles of 94°C for 30 s, 56°C for 30 s, and 72°C for 90 s; 72°C for 5 min. PCR products were purified and sequenced using their corresponding primers. The amplified sequences were submitted for blastx analysis. The multiple alignment analysis was

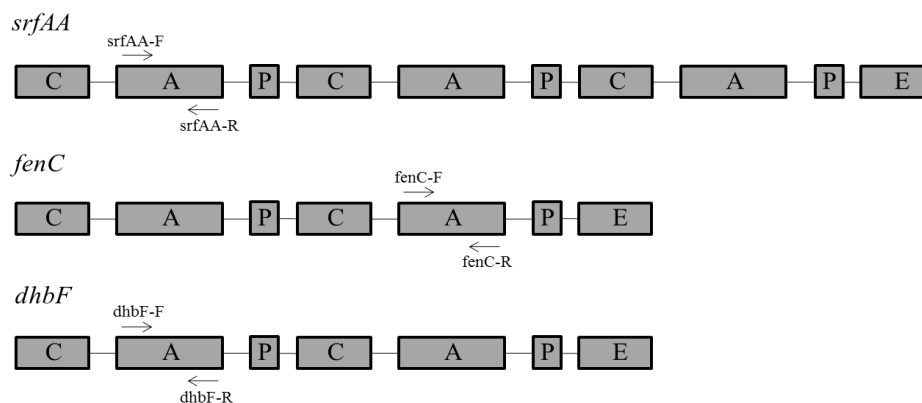


**Figure 1.** Schematic representation of *srfAA*, *fenC* and *dhbF* coding regions and primer-binding positions. Letters indicate the genomic regions that code for different NRPS functional domains. C, condensation domain; A, adenylation domain; P, peptidyl carrier protein domain; E, epimerization domain. Arrows indicate the primer positions and directions.

**Table 1.** Primers used for amplification of target NRPS genes in this study

Primer	Target gene	NRP	Primer sequence (5'→3')
srfAA-F	<i>srfAA</i>	Surfactin	CCGATCTGACCGTGTTATTGCG
srfAA-R			CGCGGACTTTCCTTGATCGTC
fenC-F	<i>fenC</i>	Fengycin	CTGAACGAACGGGCTAACAG
fenC-R			CCGATAACCGCGGATTTTCAC
dhbF-F	<i>dhbF</i>	Bacillibactin	CTATGCCGAATTGAACAAGCG
dhbF-R			CGGCTCTGCTGATATAATCAAG

performed between the deduced amino acid sequences of strains 1021, 2211 and 3210 and their related amino acid sequences, using the program Clustal W. Gaps were manually removed, and phylogenetic trees were reconstructed, using the neighbour-joining method. The bootstrap analysis was performed with 1,000 re-samplings.

### 3. Results and Discussion

Strains 1021, 2211 and 3210 were originally isolated from root, stem and leaf surfaces of rice plants, respectively [13]. Their antagonism against *P. oryzae* was previously shown, using dual-culture assay on PDA plates [13]. This indicated the antagonistic activities may involve the production of extracellular antibiotic compounds. The supernatants from bacterial cultures grown in NB medium were obtained and used to prepare the crude extracts. However, they failed to suppress fungal growth when tested by disc-diffusion assay [13]. In the present work, the determination of medium effects on the antagonistic activity of these strains was carried out (Figure 2). The use of PDB for bacterial culture increased the antagonistic activity of all three

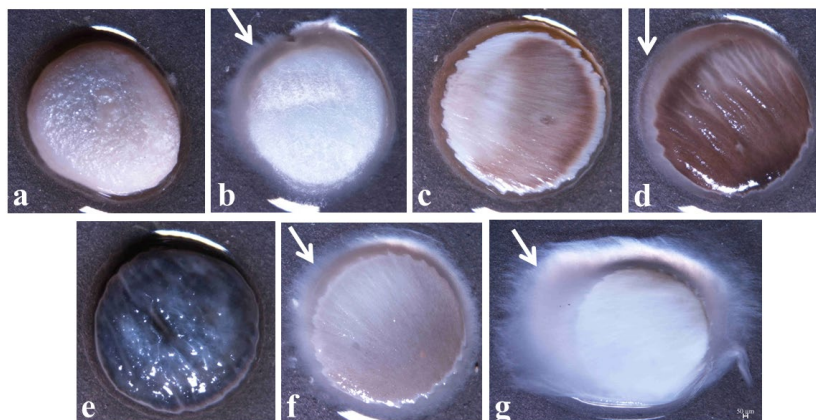


**Figure 2.** *Pyricularia oryzae* mycelial plugs incubated in PDB- (a, c, e) and NB-derived (b, d, f) supernatants of strains 1021 (a, b), 2211 (c, d) and 3210 (e, f), compared with sterilized distilled water (g). Arrows indicate mycelial growth of *P. oryzae* around the edge of the plugs.

strains when compared to NB. This was indicated by the absence of mycelial growth from the plugs that were incubated in PDB-derived supernatants. In contrast, mycelial growth was still visible when the plugs were submerged in NB-derived supernatants. Extensive mycelial growth of the control group that was treated with sterilized distilled water was clearly visible. This suggested PDB was more suitable for induction of the antagonistic activity in strains 1021, 2211 and 3210.

Strains 1021, 2211 and 3210 were previously tested positive for antagonistic activities against *P. oryzae*, the causative agent of leaf blast in rice [13]. The inhibition of the fungal mycelial growth by filter-sterilized supernatants suggested that the mechanism for the activity was the production of extracellular antibiotics. Additionally, the activity depended on the medium used for bacterial culture. The PDB-based supernatants exhibited a stronger inhibitory effect against *P. oryzae* than the ones obtained with NB medium. The result presented here was rather counterintuitive, regarding the purposes of both media. PDB is generally used for growing fungi, while NB is commonly used in bacterial culture. However, a previous study showed that *Bacillus pumilus*, cultured in PDB, produced antifungal metabolites that inhibited growth of several species of genera *Aspergillus*, *Penicillium* and *Fusarium* [25]. Another study showed that the use of PDB as the fermentation medium with *Bacillus natto* NT-6 yielded the highest level of surfactin production, compared to lysogeny broth, NB and Landy medium [26]. Additionally, modified PDB medium was used to induce bioactive compounds by *Bacillus subtilis* 7PJ-16 to reduce mulberry fruit sclerotinose in a field experiment [27]. Based on these observations, PDB may be more appropriate than NB for inducing the antagonistic activity in strains 1021, 2211 and 3210.

Strains 1021, 2211 and 3210 were primarily affiliated with the genus *Bacillus* based on approximately 900-bp 16S rRNA gene sequences [13]. To understand their phylogenetic positions, approximately 1,400-bp long 16S rRNA gene sequences were obtained here. The pairwise alignment of the sequences was analyzed on the EzBioCloud database. Strain 1021 showed the highest similarity (100%) with *Bacillus siamensis* KCTC 13613<sup>T</sup>. On the other hand, the similarity levels with *Bacillus velezensis* CR-502<sup>T</sup> for strains 2211 (99.93%) and 3210 (99.86%) were the highest. Based on the reconstructed phylogenetic tree, the three strains were phylogenetically related to *B. siamensis* KCTC13613<sup>T</sup>, *B. amyloliquefaciens* DSM7<sup>T</sup> and *B. velezensis* CR-502<sup>T</sup> (Figure 3). Both the maximum-parsimony and maximum-likelihood methods showed similar matches.

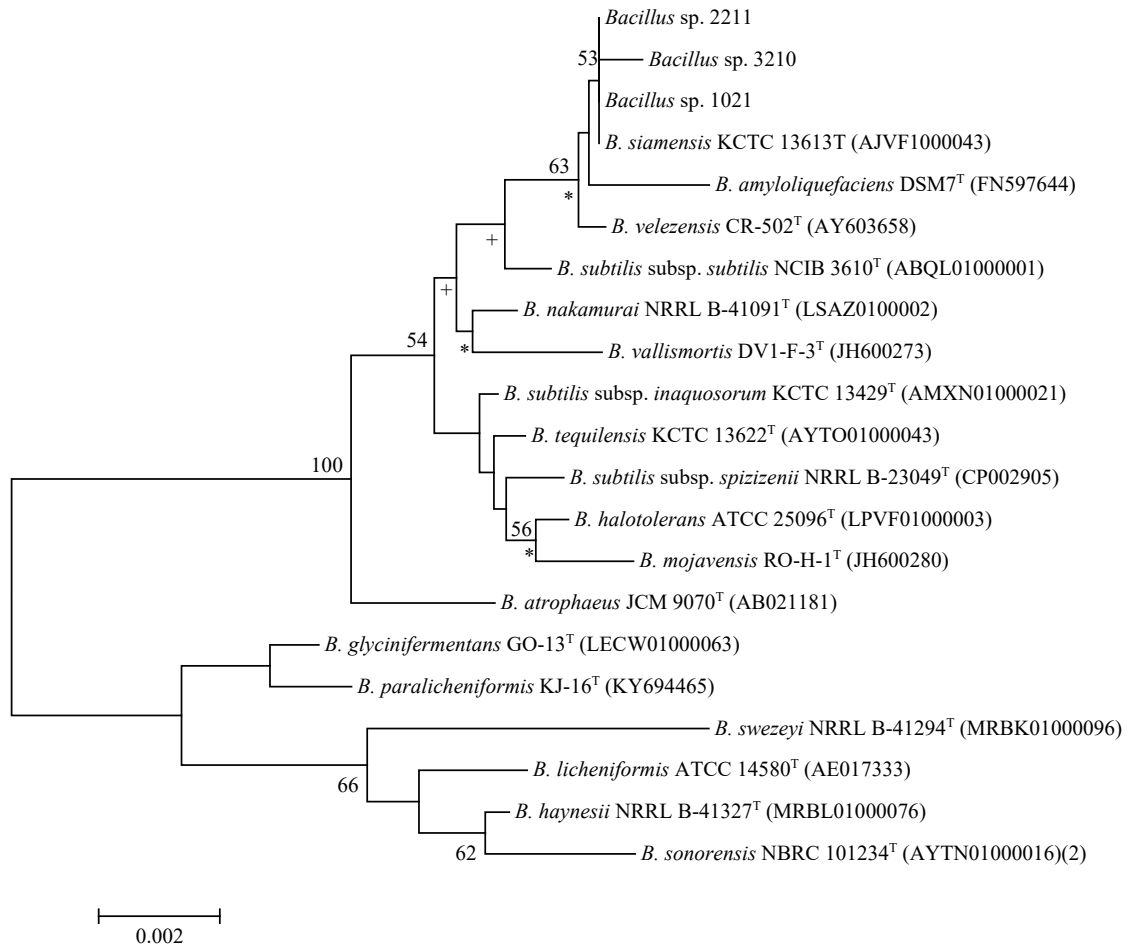


**Figure 3.** Phylogenetic tree reconstructed from partial 16S rRNA gene sequences of strains 1021, 2211, 3210 and other related *Bacillus* strains using the neighbour-joining method. Only bootstrap levels higher than 50% are shown on nodes. + indicates branches that were also found using the maximum-likelihood method. \* indicates branches that were also found using both maximum-parsimony and maximum-likelihood methods. Bar represents 0.002 substitutions per nucleotide position.

Phylogenetic analysis of the 16S rRNA gene sequences indicated that strains 1021, 2211 and 3210 were related to *B. siamensis* KCTC13613<sup>T</sup>, *B. amyloliquefaciens* DSM7<sup>T</sup> and *B. velezensis* CR-502<sup>T</sup>. Consistently, strains of these *Bacillus* species were reported as antagonistic bacteria against the phytopathogenic fungus that caused the blast disease in rice [28-30]. Additionally, some strains were antagonistic against other phytopathogenic fungi, e.g., *Fusarium graminearum* [31], *Botrytis cinerea* [32], *Rhizoctonia solani* [33], *Fusarium solani* and *Fusarium oxysporum* [34]. Applications of these *Bacillus* species as biocontrol agents were effective against various plant diseases including tomato crown gall [35], potato common scab [36] and *Fusarium* head blight in wheat [37].

Several *Bacillus* species were known to carry various NRPS gene clusters [1, 7, 28]. Complete genome sequences of *B. siamensis* SCSIO 05746 (accession number: CP025001), *B. amyloliquefaciens* DSM7<sup>T</sup> (FN597644) and *B. velezensis* FZB42 (CP000560) were obtained from the GenBank database. Based on the antiSMASH server, all three bacterial genomes were predicted to carry biosynthesis gene clusters for three different NRPs, including surfactin, fengycin and bacillibactin. The similarity levels ranged from 82% to 100%. This information was used to investigate the presence of the core biosynthesis genes for surfactin (*srfAA*), fengycin (*fenC*) and bacillibactin (*dhbF*) in strains 1021, 2211 and 3210. Amplification of *srfAA* [38], *fenC* [39] and *dhbF* [40] was previously used as indirect indicators of antagonistic *Bacillus* strains against phytopathogenic fungi. Non-degenerate primers were designed for amplification of the adenylation domain of the genes. The amplified product was approximately 1,000 bp (Figure 4). The *srfAA* and *dhbF* genes were amplified in all three strains, while *fenC* was detected only in strains 1021 and 2211. Sequences of the DNA fragments were used for the blastx analysis (Table 2). The sequence similarities ranged from 98.4% to 100%. The sequences of strain 1021 were similar to NRPS sequences of *B. siamensis*. The sequences of strain 2211 were similar to those of *B. amyloliquefaciens*. In contrast, the *srfAA* sequence of strain 3210 was similar to *B. amyloliquefaciens*, while its *dhbF* sequence was more similar to that of *B. velezensis*.

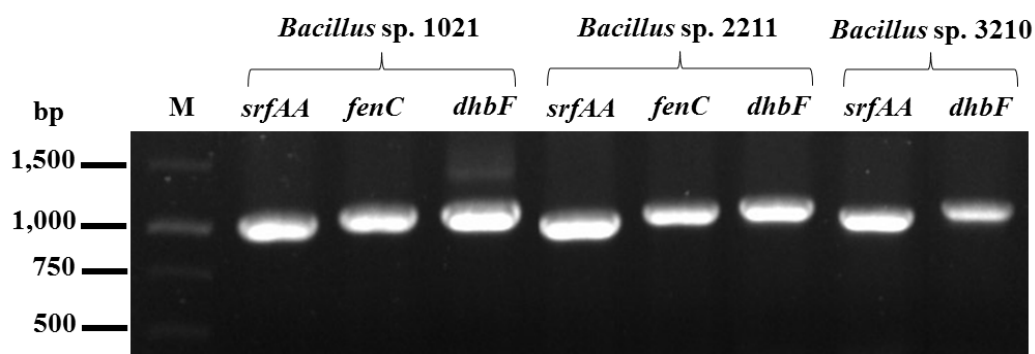


**Figure 4.** Amplified NRPS gene fragments of strains 1021, 2211 and 3210. M: 1kb DNA ladder

The predicted NRP products from the complete genomes of *B. siamensis* SCSIO 05746, *B. amyloliquefaciens* DSM7<sup>T</sup> and *B. velezensis* FZB42 enabled the selection of *srfAA*, *fenC* and *dhbF* genes to be determined in the three strains. Successful amplification of *srfAA* and *dhbF* was observed in all three strains. In contrast, *fenC* was amplified only in strains 1021 and 2211, which suggested the absence of *fenC* in strain 3210 or the primers may alternatively fail to bind to the *fenC* gene of strain 3210. The blastx analysis consistently showed that all amplicons were parts of the NRPS genes. This result indicated that the complete genome sequences of *Bacillus* strains could be valuable for the study of NRPS genes in related bacteria whose genome sequences were not yet available. It also showed that non-degenerate primers could amplify the NRPS gene targets. Previously, other studies used degenerate primers for amplification of NRPS genes [41, 42], as opposed to the non-degenerate primers used here. Another previous study used non-degenerate primers to amplify five biosynthesis genes of bacyllosmycin, fengycin, iturin, surfactin and bacilysin in four *Bacillus* strains [43]. However, the amplified products ranged from 269 bp to 498 bp and were relatively shorter than the ones obtained here.

**Table 2.** Blastx results of the nucleotide sequences of strains 1021, 2211 and 3210

Strains	Amplicon fragments	Most similar proteins	Accession number	Sequence similarity
1021	<i>srfAA</i>	non-ribosomal peptide synthetase, partial ( <i>Bacillus siamensis</i> )	WP_016936794	98.40%
1021	<i>fenC</i>	non-ribosomal peptide synthetase ( <i>Bacillus siamensis</i> )	WP_081484472	100%
1021	<i>dhbF</i>	non-ribosomal peptide synthetase ( <i>Bacillus siamensis</i> )	WP_095241403	98.47%
2211	<i>srfAA</i>	Surfactin non-ribosomal peptide synthetase SrfAA ( <i>Bacillus amyloliquefaciens</i> )	WP_115996107	100%
2211	<i>fenC</i>	Plipastatin synthase subunit C ( <i>Bacillus amyloliquefaciens</i> )	CUB46431	99.28%
2211	<i>dhbF</i>	non-ribosomal peptide synthetase ( <i>Bacillus amyloliquefaciens</i> )	WP_115996640	100%
3210	<i>srfAA</i>	non-ribosomal peptide synthetase ( <i>Bacillus amyloliquefaciens</i> )	WP_021494208	100%
3210	<i>dhbF</i>	non-ribosomal peptide synthetase ( <i>Bacillus velezensis</i> )	WP_095273337	99.70%

The higher antagonistic activity of PDB-derived culture filtrate was similar between strains 1021, 2211 and 3210. The presence of the core biosynthesis genes indirectly indicated strains 1021 and 2211 were potential producers of surfactin, fengycin and bacillibactin, whereas strain 3210 was likely able to produce surfactin and bacillibactin. Previously, the regulation of surfactin production was shown to be regulated by quorum sensing which involved the critical cell density [44]. Thus, the greater effect of PDB over NB in this study may be derived from different growth rates in the two media. Additionally, as a preliminary study, the phylogenetic relationship between the deduced amino acid sequences of the amplified products was investigated. The sequences of strain 1021 were closely related to those of *B. siamensis* and distant from the sequences of strains 2211 and 3210 which were more related to *B. amyloliquefaciens* and *B. velezensis* (Figures 5-7). Based on this analysis, we hypothesized that the amino-acid compositions of NRP molecules produced by strain 1021 and those by strains 2211 and 3210 may be different. This was because the amplified fragments were derived from the adenylation domain that functioned in amino acid selection of the biosynthesis of NRP molecules [5]. Further characterization of the antibiotic compounds produced by these antagonistic strains is needed to confirm this hypothesis.

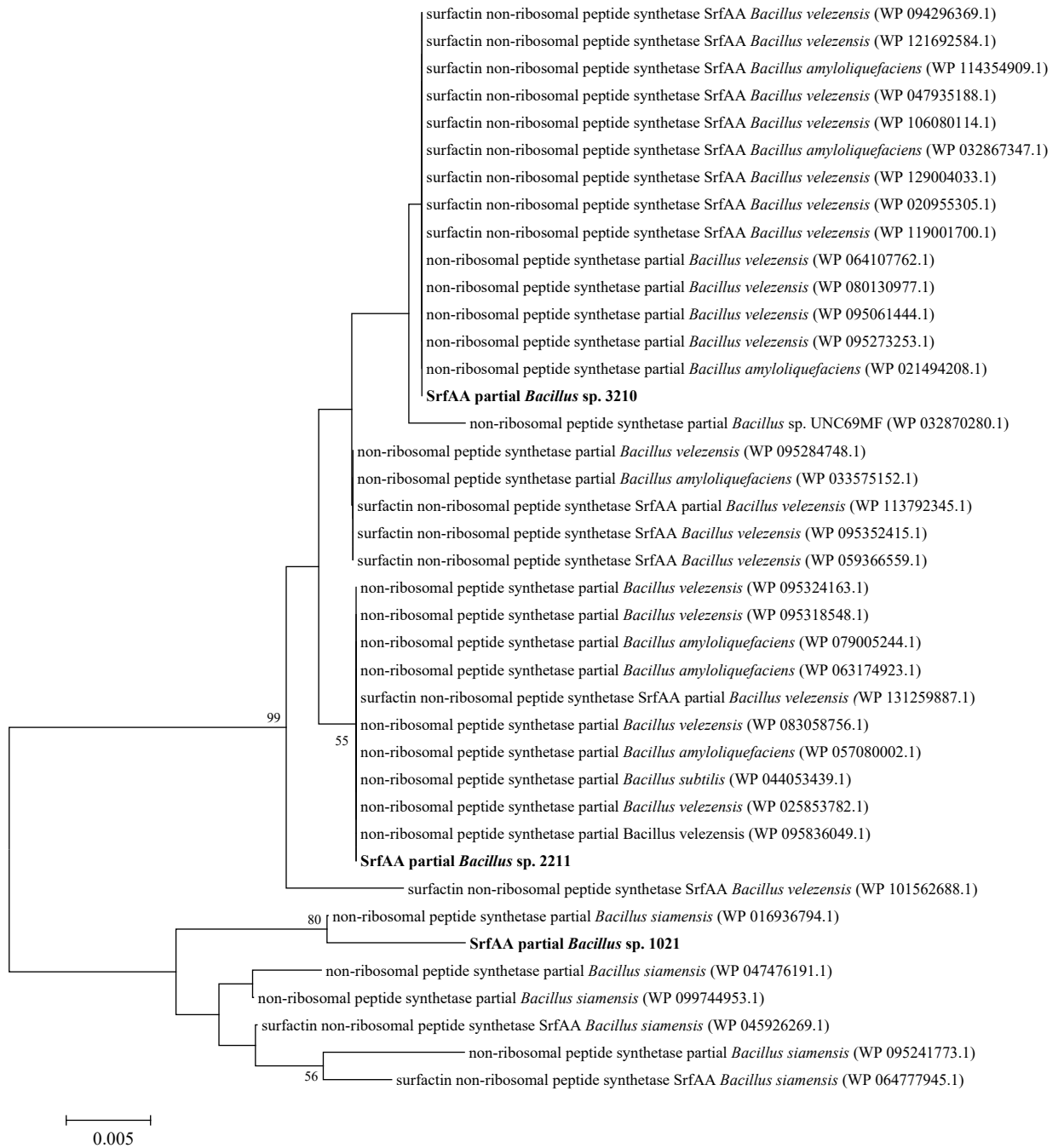


**Figure 5.** The phylogenetic tree based on the SrfAA sequences of strains 1021, 2211 and 3210 and other related NRPS sequences. The tree was reconstructed, using the neighbour-joining method. Only bootstrap levels higher than 50% are shown on the nodes. The bar indicates 0.005 substitutions per amino acid position.

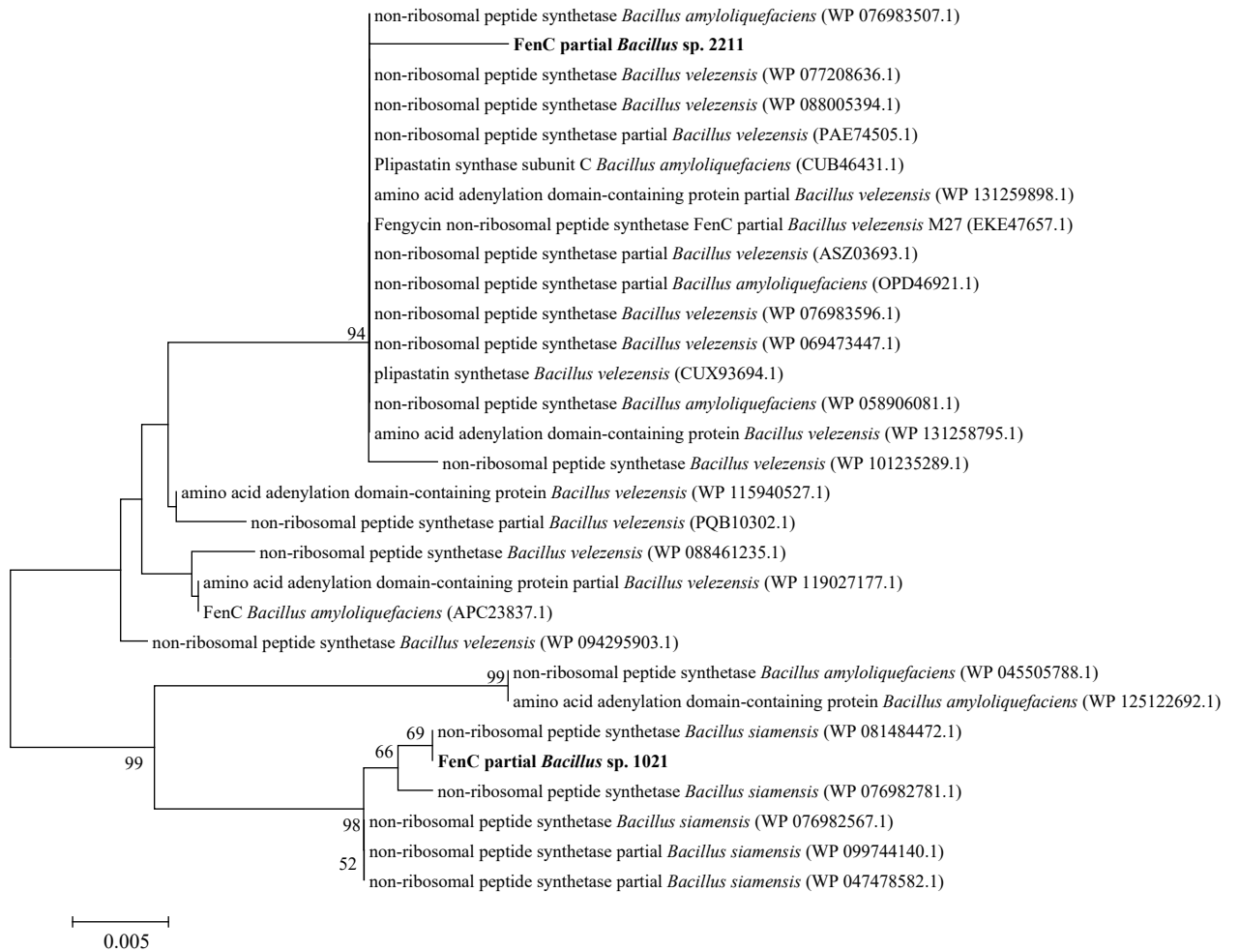


**Figure 6.** The phylogenetic tree based on the FenC sequences of strains 1021, 2211 and other related NRPS sequences. The tree was reconstructed, using the neighbour-joining method. Only bootstrap levels higher than 50% are shown on the nodes. The bar indicates 0.005 substitutions per amino acid position.

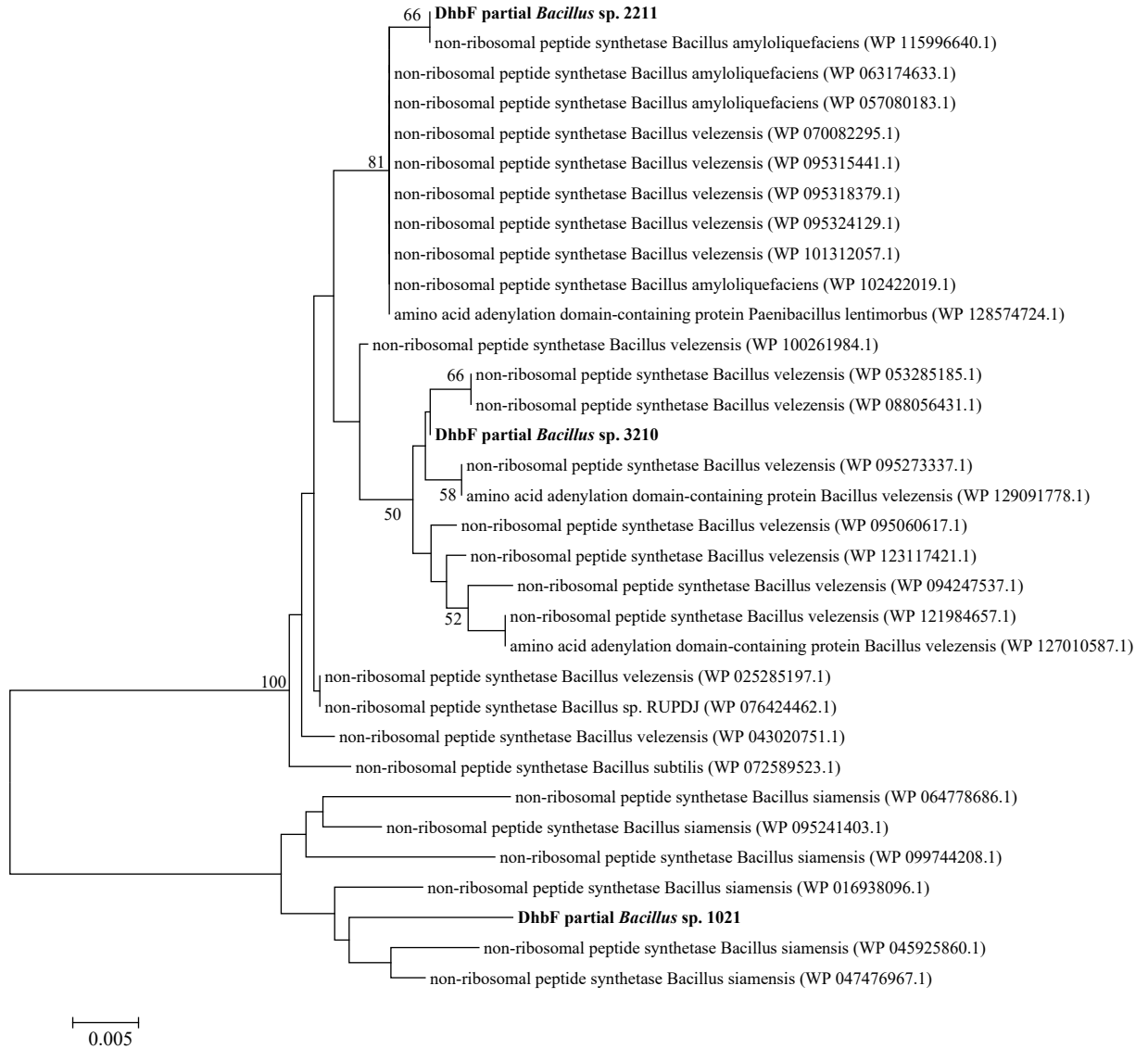


**Figure 7.** The phylogenetic tree based on the DhbF sequences of strains 1021, 2211, 3210 and other related NRPS sequences. The tree was reconstructed, using the neighbour-joining method. Only bootstrap levels higher than 50% are shown on the nodes. The bar indicates 0.005 substitutions per amino acid position.

#### 4. Conclusions

The present study showed that the antibiotic production of *Bacillus* spp. 1021, 2211 and 3210 grown in PDB was likely higher than NB. The phylogenetic analysis of the 16S rRNA gene sequence indicated that the three strains were closely related to *B. siamensis* KCTC13613<sup>T</sup>, *B. amyloliquefaciens* DSM7<sup>T</sup> and *B. velezensis* CR-502<sup>T</sup>. Non-degenerate primers of the core biosynthesis genes *srfAA*, *fenC* and *dhbF* were designed and used for detection of the partial fragments of these genes in strains 1021, 2211 and 3210. All three genes were detected in strains 1021 and 2211, while only *srfAA* and *dhbF* were amplified in strain 3210. The phylogenetic analysis of the deduced amino acid sequences indicated the distinction between the sequences of strain 1021 and those of strains 2211 and 3210.

#### 5. Acknowledgements

The culture of *P. oryzae* was kindly provided by Asst. Prof. Dr. Nonglak Parinthewong of the Faculty of Agricultural Technology, King Mongkut's Institute of Technology Ladkrabang.

#### References

- [1] Sumi, D., Yang, B.W., Yeo, I.C. and Hahmn, Y.T., 2015. Antimicrobial peptides of the genus *Bacillus*: a new era for antibiotics. *Canadian Journal of Microbiology*, 61, 93-103.
- [2] Zhao Z., Wang, Q., Wang, K., Brian, K. Liu, C. and Gu, Y., 2010. Study of the antifungal activity of *Bacillus vallismortis* ZZ185 *in vitro* and identification of its antifungal components. *Bioresource Technology*, 101(1), 292-297.
- [3] Benitez, L.B., Velho, R.V., Lisboa, M.P., Medina, L.F. and Brandelli, A., 2010. Isolation and characterization of antifungal peptides produced by *Bacillus amyloliquefaciens* LBM5006. *Journal of Microbiology*, 48, 791-797.
- [4] Yaseen Y., Diop, A., Gancel, F., Béchet, M., Jacques, P. and Drider, D., 2018. Polynucleotide phosphorylase is involved in the control of lipopeptide fengycin production in *Bacillus subtilis*. *Archives of Microbiology*, 200(5), 783-791.
- [5] Reimer, J.M., Haque, A.S., Tarry, M.J. and Schmeing, T.M., 2018. Piecing together nonribosomal peptide synthesis. *Current Opinion in Structural Biology*, 49, 104-113.
- [6] Challis, G.L. and Naismith, J.H., 2004. Structural aspects of non-ribosomal peptide biosynthesis. *Current Opinion in Structural Biology*, 14, 748-756.
- [7] Aleti, G., Sessitsch, A. and Brader, G., 2015. Genome mining: Prediction of lipopeptides and polyketides from *Bacillus* and related *Firmicutes*. *Computational and Structural Biotechnology Journal*, 13, 192-203.
- [8] Ayuso-Sacido, A. and Geniiloud, O., 2005. New PCR primers for the screening of NRPS and PKS-I systems in actinomycetes: detection and distribution of these biosynthetic gene sequences in major taxonomic groups. *Microbial Ecology*, 49, 10-24.
- [9] Jasim, B., Mathew, J. and Radhakrishnan, E.K., 2016. Identification of a novel endophytic *Bacillus* sp. from *Capsicum annuum* with highly efficient and broad spectrum plant probiotic effect. *Journal of Applied Microbiology*, 121(4), 1079-1094.
- [10] Kamedi, J., Imanparast, S. and Mohammadipanah, F., 2015. Molecular, chemical and biological screening of soil actinomycete isolates in seeking bioactive peptide metabolites. *Iran Journal of Microbiology*, 7, 23-30.

- [11] Mora, I., Jordi, C. and Montesinos, E., 2011. Antimicrobial peptide genes in *Bacillus* strains from plant environments. *International Microbiology*, 14, 213-223.
- [12] Rokni-Zadeh, H., Mangas-Losada, A. and De Mot, R., 2011. PCR detection of novel non-ribosomal peptide synthetase genes in lipopeptide-producing *Pseudomonas*. *Microbial Ecology*, 62, 941-947.
- [13] Apimeteethamrong, S. and Kittiwongwattana, C., 2019. Diversity and plant growth promoting activities of rice epiphytic bacteria. *Current Applied Science and Technology*, 19, 66-79.
- [14] Hongoh, Y., Yuzawa, H., Ohkuma, M. and Kudo, T., 2003. Evaluation of primers and PCR conditions for the analysis of 16S rRNA genes from a natural environment. *FEMS Microbiology Letters*, 221, 299-304.
- [15] Mao, D., Zhou, Q., Chen, C. and Quan, Z., 2012. Coverage evaluation of universal bacterial primers using the metagenomic datasets. *BMC Microbiology*, 12, 66.
- [16] Yoon, S.H., Ha, S.M., Kwon, S., Lim, J., Kim, Y., Seo, H. and Chun, J., 2017. Introducing EzBioCloud: a taxonomically united database of 16S rRNA gene sequences and whole-genome assemblies. *International Journal of Systematic and Evolutionary Microbiology*, 67(5), 1613-1617.
- [17] Thompson, J.D., Higgins, D.G. and Gibson, T.J., 1994. CLUSTAL W: improving the sensitivity of progressive multiple sequence alignment through sequence weighting, position-specific gap penalties and weight matrix choice. *Nucleic Acids Research*, 22, 4673-4680.
- [18] Saitou, N. and Nei, M., 1987. The neighbor-joining method: a new method for reconstructing phylogenetic trees. *Molecular Biology and Evolution*, 4, 406-425.
- [19] Fitch, W.M., 1971. Toward defining the course of evolution: minimum change for a specific tree topology. *Systematic Zoology*, 20, 406-416.
- [20] Felsenstein, J., 1981. Evolutionary trees from DNA sequences: a maximum likelihood approach. *Journal of Molecular Evolution*, 17, 368-376.
- [21] Kumar, S., Stecher, G. and Tamura, K., 2016. MEGA7: Molecular evolutionary genetics analysis version 7.0 for bigger datasets. *Molecular Biology and Evolution*, 33(7), 1870-1874.
- [22] Felsenstein, J., 1985. Confidence limits on phylogenies: An approach using the bootstrap. *Evolution*, 39, 783-791.
- [23] Blin, K., Wolf, T., Chevrette, M.G., Lu, X., Schwalen, C.J., Kautsar, S.A., Suarez Duran, H.G., de Los Santos, E.L.C., Kim, H.U., Nave, M., Dickschat, J.S., Mitchell, D.A., Shelest, E., Breitling, R., Takano, E., Lee, S.Y., Weber, T. and Medema, M.H., 2017. AntiSMASH 4.0-improvements in chemistry prediction and gene cluster boundary identification. *Nucleic Acids Research*, 45(W1), W36-W41.
- [24] Chojnacki, S., Cowley, A., Lee, J., Foix, A., and Lopez, R., 2017. Programmatic access to bioinformatics tools from EMBL-EBI update. *Europe PMC*, 45(W1), W550-W553.
- [25] Munimbazi, C. and Bullerman, L.B., 1998. Isolation and partial characterization of antifungal metabolites of *Bacillus pumilus*. *Journal of Applied Microbiology*, 84, 959-968.
- [26] Sun, D., Liao, J., Sun, L., Wang, Y., Liu, Y, Deng, Q., Zhang, N., Xu, D., Fang, Z., Wang, W. and Gooneratne, R., 2019. Effect of media and fermentation conditions on surfactin and iturin homologues produced by *Bacillus natto* NT-6: LC-MS analysis. *AMB Express*, 9, 120, <https://doi.org/10.1186/s13568-019-0845-y>
- [27] Xu, W.F., Ren, H.S., Ou, T., Lei, T., Wei, J.H., Huang, C., Li, T., Strobel, G., Zhou, Z. and Xie, J., 2019. Genomic and functional characterization of the endophytic *Bacillus subtilis* 7PJ-16 strain, a potential biocontrol agent of mulberry fruit sclerotiniase. *Microbial Ecology*, 77(3), 651-663.
- [28] Xu, B.H., Lu, Y.Q., Ye, Z.W., Zheng, Q.W., Wei, T., Lin, J.F. and Guo, L.Q., 2018. Genomics-guided discovery and structure identification of cyclic lipopeptides from the

- Bacillus siamensis* JFL15. *PLoS ONE*, 13(8), e0202893, <https://doi.org/10.1371/journal.pone.0202893>
- [29] Yoshida, S., Hiradate, S., Tsukamoto, T., Hatakeda, K. and Shirata, A., 2001. Antimicrobial activity of culture filtrate of *Bacillus amyoliquefaciens* RC-2 isolated from mulberry leaves. *Phytopathology*, 91(2), 181-187.
- [30] Lim, S.M., Yoon, M.Y., Choi, G.J., Choi, Y.H., Jang, K.S., Shin, T.S., Park, H.W., Yu, N.H., Kim, Y.H. and Kim, J.C., 2017. Diffusible and volatile antifungal compounds produced by an antagonistic *Bacillus velezensis* G341 against various phytopathogenic fungi. *The Plant Pathology Journal*, 33(5), 488-498.
- [31] Palazzini, J.M., Dunlap, C.A., Bowman, M.J. and Chulze, S.N., 2016. *Bacillus velezensis* RC 218 as a biocontrol agent to reduce *Fusarium* head blight and deoxynivalenol accumulation: Genome sequencing and secondary metabolite cluster profiles. *Microbiological Research*, 192, 30-36.
- [32] Jiang, C.H., Liao, M.J., Wang, H.K., Zheng, M.Z., Xu, J.J. and Guo, J.H., 2018. *Bacillus velezensis*, a potential and efficient biocontrol agent in control of pepper gray mold caused by *Botrytis cinerea*. *Biological Control*, 126, 147-157.
- [33] Yu, G.Y., Sinclair, J.B., Hartman, G.L. and Bertagnolli, B.L., 2002. Production of iturin A by *Bacillus amyoliquefaciens* suppressing *Rhizoctonia solani*. *Soil Biology Biochemistry*, 34, 955-963.
- [34] Kim, Y.G., Kang, H.K., Kwon, K.D., Seo, C.H., Lee, H.B. and Park, Y., 2015. Antagonistic activities of novel peptides from *Bacillus amyoliquefaciens* PT14 against *Fusarium solani* and *Fusarium oxysporum*. *Journal of Agricultural and Food Chemistry*, 63, 10380-10387.
- [35] Abdallah, D.B., Frikha-Gargouri, O. and Tounsi, S., 2018. Rizhospheric competence, plant growth promotion and biocontrol efficacy of *Bacillus amyoliquefaciens* subsp. *plantarum* strain 32a. *Biological Control*, 124, 61-67.
- [36] Lin, C., Tsai, C.H., Chen, P., Wu, C.Y., Chang, W.L., Yang, Y.L. and Chen, Y.L., 2018. Biological control of potato common scab by *Bacillus amyoliquefaciens* Ba01. *PLoS ONE*, 13(4), e0196520, <https://doi.org/10.1371/journal.pone.0196520>
- [37] Chen, L., Heng, J., Qin, S. and Bian, K., 2018. A comprehensive understanding of the biocontrol potential of *Bacillus velezensis* LM2303 against *Fusarium* head blight. *PLoS ONE*, 13(6), e0198560, <https://doi.org/10.1371/journal.pone.0198560>
- [38] Plaza, G., Chojniak, J., Rudnicka, K., Paraszkiwicz, K. and Bernat, P., 2015. Detection of biosurfactants in *Bacillus* species: genes and products identification. *Journal of Applied Microbiology*, 119, 1023-1034.
- [39] Zalila-Kolsi, I., Mahmoud, A.B., Ali, H., Sellami, S., Nasfo, Z., Tounsi, S. and Jamoussi, K., 2016. Antagonistic effects of *Bacillus* spp. strains against *Fusarium graminearum* for protection of durum wheat (*Triticum turgidum* L. subsp. *Durum*). *Microbiological Research*, 192, 149-158
- [40] Lim, J.H., Ahn, C.H., Jeong, H.Y., Kim, Y.H. and Kim, S.D., 2011. Genetic monitoring of multi-functional plant growth promoting rhizobacteria *Bacillus subtilis* AH18 and *Bacillus licheniformis* K11 by multiplex and real-time polymerase chain reaction in a pepper farming field. *Environmental Science*, 54, 221-228.
- [41] Tapi, A., Chollet-Imbert, M., Scherens, B. and Jacques, P., 2010. New approach for the detection of non-ribosomal peptide synthetase genes in *Bacillus* strains by polymerase chain reaction. *Applied Microbiology and Biotechnology*, 85, 1521-1531.
- [42] Abderrahmani, A., Tapi, A., Nateche, F., Chollet, M., Leclère, V., Wathelet, B., Hacene, H., and Jacques, P., 2011. Bioinformatics and molecular approaches to detect NRPS genes involved in the biosynthesis of kurstakin from *Bacillus thuringiensis*. *Applied Microbiology and Biotechnology*, 92, 571-581.

- [43] Almoneafy, A.A., Kakar, K.U., Nawaz, Z., Li, B., Alisaand, M., Chun-lan, Y. and Xie, G., 2014. Tomato plant growth promotion and antibacterial related-mechanisms of four rhizobacterial *Bacillus* strains against *Ralstonia solanacearum*. *Symbiosis*, 63, 59-70.
- [44] Harwood, C.R., Mouillon, J.M., Pohl, S. and Arnau, J., 2018. Secondary metabolite production and the safety of industrially important members of the *Bacillus subtilis* group. *FEMS Microbiology Reviews*, 42, 721-738.

## Using Anthocyanin Extracts from Butterfly Pea as pH Indicator for Intelligent Gelatin Film and Methylcellulose Film

Samart Sai-Ut<sup>1\*</sup>, Phunsiri Suthiluk<sup>2</sup>, Wirongrong Tongdeesoontorn<sup>2</sup>, Saroat Rawdkuen<sup>2</sup>, Pimonpan Kaewprachu<sup>3</sup>, Thomas Karbowski<sup>4</sup>, Frédéric Debeaufort<sup>4</sup> and Pascal Degraeve<sup>5</sup>

<sup>1</sup>Department of Food Science, Faculty of Science, Burapha University, Chonburi, Thailand

<sup>2</sup>Unit of Innovative Food Packaging and Biomaterials, School of Agro-Industry, Mae Fah Luang University, Chiang Rai, Thailand

<sup>3</sup>College of Maritime Studies and Management, Chiang Mai University, Samut Sakhon, Thailand

<sup>4</sup>AgroSup Dijon, University of Burgundy, Dijon, France

<sup>5</sup>BioDyMIA research unit, Claude Bernard University Lyon 1, University of Lyon, Lyon, France

Received: 16 September 2020, Revised: 11 January 2021, Accepted: 2 March 2021

### Abstract

Among variety of intelligent food packaging, pH indicator packaging is becoming more popular, which can be made from synthetic and natural compounds. The search for natural pH indicator dyes that can be used in intelligent food packaging systems has recently focused on anthocyanins extracted from plants. Thus, this work aimed to develop and characterize an intelligent tag for pH indicator based on gelatin and methylcellulose-film with butterfly pea extract (BPE). The results showed that the colors of BPE solutions had a tendency to change from red to blue in a pH range of 4.0 to 8.0. The maximum absorption peak moved to a higher wavelength was observed at around 627 nm at pH 8.0 and shifted to 574 nm when the pH decreased to 5.0. After BPE was incorporated into the gelatin and methylcellulose-based films, the film's properties were characterized. The color of the incorporated films changed from purple to blue and blue to green in buffers with pH ranging from 2.0 to 6.0 and 7.0 to 10.0, respectively. The incorporated gelatin-based film containing BPE showed a clearer response to pH variation and showed a high pigment releasing rate when immerse in buffer of pH 10. The incorporated methylcellulose-based film containing BPE had higher water solubility than that of gelatin-based film ( $p < 0.05$ ), as well as improved mechanical properties and water vapor permeability (WVP). Therefore, it is possible to use the BPE (anthocyanins) as a visual pH indicator for food package.

**Keywords:** anthocyanin; butterfly pea; intelligent packaging; pH indicator  
DOI 10.14456/cast.2021.52

---

\*Corresponding author: E-mail: samarts@go.buu.ac.th

## 1. Introduction

Recently, packaging technologies have been developed for packaging and materials to be used as intelligent biodegradable packaging. Intelligent packaging is important in food and pharmaceutical industries to ensure food quality and safety. The main purposes of these new forms of packaging are to prolong shelf life, minimize environmental impact and communicate product changing over time to consumers. Among variety of intelligent food packaging, pH indicator packaging or real-time monitoring of food quality has become more favourite by consumer. Basically, visual pH indicators or pH sensitive dye can be made from synthetic and natural chemical compounds in which the former are avoided due to their side effects to human health. Many studies have reported prospective applications of natural pH indicator dyes in intelligent food packaging systems including anthocyanins extracted from sweet potato [1], red grapes [2], and purple cabbages [3].

The use of biopolymers in food packaging have gained increased interest in recent years because they represent an environmentally alternative to plastic-based polymers. Methylcellulose (MC) is natural biopolymer derived from cellulose, which has been widely applied in the food industry. MC presents some good properties such as water solubility, films forming ability, consistency, and hydrophilic property. Meanwhile, gelatin, fibrous protein, has been widely used as polymer base material in film formation due to its several advantages. Gelatin films present good film forming ability and oxygen barrier properties [4]. However, biopolymer-based materials can act differently when different types of ingredient are added. Protein can act as buffer systems due to their ionizable side groups resulting in uncertain responsiveness to pH changes. In addition, the mechanisms related to pH color responses of natural dye in MC films are still unknown. Formulation additives can provide a new functionality and physicochemical properties of pH indicator films.

Anthocyanins, natural plant compounds, are water soluble pigments that impart the red, purple and indigo color of many plants. Anthocyanins have the ability to change color with pH; changes that reflect structural transformations [5]. Their abilities can be suitable for use as parts of colorimetric pH indicators that can be utilized in intelligent food materials. Butterfly pea is known as a rich source of anthocyanin with blue color used for food and sweets. The butterfly pea's pigments can exhibit color at various pH, making them a natural alternative to synthetic indicators. Thus, the aims of this study are to develop pH indicator film incorporated with anthocyanin from butterfly pea and to characterize the physicochemical and mechanical properties of the indicator film.

## 2. Materials and Methods

### 2.1 Plant extract preparation

Butterfly pea (*Clitoria ternatea*) flowers were purchased from local market, Chonburi province, Thailand. The flowers were dried in hot air oven at 60°C for 24 h. The dried flowers were ground using blender. Then, sample powder (5 g) was immersed in 200 ml of 70% ethanol aqueous solution at 4°C for 24 h. After this period, the extracts were filtered through Whatman filter paper No.1. The filtrate obtained was referred to as "butterfly pea extract (BPE)." The extract was tested at different pH, ranging from pH 2 to 10 using 1 N HCl and 1 N NaOH. The pH was measured by pH meter and the sample was photographed. The absorption spectra of the BPE were measured using a UV-vis spectrophotometer. The BPE was adjusted for pH in the range of 2.0-10.0 using HCl and NaOH. The absorbances of the adjusted solutions were measured in the range of 400-700 nm.

## 2.2 Preparation of compostable film incorporated with anthocyanin extract

Compostable film incorporated with anthocyanins extract was prepared from commercial food grade bovine gelatin and methylcellulose. The gelatin film was prepared by mixing 3 g of gelatin and 0.75 g of glycerol with distilled water to obtain the film forming solution (FFS). The methylcellulose film was prepared by mixing 3 g of methylcellulose and 0.75 g of glycerol with 70% ethanol. The solution was incubated at 60°C for 30 min in a water bath with occasionally stirring. The BPE with 10% final concentration was then incorporated into the FFS. De-aerated film-forming solution was cast onto a rimmed circular plastic plate (145 mm) and dried with a ventilated oven environmental chamber at  $25 \pm 0.5^\circ\text{C}$  and  $50 \pm 5\%$  relative humidity for another 24 h. The obtained dried films were manually peeled and subjected to film characterization.

## 2.3 Determination of film thickness and color response to pH change of the indicator films

Film thickness was measured with a hand-held micrometer (Mitutoyo Absolute). Measurements were done at nine random points along the rectangular strips. The thickness values were used to calculate the mechanical properties of the films. Film color was determined using CIE-Lab colorimeter in the term of lightness ( $L^*$ ), redness ( $+a^*$ ) or greenness ( $-a^*$ ), and yellowness ( $+b^*$ ) or blueness ( $-b^*$ ) of the films. The color response of the indicator films to pH changes in aqueous mediums (pH 2-10) were determined. The colorimeter was calibrated with a white standard plate. Before the measurement, the pH indicator films were immersed in 5 ml of each buffer solutions for 5 min. All measurements were taken in 4 replicates at random locations of each sample.

## 2.4 Determination of film solubility and water vapor permeability

The solubility and releasing rate of films were determined by cutting dried films into  $10 \times 10$  mm pieces and weighted. The samples were immersed in sample cup with 5 ml pH buffer solutions at  $25^\circ\text{C}$  for 30 min. After that, the solutions were removed, and then dried. When the films had dried, the samples were weighed and calculated. Their solubility was calculated by the following equation:

$$\text{Film solubility (\%)} = (W_i - W_f) / W_i \times (100) \quad (1)$$

where  $W_i$  is initial weight and  $W_f$  is final weight. The releasing rate of the films was measured after solubility tests using the aqueous mediums (pH 2-10). The amounts of monomeric anthocyanins released under different pH conditions were determined by absorbance measurement at  $\lambda_{\text{max}}$  using a UV/VIS spectrophotometer.

The WVP of the films was measured using a modified ASTM method [6]. The films were sealed onto an insertion cup containing water with grease and holder. The sample cups were placed in incubator with relative humidity at 30%. The cups were weighed every 6 h over a period of 3 days, and then the films' WVP were calculated as follows:

$$\text{WVP} = w \cdot x / A \cdot t \cdot (P_2 - P_1) \quad (2)$$

where  $w$  is the weight loss of the cup (g),  $x$  is the film thickness (mm),  $A$  is the area of exposed films ( $\text{m}^2$ ),  $t$  is the time of gain (s), and  $(P_2 - P_1)$  is the vapor pressure differential across the film (Pa). The WVP was expressed as  $\text{gH}_2\text{O/s}\cdot\text{m}\cdot\text{Pa}$ . Each film was determined in triplication. Mechanical properties were measured using a Universal Testing Machine under conditioning for 48 h at  $50 \pm 5\%$  RH at  $25^\circ\text{C}$ . Ten samples ( $2.5 \times 8$  cm) with an initial grip length of 3 cm were determined for

tensile strength (TS) and elongation at break (EAB). The cross-head speed was set at 30 mm/min with 1 kN load cell use. The wettability of the film was evaluated by contact angle measurement using a sessile-drop method. A 10  $\mu$ l drop of distilled water was applied on the surface of each film, and then the angle between the drop and the surface of the film was measured.

## 2.5 Statistical analysis

The two-sample t-test was used for comparing two means of data whereas analysis of variance (ANOVA) was used for comparing three means of data. Tukey's range test was applied as Post Hoc test for multiple comparison of groups. Analysis was performed using MINITAB.

## 3. Results and Discussion

### 3.1 VIS-spectra of BPE solutions in various pH ranges

Color variations in the BPE solutions after adjusting pH with HCl or NaOH were tested and recorded. The results of BPE showed that the color change of BPE solution is caused by the dissociation of pH (Figure 1). The BPE's original color at pH 6 was purple and then turned violet when the pH of the solution was lower than 4.0. The color of BPE solutions turned blue, dark green, and green yellow when the pH of the solution was 7.0-8.0, 9.0-10, and 12.0, respectively. The BPE solution's colors had a remarkable change at pH 2.0 to pink and 12.0 to green-yellow. The maximum absorption peak movement to a higher wavelength was observed around 627 nm at pH 8.0 and shifted to 574 nm when the pH decreased to 5.0. When the pH decreased to 2.0, the maximum absorption peak shifted to 550 nm. The change of red to blue of anthocyanin might be caused by the loss of flavylium cation and the hydrolysis of anthocyanin molecules [7]. Bathochromic shift is usually found in anthocyanin compounds which shift their color when a change in environmental conditions, such as a change of charge occurs [8-10].

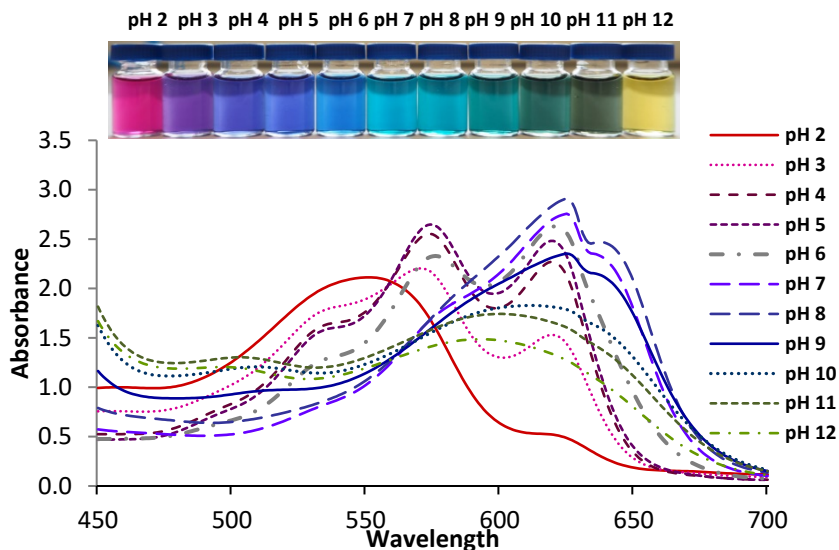


**Figure 1.** UV-Vis spectra of BPE solutions and color response variations of BPE at different pH (2-12)

### 3.2 Color response analysis of the indicator films exposed to different pH buffers

The color responses of the gelatin and methylcellulose films exposed to different pH buffers were examined by dripping the films in buffer solutions at pH range of 2.0 to 10.0. The result showing visible response color changes of each sample, inclining from pink to green in pH 2.0 to 10.0 buffers, are presented in Figure 2. The initial film color was blue, which turned purple when contacted with the pH 2.0 buffer solution and changed in color from blue to dark green with alkaline solution. The pH indicator film became purple in acid solution, and then showed a blue color when it was immersed in higher pH buffer solutions (pH 5.0-6.0). Thereafter, the film color changed to a light green color in pH 8.0 to 10.0 buffers. The color parameters of the pH indicator films after immersion in the pH buffers were measured using a CIE-Lab colorimeter. The colorimetric parameters of the gelatin and MC-based films containing BPE are shown in Table 1. Comparing color responses,  $a^*$  and  $b^*$  values showed significant differences in all pH buffers ( $p < 0.05$ ). The indicator films immersed in alkaline solution showed lower  $a^*$  values, but increased in  $b^*$  values. The redness of the films increased with immersion in the acid buffers due to the flavylum cation forming in anthocyanins [10]. When it reaches pH 4.0, the anthocyanin solution were liberty blue due to the less amount of flavylum cation and quinonoidal anion. When pH is increased from 4.0 to 6.0, the hydration of the flavylum cation generates a colorless carbinol pseudo-base resulting from nucleophilic attack by water [11,12]. At alkaline pH (8.0-10.0), blue color solution were formed due to deprotonation of the quinonoid molecule [10]. In contrast, when pH is increased to alkaline condition, the films appear blue-green in color which is due to the anionic quinoidal base representing deep blue becoming more prominent [13]. Color properties in terms of  $a^*$  and  $b^*$  had significant color response variations influenced by acid-alkaline condition. It can be considered that the films incorporated with BPE had unequivocal colors in various pH environments.

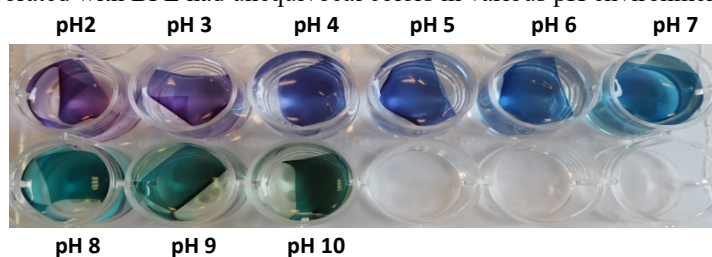


**Figure 2.** Color response of the gelatin film containing BPE in different pH buffers

**Table 1.** Colorimetric parameters of gelatin and MC-based films containing BPE

pH value	Gelatin-based film			MC-based film		
	$L^*$	$a^*$	$b^*$	$L^*$	$a^*$	$b^*$
pH 2	58.47 ± 0.64	24.52 ± 0.97	-14.55 ± 0.59	53.16 ± 3.33	27.61 ± 1.70	-19.89 ± 4.41
pH 3	54.41 ± 0.83	17.71 ± 1.29	-17.76 ± 1.47	49.08 ± 1.16	24.75 ± 1.65	-22.00 ± 0.85
pH 4	50.33 ± 0.73	17.55 ± 1.81	-27.26 ± 1.22	49.28 ± 1.44	20.72 ± 0.19	-29.34 ± 0.90
pH 5	51.84 ± 1.21	15.91 ± 0.94	-28.63 ± 0.94	45.36 ± 1.27	19.41 ± 1.90	-28.44 ± 3.51
pH 6	54.67 ± 1.30	8.30 ± 0.51	-26.64 ± 1.16	47.39 ± 0.85	11.38 ± 0.58	-24.96 ± 1.38
pH 7	55.68 ± 2.25	-5.32 ± 1.73	-19.27 ± 1.51	47.39 ± 1.69	4.18 ± 1.85	-19.33 ± 0.72
pH 8	54.44 ± 0.74	-7.13 ± 0.30	-9.77 ± 0.31	50.27 ± 2.59	-6.12 ± 2.11	-11.49 ± 2.08
pH 9	55.04 ± 1.90	-3.71 ± 0.36	-4.99 ± 0.24	50.40 ± 0.66	-6.67 ± 0.49	-8.04 ± 0.73
pH 10	59.03 ± 1.71	-2.88 ± 0.83	-2.26 ± 0.67	44.32 ± 1.33	-0.47 ± 0.79	-3.08 ± 0.34

### 3.3 Film solubility and releasing rate of the pH indicator films

The solubility in different pH buffers is a significant property that determines the indicator film pertinence. The solubility of both gelatin and MC-based films was measured at pH 2.0-10.0. The gelatin films at neutral close pH showed a lower solubility (8.5% at pH 6), whereas the films in acid buffer presented the highest solubility (79.7% at pH 2) (Table 2). The difference in solubility of the films was affected by the pH of aqueous solution. Theoretically, proteins have a minimum solubility at the protein isoelectric point, at which the net charge of protein molecules is zero. Proteins basically present high solubility in acid or alkaline pH regions due to the excesses of charges on protein, which conduct repulsion among the molecules, thus favoring greater solubility. In contrast, MC-based films showed significantly higher solubility than that of gelatin films. The decreased film solubility of gelatin film compared with MC-based films was attributed to the cross linking effect of phenolic compounds presented in the butterfly pea extract. Similarly, reduced solubility of chitosan film incorporating anthocyanin in water was attributed to hydrogen bond development [14]. The higher solubility of methylcellulose films was due to a hydrophilic polymer involving the penetration of water to the polymer bulk, causing swelling, and then disruption of hydrogen and Van der Waals forces between MC polymer chains [15]. Anthocyanin molecules of PBE possibly caused a decrease in intermolecular interactions in the MC-based film. Therefore, the free side groups of the molecules might interact with water and increase water absorbency [16].

**Table 2.** Film solubility of BPE incorporated gelatin and MC-based films

pH	Film solubility (%)	
	Gelatin-based film	MC-based film
2	79.7 ± 4.8 <sup>a</sup>	89.8 ± 4.5 <sup>a</sup>
3	71.8 ± 4.5 <sup>ab</sup>	85.8 ± 3.5 <sup>abc</sup>
4	60.0 ± 10.2 <sup>b</sup>	77.0 ± 6.1 <sup>abcd</sup>
5	13.4 ± 8.5 <sup>de</sup>	73.5 ± 6.4 <sup>bcd</sup>
6	8.5 ± 3.1 <sup>e</sup>	69.2 ± 1.9 <sup>cd</sup>
7	24.7 ± 0.7 <sup>cde</sup>	70.7 ± 7.2 <sup>cd</sup>
8	31.8 ± 4.0 <sup>cd</sup>	62.8 ± 1.8 <sup>d</sup>
9	26.4 ± 3.4 <sup>cde</sup>	79.7 ± 2.3 <sup>abc</sup>
10	39.3 ± 11.8 <sup>c</sup>	80.5 ± 7.1 <sup>abc</sup>

Note: Different superscript letters indicate significant differences between means in the same column ( $p < 0.05$ ).

The releasing properties of BPE in gelatin and MC-based film were determined under pH 2-10. The gelatin films showed that the releasing properties of the extract were in the range of 34.7% to 70.8%, whereas MC-based film had the releasing properties of 28.0% to 88.0% (Table 3). In acid solution, the releasing ability of the both films were lower than those in alkaline solution. Reduction in releasing properties of the extract from the gelatin and methylcellulose-based films was due to the interactions with the polymeric chains; between protein and phenol compounds and also methylcellulose and phenol compounds. These interactions, which lowered relaxation ability, led to lower swelling and thereby reduced the extract release rate. With increasing of pH to alkaline, the films significantly released anthocyanin into the solution. This indicates that the anthocyanin from the extract was dependently physico-chemically immobilized. At higher pH, negative charge unfolded the protein structure, and more anthocyanin residues were exposed to the solution and displayed increased anthocyanin release properties. Similar results were reported by Wu *et al.* [17],

**Table 3.** Releasing properties of BPE in gelatin and MC-based films

pH	$\lambda_{\max}$	Releasing properties of BPE in film (%)	
		Gelatin-based film	MC-based film
2	550	37.7 ± 1.8 <sup>cdeA</sup>	32.5 ± 5.4 <sup>cdB</sup>
3	570	35.4 ± 4.5 <sup>deA</sup>	33.4 ± 0.2 <sup>cdA</sup>
4	574	34.7 ± 3.2 <sup>eA</sup>	34.6 ± 4.2 <sup>cdA</sup>
5	574	41.4 ± 1.5 <sup>bcdA</sup>	28.0 ± 2.3 <sup>dB</sup>
6	621	40.0 ± 1.0 <sup>cdA</sup>	31.1 ± 1.8 <sup>cdB</sup>
7	625	48.5 ± 4.9 <sup>bcA</sup>	42.0 ± 2.5 <sup>bcB</sup>
8	625	46.7 ± 3.6 <sup>bcdA</sup>	49.1 ± 5.7 <sup>bA</sup>
9	625	51.9 ± 4.9 <sup>bbB</sup>	79.2 ± 6.5 <sup>aA</sup>
10	600	70.8 ± 7.0 <sup>abB</sup>	88.0 ± 7.0 <sup>aA</sup>

Note: Two sample t-test was used for comparing 2 means in row. Different superscript letters indicate significant differences between means in the same column ( $p < 0.05$ ) and different superscript capital letters indicate significant differences between means in the same row ( $p < 0.05$ ).

who observed that the releasing properties of indicator dyes were affected by pH, and especially under alkaline solution.

### 3.4 Effect of BPE on the mechanical and physicochemical properties of films

The effect of BPE on the mechanical and physicochemical properties of the films were evaluated by testing the tensile strength (TS) and elongation at break (E%) of the films. The colored film thickness ranged between 50 and 55  $\mu\text{m}$  (data not shown). The incorporation of BPE had no effect on the gelatin films' thickness. As the results shown in Table 4, colored films showed no significant difference in tensile strength and elongation at break when compared to control films, except in the case of tensile strength for gelatin film. Incorporation of BPE into formulations tended to improve the mechanical properties of MC-based films, but decreased those properties of gelatin-based films. Normally, the mechanical properties of compostable films rely on the interactions between the constituents of the film matrix. The enhanced TS and E% in MC-based film could be ascribed to intermolecular interactions between anthocyanins and methylcellulose chains. However, enormous incorporation of the phenolic compound sorely exhausted the molecular interaction between the methylcellulose polymers [18]. For gelatin-based film, the TS decreased after the addition of BPE, suggesting the anthocyanins-rich extract interrupted the formation of intra/interchain hydrogen bonds of gelatin. The decrease in TS is due to weakening of interactions between protein and phenol groups. Similar effects on mechanical properties were found in the case of anthocyanin used as color indicator in gelatin films [19].

The contact angle and WVP of pH indicator films are shown in Table 4. Incorporation of BPE into the films resulted in significantly higher WVP of films ( $p < 0.05$ ). To develop the film as an indicator, a higher WVP should be examined. The films should have high volatile permeate ability for monitoring deterioration of food products. The pH indicator gelatin film showed significantly lower WVP than the methylcellulose-based film ( $p < 0.05$ ). The increase in WVP for the pH indicator films might be due to the incorporation of the hydrophilic BPE. Polyphenolic molecules of BPE possibly caused low in intermolecular interactions in the film network. Thus, the hydroxyl groups of BPE molecules might cooperate with water and intervene in the network by

**Table 4.** Mechanical properties of gelatin and MC-based films incorporated with BPE

Film	Tensile (MPa)	Elongation at break (mm)	WVP $\times 10^8$ (gH <sub>2</sub> O/s·m·Pa)	Contact angle (degree)
Gelatin-based film	51.1 $\pm$ 4.3 <sup>abA</sup>	58.9 $\pm$ 3.4 <sup>aA</sup>	10.54 $\pm$ 0.92 <sup>bb</sup>	70.56 $\pm$ 5.07 <sup>bb</sup>
Gelatin-based film with BPE	39.4 $\pm$ 1.2 <sup>bb</sup>	59.8 $\pm$ 2.3 <sup>aA</sup>	12.27 $\pm$ 0.82 <sup>ba</sup>	83.51 $\pm$ 9.09 <sup>aA</sup>
MC-based film	61.2 $\pm$ 22.2 <sup>abA</sup>	69.0 $\pm$ 7.0 <sup>ba</sup>	10.83 $\pm$ 0.44 <sup>bb</sup>	64.38 $\pm$ 3.23 <sup>bcA</sup>
MC-based film with BPE	65.5 $\pm$ 14.2 <sup>aa</sup>	71.0 $\pm$ 4.8 <sup>ba</sup>	20.20 $\pm$ 2.27 <sup>aA</sup>	54.62 $\pm$ 7.81 <sup>cb</sup>

Note: ANOVA and Tukey's test were used for comparison. Different superscript letters indicate significant differences between means in the same column ( $p < 0.05$ ), and different superscript capital letters indicate significant differences between means in the same based film's type (with/without BPE) ( $p < 0.05$ ).

hydrogen bonds and thus increase water vapor permeability [20]. The WVP increased when incorporated with bioactive compounds. Similar results were found in some reports of incorporating bioactive compounds containing the hydroxyl group into active films [21-23]. The contact angle technique is used to investigate the surface structures of the films for their hydrophobicity properties. Larger angle value represents more hydrophobicity of the pH indicator films. The contact angle for the gelatin-based film was higher after BPE incorporation, in contrast to the MC-based film, which showed a lower contact angle value after BPE incorporation (Table 4). This might be due to a greater number of hydrophilic sites for the water soluble components present on the MC-based film. In addition, the high amount of BPE in the MC-based films resulted in high polarity bonds groups of anthocyanin that can interact with water molecules and the contact angle consequently decreases by expanding water on the surface of the film.

#### 4. Conclusions

The intelligent gelatin film incorporated with BPE presented a color variation as a function of pH ranges. Butterfly pea is suitable to be used as pH color response indicator in both gelatin and MC-based films due to its high sensitivity and variety of color shades. The pigment releasing properties showed that anthocyanin from butterfly pea in the extract was bonded loosely on the MC-based films. However, the mechanical properties and WVP need to be improved, when considering its application as a pH-responsive indicator for varieties of food products. Thus, development of color response film by incorporating anthocyanin from butterfly pea can be used as novel food smart packaging for pH sensitive product and spoilage detection for perishable food.

#### 5. Acknowledgements

This work was financially supported by the Ministry of Higher Education, Science, Research and Innovation (MEHSI) of Thailand, the Ministry of Europe and Foreign Affairs (MEAE) and the Ministry of Higher Education, Research and Innovation (MESRI) of France under Franco-Thai Mobility Programme/PHC SIAM "ActiFoodCoat." The authors greatly thank Burapha University, Mae Fah Luang University, University of Burgundy and University of Lyon for offering many conveniences.

## References

- [1] Cevallos-Casals, B.A. and Cisneros-Zevallos, L., 2004. Stability of anthocyanin-based aqueous extracts of Andean purple corn and red-fleshed sweet potato compared to synthetic and natural colorants. *Food Chemistry*, 86(1), 69-77.
- [2] Golasz, L.B., da Silva, J. and da Silva, S.B., 2013. Film with anthocyanins as an indicator of chilled pork deterioration. *Food Science and Technology*, 33, 155-162.
- [3] Chen, X. and Gu, Z., 2013. Absorption-type optical pH sensitive film based on immobilized purple cabbage pigment. *Sensors and Actuators B. Chemical*, 178, 207-211.
- [4] Nilsuwan, K., Benjakul, S. and Prodpran, T., 2016. Influence of palm oil and glycerol on properties of fish skin gelatin-based films. *Journal of Food Science and Technology*, 53(6), 2715-2724.
- [5] Heredia, F.J., Francia-Aricha, E.M., Rivas-Gonzalo, J.C., Vicario, I.M. and Santos-Buelga, C., 1998. Chromatic characterization of anthocyanins from red grapes-I. pH effect. *Food Chemistry*, 63(4), 491-498.
- [6] ASTM, 1983. Standard test method for water vapor transmission of materials. E 96-80. In: *Annual Book of ASTM Standards*. Philadelphia: American Society for testing and Materials, pp. 761-770.
- [7] Goto, T. and Kondo, T., 1991. Structure and molecular stacking of anthocyanins-flower color variation. *Angewandte Chemie International Edition*, 30(91), 17-33.
- [8] Asen, S., Stewart, R.N. and Norris, K.H., 1972. Co-pigmentation of anthocyanins in plant tissues and its effect on color. *Phytochemistry*, 11(3), 1139-1144.
- [9] Bakowska-Barczak, A., Kucharska, A.Z. and Oszmianski, J., 2003. The effects of heating, UV irradiation, and storage on stability of the anthocyanin-polyphenol copigment complex. *Food Chemistry*, 81(3), 349-355.
- [10] Choi, I., Lee, J.Y., Lacroix, M. and Han, J., 2017. Intelligent pH indicator film composed of agar/potato starch and anthocyanin extracts from purple sweet potato. *Food Chemistry*, 218, 122-128.
- [11] Castaneda-Ovando, A., Pacheco-Hernandez, M.D.L., Paez-Hernandez, M.E., Rodriguez, J.A. and Galan-Vidal, C.A., 2009. Chemical studies of anthocyanins: A review. *Food Chemistry*, 113(4), 859-871.
- [12] Schwarz, M. and Winterhalter, P., 2003. A novel synthetic route to substituted pyranoanthocyanins with unique colour properties. *Tetrahedron Letters*, 44(41), 7583-7587.
- [13] Halász, K. and Csóka, L., 2018. Black chokeberry (*Aronia melanocarpa*) pomace extract immobilized in chitosan for colorimetric pH indicator film application. *Food Packaging and Shelf Life*, 16, 185-193.
- [14] Yoshida, C.M.P., Maciel, V.B.V., Mendonça, M.E.D. and Franco, T.T., 2014. Chitosan biobased and intelligent films: Monitoring pH variations. *LWT - Food Science and Technology*, 55(1), 83-89.
- [15] Turhan, K.N. and Sahbaz, F., 2004. Water vapor permeability, tensile properties and solubility of methylcellulose-based edible films. *Journal of Food Engineering*, 61(3), 459-466.
- [16] Pourjavaher, S., Almasi, H., Meshkini, S., Pirsá, S. and Parandi, E., 2017. Development of a colorimetric pH indicator based on bacterial cellulose nanofibers and red cabbage (*Brassica oleraceae*) extract. *Carbohydrate Polymers*, 156, 193-201.
- [17] Wu, L.T., Tsai, I.L., Ho, Y.C., Hang, Y.H., Lin, C., Tsai, M.L. and Mi, F.L., 2021. Active and intelligent gellan gum-based packaging films for controlling anthocyanins release and monitoring food freshness. *Carbohydrate Polymers*, 254, 117410, <https://doi.org/10.1016/j.carbpol.2020.117410>

- [18] Sun, G., Chi, W., Zhang, C., Xu, S., Li, J. and Wang, L., 2019. Developing a green film with pH-sensitivity and antioxidant activity based on  $\kappa$ -carrageenan and hydroxypropyl methylcellulose incorporating *Prunus maackii* juice. *Food Hydrocolloids*, 94, 345-353.
- [19] Rawdkuen, S., Faseha, A., Benjakul, S. and Kaewprachu, P., 2020. Application of anthocyanin as a color indicator in gelatin films. *Food Bioscience*, 36, 100603, <https://doi.org/10.1016/j.fbio.2020.100603>
- [20] Acevedo-Fani, A., Salvia-Trujillo, L., Rojas-Graü, M.A. and Martín-Belloso, O., 2015. Edible films from essential-oil-loaded nanoemulsions: Physicochemical characterization and antimicrobial properties. *Food Hydrocolloids*, 47, 168-177.
- [21] Suppakul, P., Sonneveld, K., Bigger, S.W. and Miltz, J., 2011. Diffusion of linalool and methylchavicol from polyethylene-based antimicrobial packaging films. *LWT - Food Science and Technology*, 44(9), 1888-1893.
- [22] Li, M., Zhang, F., Liu, Z., Guo, X., Wu, Q. and Qiao, L., 2018. Controlled release system by active gelatin film incorporated with  $\beta$ -cyclodextrin-thymol inclusion complexes. *Food and Bioprocess Technology*, 11, 1695-1702.
- [23] Yong, H., Liu, J., Qin, Y., Bai, R., Zhang, X. and Liu, J., 2019. Antioxidant and pH-sensitive films developed by incorporating purple and black rice extracts into chitosan matrix. *International Journal of Biological Macromolecules*, 137, 307-316.

## Electrical Properties of Bistable Device Based on Graphene Oxide Compositing with Polyvinylpyrrolidone Thin Films

Thutiyaoporn Thiawong, Potiyan Songkeaw, Korakot Onlaor\* and Benchapol Tunhoo

Electronics and Control Systems for Nanodevices Research Laboratory,  
College of Nanotechnology, King Mongkut's Institute of Technology Ladkrabang,  
Bangkok, Thailand

Received: 3 November 2020, Revised: 17 February 2021, Accepted: 17 March 2021

### Abstract

This research studied the bistable properties of synthesized graphene oxide (GO) compositing with polyvinylpyrrolidone (PVP). The devices were fabricated using a spin coating process on indium tin oxide (ITO)/glass substrate, and the top electrodes were prepared by thermal evaporation with the device structure of ITO/PVP:GO/Al. The PVP:GO films were characterized by Raman spectroscopy, Fourier-transform infrared spectroscopy, X-ray photoemission spectroscopy, and scanning electron microscopy. The current-voltage (I-V) characteristics of the fabricated device exhibited a maximum ON/OFF current ratio in the order of about  $10^4$  at a GO concentration of 4 wt%. The mechanism was explained by fitting with the results of the I-V measurement. Moreover, the retention test of the device was more than  $2 \times 10^4$  s. The device showed the important characteristics of memory to be a candidate for data storage.

**Keywords:** graphene oxide; memory device; polymer; composite; nanomaterials  
DOI 10.14456/cast.2021.53

### 1. Introduction

Graphene oxide (GO) is a family group of chemically modified graphene (CMG) materials [1]. Typically, GO can be synthesized by a chemical oxidation technique that can be prepared for mass scale production [2]. The structure of GO is composed of a graphene sheet to which various functional groups, such as carbonyl, hydroxyl, carboxylic groups and so on, are attached to the plane and edges of a graphene sheet [3]. Thus, the various physical properties of GO comprising electronic, optical, mechanical properties etc. depend on the order of the oxidization of the functional groups on the graphene sheet [4]. In recent years, studies in GO material have received much interest because of the numerous advantages like the simple preparation process and low cost. Moreover, GO was studied to be applied in various fields of application including sensors, energy storage, optoelectronic devices, etc. [5-7].

---

\*Corresponding author: Tel.: (+66) 23298000 ext. 3128  
E-mail: korakot.onlaor@gmail.com

For an electronics system, the memory device plays an important part for remembering the data in the system. A resistive random access memory device is a candidate of a novel memory device due to its exhibited advantageous properties including low operating voltage, high speed, simple fabrication process, etc. [8]. Bistable memory device can be prepared from various materials like nanoparticles, polymers, ceramics, and carbon-based materials. Bistable devices with a structure of nanoparticle-polymer composite materials have been extensively studied as they offer a variety of beneficial properties; e.g., simple fabrication and flexibility [9]. In this kind of device structure, the polymer acts as the host matrix for dispersal of nanoparticles. Many kinds of polymers could be used, such as poly (9-vinylcarbazole) (PVK), poly (methyl methacrylate) (PMMA), polyvinylpyrrolidone (PVP), etc. [10]. Among these, the PVP polymer was shown to be a dielectric polymer material with a large energy band gap that had a low cost and good thermal stability [11]. However, the PVP composites with the nanoparticles as a charge trap were reported to improve the performance of the bistable device [12]. Additionally, various materials; for example, ZnO [13],  $\text{Cu}_2\text{ZnSnS}_4$  [14], multiwalled carbon nanotube [15],  $\text{MoS}_2$  [16], and  $\text{Co}_9\text{Se}_8$  quantum dots were composited with PVP to improve the performance of the device [17].

In this current study, synthesized GO particles were composited with PVP polymer to fabricate the bistable device with the structure of ITO/PVP:GO/Al. The electrical behavior and conduction mechanisms of the bistable device were studied and explained. The time retention measurement of the fabricated device was also presented.

## 2. Materials and Methods

Graphite powder (Arcos Organics, USA) was used as a precursor, and a modified Hummer's method [18] was used to synthesis the GO. The graphite powder was oxidized to produce GO that could be exfoliated into GO particles. First, the graphite powder,  $\text{H}_2\text{SO}_4$  (96%), and  $\text{NaNO}_3$  were mixed together at a ratio of 1 g: 50 ml: 1 g, respectively. The mixed solution was kept at a temperature below  $20^\circ\text{C}$ . After that, 6 g of  $\text{KMnO}_4$  was slowly added to the mixed solution. Next, 70 ml of distilled water was added to the solution at a temperature of  $90^\circ\text{C}$  for two h. Finally, distilled water and  $\text{H}_2\text{O}_2$  were added to stop the oxidized reaction. To collect the synthesized product, the GO particles were washed several times with distilled water and baked at  $100^\circ\text{C}$  until they became dry black particles.

To fabricate the bistable device, the PVP:GO solution was prepared by a fixed PVP concentration in ethanol at 70 mg/ml. The GO particles were added at 0%, 2%, 4%, and 6% by weight (wt%) of the PVP and ultrasonicated for 20 min for complete dispersion. A commercial indium tin oxide (ITO) on glass substrate was used as the bottom electrode. The ITO substrate was patterned with two parallel line masks of 3 mm in width. After etching the electrodes, the ITO substrate was cleaned with deionized water, methanol, acetone, and isopropanol in an ultrasonication bath for 15 min for each solvent. The PVP:GO active layer was fabricated by spin coating with speed conditions of 500 rpm for 3 s and 1,500 rpm for 10 s, respectively. After the spinning process, the prepared film was baked at  $50^\circ\text{C}$  for one h. The top electrodes were 100 nm thick aluminum that was prepared by thermal evaporation in a high vacuum. Figure 1 depicts the schematic structure of the device.

The thickness of the PVP:GO films was measured as cross-section images from a field emission scanning electron microscope (FESEM, JEOL JSM-7001F). The properties of the PVP:GO composite films were evaluated using a Raman spectrophotometer (DXR smart Raman, Thermo scientific) with 532 nm of an exciting light source, Fourier-transform infrared spectroscopy (FTIR) analysis in UTR mode (Thermo and Perkin Elmer), and X-ray photoelectron

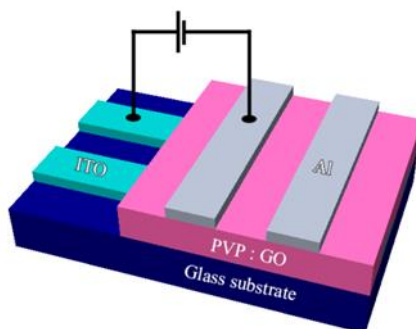


**Figure 1.** The structure of the ITO/PVP:GO/Al device

spectroscopy (XPS, AXIS Ultra DLD, Kratos), respectively. The electrical properties of the device were measured in terms of the current-voltage (I-V) characteristics and time retention test by a precision source meter (Keithley 2410).

### 3. Results and Discussion

Raman spectroscopy is a non-destructive characterization technique for carbon family materials, which can be used to confirm the structure of synthesized GO materials [19]. Figure 2a depicts the three components in the Raman spectrograph of the GO particles. The observed peak positions at 1350, 1580, and 2924  $\text{cm}^{-1}$  could be assigned to the D peak from the  $\text{sp}^3$  defect, G peak from  $\text{sp}^2$  in the carbon bonding, and 2D band of the graphene sheet [19], respectively. The intensity ratio of the D/G peaks was 0.89, which confirmed the synthesized GO in this study [20-22]. Moreover, the intensity ratio of the 2D/G peaks was 0.08, which was related to the multilayered synthesized GO sheet [20, 21].

FTIR was used to characterize the function groups of the PVP:GO layer; an example result from the PVP:GO 4 wt% is shown in Figure 2b. The absorption band at 3406  $\text{cm}^{-1}$  was assigned to the O-H stretching vibration due to the water molecule absorption of the materials [23]. The absorption band at 2940  $\text{cm}^{-1}$  was assigned to C-H and corresponds to asymmetric stretching vibration of the vinyl groups in the PVP. The absorption peak at 1279  $\text{cm}^{-1}$  and 1647  $\text{cm}^{-1}$  could be assigned to the C-N vibration and C=O stretching vibration in the pyrrolidone ring of the PVP molecule. The absorption peak at 1433  $\text{cm}^{-1}$  was assigned to the  $\text{CH}_2$  bending vibration of the PVP polymer [24, 25]. In the case of the PVP:GO layer, these peaks exhibited higher intensity, which was proportional to the concentrate of the GO. In addition, the other absorption peaks at 1080  $\text{cm}^{-1}$  and 1377  $\text{cm}^{-1}$  could be assigned to the C-O vibration of the alkoxy and epoxy function groups, respectively. The FTIR confirmed the composite materials of the PVP and GO.

XPS is a technique for determining the elements and composition of the material. A high resolution spectrograph of the C1s and O1s components from the PVP:GO 4wt% is shown in Figures 2c-2d. These peaks were fitted with Lorentz-Gaussian distribution functions. The O1s peak exhibited three components with binding energies of 530.70, 531.70, and 532.62 eV, respectively, which were identified as C=O, C-O, and O-H bonds, respectively [26, 27]. It was observed that the high intensity of the C-O and O-H peaks could confirm the composited material with the PVP and GO. Simultaneously, the C1s peak showed four components that had binding energies of 284.49, 285.44, 287.16, and 288.15 eV, respectively, which could be identified as the C-C, C-N, C-O, and C=O bonds, respectively [26-29].

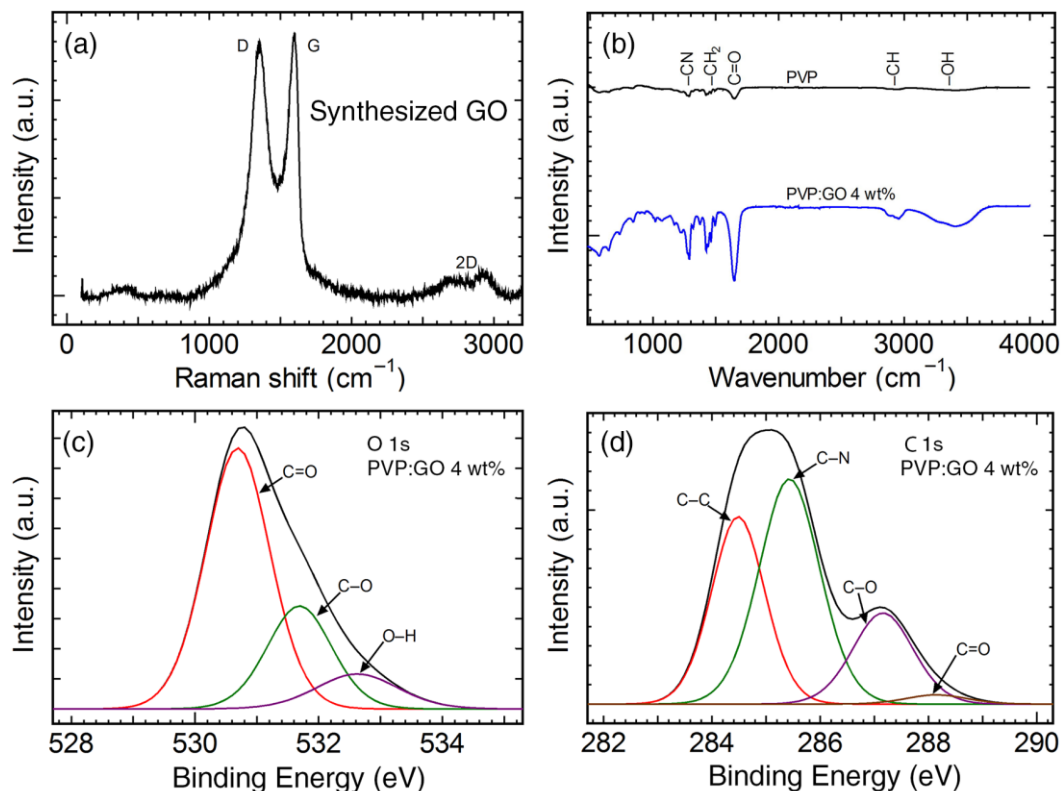


**Figure 2.** (a) Raman spectrogram of the synthesized GO particles; (b) FTIR spectrogram of the PVP:GO 4wt% layer. The high resolution XPS spectrogram of the PVP:GO 4wt% layer at (c) O 1s and (d) C 1s.

A cross-section scanning electron microscope was used to obtain the thickness of the prepared films (Figure 3). The direct estimate from the images represented the thicknesses of the PVP and PVP:GO at  $121.14 \pm 13.19$  and  $111.20 \pm 5.35$  nm, respectively (measured in 10 randomly selected cross-section points, and the thicknesses are average values with standard deviations). The thicknesses of the films were quite uniform throughout the films. In the case of the ITO electrode, the thickness was  $155 \pm 20$  nm (data from Xinyan Technology Ltd.) whereas the 100 nm-thick Al electrodes of all devices were prepared under the same conditions and monitored by a high-resolution thickness monitor (XTC/2, INFICON).

The electrical properties of the device were assessed with I-V measurement. Applied voltage was swept from 0 V to +5 V for Step 1, +5 V to -5 V for Step 2, and -5 V to 0 V for Step 3. Figure 4 depicts the relationship between the current and voltage. For the 2 wt% and 4 wt% of the GO concentrations, the results exhibited two states of current that were defined as low current (OFF state) and high current (ON state). In the case of only the PVP layer, the ratio of the current of the ON state and OFF state (ON/OFF ratio) was small, as the applied voltage into the device was not sufficient to change the electrical conduction of the PVP polymer. Furthermore, at 2 wt% of GO concentration in the film, the hysteresis loops of the device still showed a small hysteresis, as shown in the inset of Figure 4. The highest ON/OFF ratio was observed at the GO concentration of 4 wt% with a writing voltage of +5 V, a reading voltage of +1 V and the ON/OFF current ratio

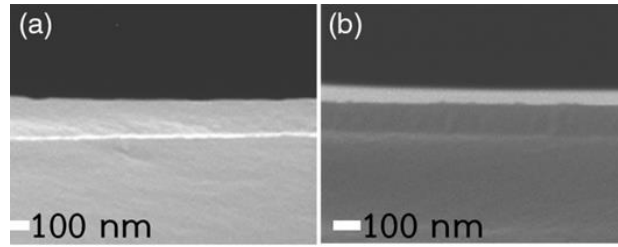


**Figure 3.** Cross-section SEM images of (a) PVP on the glass substrate, and (b) PVP:GO 4 wt% on the glass substrate

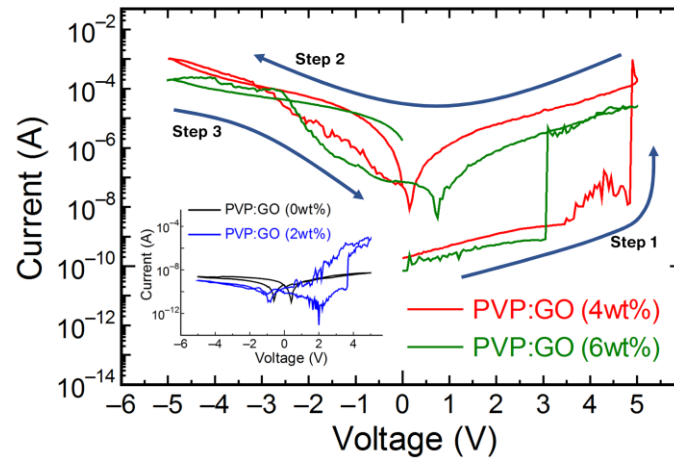


**Figure 4.** I-V characteristics of the memory device with different GO concentrations

of approximately  $10^4$ . Moreover, the I-V curve characteristics remained in the ON state although a negative bias voltage was applied. The behavior of the device indicated the characteristic of a write-once-read-many (WORM) memory device. However, when the concentration of the GO is increased to 6 wt%, the switching voltage and ON/OFF current ratio went down, and the effect of GO concentration is discussed in the next section.

The ITO/PVP:GO (4 wt%)/Al device showed optimal memory properties with the highest ON/OFF current ratio of memory device. Therefore, to explain the conduction mechanisms of the device, the I-V curves of the GO 4wt% were fitted with an electrical conduction model. The fitted curve was optimized with the models of thermionic emission (TE) and space charge limited current (SCLC).

First, TE had the expression as [30]:

$$I \propto T^2 \exp \left[ \frac{-(\phi_b - q\sqrt{qV/4\pi d\epsilon_i})}{k_b T} \right] \quad (1)$$

where T is the absolute temperature, q is the charge constant,  $\phi_b$  is the barrier height,  $\epsilon_i$  is the insulator permittivity, and  $k_b$  is the Boltzmann's constant. The equation could be rearranged with a linear equation between  $\ln(I) \propto V^{1/2}$ . The SCLC had the expression as follows:

$$I \propto V^\alpha \quad (2)$$

Where  $\alpha$  is constant with  $\alpha = 1$  is Ohmic conduction  
 $\alpha = 2$  is SCLC  
 $\alpha \gg 2$  is the trap filled limit of SCLC.

In the OFF state, the dominating conduction was the thermal injection over the barrier that corresponded to the TE model (Figure 5a). In the ON state, the electrical models changed to SCLC with the slope of the curve corresponding to  $\alpha = 2.35$  (Figure 5b). The theoretical trap free SCLC showed  $\alpha = 2$ , so,  $\alpha$  more than 2 should affect the trap fill SCLC [31]. This could imply that the GO acts like a carrier trap [31] in the PVP.

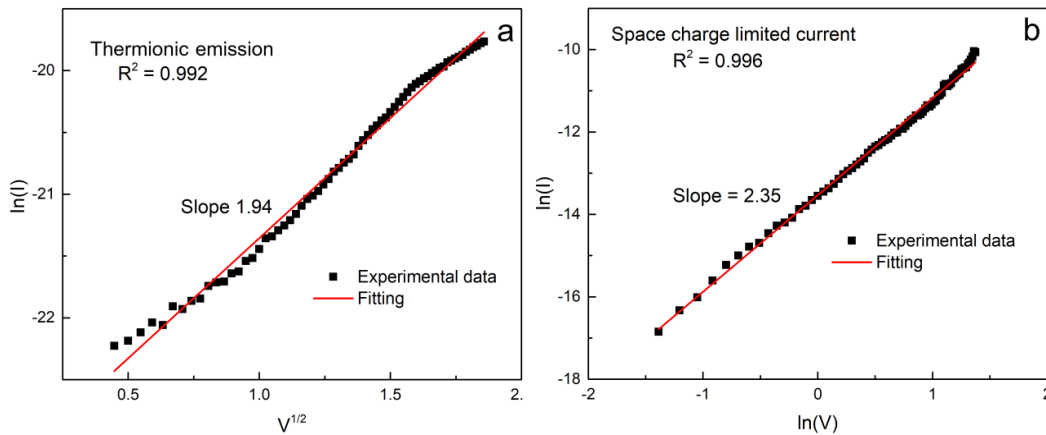


**Figure 5.** I-V curves fitting of the ITO/PVP:GO (4 wt%)/Al device  
 (a) TE mechanism at the OFF state and (b) SCLC mechanism at the ON state

To explain more about the behavior of the device, the mechanism models of ITO/PVP:GO/Al were proposed in terms of the energy band diagram. In other studies [32], the LUMO and HOMO energy levels of the PVP material were located at -2.01 and -5.93 eV, respectively. For the GO material, the energy levels also depended on the structure of the GO. Kim *et al.* [33] reported on the estimated conduction and valence energy levels of the GO and rGO in ranges of -2.245 to -2.525 eV and -5.445 to -5.115 eV. Those values were closer when the GO was reduced to become the rGO. Liu *et al.* [34] reported on the value of the GO ribbon with the LUMO and HOMO levels that were located at -3.5 and -5.3 eV, respectively. It could be seen that the conduction level of the GO and rGO was also lower than the LUMO level of the PVP. On the other hand, the valence levels of the GO and rGO were also higher than the HOMO level of the PVP. Therefore, Figure 6a depicts the proposed models of the device. First, the electrons were injected through the barrier from the Al electrode into the PVP:GO layer due to thermal injection that resulted from the TE model in the OFF state (Figure 6b). After that, when the GO trapping states were filled by the electrons, the device changed to the ON state, which corresponded to the trap filled limit SCLC (Figure 6c). The electrons could be released from the PVP:GO layer although a negative voltage was applied because of the trapped electrons in the layer and the injected electrons from the electrode (Figure 6d). Therefore, the devices maintained the ON state with a small drop of current due to the effect of the barrier height between the positive and negative voltages.

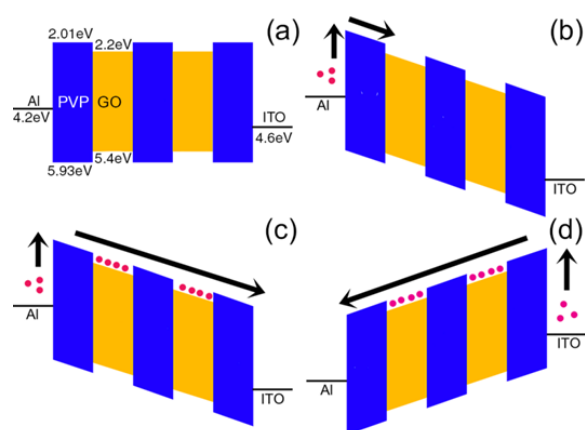


**Figure 6.** Schematic energy band diagram of the GO blend in PVP at 4 wt% corresponding to the carrier trap mechanism of (a) 0 V, (b) OFF state, (c) ON state, and (d) negative voltage

Moreover, the GO concentration had an effect on the conduction of the device. For the condition of the mechanism of the GO 4-6 wt%, the devices might have a shorter width barrier of PVP due to the PVP being separated by the GO resulting in the electrons being easier to be injected by thermal energy across the interface barrier between the ITO and PVP. However, the higher barrier height at the interface led to the low conduction of the device; the hypothesis could be supported by the negative voltage when the electrons were injected from the ITO electrode.

In addition, the time retention characteristic was shown to be an important parameter of the bistable device [35, 36]. This characteristic could be demonstrated in the retention of the GO 4wt% composites PVP device in both the ON and OFF states for various long periods of time measurement. The test was performed with a continuous reading at +1 V every 300 ms to acquire the retention of the OFF state. After that, a voltage pulse of +5 V was applied to the device as a writing process. Then, the device was continuously read at +1 V every 300 ms to acquire the retention of the ON state. Figure 7 depicts the retention characteristic of the GO composite PVP device. It could be seen that the device exhibited more retention time at  $2 \times 10^7$  seconds with the ON/OFF ratio still remaining about  $10^4$ . The fluctuation of the current states might have been due to the effect of the charge disturbance of the low current. However, the ON/OFF current ratio was still higher than  $10^4$ , which ensured protecting against the misreading process [37].

In comparison with previous studies, the summary of the GO composite bistable device is shown in Table 1. Liu *et al.* [38] reported on the resistive switching characteristics of the graphene oxide-polypyrrole-polyvinylferrocene ternary nanocomposite for which the device exhibited an ON/OFF current ratio of  $10^3$  and time retention stability over a period of 5,000 s. Khuran *et al.* [39] demonstrated the flexibility of the resistive random access memory of zinc oxide nanorods incorporating GO sheets. That device had an ON/OFF ratio of about 100 with an endurance cycle of over 200 cycles. Kim *et al.* [40] reported the resistive switching behavior of the PVA/GO+PVA composite/PVA. That device demonstrated an ON/OFF ratio of about  $10^4$  with a retention time of  $2 \times 10^3$  s. It could be seen that the bistable device based on the structure of the GO and PVP composites exhibited appropriate performances of bistable behavior for a resistive random access memory device.

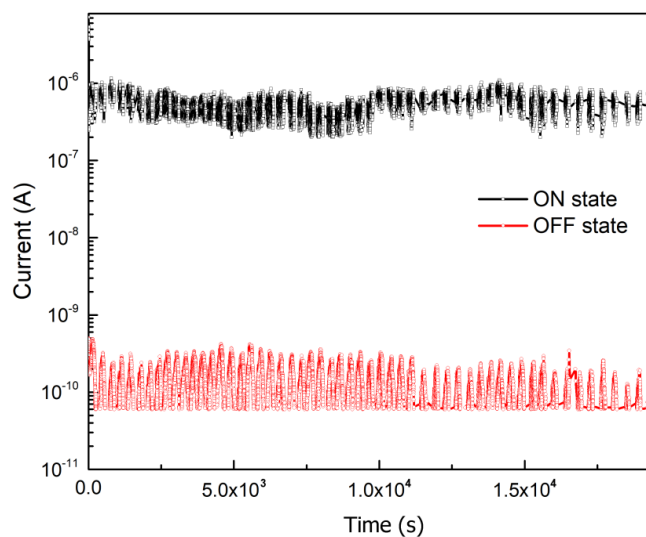


**Figure 7.** The retention time of the reading data at 1 V of the PVP:GO 4 wt% condition.

**Table 1.** Summary of the bistable device based on the polymer-GO thin films

Structure	ON/OFF ratio	Retention time (s)	Reading voltage (V)	Mechanism	Ref.
ITO/GO-PyVf/Al	$10^3$	$>5 \times 10^3$	+0.1	trapping	[38]
Al/GOZNS/ITO	$10^2$	$>10^4$	+0.1	filamentary	[39]
PVA/GO+PVA/PVA	$10^4$	$>2 \times 10^3$	+1	filamentary	[40]
Al/PTPEB-g-RGO/ITO	$10^4$	$>10^4$	+0.1	trapping	[41]
Al/PAE-g-RGO/ITO	$10^3$	$>10^4$	-1	trapping	[42]
ITO/PMMA-GOs/Al	$10^4$	$>10^4$	N/A	trapping	[43]
Al/PVP-GO/ITO	$10^4$	$>10^4$	+1	trapping	This work

#### 4. Conclusions

A bistable device based on composite films of GO and PVP was fabricated with a device structure of ITO/PVP:GO/Al. The current-voltage characteristics of the device demonstrated non-volatile WORM memory behavior. The conduction mechanisms based-on TE and SCLC in the OFF and ON states were observed from the I-V fitting model, respectively, with the GO acting to create trapping states in the composites film. The optimized current ON/OFF ratio was observed to be in the order of about  $10^4$  from the GO concentration of 4 wt% with +1 V reading voltage. Moreover, the retention time of device was more than  $2 \times 10^4$  s for each state.

## 5. Acknowledgements

This work was supported by King Mongkut's Institute of Technology Ladkrabang (grant number: KREF146203). The authors acknowledge the facilities, and technical assistance from Nanotechnology and Materials Analytical Instrument Service Unit (NMIS) of College of Nanotechnology, King Mongkut's Institute of Technology Ladkrabang.

## References

- [1] Zhu, Y., Murali, S., Cai, W., Li, X., Suk, J.W., Potts, J.R. and Ruoff, R.S., 2011. Graphene and graphene oxide: Synthesis, properties, and applications. *Advanced Materials*, 22, 3906-3924.
- [2] Gómez-Navarro, C., Meyer, J.C., Sundaram, R.S., Chuvilin, A., Kurasch, S., Burghard, M., Kern, K. and Kaiser, U., 2010. Atomic structure of reduced graphene oxide. *Nano Letters*, 10, 1144-1148.
- [3] Ban, F.Y., Majid, S.R., Huang, N.M. and Lim, H.N., 2012. Graphene oxide and its electrochemical performance. *International Journal of Electrochemical Science*, 7, 4345-4351.
- [4] Panin, G.N., Kapitanova, O.O., Lee, S.W., Baranov, A.N. and Kang, T.W., 2011. Resistive switching in Al/graphene oxide/Al structure. *Japanese Journal of Applied Physics*, 50, 070110, <https://doi.org/10.1143/JJAP.50.070110>
- [5] Maccaferri, G., Terzi, F., Xia, Z., Vulcano, F., Liscio, A., Palermo, V. and Zanardi, C., 2019. Highly sensitive amperometric sensor for morphine detection based on electrochemically exfoliated graphene oxide. Application in screening tests of urine samples. *Sensors and Actuators B: Chemical*, 281, 739-745.
- [6] Ye, M., Gao, J., Xiao, Y., Xu, T., Zhao, Y. and Qu, L., 2017. Metal/graphene oxide batteries. *Carbon*, 125, 299-307.
- [7] Santiago, S.R.M.S., Chang, C.-H., Lin, T.-N., Yuan, C.-T. and Shen, J.-L., 2019. Diethylenetriamine-doped graphene oxide quantum dots with tunable photoluminescence for optoelectronic applications. *ACS Applied Nano Materials*, 2, 3925-3933.
- [8] Hong, S.K., Kim, J.E., Kim, S.O., Choi, S. and Cho, B.J., 2010. Flexible resistive switching memory device based on graphene oxide. *IEEE Electron Device Letters*, 31, 1005-1007.
- [9] Son, D.-I., Park, D.-H., Choi, W.K., Cho, S.-H., Kim, W.-T. and Kim, T.W., 2009. Carrier transport in flexible organic bistable devices of ZnO nanoparticles embedded in an insulating poly(methyl methacrylate) polymer layer. *Nanotechnology*, 20, 195203.
- [10] Marsden, A.J., Papageorgiou, D.G., Vallés, C., Liscio, A., Palermo, V., Bissett, M.A., Young, R.J. and Kinloch, I.A., 2018. Electrical percolation in graphene-polymer composites. *2D Materials*, 5(3), 032003, <https://doi.org/10.1088/2053-1583/aac055>
- [11] Huang, S., Zhou, L., Li, M.-C., Wu, Q., Kojima, Y. and Zhou, D., 2016. Preparation and properties of electrospun poly(vinyl pyrrolidone)/cellulose nanocrystal/silver nanoparticle composite fibers. *Materials*, 9(7), 523, <https://doi.org/10.3390/ma9070523>
- [12] Gu, C., Mao, H.-W., Tao, W.-Q., Zhou, Z., Wang, X.-J., Tan, P., Cheng, S., Huang, W., Sun, L.-B., Liu, X.-Q., Liu, X.-Q. and Liu, J.-Q., 2019. Facile synthesis of Ti<sub>3</sub>C<sub>2</sub>T<sub>x</sub>-Poly(vinylpyrrolidone) nanocomposites for nonvolatile memory devices with low switching voltage. *ACS Applied Materials & Interfaces*, 11, 38061-38067.
- [13] Onlaor, K., Thiwawong, T. and Tunhoo, B., 2014. Electrical switching and conduction mechanisms of nonvolatile write-once-read-many-times memory devices with ZnO nanoparticles embedded in polyvinylpyrrolidone. *Organic Electronics*, 15, 1254-1262.

- [14] Kim, Y.N., Yun, D.Y., Arul, N.S. and Kim, T.W., 2015. Carrier transport mechanisms of multilevel nonvolatile memory devices with a floating gate consisting of hybrid organic/inorganic nanocomposites. *Organic Electronics*, 17, 270-274.
- [15] Kim, W.T., Jung, J. H. and Kim, T.W., 2009. Carrier transport mechanisms in nonvolatile memory devices fabricated utilizing multiwalled carbon nanotubes embedded in a poly-4-vinyl-phenol layer. *Applied Physics Letters*, 95(2), 022104, <https://doi.org/10.1063/1.3174913>
- [16] Wu, Z., Wang, T., Sun, C., Liu, P., Xia, B., Zhang, J., Liu, Y. and Gao, D., 2017. Resistive switching effect of N-doped MoS<sub>2</sub>-PVP nanocomposites films for nonvolatile memory devices. *AIP Advances*, 7(12), 125213, <https://doi.org/10.1063/1.4994227>
- [17] Zhang, P., Xu, B., Gao, C., Chen, G. and Gao, M., 2016. Facile synthesis of Co<sub>9</sub>Se<sub>8</sub> quantum dots as charge traps for flexible organic resistive switching memory device. *ACS Applied Materials & Interfaces*, 8, 30336-30343.
- [18] Yu, H., Zhang, B., Bulin, C., Li, R. and Xing, R., 2016. High-efficient Synthesis of Graphene Oxide Based on Improved Hummers Method. *Scientific Reports*, 6, 36143, <https://doi.org/10.1038/srep36143>
- [19] Wu, J.-B., Lin, M.-L., Cong, X., Liu, H.-N. and Tan, P.-H., 2018. Raman spectroscopy of graphene-based materials and its applications in related devices. *Chemical Society Reviews*, 47, 1822-1873.
- [20] Khan, Q.A., Shaur, A., Khan, T.A., Joya, Y.F. and Awan, M.S., 2017. Characterization of reduced graphene oxide produced through a modified Hoffman method. *Cogent Chemistry*, 3, 1298980, <https://doi.org/10.1080/23312009.2017.1298980>
- [21] Kim, H.J., Lee, S.-M., Oh, Y.-S., Yang, Y.-H., Lim, Y.S., Yoon, D.H., Lee, C., Kim, J.-Y. and Ruoff, R.S., 2014. Unoxidized graphene/alumina nanocomposite: Fracture- and wear-resistance effects of graphene on alumina matrix. *Scientific Reports*, 4, 5176, <https://doi.org/10.1038/srep05176>
- [22] Ray, S.C., Bhunia, S.K., Saha, A. and Jana, N.R., 2015. Graphene oxide (GO)/reduced-GO and their composite with conducting polymer nanostructure thin films for non-volatile memory device. *Microelectronic Engineering*, 146, 48-52.
- [23] Abdelghany, A.M., Mekhail, M.S., Abdelrazek, E.M. and Aboud, M.M., 2015. Combined DFT/FTIR structural studies of monodispersed PVP/gold and silver nanoparticles. *Journal of Alloys and Compounds*, 646, 326-332.
- [24] Koczur, K.M., Mourdikoudis, S., Polavarapu, L. and Skrabalak, S.E., 2015. Polyvinylpyrrolidone (PVP) in nanoparticle synthesis. *Dalton Transaction*, 44, 17883-17905.
- [25] Song, Y.J., Wang, M., Zhang, X.Y., Wu, J.Y. and Zhang, T., 2014. Investigation on the role of the molecular weight of polyvinyl pyrrolidone in the shape control of high-yield silver nanospheres and nanowires. *Nanoscale Research Letters*, 9, 17, <https://doi.org/10.1186/1556-276X-9-17>
- [26] Zang, L., Cao, X., Zhang, Y., Sun, L., Qin, C. and Wang, C., 2015. Microfluidic generation of graphene beads for supercapacitor electrode materials. *Journal of Materials Chemistry A*, 3, 22088-22093.
- [27] Cheng, D., Xie, R., Tang, T., Jia, X., Cai, Q. and Yang, X., 2016. Regulating micro-structure and biomineralization of electrospun PVP-based hybridized carbon nanofibers containing bioglass nanoparticles via aging time. *RSC Advances*, 6, 3870-3881.
- [28] Li, S.K., Yan, Y.X., Wang, J.L. and Yu, S.H., 2013. Bio-inspired in situ growth of monolayer silver nanoparticles on graphene oxide paper as multifunctional substrate. *Nanoscale*, 5, 12616-12623.

- [29] Wang, Z.-L., Yan, J.-M., Zhang, Y.-F., Ping, Y., Wang, H.-L. and Jianga, Q., 2014. Facile synthesis of nitrogen-doped graphene supported AuPd-CeO<sub>2</sub> nanocomposites with high-performance for hydrogen generation from formic acid at room temperature. *Nanoscale*, 6(6), 3073-3077.
- [30] Chen, K.H., Tsai, T.M., Cheng, C.M., Huang, S.J., Chang, K.C., Liang, S.P. and Young, T.F., 2018. Schottky emission distance and barrier height properties of bipolar switching Gd:SiO<sub>x</sub> RRAM devices under different oxygen concentration environments. *Materials*, 11, 43, <https://doi.org/10.3390/ma11010043>
- [31] Ikuno, T., Okamoto, H., Sugiyama, Y., Nakano, H., Yamada, F. and Kamiya, I., 2011. Electron transport properties of Si nanosheets: Transition from direct tunneling to Fowler-Nordheim tunneling. *Applied Physics Letters*, 99, 023107, <https://doi.org/10.1063/1.3610486>
- [32] Yu, X., Yu, X., Zhang, J., Zhang, D., Caib, H. and Zhao, Y., 2015. Interfacial modification for improving inverted organic solar cells by poly(N-vinylpyrrolidone). *RSC Advances*, 5, 58966-58972.
- [33] Kim, J., Ganorkar, S., Kim, Y.H. and Kim, S.I., 2015. Graphene oxide hole injection layer for high-efficiency polymer light-emitting diodes by using electrophoretic deposition and electrical reduction. *Carbon*, 94, 633-640.
- [34] Liu, J., Xue, Y., Gao, Y., Yu, D., Durstock, M. and Dai, L., 2012. Hole and electron extraction layers based on graphene oxide derivatives for high-performance bulk heterojunction solar cells. *Advanced Materials*, 24, 2228-2233.
- [35] Zhang, X., Xu, J., Zhang, X., Shi, S., Zhao, X. and Li, L., 2017. Electrical bistable properties of nonvolatile memory device based on hybrid ZCIS NCs: PMMA film. *Materials Science in Semiconductor Processing*, 57, 105-109.
- [36] Huang, J., Zhao, X., Zhang, H., Bai, J., Wang, S., Wang, C., Mad D. and Hou, Y., 2019. Flash memory devices and bistable nonvolatile resistance switching properties based on PFO doping with ZnO. *RSC Advances*, 9, 9392-9400.
- [37] Ling, Q.D., Liaw, D.J., Teo, E.Y.H., Zhu, C., Chan, D.S.H., Kang, E.T. and Neoh, K.G., 2007. Polymer memories: Bistable electrical switching and device performance. *Polymer*, 48, 5182-5201.
- [38] Liu, R., Ni, X. and Lin, J., 2019. Preparation of graphene oxide-polypyrrole-polyvinylferrocene ternary nanocomposite and its resistive-switching characteristic. *Journal of Materials Science: Materials in Electronics*, 30, 1001-1008.
- [39] Khurana, G., Misra, P., Kumar, N. and Katiyar, R.S., 2014. Tunable power switching in nonvolatile flexible memory devices based on graphene oxide embedded with ZnO nanorods. *Journal of Physical Chemistry C*, 118, 21357-21364.
- [40] Kim, T., Kim, D.K., Kim, J. and Pak, J.J., 2019. Resistive switching behaviour of multi-stacked PVA/graphene oxide + PVA composite/PVA insulating layer-based RRAM devices. *Semiconductor Science and Technology*, 34, 065006, <https://doi.org/10.1088/1361-6641/ab1403>
- [41] Cao, Y., Fu, Y., Li, D., Zhu, C., Zhang, B. and Chen, Y., 2019. Organophosphorus-based polymer covalently functionalized reduced graphene oxide: In-situ synthesis and nonvolatile memory effect. *Carbon*, 141, 758-767.
- [42] Sun, S., Zhuang, X., Liu, B., Wang, L., Gu, L., Song, S., Zhang, B. and Chen, Y., 2016. In situ synthesis and characterization of poly(aryleneethynylene)-grafted reduced graphene oxide. *Chemistry-A European Journal*, 22, 2247-2252.
- [43] Gogoi, K.K. and Chowdhury, A., 2019. Electric field induced tunable memristive characteristics of exfoliated graphene oxide embedded polymer nanocomposites, *Journal of Applied Physics*, 126, 025501, <https://doi.org/10.1063/1.5102145>

## **Allelopathic Effect of West Java Local Black Rice Varieties on Barnyard Grass (*Echinochloa crus-galli* (L.) Beauv.) at Germination Stage**

Muhamad Kadapi\*, Denny Sobardini, Elissa Helena, Haritsa Hanindianingrum, Fachryansah Noor, Noladhi Wicaksana and Sumadi

Faculty of Agriculture Universitas Padjadjaran, Jatinangor, Indonesia

Received: 20 July 2020, Revised: 4 March 2021, Accepted: 23 March 2021

### **Abstract**

Some colored rice varieties are able to release root exudates that contained allelochemicals which can inhibit the growth of other plant species including weeds. This capability is required if rice is to compete with weeds from the germination stage onwards. One of the dominant weeds in rice fields is barnyard grass, which can have negative effects on rice growth at every stage, particularly at the germination stage. Therefore, the objective of this study was to evaluate the response of local black rice varieties originated from West Java, Indonesia against barnyard grass at the germination stage. In this study, four local black rice varieties that originated in three West Java districts, two from Subang (SB and SB II), one from Sukabumi (SMI) and one from Tasikmalaya (TSK), were sowed together with *Echinochloa crus-galli* in petri dishes with six replications. The experiment was conducted in a plant breeding and seed technology laboratory in order to observe  $T_{50}$ , germination percentage, vigour index, shoot and root length at 7 and 14 days after sowing (DAS). The results showed that the four local black rice cultivars had allelopathic potential, as indicated by vigour traits at germination stages of barnyard grass. Besides, the presence of barnyard grass showed an inhibitory or stimulatory effect on black rice growth in its early germination stage (7 DAS). However, the local black rice that originated from Subang (SB II) showed growth recovery and inhibitory effect towards barnyard grass at the second germination stage (14 DAS), as measured by vigour index, shoot length and inhibitory percentage. This study suggested that the ability to recover at the second stages of germination is a useful trait to be considered when conducting breeding program for the efficiency of weed management.

**Keywords:** allelochemical; tolerance; variation; black rice; weed  
DOI 10.14456/cast.2021.54

### **1. Introduction**

Rice is one of the important crops for more than half of human consumption in the world. The average of world rice consumption has been increasing every year [1]. Among the countries of Asia, Indonesia is the third country in rice consumption after India and China [2]. More than 40,000

---

\*Corresponding author: Tel.: (+62) 8812279027  
E-mail: kadapi@unpad.ac.id

varieties of rice have been registered around the world which can be differentiated according to shape and color [3]. Colored rice, such as black rice is mainly cultivated in Asia and the biggest country that produces this kind of rice is China, followed by Sri Lanka, Indonesia, India and Philippines [3]. The color of black rice is commonly found in the aleurone coat that contains anthocyanin [4].

Breeding program for black rice has been paid much attention on anthocyanin content due to its benefits to human health [5]. However, another potential of black rice has been reported by Kato-Noguchi *et al.* [6] that Japanese black rice has allelopathic potential that can inhibit hypocotyls and root growth of lettuce and white clover. This potential is important for rice during the growth and developmental stage to compete with weeds [7]. The control of weeds in rice fields over several periods involved the use of synthetic chemicals as herbicides that caused the ecological problems and finally led to the emergence of rice weeds resistant to herbicides [8-10]. Allelopathy is well known as a phenomenon that occurs due to interactions among plants and causes allelochemicals release into the plant rhizosphere. Allelochemicals can be released by several mechanisms such as root exudation, degradation of plant residues, volatilization and leaching from leaves. Allelochemicals can influence the neighboring plants causing inhibitory and stimulatory effects on plant growth [11]. Therefore, the development and cultivation of allelopathic rice that can release allelochemicals causing damage to weeds or having inhibitory effect on weeds, has become an important step in the reduction of the negative impact of herbicides [12, 13]. At the preliminary stage, the revealing of the allelopathic potential of various rice strains can provide important information needed to improve the new rice varieties in breeding program [14, 15]. It has been reported that the allelopathic rice varieties depend on genetic factors [16-18].

Variations of allelopathic rice potential have been reported to inhibit the growth of several weed species when planted together in field conditions or in the laboratory [19, 20]. One of the dominant and most harmful weeds in rice cultivation field is barnyard grass (*Echinochloa crus-galli* (L.) Beauv.). This weed can reduce the yield from 35% to 95% [21-23]. Therefore, the current study of allelopathic rice on the barnyard grass growth has become more intensive [7, 24]. In the quest to evaluate and discover the allelopathic potential of rice varieties, several screening approaches have been established [19, 25, 26]. One of the useful methods is laboratory screening and the results showed a significant correlation between laboratory and field performance of rice seed vigour traits [25]. However, environmental conditions affect the correlation between field and laboratory investigations [27]. In addition, Berendji *et al.* [28] reported that barnyard grass seedling growth traits were inhibited by Iranian rice cultivars. The inhibition caused by rice was due to allelochemicals released by rice root exudates [20]. Furthermore, seed vigour is a physiological trait that is required to ensure the uniform emergence of plants in the field under sub-optimal conditions [29]. This trait is useful for the breeding program, even though this trait is often absent from breeding programs, which are frequently directed toward yield traits [30, 31]. Therefore, the aims of this study were to evaluate the allelopathic potential of local black rice against barnyard grass and to reveal the particular vigour traits that might be useful for the breeding program in order to develop new allelopathic rice as one of practices in environmentally friendly of weed management by farmers.

## 2. Materials and Methods

Four out of seven West Java local rice (*Oryza sativa* L.) seeds from a plant breeding and seed technology laboratory were selected according to their allelopathic potential against lettuce, color and viability of seed [32]. The screening method used was in accordance with the following method with brief modification [33] in which 20 seeds of rice and 50 seeds of check plant were planted

together. The local black varieties were collected from local farmers in three districts of West Java, Indonesia (Subang, Sukabumi, and Tasikmalaya) (Figure 1) while barnyard grass (*Echinochola crus-galli* (L.) Beauv.) seeds were purchased from (Prairie Moon Nursery) Minnesota, USA.

The experiment was conducted in a plant breeding and seed technology laboratory at the Universitas Padjadjaran under room conditions, with 26/24°C day/night temperature, 60-70% relative humidity (RH), and 12 h daily light. The germination test used was the top of paper method [7]. In this study, we put 20 rice seeds of each variety into 90 mm petri dishes containing a filter paper (Whatman™ no. 42) and 10 ml distilled water. The first day count (FDC) of germination percentage (%) was calculated at 7 days after sowing (DAS) and 14 DAS as last day count (LDC) using ISTA formula [34]:

$$GP (\%) = \frac{\text{Total seeds germinated}}{\text{Number of initial seed used}} \times 100\% \quad (1)$$

The germination test for barnyard grass seed used 100 seeds with the same method. The potential allelopathy of rice was tested using the method that was adapted [18, 19, 35] with a slight modification. Fifteen seeds of each variety of rice and 30 seeds of barnyard grass were planted together in 90 mm petri dishes that contains filter paper (Whatman No. 42) and 10 ml distilled water. All of the petri dishes were placed at room condition. The germination rate (%) of weeds and black rice was recorded every day until 14 days after sowing as LDC of rice seed using the same formula as mentioned above and vigour parameter such as  $T_{50}$  using the methods described by Coolbear *et al.* [36] and Farooq *et al.* [37], vigour index, and inhibition percentage were calculated by the following equation [38].

$$\text{Vigour Index} = \frac{N}{\text{Total number of seeds}} \times \text{Total length of seedling} \quad (2)$$

N: total of normal seeds germinated at 14 days after sowing

$$T_{50} = t_i + [(N / 2 - n_i) (t_i - t_j)] / n_i - n_j \quad (3)$$

N: the final number of germination and  $n_i$ ,  $n_j$  cumulative and number of seeds germinated by adjacent counts at times  $t_i$  and  $t_j$

$$\text{Inhibition Percentage} = \frac{\text{control} - \text{treatments}}{\text{control}} \times 100\% \quad (4)$$

In this study, we also measured the shoot length (cm) and root length (cm) of weeds at 7 and 14 days after sowing of both species. The inhibition percentages of the treatments were to identify the interaction between two species, and the negative values of this trait indicated a stimulatory effect whereas positive values indicated inhibitory effect [12]. The treatments were conducted with six replications, and in order to reveal the differences between treatments and control, t-test at  $\alpha$  0.05 levels was performed. A statistical analysis was calculated using software SPSS v. 2

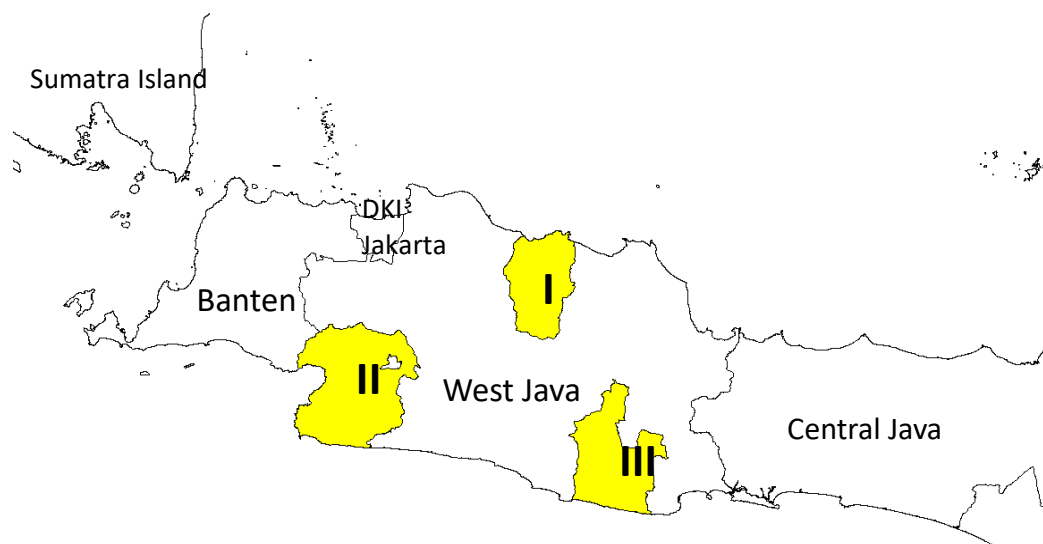


**Figure 1.** The location of local black rice varieties in West Java Province, Indonesia, I is Subang District, II is Sukabumi District, and III is Tasikmalaya District. The map was created with DIVA-GIS at scale 1: 2000000.

### 3. Results and Discussion

This study observed the allelopathic potential of local black rice root exudates that originated from West Java, Indonesia. The selected local black rice varieties that originated from different districts of West Java were used against barnyard grass, which was the dominant weed in rice fields. Two local varieties were derived from Subang (SB and SB II), one variety from Sukabumi (SMI), and one variety from Tasikmalaya (TSK). Various tests at germination stage to examine the potential of local black rice against barnyard grass were used in this study including time of 50% germination ( $T_{50}$ ), germination percentage (GP), vigour index (VI), shoot and root length (SL and RL), and inhibitory percentage (IP), and the results are presented in Table 1 and Figure 2.

The results showed that the various different responses of local black rice against barnyard grass were revealed using these assessments. However, the GP at 7 and 14 days showed no significant difference to control. The speed of germination was revealed by the time of 50% germination (days), and the results showed that three out of four varieties (SB, SB II, and TSK) were significantly different when compared to control. The SB and TSK varieties germinated at 3.37 and 2.38 days, which were faster than the controls at 4.2 and 3.4 days, respectively. However, the SB II variety germinated at 3.65 days, which was slower than the control at 2.53 days, as displayed in Table 1. Interestingly, the germination percentage at 7 and 14 days after sowing showed that there were no significant different compared to control, where the range of GP was 87.78% to 95.56% at 7 days after sowing and 91.11% to 97.78% at 14 days after sowing. However, the SB II local black rice varieties showed negative inhibitory percentage (IP) at 7 and 14 days after sowing, while the other varieties were positive (-0.58% and -1.15%) as presented in Figure 2A. The vigour index of SB (7.83) and SMI (8.91) varieties were higher than the controls, which

**Table 1.** The response of West Java local black rice against barnyard grass at germination stages

Traits	Treatments	Rice Varieties (Mean ± Std Err)			
		SB	SB II	SMI	TSK
T <sub>50</sub> (days)	Control	4.16±0.10	2.53±0.26	3.40±0.25	3.44±0.30
	+BG	3.37±0.22	3.65±0.06	3.29±0.26	2.38±0.38
	t test	*	*	ns	*
GP Rice 7 (%)	Control	91.75%±0.02	95.00%±0.02	91.67%±0.03	93.33%±0.03
	+BG	90.00%±0.04	95.56%±0.01	87.78%±0.05	90.00%±0.02
	t test	ns	ns	ns	ns
VI Rice 7	Control	4.37±0.28	8.29±0.37	5.21±0.20	9.31±0.77
	+BG	7.83±0.57	7.38±0.26	8.91±0.51	7.80±0.40
	t test	*	ns	*	ns
GP Rice 14 (%)	Control	92.96%±0.02	96.67%±0.02	96.67%±0.02	93.15%±0.03
	+BG	91.11%±0.04	97.78%±0.01	93.33%±0.05	94.44%±0.01
	t test	ns	ns	ns	ns
VI Rice 14	Control	11.14±0.47	14.70±1.02	20.19±0.66	20.20±0.95
	+BG	14.76±1.01	17.38±0.63	18.44±1.05	18.78±0.73
	t test	*	*	ns	ns
SL 7 (cm)	Control	2.87±0.13	4.10±0.10	2.76±0.14	4.87±0.48
	+BG	4.71±0.18	3.81±0.10	6.21±0.15	4.71±0.17
	t test	*	ns	*	ns
SL 14 (cm)	Control	8.49±0.24	7.30±0.98	11.13±0.50	10.76±0.90
	+BG	11.72±0.66	12.34±0.53	14.53±0.43	15.20±0.53
	t test	*	*	*	*
SL Δ714 (cm)	Control	5.62±0.11	4.75±1.03	8.37±0.63	5.88±0.69
	+BG	7.00±0.61	8.53±0.47	8.32±0.36	10.90±0.41
	t test	ns	*	ns	*
RL 7 (cm)	Control	1.87±0.09	4.61±0.13	2.92±0.08	5.12±0.45
	+BG	3.95±0.26	3.91±0.19	3.95±0.20	3.95±0.26
	t test	*	*	*	*
RL 14 (cm)	Control	3.47±0.06	8.00±0.38	9.82±0.46	10.93±0.55
	+BG	4.47±0.24	5.42±0.33	5.27±0.23	4.67±0.34
	t test	*	*	*	*
RL Δ714 (cm)	Control	1.60±0.04	3.98±0.77	6.90±0.40	5.81±0.87
	+BG	0.52±0.24	1.51±0.35	1.32±0.36	0.87±0.40
	t test	*	*	*	*

Note: \* indicates significance at 0.05 by t test. SB is Subang, SB II is Subang II, SMI is Sukabumi, and TSK is Tasikmalaya, +BG is the rice placed together with barnyard grass, T<sub>50</sub> is time to reach 50% germination, GP is germination of percentage, VI is vigour index, SL is shoot length, RL is root length, and Δ714 is the deviation of the traits between two times (7 and 14 days after sowing).

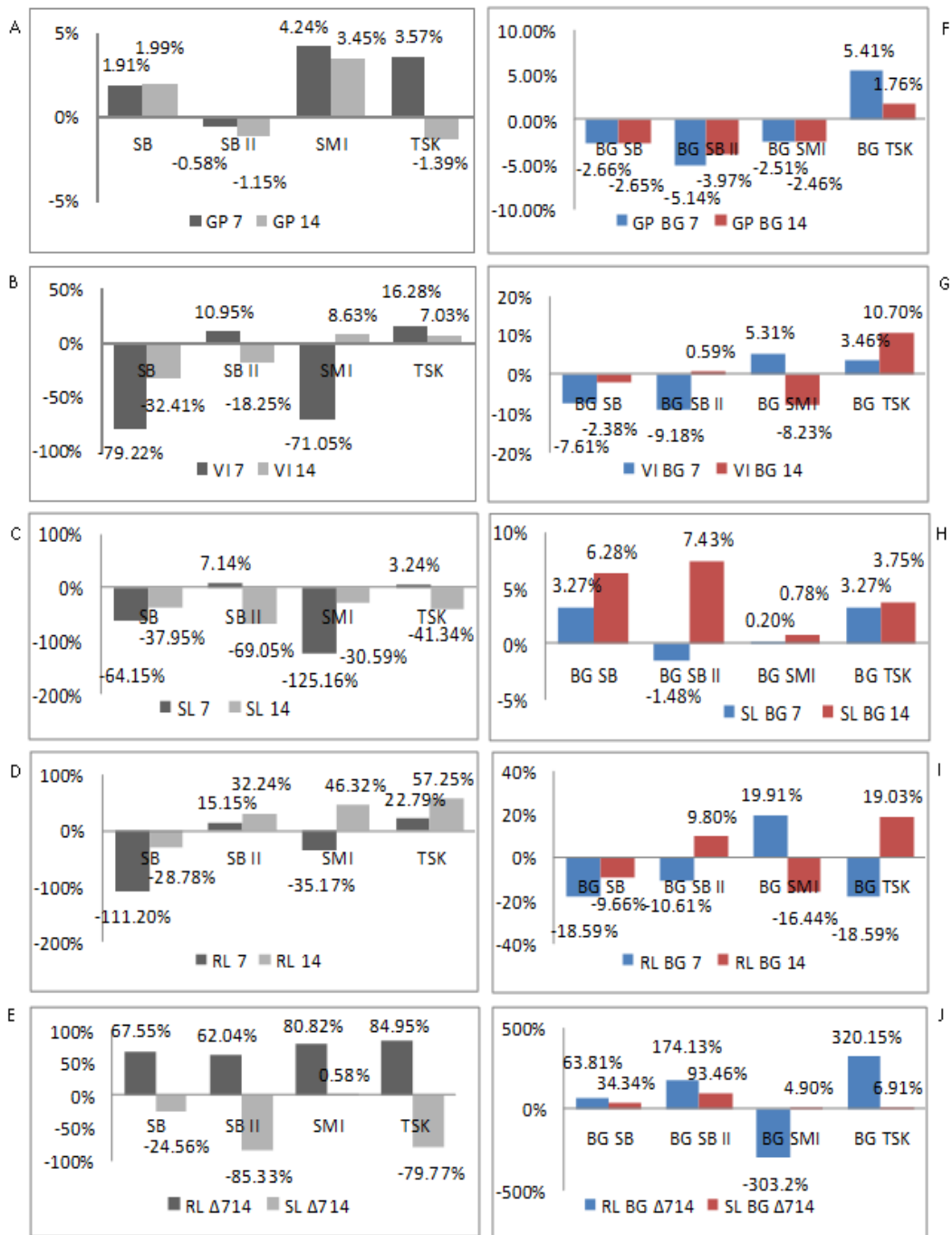


**Figure 2.** The inhibitory percentage of rice against barnyard grass (A-E) and barnyard grass against rice (F-J) in vigour traits. BG is Barnyard grass, SB is Subang, SB II is Subang II, SMI is Sukabumi, and TSK is Tasikmalaya. The positive values indicated inhibitory effect and negative values indicated stimulatory effect.

were 4.37 and 5.21, respectively, after sowing for 7 days. Moreover, the vigour index of SB (14.76) and SB II (17.38) varieties had a higher value than the controls at 11.14 and 14.70, respectively, after sowing for 14 days as could be seen in Table 1. In Figure 2B, only the SB local black variety showed negative IP at 7 and 14 days after sowing (-79.22% and -32.41%).

Table 1 shows the growth seedling traits, shoot and root length (SL and RL) at 7 to 14 days after sowing. Furthermore, the inhibitory percentages are shown in Figures 2C and 2D. Table 1 shows that based on two observations, the local varieties, SB and SMI had significantly higher SL traits at 4.71 and 6.21 cm length compared to the controls, which were 2.87 and 2.76 cm, respectively. In addition, at day 7 after sowing, the SL traits of these two varieties were 11.72 and 14.53 cm, compared to the controls, which were 8.49 and 11.13 cm respectively at 14 days. The other two local varieties, SB II and TSK showed higher significance in SL traits at 12.34 and 15.20 cm compared to those of the controls, which were 7.30 and 10.76 cm, respectively, at 14 days after sowing. Also, the RL trait of the SB local black rice variety was significantly higher at 3.95 cm than was the control which was 1.87 cm, at the 7 day. While at 14 days, the RL trait of this variety and the control were 4.47 and 3.47 cm, respectively. Thus, the value of inhibitory percentage of the SB variety showed negative value at two observation times, -111.20% and -28.78% respectively. The deviation between two times of SL and RL measurement (SL  $\Delta$ 714 and RL  $\Delta$ 714) showed the increase in the growth values. In SL  $\Delta$ 714, all local black rice varieties showed values higher than control. However, the SB II and TSK varieties showed significantly higher values compared to those of control in SL  $\Delta$ 714 traits. The SL  $\Delta$ 714 traits of the SB II and TSK varieties were 8.53 and 10.90 cm, respectively. These values were higher than the controls of these varieties, which were 4.75 and 5.88 cm, respectively. Besides, these two local black rice varieties had negative values of more than 50%, at -85.3% and -79.8%, respectively. Furthermore, the controls showed significantly higher than all local varieties for the RL  $\Delta$ 714 trait, as the values of the trait were 0.52 cm for SB, 1.51 cm for SB II, 1.32 cm for SMI and 0.87 cm for TSK. Meanwhile, for the controls, they were 1.60, 3.98, 6.90, and 5.81 cm, respectively. Thus, there were no negative values in the inhibitory percentage (IP) for all varieties (Figure 2E).

The local black rice varieties provided different allelopathic potential on barnyard grass at germination stage. A comparison of the responses of barnyard grass between the control (without rice) and barnyard grass sowed with rice showed inhibitory and/or stimulatory effects on barnyard grass at germination stage (Table 2 and Figures 2F to 2J). The local black rice originated from Subang (SB II) showed significant stimulatory effects on barnyard grass  $T_{50}$ . The barnyard grass reached 50% at 1.04 days after sowing compared to control at 1.38 days, while the other local black varieties had no stimulatory and/or inhibitory effects on  $T_{50}$  of barnyard grass. The germination percentage (GP) of barnyard grass was not affected by the presence of local black rice (Table 2). However, inhibitory percentage (IP) of GP at 7 and 14 days after sowing showed that the barnyard grass was inhibited by the presence of the local black rice from Tasikmalaya (5.41% and 1.76%), while the other varieties caused stimulatory effects on GP of barnyard grass at 7 and 14 days after sowing (Figure 2F). Furthermore, the vigour index (VI) of TSK variety during observation at 7 and 14 days had values of 8.75 and 9.08 (Table 2). It also significantly inhibited barnyard grass VI (9.06 and 10.17) at 7 and 14 days after sowing, respectively. The IP of the TSK variety at 7 and 14 days after sowing showed that the TSK variety could inhibit barnyard grass VI (3.46% and 10.7%) as presented in Figure 2G. Furthermore, the shoot and root length (SL and RL) were used to analyze the seedling growth traits of barnyard grass at 7 and 14 days after sowing, as shown in Table 2. The result showed that the growth of barnyard grass SL (6.07 cm) was inhibited in the presence of the SB and TSK varieties at 7 days after sowing, while, the control was 6.28 cm. In addition, the SL values of barnyard grass were lower than control when grown together with the SB, SB II, and TSK varieties, being 6.49 cm, 6.41 cm, and 6.67 cm, respectively, while the control was 6.93 cm. Furthermore, the inhibitory percentages of SB variety on the SL of barnyard grass at 7 and 14 days after sowing were 3.27% and 6.28%, while the SL of the TSK variety were 3.27% and 3.75%, as

shown in Figure 2H. For the root length trait, the SMI variety could inhibit the RL of barnyard grass at 7 days after sowing. This could be seen from results which showed that the RL of the grass was 3.0 cm when grown together with the SMI variety, while the control was 3.74 cm (Table 2). However, the other varieties stimulated the RL of the grass.

The SB II and TSK varieties of the local black rice showed inhibition effect on the RL trait of barnyard grass, compared to control after 14 days of sowing. This is shown in Table 2 and Figure 2I, where the RL traits of the varieties were 3.79 and 3.40 cm, while that of the control was 4.20 cm. These results were also shown by the IP, where the SB II and TSK local black rice varieties showed inhibitory effects of 9.80 and 19.03% on the RL of barnyard grass at 14 days after sowing. Furthermore, the deviation of the SL from the two times measurements (SL  $\Delta$ 714) of barnyard grass that was planted with local black rice of SB II (0.04 cm) was the lowest among the effect of other varieties on this trait, compared to the control (0.64 cm) and the IP of SB II local black rice variety on this trait was 93.46%. The TSK local black rice variety gave the lowest value on RL  $\Delta$ 714 of barnyard grass (-1.03 cm) and the highest positive value of inhibitory percentage (320.15%) which indicated higher stimulatory effect as displayed in Table 2 and Figure 2J.

According to the results, the exploration of local rice potential in Indonesia is limited in breeding programs particularly for improving local black rice. Local rice has been reported to have genetic diversity and adaptability to various environmental conditions [39]. Several researchers reported that black rice varieties have the potential to release allelopathic compounds that can inhibit the growth of other plants including weeds and increase the competitiveness of rice plants [7, 12]. This study reveals that the local black rice varieties originated in West Java have allelopathic potential which is characterized by inhibitory effects on the germination and growth of barnyard grass at germination stage. By using dendrogram obtained from Ward's method based on inhibitory percentage, it showed that the presence of barnyard grass stimulated the growth of the local black rice variety that originated from Subang (SB II) and at the same time this variety inhibited the growth of barnyard grass as revealed by the inhibitory percentage of vigour traits at germination stage (dendrogram not shown).

Various biotic or abiotic factors may play roles in the stimulation of releasing allelochemicals in rice. Barnyard grass (*Echinochloa crus-galli* (L.) Beauv.) is one of the dominant weeds in Indonesia rice field that interrupts every stage of growth and development in rice [40]. Barnyard grass has previously been shown to reveal the allelopathic potential of rice [13]. The advantages of the use allelopathic varieties are to avoid the negative effects of weeds in field and to use as breeding material for breeders [40-42]. Various inhibitory effects of rice varieties on barnyard grass at germination stage has been presented in this study that may reflect the allelopathic potential of the rice varieties and the results are in agreement with numerous studies [5, 6, 43, 44]. However, most of the previous studies examined the allelopathic effect of rice on barnyard grass or the allelopathic effect of barnyard grass on rice, and there were limited studies that observed this relationship at both sides. Thus, this study examined the effect of rice on barnyard grass and barnyard grass on rice in order to determine which varieties are useful for breeding materials and also to provide information on various responses of each rice variety against barnyard grass at germination stage. In this study, the presence of barnyard grass stimulated one TSK local black rice variety in T50, while the other varieties were inhibited by the presence of barnyard grass. However, the TSK local black rice variety did not inhibit the T50 of barnyard grass and the SMI local black rice variety stimulated the T50 of barnyard grass. This indicated that there was a different plant defense to the presence of allelochemicals that were released by barnyard grass in the early stage of germination. Also, barnyard grass responded to the presence of rice in this trait by accelerating germination. This result was in agreement with Zhang *et al.* [44] which reported that barnyard grass could recognize the presence of rice. This phenomenon occurred at every stage of germination, and was more pronounced in the more specific vigour traits such as in shoot and root length, at two times of observation.

**Table 2.** The response of barnyard grass against West Java local black rice at germination stages

Traits	Control	Barnyard grass + Rice Varieties (Mean ± Std Err)			
		BG SB	BG SB II	BG SMI	BG TSK
T <sub>50</sub> (days)	1.38±0.03 a	1.20±0.04 ab	1.38±0.02 a	1.04±0.12 b	1.29±0.05 a
GP BG 7 (%)	90.0±0.02 a	93.0±0.02 a	95.0±0.02 a	93.0±0.03 a	85.0±0.03 a
VI BG 7	9.06±0.31 a	9.75±0.23 a	9.89±0.24 a	8.58±0.28 a	8.75±0.14 a
GP BG 14 (%)	91.0±0.03 a	94.0±0.01 a	95.0±0.01 a	94.0±0.02 a	90.0±0.01 a
VI BG 14	10.17±0.27 b	10.41±0.21 ab	10.11±0.18 b	11.01±0.32 a	9.08±0.21 c
SL 7 (cm)	6.28±0.11 ab	6.07±0.10 b	6.37±0.06 a	6.27±0.09 ab	6.07±0.10 b
SL 14 (cm)	6.93±0.10 a	6.49±0.13 b	6.41±0.07 b	6.88±0.14 a	6.67±0.10 ab
SL Δ714 (cm)	0.64±0.09 a	0.42±0.12 ab	0.04±0.09 b	0.61±0.16 a	0.60±0.18 a
RL 7 (cm)	3.74±0.10 b	4.44±0.12 a	4.14±0.10 a	3.00±0.11 c	4.44±0.12 a
RL 14 (cm)	4.20±0.09 bc	4.61±0.09 ab	3.79±0.25 cd	4.89±0.15 a	3.40±0.23 d
RL Δ714 (cm)	0.47±0.13 b	0.17±0.14 bc	-0.35±0.26 c	1.90±0.22 a	-1.03±0.24 d

Note: Means followed by a different letter are indicated significant at 0.05 by t test. SB is Subang, SB II is Subang II, SMI is Sukabumi, and TSK is Tasikmalaya, BG initial rice is the barnyard grass placed together with rice, T<sub>50</sub> is time to reach 50% germination, GP is germination of percentage, VI is vigour index, SL is shoot length, RL is root length, and Δ714 is the deviation of the traits between two times (7 and 14 days after sowing)

The rice and barnyard grass reached the maximum germination percentage (GP) as shown by value of GP above 80%. However, the vigour index (VI), shoot and root length (SL and RL) revealed that there were different responses of rice and barnyard grass when they were placed together. These indicated that need for more specific traits to discover the allelopathy of both plants. Xuan *et al.* [7] reported that the root exudates released by barnyard grass possessed phytotoxic effect on root and shoot length of rice. However, this study revealed that the presence of barnyard grass may stimulate the shoot and root growth of rice during germination stage. Similar results have been reported by Khoo *et al.* [5] that the reactions of allelopathic rice in the presence of barnyard grass increased shoot and root length. As presented in this study, the local black rice variety originated from Subang (SB II) underwent recovery during 7 to 14 days after sowing. The germination percentage (GP), vigour index (VI), and shoot length (SL) of SB II variety were stimulated by the presence of barnyard grass after sowing for 14 days. Additionally, during the recovery of SB II

growth, this variety showed an inhibitory effect on the growth of barnyard grass as displayed by positive values of inhibitory percentage in the VI, SL, and RL traits of barnyard grass.

These results were consistent with a recent study which showed that allelopathic rice influenced the plant architecture of barnyard grass [44]. This indicated that this rice had a different defense mechanism from the other varieties; one in which the variety struck back at the competitor, probably by releasing an allelochemical. This phenomenon is called “counter-offensive defense mechanism”. This mechanism probably occurs by two factors. The first factor is that the level of allelopathic effect of barnyard grass on this variety did not interfere in the beginning stage. The second factor is that allelochemical compounds arose more than released by this rice variety at later germination stage. However, the actual mechanisms in terms of the metabolism of the allelopathic interactions between these two species remain unclear and further research is needed. According to these results, the selection of rice varieties with allelopathic effects gave promising results in early stages of plant growth (germination stage), and this was indicated by the morphological traits observed during the seedling stage, through the vigour index, shoot and root length, and inhibitory percentage. These traits were useful in rice breeding programs, particularly in the effort to release new allelopathic rice varieties. As suggested by Kim and Shin [45], the identification of allelopathy effects should precede efforts to reveal allelopathy genes, knowledge of which can be used to improve cultivars by conventional or modern techniques of breeding.

#### **4. Conclusions**

The allelopathic potential of local black rice originated from West Java, Indonesia against barnyard grass varies as indicated by vigour traits such as  $T_{50}$ , germination percentage, vigour index, shoot and root length and inhibitory percentage. In the early (7 DAS) and the second germination stages (14 DAS), it could be seen that several varieties were inhibited and stimulated by barnyard grass presence. Furthermore, the inhibitory percentage showed that barnyard grass was inhibited by rice presence. The Subang (SB II) variety displayed recovery mechanism that occurred in the second stage of germination, whilst it had shown the sign of suppressed in the early germination stage as revealed by inhibitory percentage in several vigour traits. These results unveiled that rice allelopathy may increase as part of the recovery mechanism. Besides, the vigour index and shoot length that also reflected by the inhibitory percentage in these two traits were indicated as useful traits for allelopathic rice breeding program. These findings suggest that an allelopathic rice variety that contains a richness of allelopathic compounds and can inhibit the growth of barnyard grass will be, in the future, one part of an environmentally-sound weed management program used by farmers. Furthermore, further study is needed to identify the physiological mechanisms of the release of allelochemicals from root exudates in rice and barnyard grass and also to obtain the right concentration of allelochemicals that could stimulate and inhibit the interactions of these species at several growth stages.

#### **5. Acknowledgements**

The authors are grateful to Universitas Padjadjaran for funding this work through HIU (internal grant of UNPAD).

## References

- [1] FAO, 2018. *Supply and Demand World Rice*. [online] Available at: <https://app.amis-outlook.org/#/market-database/supply-and-demand-overview>
- [2] Sawe, B.E., 2019. *World Atlas Top 10 Rice Consuming Countries 2019* [online] Available at: <https://www.worldatlas.com/articles/top-10-rice-consuming-countries.html>
- [3] Kushwaha, U.K.S., 2016. *Black Rice: Research, History and Development*. Geneva: Springer.
- [4] Hao, J., Zhu, H., Zhang, Z., Yang, S. and Li, H., 2015. Identification of anthocyanin in black rice (*Oryza sativa* L.) by UPLC/Q-TOF-MS and their *in vitro* and *in vivo* antioxidant activities. *Journal Cereal Science*, 64, 92-99.
- [5] Khoo, H.E., Azlan, A., Tang, S.T., and Lim, S.M., 2017. Anthocyanidins and anthocyanins: colored pigments as food, pharmaceutical ingredients, and the potential health benefits. *Food & Nutrition Research*, 61(1), 1361779, <https://doi.org/10.1080/16546628.2017.1361779>
- [6] Kato-Noguchi, H., Nitta, K. and Itani, T., 2013. Allelopathic potential of white, red and black rice cultivars. *Plant Production Science*, 16, 305-308.
- [7] Xuan, T.D., Chung, I.M., Khanh, T.D. and Tawata, S., 2006. Identification of phytotoxic substances from early growth of barnyard grass (*Echinochloa crus-galli*) root exudates. *Journal of Chemical Ecology*, 32, 895-906.
- [8] Kropff, M.J. and Walter, H., 2000. EWRS and the challenges for weed research at the start of a new millennium. *Weed Research*, 40, 7-10.
- [9] Nicolopoulou-Stamati, P., Maipas, S., Kotampasi, C., Stamatis, P. and Hens, L., 2016. Chemical pesticides and human health: The urgent need for a new concept in agriculture. *Frontiers in public health*, 4, 148, <https://doi.org/10.3389/fpubh.2016.00148>
- [10] Lushchak, V.I., Matviishyn, T.M., Husak, V.V., Storey, J.M. and Storey, K.B., 2018. Pesticide toxicity. A mechanistic approach. *Experimental and Clinical Science Journal*, 17, 1101-1136.
- [11] Chung, I.M., Kim, J.T. and Kim, S.H., 2006. Evaluation of allelopathic potential and quantification of momilactone A, B from rice hull extracts and assessment of inhibitory bioactivity on paddy field weeds. *Journal of Agricultural and Food Chemistry*, 54, 2527-2536.
- [12] Kong, C.H., Xuan, T.D., Khanh, T.D., Tran, H.D., and Trung, N.T., 2019. Allelochemicals and signaling chemicals in plants. *Molecules*, 24, 2737, <https://doi.org/10.3390/molecules24152737>
- [13] Khanh, T.D., Cong, L.C., Chung, I.M., Xuan, T.D. and Tawata, S., 2008. Variation of weed-suppressing potential of Vietnamese rice cultivars against barnyard grass (*Echinochloa crus-galli*) in laboratory, greenhouse and field screenings. *Journal of Plant Interactions*, 4, 209-218.
- [14] Li, Y., Xu, L., Letuma, P. and Lin, W., 2020. Metabolite profiling of rhizosphere soil of different allelopathic potential rice accessions. *BMC Plant Biology*, 20, 265, <https://doi.org/10.1186/s12870-020-02465-6>.
- [15] Olofsdotter, M., Jensen, L.B. and Courtois, B., 2002. Improving crop competitive ability using allelopathy -An example from rice. *Plant Breeding*, 121, 1-9.
- [16] Duke, S.O., Scheffler, B.E., Dayan, F.E., Weston, L.A. and Ota, E., 2001. Strategies for using transgenes to produce allelopathic crops. *Weed Technology*, 15, 826-834.
- [17] Gealy, D.R., Estorninos, L.E., Gbur, E.E. and Chavez, C.R.S., 2005. Interference interactions of two rice cultivars and their F3 cross with barnyard grass (*Echinochloa crus-galli*) in a replacement series study. *Weed Science*, 53, 323-330.
- [18] Olofsdotter, M., 2001. Getting closer to breeding for competitive ability and the role of allelopathy—an example from rice (*Oryza sativa*). *Weed Technology*, 15, 798-806.

- [19] Khang, D.T., Anh, L.H., Thu, H.P.T., Tuyen, P.T., Quan, N.V., Minh, L.T., Quan, N.T., Minh, T.N., Xuan, T.D., Khanh, T.D and Trung, K.H., 2016. Allelopathic activity of dehulled rice and its allelochemicals on weed germination. *International Letters of Natural Sciences*, 58, 1-10.
- [20] Kato-Noguchi, H., 2011. Barnyard grass-induced rice allelopathy and momilactone B. *Journal of Plant Physiology*, 168, 1016-1020.
- [21] Kim, S.Y., Madrid, A.V., Park, S.T., Yang, S.J. and Olofsson, M., 2005. Evaluation of rice allelopathy in hydroponics. *Weed Research*, 45, 74-79.
- [22] Rao, A.N., Johnson, D.E., Sivaprasad, B., Ladha, J.K. and Mortimer, A.M. 2007. Weed management in direct-seeded rice. *Advances in Agronomy*, 93, 153-255.
- [23] Heidarzade, A., Esmaili, M. and Pirdashti, H., 2012. Common allelochemicals in root exudates of Barnyard grass (*Echinochloa crusgalli* L.) and inhibitory potential against rice (*Oryza sativa*) cultivars. *International Research Journal of Applied and Basic Science*, 3, 11-17.
- [24] Gealy, D.R., Rohila, J.S. and Boykin, D.L., 2019. Genetic potential of rice under alternate-wetting-and-drying irrigation management for barnyard grass (*Echinochloa crus-galli*) suppression and grain yield production. *Weed Science*, 67, 453-462.
- [25] Seal, A.N., Pratley, J.E. and Haig, T.J., 2005. Evaluation of rice varieties for allelopathic effects on Australian rice weeds-linking laboratory to field. *Proceedings of 4<sup>th</sup> World Congress on Allelopathy*, Wagga Wagga, New South Wales, Australia, 21-26 August 2005, 164-167.
- [26] Wu, H., Pratley, J. and Lemerle, D., 2001. Screening methods for the evaluation of crop allelopathic potential. *The Botanical Review*, 67, 403-415.
- [27] Olofsson, M., Navarez, D., Rebulanan, M. and Streibig, J.C., 1999. Weed-suppressing rice cultivars - Does allelopathy play a role? *Weed Research*, 39, 441-474.
- [28] Berendji, S., Asghari, J. and Matin, A.A., 2008. Allelopathic potential of rice (*Oryza sativa*) varieties on seedling growth of barnyard grass (*Echinochloa crus-galli*). *Journal of Plant Interactions*, 3, 175-180.
- [29] Ventura, L., Dona, M., Macovei, A., Carbonera, D., Buttafava, A. and Mondoni, A., 2012. Understanding the molecular pathways associated with seed vigour. *Plant Physiology and Biochemistry*, 60, 196-206.
- [30] Munamava, M.R., Goggi, A.S. and Pollak, L., 2004. Seed quality of maize inbred lines with different composition and genetic backgrounds. *Crop Science*, 44, 542-548.
- [31] Goggi, A.S., Caragea, P., Pollak, L., McAndrews, G., DeVries, M. and Montgomery, K., 2008. Seed quality assurance in maize breeding programs: Tests to explain variations in maize inbreds and populations. *Agronomy Journal*, 100(2), 337-343.
- [32] Helena, E., 2019. *Evaluasi Vigor Benih Padi Hitam (Oryza sativa L.) Lokal Jawa Barat Pada Beberapa Taraf Konsentrasi Eksudat Akar Gulma Echinochloa crus-galli (L.) Beauv.* BSc. Universitas Padjadjaran. (Indonesian)
- [33] Ma, Y., Zhang, M., Li, Y., Shui, J. and Zhou, Y., 2014. Allelopathy of rice (*Oryza sativa* L.) roots exudates and its relations with *Orobanche cumana* Wallr. and *Orobanche minor* Sm. germination, *Journal of Plant Interactions*, 9, 722-730
- [34] International Seed Testing Association, 1999. International rules for seed testing. Rules 1999. *Seed Science and Technology*, 27 (Suppl.), 1-288.
- [35] Khanh, T.D., Cong, L.C., Chung, I.M., Xuan, T.D. and Tawata, S., 2009. Variation of weed-suppressing potential of Vietnamese rice cultivars against barnyard grass (*Echinochloa crus-galli*) in laboratory, greenhouse and field screenings. *Journal of Plant Interactions*, 4, 209-218.
- [36] Coolbear, P., Francis, A. and Grierson, D., 1984. The effect of low temperature pre-sowing treatment under the germination performance and membrane integrity of artificially aged tomato seeds. *Journal of Experimental Botany*, 35, 1609-1617.

- [37] Farooq, M., Basra, S.M., Ahmad, N. and Hafeez, K., 2005. Thermal hardening: A new seed vigour enhancement tool in rice. *Journal of Integrative Plant Biology*, 47, 187-193.
- [38] Abdul-Baki, A.A. and Anderson, J.D., 1973. Vigour determination in soybean seed by multiple criteria. *Crop Science*, 13, 630-633.
- [39] Muhamad, K., Ebana, K., Fukuoka, S. and Okuno, K., 2015. Diversity and differentiation of *Oryza sativa* and *O. rufipogon* in Indonesia. *Genetic Resources and Crop Evolution*, 64, 41-54.
- [40] Usman, P., B.S., Syukur, M. and Guntoro, D., 2016. Toleransi Galur Harapan Padi Sawah (*Oryza sativa* L.) pada Persaingan dengan Gulma *Echinochloa crus-galli*. *Jurnal Agronomi Indonesia*, 44, 111-118. (in Indonesian)
- [41] Khanh, T.D., Xuan, T.D. and Chung, I.M., 2007. Rice allelopathy and the possibility for weed management, *Annals of Applied Biology*, 151, 325-339.
- [42] Kong, C.H., Chen, X.H., Hu, F. and Zhang, S.Z., 2011. Breeding of commercially acceptable allelopathic rice cultivars in China. *Pest Management Science*, 67(9), 1100-1106.
- [43] Ahn, J.K. and Chung, I.M., 2000. Allelopathic potential of rice hulls on germination and seedling growth of barnyardgrass. *Agronomy Journal*, 92(6), 1162-1167.
- [44] Zhang, T., Fan, B. and Wang, P., 2018. Barnyardgrass root recognition behaviour for rice allelopathy. *Agronomy*, 8(4), 39, <https://doi.org/10.3390/agronomy8040039>
- [45] Kim, K.-U. and Shin, D.-H., 2008. Progress and prospect of rice allelopathy research. In: R.S. Zeng, A.U. Mallik and S.M. Luo, eds. *Allelopathy in Sustainable Agriculture and Forestry*. New York: Springer, pp. 189-213.

# Facile and Green Synthesis of Melamine-Formaldehyde@rGO Foam with Enhanced Superhydrophobicity for Oil Removal Application

Natcha Jirasuttisarn<sup>1</sup> and Chaval Sriwong<sup>1,2,3\*</sup>

<sup>1</sup>Department of Chemistry, Faculty of Science, King Mongkut's Institute of Technology Ladkrabang, Bangkok, Thailand

<sup>2</sup>Center of Excellence in Smart Materials Research and Innovation, King Mongkut's Institute of Technology Ladkrabang, Bangkok, Thailand

<sup>3</sup>Smart Materials Research and Innovation Unit, Faculty of Science, King Mongkut's Institute of Technology Ladkrabang, Bangkok, Thailand

Received: 7 December 2020, Revised: 24 February 2021, Accepted: 30 March 2021

## Abstract

This research presented a more effective method to synthesize superhydrophobic melamine-formaldehyde (MF) foam coated with reduced graphene oxide (MF@rGO) by a conventional heating process. This is a facile and green method based on the use of graphene oxide, GO, as a precursor, and vitamin C as a reductant. The effect of recoating GO onto MF@rGO to form MF@rGO-recoat foam on superhydrophobicity was also investigated. Then, pristine GO, rGO, MF and as-synthesized MF@rGO foams were analyzed and their structures confirmed by several techniques including FTIR, Raman, SEM, TEM, and water contact angle (WCA). The results indicated that the WCA values of MF@rGO and MF@rGO-recoat foams were increased from 144.1° to 156.9°, respectively. Furthermore, the adsorption capacity ( $Q_c$ ), oil removal performance, and recyclability of MF@rGO-recoat foam were investigated. The adsorption capacity of MF@rGO-recoat foam was higher than 103.8 g.g<sup>-1</sup> for all the oils tested (palm oil, gasoline, diesel and lubricant oil), and the highest value was 115.9 g.g<sup>-1</sup> for lubricant oil. Besides, MF@rGO-recoat foam can be easily recycled up to 10 times for removal of all oils tested. Thus, this work provides a new alternative eco-friendly way to synthesize MF foam coated with rGO sheets and the synthesized MF@rGO foam can be applied and reused for the removal of oil spillages from water or wastewater.

**Keywords:** superhydrophobicity; reduced graphene oxide (rGO); melamine-formaldehyde (MF) foam; adsorbent; vitamin C; oil removal; water pollution  
DOI 10.14456/cast.2021.55

## 1. Introduction

With the rapid development and growth of industry, the spillage of oils, petroleum, and organic solvents into water system has caused serious environmental and ecological damages [1, 2]. This has led to incentives to research and develop new techniques in the challenging area of oil-water

---

\* Corresponding author: Tel.: (+66) 23298000-11  
E-mail: chaval.sr@kmitl.ac.th

separation. For this reason, new varieties of adsorbents or adsorber materials that can more effectively adsorb, remove, and transfer spilled oils or toxic organic solvent contaminants from water are urgently desired to help preserve and treat the water pollution [3, 4].

In the past few years, several commercially available polymer sponges or foams, for example, polyurethane (PU), polyethylene (PE), polypropylene (PP), melamine-formaldehyde (MF), and melamine, have been widely used to separate and cleanup oil spills from water because of their low operational costs, lightweight, good flexibility, easy to use and ready availability [2, 4, 5]. However, certain properties of these polymer foams, including their low oil adsorption capacity, poor selectivity, and low chemical stability in organic solvents have limited their applicability [5, 6]. In order to overcome these problems, the modifications of the commercial polymer foams are needed [7, 8].

As a single-atom sheet of two-dimensional (2D) carbon nanomaterial, graphene derivative namely reduced graphene oxide (rGO) has attracted much attention owing to its unique excellent hydrophobicity, thermal and chemical stability, very large surface area, and good flexibility [9, 10]. Recently, rGO sponges and its coating onto polymer foams have been used commonly for removing spilled oils and organic solvents from water. Usually, rGO can be produced from graphene oxide (GO) precursor by both chemical and thermal reduction processes. Unfortunately, the former process has some drawbacks in that it frequently involves the use of several toxic reductants, for instance, hydrazine ( $N_2H_4$ ), hydrogen sulphide ( $H_2S$ ), sodium borohydride ( $NaBH_4$ ) and boron hydride ( $B_2H_6$ ) [11, 12].

Recently, we have reported a simple, green, and effective method for the preparation of MF foam coated with rGO to form MF/rGO foams by using different types of GO as precursors and vitamin C as a reductant [13]. In this research, vitamin C was used as a reducing agent as it is natural reducing agent, environmentally friendly, non-toxicity, inexpensive and readily available. However, all the obtained MF/rGO foams had low oil adsorption ability because of their hydrophobic properties, and had water contact angle below  $150^\circ$ . Although the effect of high content of GO for the preparation of MF/GO was studied, a decrease in the water contact angle was observed [13].

Therefore, to further improve the superhydrophobic property of MF foam coated with rGO, this work aimed to investigate effect of GO precursors coated and recoated onto MF foam to form MF@rGO and MF@rGO-recoat foams using vitamin C as a reducing agent. To the best of our knowledge, moreover, none of the published research had reported on MF foam recoated with rGO by a facile, green, and effective method involving a direct mixing of MF@rGO foam, GO precursor, and vitamin C reductant. In this study, we found that vitamin C not only functioned as a reductant, but it also acted as a surface modifier of MF foam, enhancing the strong interaction between GO sheet precursor and the skeleton surface of MF foam. The results indicated that the as-synthesized MF@rGO-recoat foam in this present work shows a superhydrophobic property which is higher than water contact angle (as  $156.9^\circ$ ) of  $150^\circ$ . Besides, the adsorption capacity ( $Q_e$ ), oil removal performance, and recyclability of MF@rGO-recoat foam were also studied and reported.

## 2. Materials and Methods

### 2.1 Chemicals and materials

Melamine-formaldehyde (MF) foam was supplied from Scotch Brite, 3M Co., Ltd, Thailand. Graphite powder (99% purity), hydrogen peroxide ( $H_2O_2$ , 30%) and vitamin C, (vit C,  $C_6H_8O_6$ , 99%) were purchased from Sigma-Aldrich (USA). Potassium permanganate ( $KMnO_4$ ) and sulfuric acid ( $H_2SO_4$ , 98%) were obtained from Merck (Germany). Ethanol ( $C_2H_5OH$ , 95%) was obtained from Baker (USA). All chemicals were used as received without any further purification.

## 2.2 Synthesis of melamine-formaldehyde/rGO (MF@rGO) foams

### 2.2.1 Synthesis of GO precursor and rGO samples

First, graphite oxide was synthesized through a modified Hummers method [14]. Then, the synthesized graphite oxide powder was added in DI water under sonication for 90 min, followed by centrifuging. Finally, the aqueous suspension of GO precursor (at the concentration of 5 mg/ml) was obtained. Meanwhile, rGO sample was easily synthesized by a conventional heating method at 90°C for 30 min using GO suspension and vitamin C solution, as precursor and reductant, respectively [15].

### 2.2.2 Synthesis of MF@rGO foams

In this work, a commercial MF foam sheet was used, and then cut into (2.0 cm × 2.0 cm × 1.0 cm) cubes. Afterward, the MF foam pieces were cleaned and treated with distilled water, ethanol, and then dried at 60°C in an oven for 30 min. The MF foam coated with rGO (MF@rGO) was synthesized by a method based on Jirasuttisarn and Sriwong [13], using a conventional heating process. In brief, the MF foam was firstly immersed into 50 ml of distilled water and followed by adding a few drops of vitamin C solution to adjust the pH of distilled water to 3. Then, 10 mg of GO precursor was added and stirred for 5 min, followed by heating at 90°C for 30 min under stirring. Subsequently, the MF@rGO foam product was taken out and then washed with distilled water and ethanol several times. After drying in an oven at 60°C for 3 h, the MF@rGO-10 foam was obtained. Meanwhile, the recoated MF@rGO foam was also synthesized as described above, but using MF@rGO-10 foam as a starting foam with a new GO precursor at the content of 10 mg. The obtained product was named as MF@rGO-recoat foam.

## 2.3 Characterizations

The functional groups of GO, rGO, MF and all MF@rGO foam samples were analyzed via Fourier-transformed infrared spectroscopy (FT-IR) (Nicolet iS50, Thermo Fisher Scientific Inc., USA). The chemical structures of the samples were also well-confirmed by Raman spectroscopy technique (DXR Smart, Thermo Fisher Scientific Inc., USA). The microstructures of the samples were investigated using scanning electron microscopy (SEM), (JEOL-JSM5800LV, Japan) and transmission electron microscopy (TEM), (JEJOL-JM-2010, Japan). Water contact angle (WCA) measurements of all MF@rGO foams were performed through a contact angle analyzer using a water droplet of volume 5 ul.

## 2.4 Measurements of oils adsorption capacity

The MF@rGO-recoat foam was dipped into various oils, such as, gasoline, diesel, palm oil, and lubricant oil for 3 min. The adsorption capacity,  $Q_e$  (g/g) was calculated by Equation (1),

$$Q_e = (m_t - m_i)/m_i \quad (1)$$

where  $m_i$  and  $m_t$  are the weights (g) of the foam sample before and after adsorption, respectively [10, 16]. The average adsorption capacity of MF@rGO-recoat foam for removal of various oils was obtained by using 3 pieces of each foam sample per test.

## 2.5 Recyclability

The recyclability of the MF@rGO-recoat foam was measured by repeated adsorption-squeezing methods without any washing and drying of the foam sample. This method was carried out by immersing pieces of MF@rGO-recoat foam into palm oil, gasoline, diesel or lubricant oil until the foam became saturated, and then manually squeezing the foam to separate out adsorbed oils, a process that was repeated 10 times in order to test the recyclable performance of the MF@rGO-recoat foam.

## 3. Results and Discussion

### 3.1 Synthesis of MF@rGO foams

The photographs of pristine MF, MF@rGO-10 and MF@rGO-recoat foam samples are shown in Figure 1. It can be clearly seen that the surface of the pristine MF foam was white in color [as can be seen in Figure 1(a)], whereas both MF@rGO foams were of black color [Figures 1(b) and (c)]. This result confirmed that the surfaces of both MF@rGO foams were coated or well-covered with rGO sheet particles [10]. As a result, vitamin C not only functioned as a reducing agent, but it also acted as a surface modifier of the MF foam with the positive charges of  $H^+$  ions on the surface of the MF foam. Therefore, the negative charges on the skeleton of GO sheets could easily adhere to the skeleton of MF surface through strong electrostatic interaction [17]. Moreover, vitamin C molecules can also react with GO molecules via good hydrogen bonding and  $\pi$ - $\pi$  stacking, resulting in better interaction of GO precursor and vitamin C reductant, which enhances the reduction of GO to rGO. After the reduction, rGO nanosheets were easily produced from GO precursor, and still maintained cover and impregnation on the surfaces of all as-synthesized MF@rGO foams.

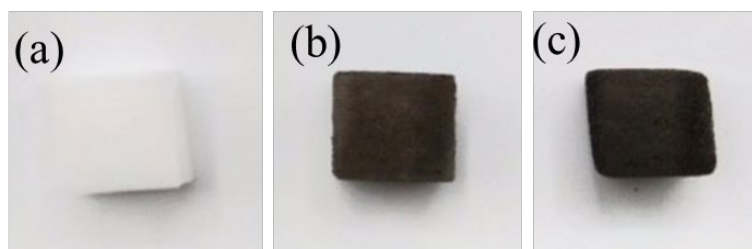


**Figure 1.** Photographs of (a) pristine MF, (b) MF@rGO-10 and (c) MF@rGO-recoat foams

### 3.2 Analysis of GO precursor and rGO

To confirm the characteristics of GO precursor and as-synthesized rGO samples, Raman, FTIR, SEM and TEM techniques were carried out, all the results of which are displayed in Figure 2. It can be observed that the Raman peaks of GO precursor and rGO are exhibited as two broad peaks at around  $1336\text{ cm}^{-1}$  and  $1586\text{ cm}^{-1}$  [see in Figure 2(a)], which are related to disordered carbon (D band) and graphitic  $sp^2$  carbon (G band), respectively [6, 18]. Compared to the GO, the  $I_D/I_G$  intensity ratio of rGO was increased, which can be attributed to the transformation of GO to rGO after the reduction method using vitamin C [8, 12]. This is confirmed by the color change of GO (brown) and rGO (black) suspensions, as shown in inset of Figure 2(a) [10, 12]. Meanwhile, the FTIR spectra of GO precursor and rGO samples are also shown in Figure 2(b). After the reaction of

GO precursor, the absorption bands of some oxygen-functional groups, for instance, hydroxyl (-OH), carbonyl (-C=O) and epoxy (C-O-C) were mostly removed [6, 19]. This result indicated that the GO precursor was transformed into rGO by the chemical reduction method using vitamin C as reductant. Figure 2(c) displays the SEM image of the rGO sample. It can be seen that the morphology of rGO particles was flake-like structure of very small sizes and high aggregation. This result agrees with the TEM image in Figure 2(d), in which it can be seen that rGO particles had formed very thin sheets [13, 17].

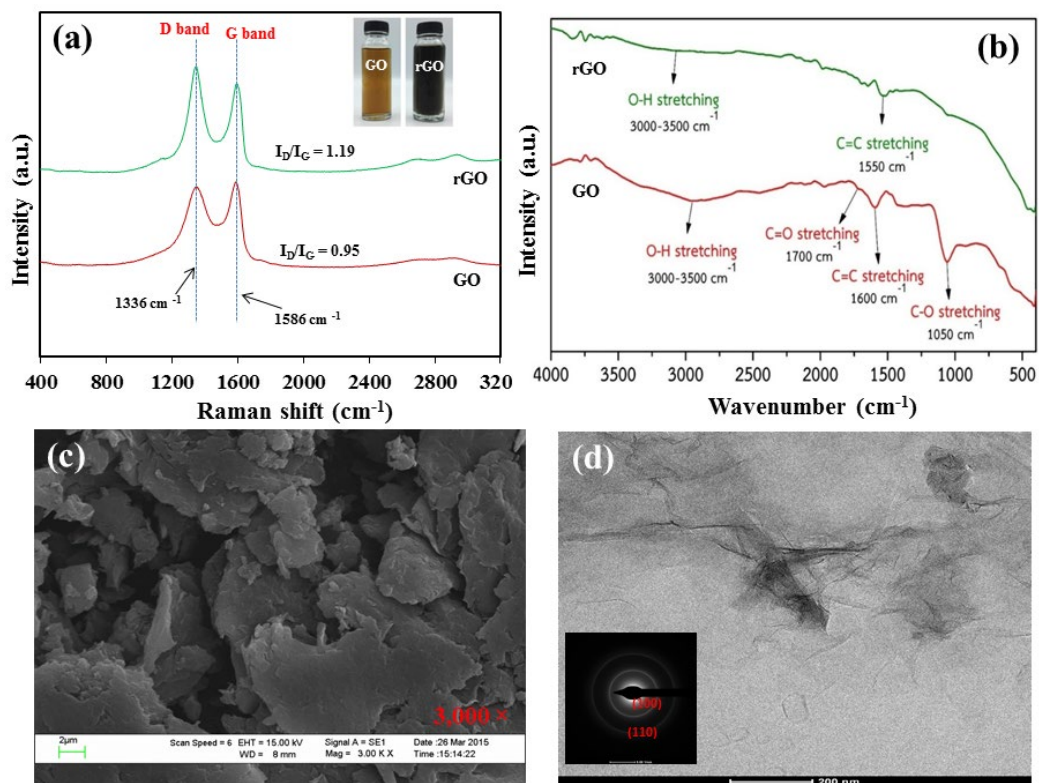


**Figure 2.** (a) Raman, (b) FTIR spectra of GO precursor and synthesized rGO samples; and (c) SEM and (d) TEM images of rGO sheets

### 3.3 SEM characterization of MF@rGO foams

Figure 3 displays the surface morphology of the pristine MF, as-synthesized MF@rGO-10 and MF@rGO-recoat foams. It can be obviously seen that the skeleton template of pristine MF foam had a very smooth surface (see in Figure 3(a), whereas both the MF@rGO foams showed rough surfaces being coated and covered with rGO sheet particles on the skeletons of the MF@rGO foams [see in Figure 3(b) – 3(c)] [13]. Compared to the MF@rGO-10 foam, the surface roughness of the MF@rGO-recoat foam has more covering of rGO nanosheets on the skeleton of the MF surface. This result indicates the recoating of MF@rGO foam can enhance the impregnation and cover of rGO particles on the foam surface.

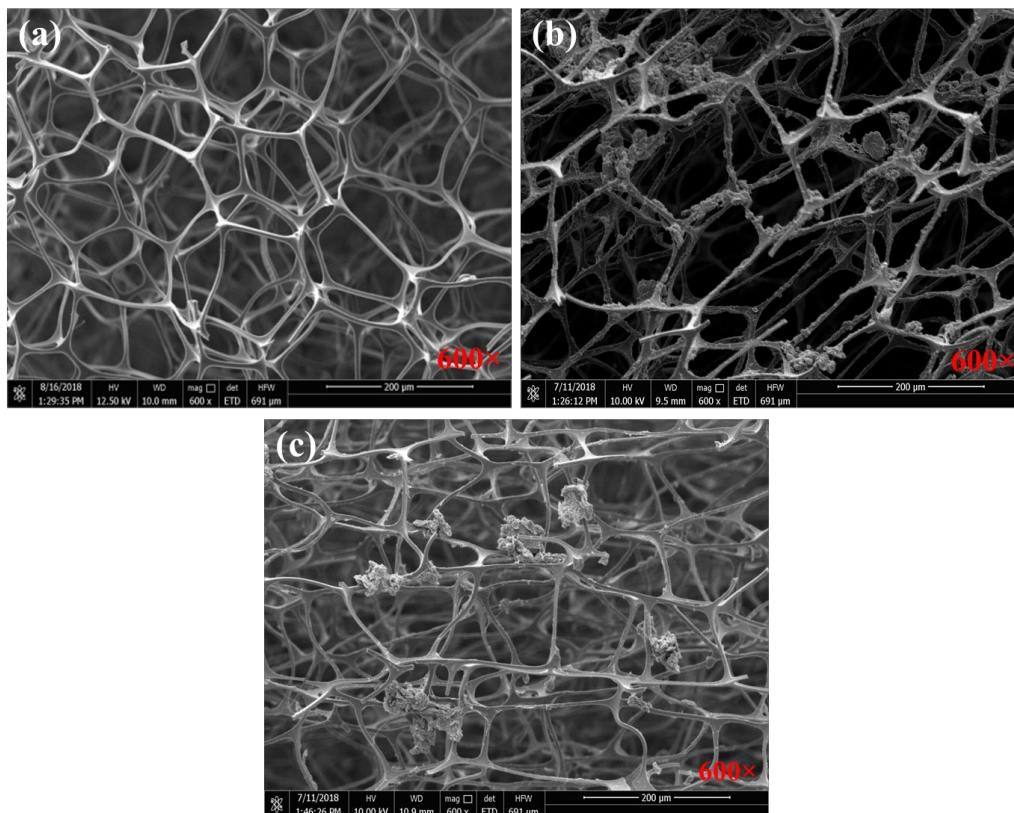


**Figure 3.** SEM images of (a) pristine MF, (b) MF@rGO-10 and (c) MF@rGO-recoat foams

### 3.4 FTIR analysis of pristine MF and MF@rGO foams

Figure 4 illustrates the FTIR spectra of pure MF and all MF/rGO foams. For the pristine MF foam, the typical absorption bands that appeared at around  $3340\text{ cm}^{-1}$ ,  $2910\text{--}2848\text{ cm}^{-1}$ ,  $1556\text{ cm}^{-1}$ ,  $1450\text{ cm}^{-1}$ ,  $1320\text{ cm}^{-1}$ ,  $1018\text{ cm}^{-1}$  and  $800\text{ cm}^{-1}$  were assigned to the functional groups of MF foam structure, such as, -N-H or -O-H stretching, -C-H stretching of  $-\text{CH}_2$ , the aromatic ring stretching of -C-N and -C=N groups, and triazine ring bending vibrations of MF [5, 20]. Compared to the MF foam, all the absorption bands of the MF@rGO foams can be observed but it needs to be remarked that the intensities of all characteristic bands of MF in MF@rGO foams were slightly decreased and broadened upon its coating and recoating. This result well confirmed the increase of rGO nanosheet particles that had interacted with, covered, and impregnated the surface of MF@rGO foams [13, 18, 21].

### 3.5 Raman analysis of MF@rGO foams

Figure 5 displays the Raman spectra of as-synthesized MF@rGO-10 and MF@rGO-recoat foam samples. In the Figure 5, two obvious peaks at around  $1336\text{ cm}^{-1}$  (D band) and  $1588\text{ cm}^{-1}$  (G band) of rGO can be seen with all the MF@rGO foams. The characteristic absorption peaks of rGO were more clearly observed and slightly increased along with the recoating of the foam sample. However,

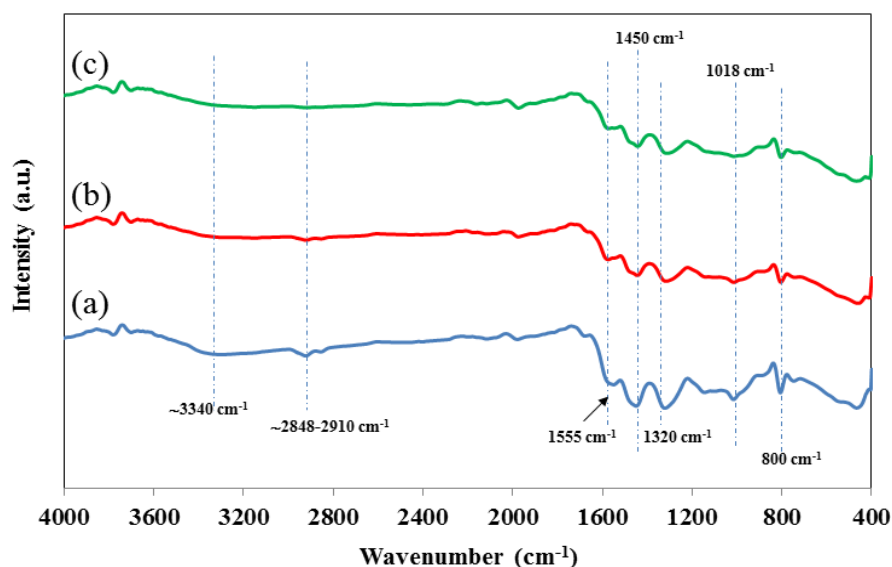


**Figure 4.** FTIR spectra of (a) pristine MF, (b) MF@rGO-10 and (c) MF@rGO-recoat foams

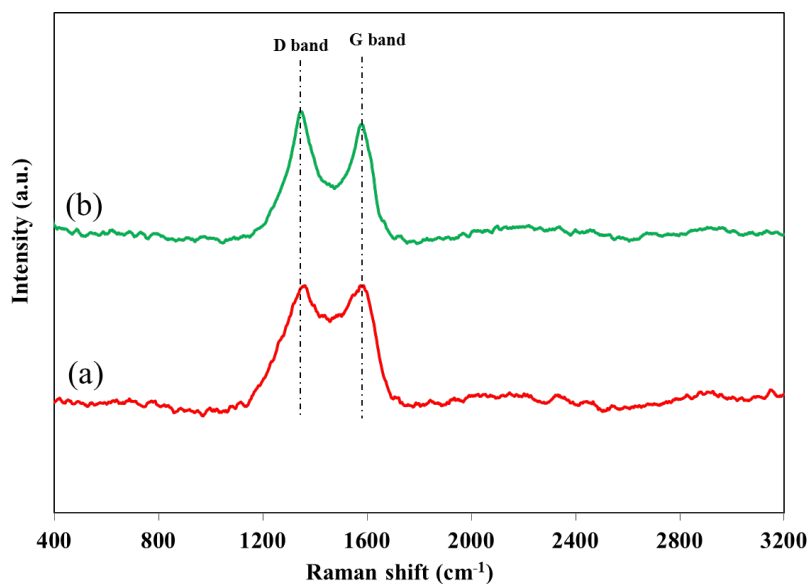


**Figure 5.** Raman spectra of (a) MF@rGO-10 and (b) MF@rGO-recoat foams

the typical peaks, such as a triazine ring breathing mode (at around 980-990 cm<sup>-1</sup>) and C–H stretching (at around 2960 cm<sup>-1</sup>) vibrations of MF structure [22] were not observed in both MF@rGO foams. This result further confirmed the rGO sheet particles had become well impregnated into and better covered the surface of the MF@rGO-recoat foam.

### 3.6 Water contact angle of MF@rGO foams

To understand the hydrophobic properties of all foam samples, the water contact angle (WCA) measurements were investigated, and the results are presented in Figure 6. It was found that the WCA values of the MF@rGO-10 and MF@rGO-recoat foams had increased from  $144.1^\circ$  to  $156.9^\circ$ , respectively. The WCA of MF@rGO-recoat foam had a WCA value of  $156.9^\circ$  which was higher than  $150^\circ$ , indicating that this foam was superhydrophobic as well as having excellent ability for oil adsorption. These results were directly related to the higher content of rGO sheets which existed, covered, and were coated on the surface of the MF@rGO foams. These results can be related to the data from SEM and Raman techniques. As a result, it can be concluded that the higher water contact angle of the MF@rGO-recoat foam coincided with its superhydrophobic behavior, resulting in its superior oil adsorption ability [23].

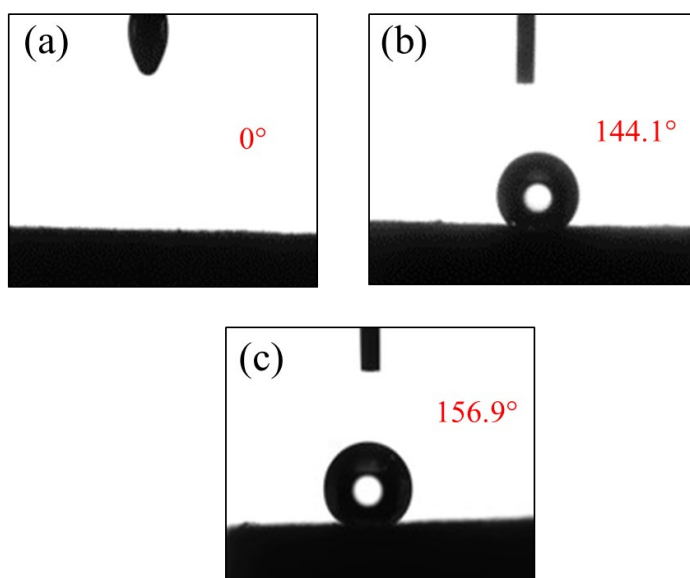


**Figure 6.** Water contact angle (WCA) of (a) pristine MF, (b) MF@rGO-10 and (c) MF@rGO-recoat foams

### 3.7 Oil removal ability of MF/rGO-recoat foam

To understand the oil removal ability, oil-water separation from water was tested using the as-synthesized MF@rGO-recoat foam. The hydrophobicity of the foam was measured by placing palm oil and water droplets on the MF@rGO-recoat foam surface, as shown in Figure 7(a). It was found that water droplets of spherical shape were still maintained on the surface of the synthesized MF@rGO foam; in contrast, the oil droplets were immediately adsorbed into the foam and disappeared. Furthermore, the removal performance of the MF@rGO-recoat for palm oil from water was also studied. As can be seen in Figures 7(b) and 7(c), when the MF@rGO-recoat foam contacted with the oil and chloroform in the water, both the palm oil and chloroform were quickly adsorbed into the foam sample within a few seconds [10, 12, 24], and moreover the adsorbed oil could be easily released by the squeezing process. These results pointed out that the synthesized MF@rGO-recoat foam had excellent ability to adsorb oil or non-polar solvents from water.

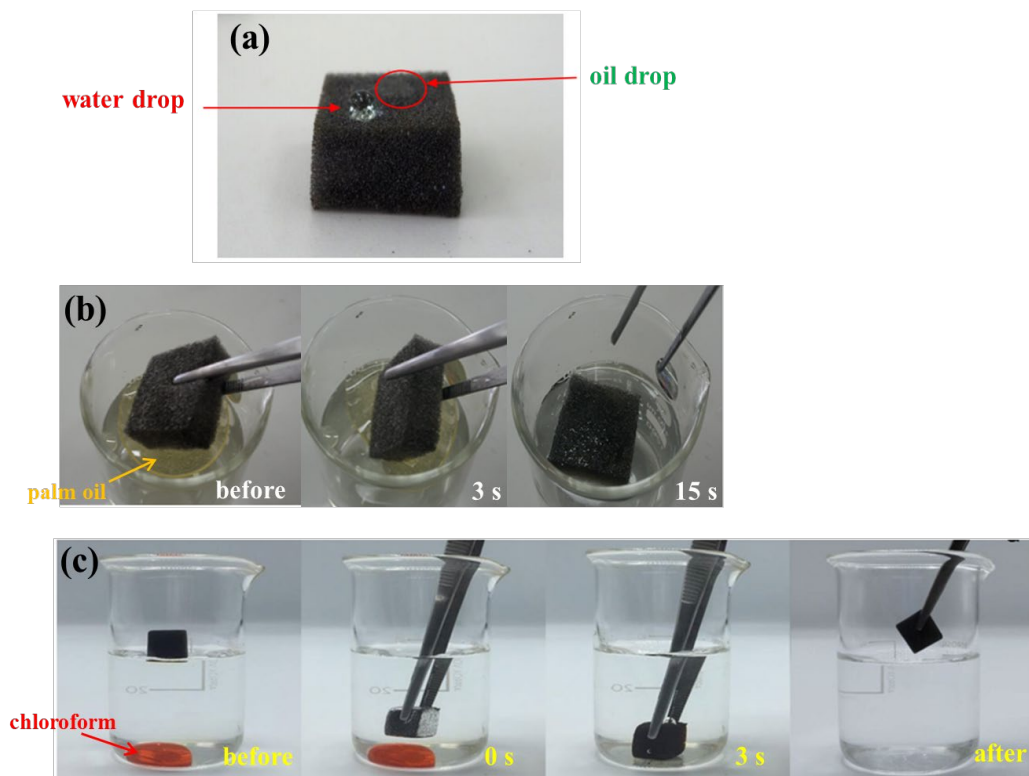


**Figure 7.** Photographs of (a) oil and water droplets on the surface of MF@rGO-recoat foam; (b) the removal of palm oil and (c) chloroform from water using MF@rGO-recoat foam

### 3.8 Recyclability of MF@rGO-recoat foam

The reusability of adsorbents is very important for practical applications. In this study, the MF/rGO-recoat foam was tested by repeated adsorption-squeezing processes. Figure 8 shows the adsorption capacity and recyclability (up to 10 times) of as-synthesized MF@rGO-recoat foam for absorbing palm oil, gasoline, diesel, and lubricant oil. From the first use, the MF@rGO-recoat foam exhibited the highest  $Q_e$  values were about  $103.8 \text{ g.g}^{-1}$ ,  $108.6 \text{ g.g}^{-1}$ ,  $112.7 \text{ g.g}^{-1}$  and  $115.9 \text{ g.g}^{-1}$  for gasoline, diesel, palm oil and lubricant oil, respectively. The lubricant oil showed the highest  $Q_e$  value compared to the other oils. Normally, excellent adsorption performance of a foam depends on the polarity and density of various oils [19, 23]. Thus, the highest  $Q_e$  value of lubricant oil with MF@rGO-recoat foam is due to the high density as well as the low polarity of this oil. After 10 cycles of all oil removal tests, the adsorption capacity values of the MF@rGO-recoat had slightly decreased but were still higher than  $100 \text{ g.g}^{-1}$ . This indicates that the MF@rGO-recoat foam retained a high and stable adsorption capacity to remove oil from water.

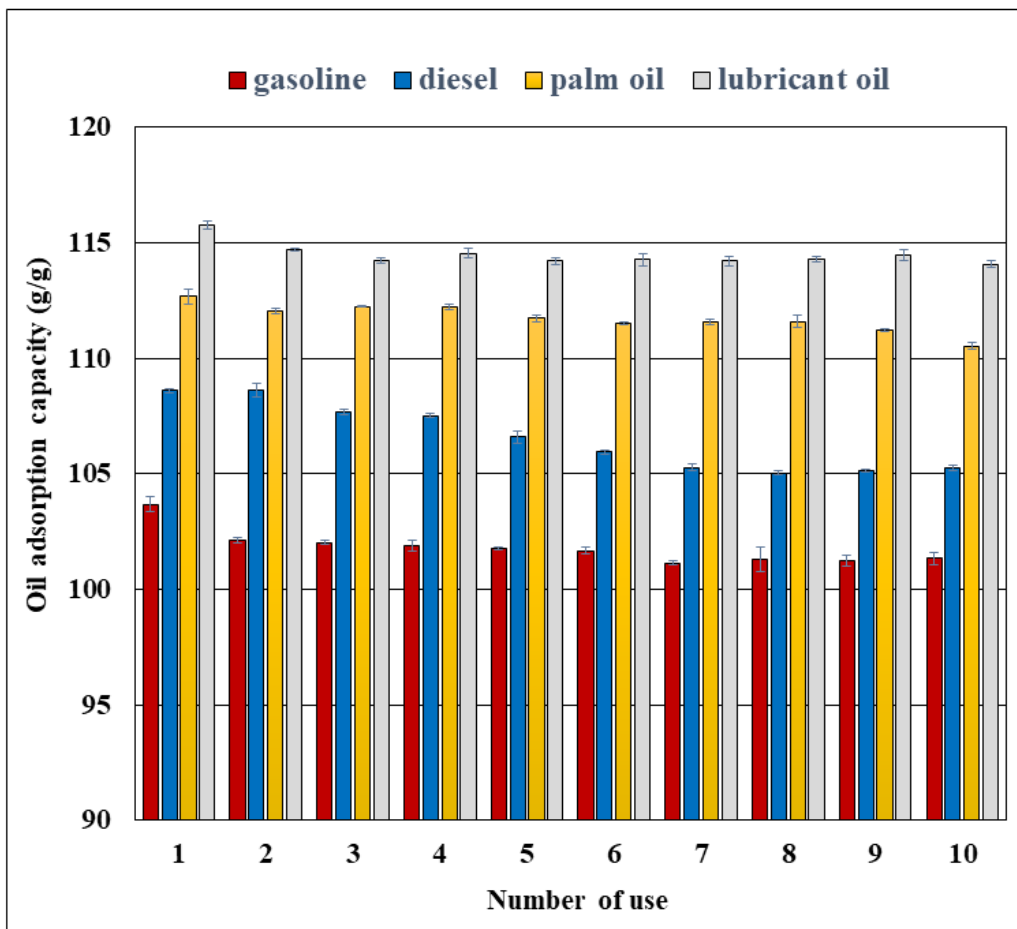


**Figure 8.** Oil adsorption capacity and recyclability of as-synthesized MF@rGO-recoat foam for adsorbing gasoline, diesel, palm oil, and lubricant oil, respectively.

#### 4. Conclusions

In summary, the MF@rGO-recoat foam with excellent oil-water separation ability was successfully synthesized by a green and conventional heating process using GO as precursor, and vitamin C as reductant. The characteristics of the samples were well-confirmed and analyzed by FTIR, Raman, SEM, and TEM techniques. Depending on the appropriate content of GO and recoating cycle, the as-synthesized MF@rGO-recoat foam exhibited the highest water contact angle ( $156.9^\circ$ ) as well as excellent superhydrophobicity. The adsorption capacity ( $Q_e$ ) of the MF@rGO-recoat foam was higher than  $103.8 \text{ g}\cdot\text{g}^{-1}$  in all the oil removal tests, and the highest value seen was about  $115.9 \text{ g}\cdot\text{g}^{-1}$  for lubricant oil. Besides, the synthesized MF@rGO foam can be used easily and recycled up to 10 times for all the oils tested in the oil removal from water.

## 5. Acknowledgement

The authors would like to thank the Department of Chemistry, Faculty of Science, King Mongkut's Institute of Technology Ladkrabang (KMITL) for the financial support.

## References

- [1] Allgayer, R., Yousefi, N. and Tufenkji, N., 2020. Graphene oxide sponge as adsorbent for organic contaminant: comparison with granular activated carbon and influence of water chemistry. *Environmental Science Nano*, 7, 2669-2680.
- [2] Baig, N., Ihsa, N., Sajid, M. and Saleh, T.A., 2019. Graphene-based adsorbents for the removal of toxic organic pollutants: A review. *Journal of Environmental Management*, 244, 370-382.
- [3] Xu, T., Wang, Z., Ding, Y., Xu, W., Wu, W., Zhu, Z. and Fong, H., 2018. Ultralight electrospun cellulose sponge with super-high capacity on absorption of organic compounds. *Carbohydrate Polymers*, 179, 164-172.
- [4] Periasamy, A.P., Wu, W.P., Ravindranath, R., Roy, P., Lin, G.L. and Chang, H.T., 2017. Polymer/reduced graphene oxide functionalized sponges as superabsorbents for oil removal and recovery. *Marine Pollution Bulletin*, 114, 888-895.
- [5] Xu, M., Ma, Y., Liu, R., Liu, Y., Bai, Y., Wang, X., Huang, Y. and Yuan, G., 2020. Melamine sponge modified by graphene/polypyrrole as highly compressible supercapacitor electrodes. *Synthetic Metals*, 267, 116461, <https://doi.org/10.1016/j.synthmet.2020.116461>
- [6] Lu, X., Cui, Z., Wei, W., Jiang, J., Huang, J. and Liu, J., 2016. Constructing polyurethane sponge modified with silica/graphene oxide nanohybrids as a ternary sorbent. *Chemical Engineering Journal*, 284, 478-486.
- [7] Liu, C., Yang, J., Tang, Y., Yin, L., Tang, H. and Li, C., 2015. Versatile fabrication of the magnetic polymer-based graphene foam and application for oil-water separation. *Colloids and Surface A: Physicochemical and Engineering Aspects*, 468, 10-16.
- [8] Peng, M., Chen, G., Zeng, G., Chen, A., He, K., Huang, Z., Hu, L., Shi, J., Yuan, L. and Huang, T., 2018. Superhydrophobic kaolinite modified graphene oxide-melamine sponge with excellent properties for oil-water separation. *Applied Clay Science*, 163, 63-71.
- [9] Rahmani, Z., Samadi, M. T., Kazemi, A. and Rashidi, A.M., 2017. Nanoporous graphene and graphene oxide-coated polyurethane sponge as a highly efficient superhydrophobic, and reusable oil spill absorbent. *Journal of Environmental Chemical and Engineering*, 5, 5025-5032.
- [10] He, Y., Liu, Y., Wu, T., Ma, J., Wang, X., Gong, Q., Kong, W., Xing, F., Liu, Y. and Gao, J., 2013. An environmentally friendly method for the fabrication of reduced graphene oxide foam with a super oil absorption capacity. *Journal of Hazardous Materials*, 260, 796-805.
- [11] Guo, T., Chen, X., Su, L., Li, C., Huang, X. and Tang, X.Z., 2019. Stretched graphene nanosheets formed the obstacle walls in melamine sponge toward effective electromagnetic interference shielding applications. *Materials and Design*, 182, 108029, <https://doi.org/10.1016/j.matdes.2019.108029>
- [12] Zhang, C., Li, H., Zhuo, Z., Dugnan, R., Sun, C., Chen, Y. and Liu, H., 2017. Facile fabrication of ultra-light and highly resilient PU/RGO foams for microwave absorption. *RSC Advances*, 7, 41321-41329.
- [13] Jirasuttisarn, N. and Sriwong, C., 2020. Effect of graphene oxide precursor loading on the surface of melamine-formaldehyde/rGO sponge with enhanced ultra-hydrophobicity for oils removal. *American Journal of Nano Research and Applications*, 8(2), 22-27.

- [14] Phompet, C., Sriwong, C. and Ruttanapun, C., 2019. Mechanical, dielectric, thermal and antibacterial properties of reduced graphene oxide (rGO)-nanosized C3AH6 cement nanocomposites for smart cement-based materials. *Composites Part B: Engineering*, 175, 107128, <https://doi.org/10.1016/j.compositesb.2019.107128>
- [15] Sriwong, C., Choojun, K. and Kongtaweelert, S., 2017. Investigation of the influences of reaction temperature and time on the chemical reduction of graphene oxide by conventional method using vitamin C as a reducing agent. *Materials Science Forum*, 909, 225-230.
- [16] Dashairya, L., Sahu, A. and Saha, P., 2019. Stearic acid treated polypyrrole-encapsulated melamine formaldehyde superhydrophobic sponge for oil recovery. *Advanced Composites and Hybrid Materials*, 2, 70-82.
- [17] Li, D., Muller, M.B., Gilje, S., Kaner, R.B. and Wallace, G.G., 2008. Processable aqueous dispersions of graphene nanosheets. *Nature Nanotechnology*, 3, 101-105.
- [18] Liu, Y., Ma, J., Wu, T., Wang, X., Huang, G., Liu, Y., Qiu, H., Li, Y. and Wang, W., 2013. Cost-effective reduced graphene oxide-coated polyurethane sponge as a highly efficient and reusable oil-absorbent. *ACS Applied Materials & Interfaces*, 5, 10018-10026.
- [19] Qiu, L., Zhang, R., Zhang, Y., Li, C., Zhang, Q. and Zhou, Y., 2018. Superhydrophobic, mechanically flexible and recyclable reduced graphene oxide wrapped sponge for highly efficient oil/water separation. *Frontiers of Chemical Science and Engineering*, 12, 390-399.
- [20] Merline, D.J., Vukusic, S. and Abdala, A.A., 2013. Melamine formaldehyde: curing studies and reaction mechanism. *Polymer Journal*, 45, 413-419.
- [21] Yousefi, N., Wong, K., Hosseinidoust, Z., Sørensen, H.O. and Tufenkji, N., 2018. Hierarchically porous, ultra-strong reduced graphene oxide-cellulose nanocrystal sponges for exceptional adsorption of water contaminants. *Nanoscale*, 10, 7171-7184.
- [22] Nakanishi, K. and Hofmann, S., 2020. Ordered graphitic microfoams via shrinkage and catalytic conversion of polymer scaffolds. *APL Materials*, 8, 021106, <https://doi.org/10.1063/1.5136235>
- [23] Zhu, H., Chen, D., Yang, S., Li, N., Xu, Q., Li, H., Wang, L., He, J., Jiang, J. and Lu, J., 2016. A versatile and cost-effective reduced graphene oxide-cross-linked polyurethane sponge for highly effective wastewater treatment. *RSC Advances*, 6, 38350-38355.
- [24] Liu, W., Li, M., Jiang, H., Zhang, X. and Qiao, J., 2019. High performance graphene-melamine sponge prepared via eco-friendly and cost-effective process. *Journal of Nanoparticles Research*, 21, 36, <https://doi.org/10.1007/s11051-018-4457-2>

## Quality Improvement of Marinated Pork Stew in Retort Pouch for the Elderly

Porn-tip Wiriyawattana\*

Department of Food Technology, Faculty of Science, Ramkhamhaeng University,  
Bangkok, Thailand

Received: 5 November 2020, Revised: 2 March 2021, Accepted: 5 April 2021

### Abstract

Population aging, which affects virtually every country in the world, involves growth in the number and proportion of older people in the population. The aim of this study was to develop a marinated pork stew packed in a retort pouch that provided food properties suitable for the elderly. Pork loin was treated with different alkaline solution marinades including 5% sodium chloride (M-SC), 5% sodium bicarbonate (M-SBC) or 5% sodium tripolyphosphate (M-STPP) and compared with the control (non-marinated pork). The marinated pork increased pH, cooking yield, redness ( $a^*$  value) and color difference ( $\Delta E^*$ ), while decreased cooking loss, lightness ( $L^*$  value), yellowness ( $b^*$  value) and enhanced texture properties of pork. M-SBC gave significantly ( $p \leq 0.05$ ) the lowest cooking loss and lightness as well as hardness and shear force value. Therefore, M-SBC was selected to develop marinated pork stew through thermal processing by retort technology to produce convenient food for the elderly. The products after sterilizing could be stored at normal temperature and had longer shelf life. The  $F_0$  value of 6.0 was found to be adequate for marinated pork stew. After thermal processing, the  $L^*$  and  $b^*$  values of stew color significantly increased ( $p \leq 0.05$ ) whilst the  $a^*$  value of stew color significantly decreased ( $p \leq 0.05$ ). The texture of the marinated pork improved as indicated by decrease in hardness, cohesiveness, chewiness, and shear force value. Nevertheless, the protein content of marinated pork stew significantly ( $p \leq 0.05$ ) increased after thermal processing. The final marinated pork stew product was evaluated by the elderly folks and accepted with a moderate liking score.

**Keywords:** marination; pork stew; retort pouch; the elderly  
DOI 10.14456/cast.2021.56

### 1. Introduction

Population aging, an inevitable increase in the number of elderly people resulting from declining fertility and expanding longevity, is taking place around the world. In 2019, the global population aged 65 and over amounted to 703 million. East and Southeast Asia were home to the highest proportion of the world's older population, followed by Europe and North America. The number of elderly people is projected to double to 1.5 billion by 2050 [1].

Aging can be biologically considered to be a morpho-functional involvement, variably affecting major physiological systems [2]. Several physiological changes that occur in the healthy aging process are associated with a declining gustatory function in the elderly such as

---

\* Corresponding author: Tel.: (+66) 863863493 Fax: (+66) 23108407  
E-mail: porn-tip.w@ru.ac.th, porn-tip.w.ru@gmail.com

chemosensory perception, oral health, and olfactory function [3]. Decrease in taste perception is possibly caused by an age-related reduction in the number of taste buds on the tongue papillae and a shorter life span of the receptor cells. The loss of threshold sensitivity in the elderly presumably compromises their ability to recognize and appreciate subtle flavors and tastes of foods [4]. Additionally, edentulism is more frequent with advancing age and tooth loss peaks already at around 65 years. The loss of all teeth also reduces masticating efficiency and affects food taste, food preferences, and food consumption patterns. Chewing difficulties induce elderly people to limit their diet to soft foods and to avoid hard textures (such as fresh fruits and vegetables, meat, and even bread) which adversely affects their nutritional status [3, 5]. Thus, there is an urgency to develop and provide easily chewable elderly food products to maintain health and promote the nutrition of the elderly.

Texture is one of the most important aspects of meat quality affecting consumer acceptability, especially in elderly people. Other important aspects required for the acceptance of meat products are appearance or color and taste [6]. Marination is the process in which meat is immersed in different marinade solutions including alkaline or acidic solutions and water-oil emulsions [7]. Acidic solutions cause the structure of meat to loosen, allowing water absorption and producing a tenderer and juicer product but adversely affecting flavor and appearance of meat [8]. The addition of alkaline solution containing salt, phosphate and carbonate are also used to enhance the quality of pork and other meat products [9]. The mechanism responsible for the increased tenderness and juiciness is connected with higher water holding and swelling of myofibrils [10]. Effectiveness of the marination process can be affected by many factors such as type of marinade solution, marination procedure, holding time and temperature [11].

Retort thermal processing involves a combination of high temperature and pressure in a hermetically sealed flexible retort pouch to eliminate all pathogenic and spoilage microorganisms of concern in food products [12]. Overpressure water spray retort has been used for thermal processing with different types of container such as retort pouches, glass bottles, plastic or aluminium containers, etc. With directed steam injection, continuous water spray results in homogeneous heat distribution in the vessel during both sterilizing and cooling. The technical and commercial feasibilities of using retort pouches for thermal processing have been proven by various studies for different meat products like buffalo meat block [13], pork curry [12], Chettinad chicken [14] and Chettinad goat meat curry [15]. Retort pouches offer a number of advantages over metal cans including better storage stability, reduced weight and storage space, ease of opening and preparation, longer shelf life and reduced heat exposure resulting in more quality [16]. Food texture properties suitable for the elderly should be soft, moist and cohesive, while textures that are sticky, adhesive and of fibrous structures should be avoided [17]. Besides measurement by sensory texture evaluations, instrumental methods have been used to determine textural changes. Thus, this research was conducted to develop the marinated pork stew in retort pouch that provided food properties suitable for the elderly.

## **2. Materials and Methods**

### **2.1 Preparation of marinated pork**

Frozen pork loin (pH=6.09) was purchased from P.S. Food Product Co., Ltd., Thailand and transported to the laboratory under chilled condition (0-2°C). Pork was washed with potable water and cut into small cubes of 1.8 cm size using a sterilized knife. The pork cubes were dipped in marinade solution: 5% sodium chloride (M-SC) (Ajax Finechem Pty Ltd., Australia), 5% sodium

bicarbonate (M-SBC) (Continental Food Co., Ltd, Thailand) or 5% sodium tripolyphosphate (M-STPP) (SD BNI (CN) Co., Ltd., China). The mixture was applied in a ratio of meat: marinade solution of 10:1 (w/w). Non-marinade pork was used as a control. The marinade pork and control sample were packed in polyethylene bags and stored under 0-2°C for 15 h. Then, all pork cubes were precooked with steaming to reach minimum internal temperature of about 63°C [18] which was the USDA's safe temperature recommendation for pork.

## 2.2 Preparation of stew mix

A selected stew formula from three recipes was prepared as described by Spitler and Yoakam [19], with slight modification. The selected formula received the highest significant ( $p \leq 0.05$ ) 9-hedonic liking scores with greater than 7.0 (likely moderately) for appearance, flavor, taste, texture and overall liking by the elderly aged over 60 years old ( $n=50$ ). An average volume of 20 ml of each sample was served at room temperature in a 2 oz plastic cup, covered with a lid and labeled with a 3-digit random code. The ingredients used for preparation of stew were as follows: tomato sauce (42.2%), brown sugar (6.5%), cider vinegar (2.6%), Worcestershire sauce (1.6%), black pepper (0.1%) and water (47.0%). To this mix, predetermined quantities of tomato sauce, brown sugar, cider vinegar, Worcestershire sauce and black pepper were added to boiling water, mixed, and cooked for few min. Stew mix was precooked until the temperature reached around 90°C. All ingredients for the preparation of stew mix were purchased from Siam Makro Holding (Thailand) Limited.

## 2.3 Filling and sealing of retort pouch

Laminated flexible pouch (120x175x35 mm) made of four layers (Royal Meiwa Pax Co., Ltd., Thailand) was used for packing the pork stew, consisting of 12  $\mu\text{m}$  polyethylene terephthalate (outer layer), 15  $\mu\text{m}$  nylon, 9  $\mu\text{m}$  aluminium foil (middle layer), and 80  $\mu\text{m}$  polypropylene (inner cast). About  $72 \pm 5$  g precooked pork cubes were filled into the retort pouches. Each pouch was filled with  $48 \pm 0.5$  g of stew mix, keeping a pack weight of approximately  $120 \pm 5$  g. Controlled handling of filled pouches during and between operations was undertaken to prevent contamination of the seal area. Residual air was removed and the pouches were sealed with a vacuum packaging machine (Multivac A300/42, Germany). Initial temperature of precooked pork was measured to be about 30°C. The pouches were drilled at 30% of the pouch height and product core temperature during processing was monitored using thermocouples inserted into core of precooked pork in five of the pouches using ducts. Two thermocouples were kept in the retort chamber to monitor the chamber temperature. Filled and sealed pouches were placed flat on trays in the retort processing unit. The sealed pouches were subjected to thermal processing for optimizing the  $F_0$  value at process temperature.

## 2.4 Overpressure water spray retort

A pilot-scale overpressure retorting unit (SR Advance Technology Co., Ltd, Thailand) used for thermal processing consisted of retort, boiler, air compressor, centrifugal pump and Programmable Logical Control (PLC). The unit used in this study was similar to commercial-scale equipment which produced a high level of accuracy and reproducibility. For the thermal processing, the temperature of retort chamber was set at 116.0°C and an overpressure of 1.8 bar was maintained throughout the process cycle. After the pouches were processed to the required  $F_0$  value, they were rapidly cooled to  $50 \pm 10$ °C by spraying water under pressure. The heat penetration characteristics were determined using a general method [20]. Total process time was determined by adding

process time and the effective heating period during the come-up time i.e. 42% of the come-up time (CUT). Based on the time-temperature data recorded using the PLC, CUT, process time and cooling time were determined. The lethal rate (L) was also calculated based on equation (1) and the  $F_0$  value was able to be obtained from the area under the curve between lethal rate and time based on equation (2). The pouches were then dried, labelled and stored until further analysis.

$$L = 10^{(T-T_r)/Z} \quad (1)$$

Where T is the temperature in degree Celsius ( $^{\circ}\text{C}$ ), at which the lethal rate is calculated and  $T_r$  of  $121.1^{\circ}\text{C}$  is the reference temperature, to which the equivalent lethal effect is compared. The z-value of  $10^{\circ}\text{C}$  is the value frequently used in  $F_0$  calculation performed on low acidic foods.

$$(F_0)_i = \frac{(L_{i-1} + L_i)}{2} \times \Delta T \quad (2)$$

Where  $L_{i-1}$  is the cumulative lethal rate,  $L_i$  is the current lethal rate and  $\Delta T$  is the interval time.

## 2.5 Determination of pH and water activity ( $a_w$ )

The pH value of samples was determined according to the method of AOAC [21] using a pH meter (Mettler Toledo, S220K, Switzerland) calibrated with standard buffer solutions of pH 4.0 and 7.0. Water activity ( $a_w$ ) of samples was measured at  $25^{\circ}\text{C}$  according to the method of AOAC [21] using a water activity instrument (AquaLab, 4TE, USA).

## 2.6 Weight changes during pre-cooking

Weights of pork cubes were recorded before immersion ( $w_1$ ), before pre-cooking ( $w_2$ ) and after pre-cooking ( $w_3$ ). The following calculations were made:

$$\text{Cooking loss (\%CL)} = \frac{(w_2 - w_3)}{w_2} \times 100 \quad (3)$$

$$\text{Cooking yield (\%CY)} = \frac{(w_3/w_1) \times 100}{(3)}$$

## 2.7 Color measurement

The color of flat surface in the center of each sample and stew mix was determined using a colorimeter (Hunter Lab, Colorflex-45-2, USA). The CIE color values of each sample were reported as  $L^*$  (0=black, 100=white),  $a^*$  ( $-a^*$ =greenness,  $+a^*$ =redness) and  $b^*$  ( $-b^*$ =blueness,  $+b^*$ =yellowness). Moreover, the reported  $L^*$ ,  $a^*$  and  $b^*$  values were calculated as color difference ( $\Delta E^*$ ) via the following formula:

$$\Delta E^* = \sqrt{(L^* - L_0^*)^2 + (a^* - a_0^*)^2 + (b^* - b_0^*)^2} \quad (5)$$

where  $L^*$ ,  $a^*$  and  $b^*$  are values for the samples.  $L_0^*$ ,  $a_0^*$  and  $b_0^*$  are values for the control.

## 2.8 Texture analysis

Texture profile analysis (TPA) was performed with a texture analyzer (TA-XT Plus, Stable Micro Systems, UK) using the method of Majumdar *et al.* [22]. The samples were allowed to equilibrate

to room temperature. A load cell of 50 kg and a cylindrical probe of 50 mm diameter were used. The texture measurement included two consecutive 40% compressions of the sample at a crosshead speed of 12 mm/min. From the resulting force-time curve, the values of various texture parameters including hardness (N), cohesiveness, springiness index and chewiness (N) were recorded.

The maximum force required to cut the sample was determined as shear force value with a texture analyzer (TA-XT Plus, Stable Micro Systems, UK) using the method of Majumdar *et al.* [22]. The load cell used for shear force value was of 50 kg capacities. Each cube of cooked pork was placed individually under a Warner-Bratzler shear blade and cut at the center of the sample. The crosshead speed of the machine was maintained at 5 mm/sec. From the force-deformation curves, the maximum shear force was determined, which was indicative of toughness and expressed as N/mm.sec.

## 2.9 Proximate composition

Proximate composition of the samples was undertaken based on AOAC [21]. Moisture content was obtained using air-oven dried method (105°C). Ash was determined by incineration in a muffle furnace at 550°C. Protein content was determined by the Kjeldahl technique. The composition of fat in the samples was determined by the solvent extraction method. Carbohydrate was determined by subtracting from 100, the sum of moisture, ash, protein and fat percentages. Total energy was calculated as:  $\text{Energy} = (\text{protein} \times 4) + (\text{fat} \times 9) + (\text{carbohydrate} \times 4)$ .

## 2.10 Sensory evaluation

Panelists were invited to describe the test detail and to verify their capability to understand the test method, as well as their interest and willingness to participate in the test. This study was approved by the ethics committee of Ramkhamhaeng University (RU-HS-RESC/xd-0122/62). Fifty panelists (12 males and 38 females) aged over 60 years old participated through personal communication screening. They were recruited from the life quality development center for the elderly in Nonthaburi city municipality. The 3 samples of marinated pork and control were precooked with steaming to reach minimum internal temperature of about 63°C and served at room temperature. Samples were provided in two pieces of pork and presented in a 2 oz disposable cup, labeled with 3-digit random numbers. Presentation order was randomized to avoid any serving order bias for all panelists. The panelists were instructed to sip water between samples to cleanse the palate. Then, they were asked to evaluate liking scores using a 9-point hedonic scale (1=dislike extremely, 5=neither like nor dislike and 9=like extremely) for the attributes of appearance, flavor, tenderness, juiciness and overall likings of the samples whilst using a just about right (JAR) scale (1=not enough, 2=just about right and 3=too much) for the attributes of tenderness and juiciness [23].

For consumer acceptance test, one hundred elderly (30 males and 70 females) participated in the test through personal communication screening. The central location test (CLT) for consumer acceptance was performed. Participants were recruited from the life quality development center for the elderly in Nonthaburi city municipality. The marinated pork stew in retort pouch were provided in two pieces of pork with 20 ml of stew mix and presented in a 2 oz disposable cup, labeled with 3-digit random numbers. Then, they were asked to evaluate liking scores using a 9-point hedonic scale for the attributes of appearance, flavor, taste, tenderness, juiciness and overall liking scores as well as acceptance and buying decision.

## 2.11 Microbiological analysis

According to the Thai Food and Drug Administration (FDA), the samples were processed at the required  $F_0$  values followed the condition stated in the Notification of the Ministry of Public Health No.355 B.E.2556 (2013) Re: Food in a Hermetically Sealed Container for commercial sterilization to ensure food safety, which were as follows: total plate count (TPC), yeast and mold, coliforms, *Staphylococcus aureus*, *Salmonella* spp. [24], microbial growth at 35°C and 55°C and *Clostridium botulinum* [25].

## 2.12 Statistical analysis

The experiment was conducted according to a completely randomized design (CRD) with three replications. For each analysis, triplicate measurements were performed. Statistical analysis for sensory evaluation followed a randomized complete block design (RCBD) with subjects as blocks. Data were subjected to analysis of variances (ANOVA) using SPSS software (version 18.0; SPSS (Thailand) Co., Ltd., Bangkok, Thailand). Duncan's multiple range tests were performed to determine significant differences among treatments at 95% confidence level ( $p \leq 0.05$ ). Pearson's correlation analysis was used to investigate the relationship between instrumental measurements. Comparison of physical and chemical measurement between before and after thermal processing were tested by paired t-test.

# 3. Results and Discussion

## 3.1 Effect of marination on pork quality

The qualities of marinated pork and control after pre-cooking are shown in Table 1. The pH values of pork were increased by the alkaline solutions after marination. M-SBC gave ( $p \leq 0.05$ ) the significantly highest pH, whereas M-SC was not significant different ( $p > 0.05$ ) compared to the control. The results for pH of pre-cooked pork followed similar trends as for pH of marinated pork. Among all marinated pork, M-SBC had significantly ( $p \leq 0.05$ ) the lowest cooking loss and the highest cooking yield. Moreover, the results also showed that pH of marinated and pre-cooked pork were negatively correlated with cooking loss ( $R^2 = -0.95$  and  $R^2 = -0.89$ , respectively) and were positively correlated with cooking yield ( $R^2 = 0.86$  and  $R^2 = 0.73$ , respectively) (Table 2). Marination reduced cooking loss and increased cooking yield, presumably due to improved water holding capacity at high pH levels [10].

Pre-cooked pork color, shown in Table 1, revealed significant ( $p \leq 0.05$ ) decrease in  $L^*$  and  $b^*$  values of all marinated pork in comparison with the control. M-SBC showed significantly ( $p \leq 0.05$ ) higher  $a^*$  value than the values of others, leading to a higher  $\Delta E^*$  value with visible color change. Most food additives used in meat products caused color changes by altering the pH and chemical state of myoglobin [9]. It was found that meat with pH greater than 5.7, marinated with sodium chloride, bicarbonate and tripolyphosphate showed significantly lower  $L^*$  values. Additionally, pH of marinated pork was negatively correlated with  $L^*$  value ( $R^2 = -0.74$ ) and was positively correlated with  $a^*$  ( $R^2 = 0.64$ ) and  $\Delta E^*$  ( $R^2 = 0.73$ ) values, indicating that the higher pH decreased the lightness and increased the redness of pork (Table 2).

The texture profiles of marinated pork and control after pre-cooking are also shown in Table 1. All marinated pork had lower hardness, springiness index, cohesiveness, chewiness and shear force values than those of the control. M-SBC had significantly ( $p \leq 0.05$ ) the lowest hardness

**Table 1.** Qualities of marinated pork and control after pre-cooking

Qualities	Control*	M-SC*	M-SBC*	M-STPP*
<b>pH (marinated pork)</b>	6.09 ± 0.12 <sup>c</sup>	6.17 ± 0.08 <sup>c</sup>	6.61 ± 0.04 <sup>a</sup>	6.39 ± 0.03 <sup>b</sup>
<b>pH (pre-cooked pork)</b>	6.52 ± 0.03 <sup>c</sup>	6.49 ± 0.02 <sup>c</sup>	7.13 ± 0.04 <sup>a</sup>	6.62 ± 0.05 <sup>b</sup>
<b>%Cooking loss (%CL)</b>	22.56 ± 0.13 <sup>a</sup>	22.54 ± 0.35 <sup>a</sup>	15.97 ± 0.19 <sup>c</sup>	18.39 ± 0.24 <sup>b</sup>
<b>%Cooking yield (%CY)</b>	73.56 ± 0.43 <sup>d</sup>	82.38 ± 0.35 <sup>c</sup>	89.61 ± 0.58 <sup>a</sup>	85.61 ± 0.49 <sup>b</sup>
<b>Pre-cooked pork color</b>				
- L*	66.97 ± 0.46 <sup>a</sup>	62.96 ± 0.43 <sup>b</sup>	61.80 ± 0.27 <sup>c</sup>	62.53 ± 0.30 <sup>b</sup>
- a*	1.28 ± 0.19 <sup>b</sup>	1.32 ± 0.24 <sup>b</sup>	1.90 ± 0.06 <sup>a</sup>	1.27 ± 0.14 <sup>b</sup>
- b*	11.06 ± 0.05 <sup>a</sup>	10.06 ± 0.09 <sup>d</sup>	10.50 ± 0.07 <sup>c</sup>	10.85 ± 0.13 <sup>b</sup>
- ΔE*	-	4.14 ± 0.40 <sup>b</sup>	5.24 ± 0.27 <sup>a</sup>	4.45 ± 0.30 <sup>b</sup>
<b>Pre-cooked pork texture</b>				
- Hardness (N)	83.99 ± 2.54 <sup>a</sup>	64.28 ± 0.40 <sup>b</sup>	45.02 ± 0.64 <sup>d</sup>	56.33 ± 1.02 <sup>c</sup>
- Springiness index	2.94 ± 0.17 <sup>a</sup>	2.11 ± 0.33 <sup>b</sup>	1.01 ± 0.01 <sup>c</sup>	1.42 ± 0.33 <sup>c</sup>
- Cohesiveness	0.65 ± 0.00 <sup>a</sup>	0.64 ± 0.01 <sup>b</sup>	0.63 ± 0.00 <sup>c</sup>	0.63 ± 0.00 <sup>c</sup>
- Chewiness (N)	160.84 ± 14.88 <sup>a</sup>	86.89 ± 14.90 <sup>b</sup>	28.46 ± 0.73 <sup>c</sup>	50.52 ± 12.56 <sup>c</sup>
- Shear force (N/mm.s)	20.28 ± 0.66 <sup>a</sup>	17.94 ± 0.40 <sup>b</sup>	16.32 ± 0.26 <sup>d</sup>	17.16 ± 0.13 <sup>c</sup>

\*Values within the same row with different superscript letters are significantly different ( $p \leq 0.05$ ).

Non-marinated pork serves as a control sample. M-SC, M-SBC and M-STPP are marinated pork treated with sodium chloride, sodium bicarbonate and sodium tripolyphosphate, respectively.

and shear force value, whereas no significant ( $p > 0.05$ ) differences in springiness index, cohesiveness and chewiness were found between M-SBC and M-STPP. In addition, negative correlations were observed ( $p \leq 0.01$ ) between pH of marinated pork and hardness ( $R^2 = -0.87$ ), springiness index ( $R^2 = -0.88$ ), cohesiveness ( $R^2 = -0.81$ ), chewiness ( $R^2 = -0.83$ ), and shear force ( $R^2 = -0.81$ ) (Table 2). The results indicated that higher pH improved textural characteristics of marinated pork after pre-cooking, making the pork softer. The results of this study were consistent with those conducted by Petracci *et al.* [26] who reported that the mechanism in improving texture of meat by sodium chloride solution might increase the protein solubility and fat emulsification of the meat without the effect of pH. Hence, sodium chloride solution had a lower power to improve the water holding capacity of marinated meat than those of the others. Both sodium bicarbonate and tripolyphosphate solutions were alkaline and could increase the negative charge of protein by increasing the pH away from the isoelectric point of myofibrillar proteins [27]. Kaewthong and Wattanachant [28] reported that the smaller size of  $\text{HCO}_3^-$  ions might penetrate into meat muscle and interact with many protein side-chains, resulting in more increased repulsive force among meat proteins, compared to  $(\text{P}_3\text{O}_{10})^{5-}$  ions. Therefore, sodium bicarbonate solution had a better ability to improve water holding capacity than that sodium tripolyphosphate solution. Moreover, sodium bicarbonate solution had a superior capacity to improve the pH of meat compared to that of sodium tripolyphosphate solution, which might be due to its higher buffering capacity [29]. Besides causing change in protein charge, sodium bicarbonate solution also released carbon dioxide during cooking process improving the ability to hold water by physical entrapment of water [30]. In addition, Sheard and Tali [10] showed air-filled pockets around fiber bundles and longitudinal splits of cooked pork loin treated with sodium bicarbonate, which led to dilution of the load-bearing element and reduction of the shear force value.

**Table 2.** Pearson's correlation coefficients of various qualities of pork

	pH marinated pork	pH pre- cooked	%CL	%CY	L*	a*	b*	$\Delta E^*$	Hard ness	Springi- ness index	Cohesive- ness	Chewi- ness	Shear force
pH (marinated pork)	1												
pH (pre- cooked pork)	0.87**	1											
%CL	-0.95**	-0.89**	1										
%CY	0.86**	0.73**	-0.85**	1									
L*	-0.74**	-0.55	0.69*	-0.96**	1								
a*	0.64*	0.85**	-0.69*	0.60*	-0.47	1							
b*	-0.11	-0.07	-0.04	-0.44	0.58*	-0.14	1						
$\Delta E^*$	0.73**	0.54	-0.68*	0.96**	-1.00**	0.48	-0.60*	1					
Hardness	-0.87**	-0.76**	0.87**	-1.00**	0.94**	-0.64*	0.42	-0.94**	1				
Springiness index	-0.88**	-0.74**	0.88**	-0.95**	0.89**	-0.65*	0.26	-0.89**	0.96**	1			
Cohesiveness	-0.81**	-0.69*	0.86**	-0.91**	0.85**	-0.59*	0.19	-0.84**	0.92**	0.94**	1		
Chewiness	-0.83**	-0.68*	0.84**	-0.98**	0.95**	-0.59*	0.38	-0.94**	0.98**	0.99**	0.94**	1	

---

Shear force	-0.81**	-0.67*	0.81**	-0.98**	0.96**	-0.57	0.45	-0.95**	0.98**	0.96**	0.93**	0.99**	1
-------------	---------	--------	--------	---------	--------	-------	------	---------	--------	--------	--------	--------	---

---

\*Correlation is significant at  $p \leq 0.05$ . \*\*Correlation is significant at  $p \leq 0.01$ .

### 3.2 Effect of marination on sensory evaluation

Marination improved liking scores of appearance, flavor, tenderness, juiciness and overall in the evaluation done by the elderly compared to those of the control (Table 3). M-SBC had significantly ( $p \leq 0.05$ ) the highest liking score of tenderness among all types of marinated pork, whereas liking scores of juiciness among all marinated pork types were not significantly different ( $p > 0.05$ ). However, Santos *et al.* [31] reported that juiciness and tenderness were positively correlated. Juiciness of marinated pork loins could be described by water loss reduction from exudation and cooking process treated with alkaline brines, positively affecting the sensory characteristics [31]. Furthermore, no difference in flavor liking scores were found between M-SBC and the control which were significantly ( $p \leq 0.05$ ) lower than those of M-SC and M-STPP. Marinated pork treated with sodium bicarbonate and non-marinated pork provided meaty flavor that was disliked by some elderly. Marinated pork treated with sodium chloride and sodium tripolyphosphate provided salty and soapy flavors, respectively. Similar results were found by Sheard and Tali [10], who observed a salty flavor in samples treated with salt alone or in combination and a slight soapy flavor in samples treated with phosphate. However, they found that there were no off-flavors in samples treated with bicarbonate. This suggested that concentration of marinade solutions should be sufficient to improve tenderness and juiciness without adversely affecting color, flavor and texture. In terms of JAR rating, all marinated pork received more than 70% JAR responses for each attribute, except for juiciness of M-SC as 66% JAR and -30% net score (data not shown). This result indicated that M-SC marinated pork was a little too juicy compared to the others. Therefore, marinated pork treated with sodium bicarbonate was selected to be used in the study of thermal processing in development of marinated pork stew for the elderly because it was effective in the improvement of pork quality.

**Table 3.** Sensory attributes of marinated pork and control after pre-cooking

Attributes	Control*	M-SC*	M-SBC*	M-STPP*
Appearance	6.22 ± 1.54 <sup>b</sup>	6.72 ± 1.34 <sup>a</sup>	6.90 ± 1.37 <sup>a</sup>	6.78 ± 1.47 <sup>a</sup>
Flavor	6.24 ± 1.32 <sup>b</sup>	6.70 ± 1.37 <sup>a</sup>	6.54 ± 1.42 <sup>ab</sup>	6.72 ± 1.28 <sup>a</sup>
Tenderness	6.06 ± 1.35 <sup>c</sup>	6.60 ± 1.18 <sup>b</sup>	7.08 ± 0.90 <sup>a</sup>	6.72 ± 1.23 <sup>b</sup>
Juiciness	6.02 ± 1.36 <sup>b</sup>	6.70 ± 1.23 <sup>a</sup>	7.02 ± 1.24 <sup>a</sup>	6.74 ± 1.35 <sup>a</sup>
Overall liking	6.06 ± 1.36 <sup>b</sup>	6.80 ± 1.14 <sup>a</sup>	7.14 ± 1.11 <sup>a</sup>	6.88 ± 1.26 <sup>a</sup>

\*Values within the same row with different superscript letters are significantly different ( $p \leq 0.05$ ). Non-marinated pork serves as a control sample. M-SC, M-SBC and M-STPP are marinated pork treated with sodium chloride, sodium bicarbonate and sodium tripolyphosphate, respectively.

### 3.3 Effect of thermal processing on physical changes in marinated pork stew

The heat penetration characteristics of marinated pork stew in retort pouch are shown in Figure 1. Experimental study of thermal processing indicated that  $F_0$  value of 6.0 was optimum to achieve commercial sterility of retort processed pork stew. The total processing time included 11 min for come-up time (CUT), 42 min for processing time and 39 min for cooling time. The results of microbiological analysis, TPC, yeast and mold, and coliforms were less than 10 cfu/g, 10 cfu/g and 3 MPN/g, respectively. Moreover, there were not detection of microbial growth at 35°C and

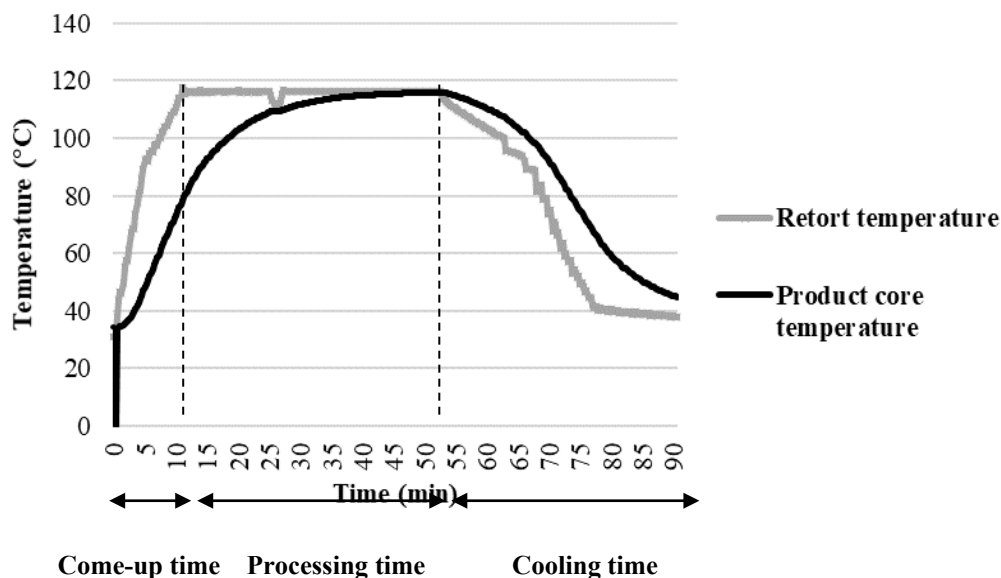


**Figure 1.** Heat penetration characteristics of marinated pork stew in retort pouch

55°C, *Staphylococcus aureus*, *Salmonella* spp. and *Clostridium botulinum* in marinated pork stew in retort pouch. According to Thai Food and Drug Administration (FDA), the  $F_0$  value used to sterilize low acidic foods must take at least 3 min to sufficiently kill *Clostridium botulinum* spores. Thermal processing of meat comes with changes in appearance, smell, taste and texture. Additionally, thermal processing also induced undesirable changes in meat quality, such as the loss of nutritional value caused by lipid oxidation and changes in composition of protein fraction [32].

The data in Table 4 shows physical changes of marinated pork stew in retort pouch after processing. Stew color showed significant ( $p \leq 0.05$ ) increase in  $L^*$  and  $b^*$  values, whereas  $a^*$  value was significant ( $p \leq 0.05$ ) decreased after processing. This indicated higher lightness and yellowness and lower redness of stew color compared to stew color before processing, resulting in visible color difference ( $\Delta E^*$ ). The release of moisture content of marinated pork into the stew during retort processing might have contributed to the lighter and yellower stew color.

The textural properties of marinated pork stew before and after processing are also shown in Table 4. The results showed that hardness, cohesiveness, chewiness and shear force value of marinated pork stew in retort pouch significantly decreased ( $p \leq 0.05$ ) after processing. However, there was no significant difference ( $p > 0.05$ ) in the springiness index of marinated pork stew in retort pouch after processing. This indicated that the pork product was softened owing to the effect of moist heat at high temperature. Girish *et al.* [12] also reported decrease in cohesiveness, chewiness, firmness and work of shear as well as increase in springiness index after retort processing of ready-to-eat pork curry product.

### 3.4 Effect of thermal processing on chemical changes in marinated pork stew

The proximate composition of marinated pork stew is shown in Table 5. Protein and fat contents increased after retort processing, which may be linked to a reduction in carbohydrate and ash

**Table 4.** Physical changes of marinated pork stew in retort pouch

Physical changes	Before processing*	After processing*
<b>Stew color</b>		
- L*	21.07 ± 0.03 <sup>b</sup>	29.13 ± 0.06 <sup>a</sup>
- a*	22.51 ± 0.03 <sup>a</sup>	21.86 ± 0.07 <sup>b</sup>
- b*	23.49 ± 0.24 <sup>b</sup>	29.24 ± 0.14 <sup>a</sup>
- ΔE*	-	9.92 ± 0.11
<b>Pork texture</b>		
- Hardness (N)	45.02 ± 0.64 <sup>a</sup>	27.04 ± 1.61 <sup>b</sup>
- Springiness index	1.01 ± 0.01 <sup>ns</sup>	0.94 ± 0.09 <sup>ns</sup>
- Cohesiveness	0.63 ± 0.01 <sup>a</sup>	0.28 ± 0.01 <sup>b</sup>
- Chewiness (N)	28.45 ± 0.73 <sup>a</sup>	7.21 ± 1.14 <sup>b</sup>
- Shear force (N/mm.s)	16.32 ± 0.27 <sup>a</sup>	7.30 ± 0.41 <sup>b</sup>

\*Mean values in the same row with different superscript letters are significantly different ( $p \leq 0.05$ ) by a paired t-test.

<sup>ns</sup> means that values in the same row are not significantly different ( $p > 0.05$ ).

**Table 5.** Chemical changes of marinated pork stew in retort pouch

Chemical changes	Before processing*	After processing*
Protein (g/100 g)	16.09 ± 0.12 <sup>b</sup>	16.42 ± 0.11 <sup>a</sup>
Fat (g/100 g)	1.25 ± 0.02 <sup>b</sup>	1.42 ± 0.04 <sup>a</sup>
Carbohydrate (g/100 g)	7.37 ± 0.31 <sup>a</sup>	6.90 ± 0.28 <sup>b</sup>
Ash (g/100 g)	1.36 ± 0.06 <sup>a</sup>	1.33 ± 0.01 <sup>b</sup>
Moisture content (%)	73.93 ± 0.21 <sup>ns</sup>	73.93 ± 0.21 <sup>ns</sup>
Water activity ( $a_w$ )	0.97 ± 0.00 <sup>ns</sup>	0.97 ± 0.00 <sup>ns</sup>
pH	5.72 ± 0.02 <sup>ns</sup>	5.74 ± 0.02 <sup>ns</sup>

\*Mean values in the same row with different superscript letters are significantly different ( $p \leq 0.05$ ) by a paired t-test.

<sup>ns</sup> means that values in the same row are not significantly different ( $p > 0.05$ ).

contents of the product. Thermal processing changed the complex meat system through the breakdown of muscle structure reflecting increased contents of protein and fat. This is in line with the assertion of Jiang *et al.* [33], who reported that prolonged high temperature cooking led to an increase in water-soluble protein contents due to the release of low molecular weight components in muscle. Girish *et al.* [12] also observed that water, soluble proteins and fats were displaced from the tissue when meat was cooked. Additionally, the results showed that there were no significant ( $p > 0.05$ ) changes in moisture content, water activity ( $a_w$ ) and pH after retort processing.

### 3.5 Acceptance and buying decision of marinated pork stew

Consumer acceptability scores of marinated pork stew by the elderly are presented in Figure 2. The overall liking score of this final product was liked moderately (7.56). In addition, acceptability scores for appearance, flavor, taste, tenderness and juiciness were also rated like moderately by elderly consumers as 7.22, 7.01, 7.11, 7.56 and 7.42, respectively. Ninety-four percent of the elderly consumers accepted the marinated pork stew in retort pouch. Eighty-six percent of the elderly consumers who responded “definitely would buy” and/or “probably would buy” were a measure of positive purchase intent for this product (data not shown). Thus, retort processing was used to alter texture of marinated pork in order to make the pork stew suitable for the elderly.

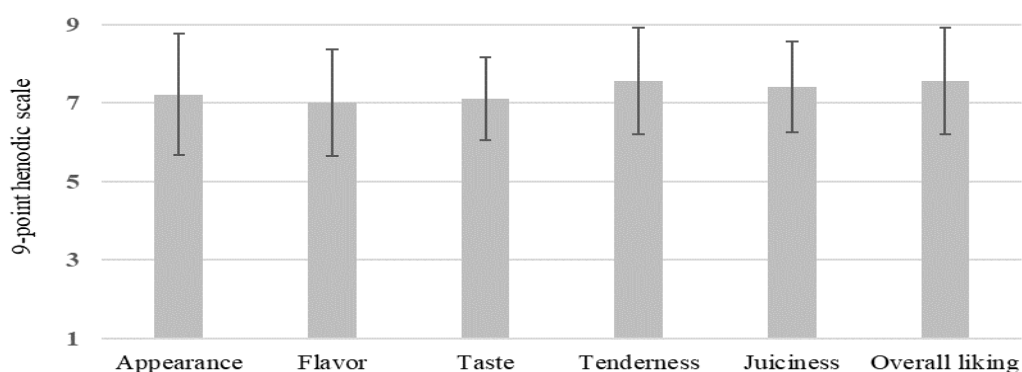


**Figure 2.** Consumer acceptance test of marinated pork stew in retort pouch

## 4. Conclusions

Based on the obtained results, pork meat showed quality improvement in color, cooking loss, cooking yield, texture and sensory characteristics after marinating with alkaline solutions, i.e. sodium chloride (M-SC), sodium bicarbonate (M-SBC) and sodium tripolyphosphate (M-STPP). M-SBC was the most effective for improving the texture of meat by raising its pH including hardness and shear force value. Furthermore, M-SBC marinated pork received the highest liking score of tenderness among all marinated pork types by the elderly. After retort processing of M-SBC pork, stew color had increased L\* and b\* values whereas it showed decreased a\* value. The texture of marinated pork had improved as indicated by decreasing in hardness, cohesiveness, chewiness and shear force value. Furthermore, protein content of marinated pork stew had increased after thermal processing. The marinated pork stew in retort pouch provided food properties suitable for the elderly.

## 5. Acknowledgements

The authors were grateful to the technical support of Department of Food Engineering, King Mongkut’s University of Technology Thonburi, Bangkok, Thailand.

## References

- [1] United Nations, 2019. *World Population Aging 2019*. [Online] Available at: <https://www.un.org/en/development/desa/population/publications/pdf/ageing/WorldPopulationAgeing2019-Highlights.pdf>
- [2] Neumann, L., Schauren, B.C. and Adami, F.S., 2016. Taste sensitivity of adults and elderly persons. *Revista Brasileira de Geriatria e Gerontologia*, 19(5), 797-808.
- [3] Sergi, G., Bano, G., Pizzato, S., Veronese, N. and Manzato, E., 2017. Taste loss in the elderly: possible implications for dietary habits. *Critical Reviews in Food Science and Nutrition*, 57(17), 3684-3689.
- [4] Wiriyawattana, P., Suwonsichon, S. and Suwonsichon, T., 2018. Effects of aging on taste threshold: a case of Asian people. *Journal of Sensory Studies*, 33(4), e12436, <https://doi.org/10.1111/joss.12436>
- [5] Gil-Montoya, J.A., de Mello, A.L., Barrios, R., Gonzalez-Moles, M.A. and Bravo, M., 2015. Oral health in the elderly patient and its impact on general well-being: a nonsystematic review. *Clinical Interventions in Aging*, 10, 461-467.
- [6] Elzerman, J.E., Hoek, A.C., van Boekel, M.A.J.S. and Luning, P.A., 2011. Consumer acceptance and appropriateness of meat substitutes in a meal context. *Food Quality and Preference*, 22(3), 233-240.
- [7] Vlahova-Vangelova, D.B., Dragoev, S.G., Balev, D.K., Assenova, B.K. and Amirhanov, K.J., 2017. Quality, microstructure, and technological properties of sheep meat marinated in three different ways. *Journal of Food Quality*, 2017(1), 5631532, <https://doi.org/10.1155/2017/5631532>
- [8] Serdaroglu, M., Abdraimov, K. and Onenc, A., 2007. The effects of marinating with citric acid solutions and grapefruit juice on cooking and eating quality of turkey breast. *Journal of Muscle Foods*, 18(2), 162-172.
- [9] Santos, V.M.O., Caldara, F.R., Seno, L.O., Feijó, G.L.D., Paz, I.C.L.A., Garcia, R.G., Nääs, I.A. and Altemio, A.C.D., 2012. Marinade with alkaline solutions for the improvement of pork quality. *Pesquisa Agropecuária Brasileira*, 47(11), 1655-1662.
- [10] Sheard, P.R. and Tali, A., 2004. Injection of salt, tripolyphosphate and bicarbonate marinade solutions to improve the yield and tenderness of cooked pork loin. *Meat Science*, 68(2), 305-311.
- [11] Gamage, H.G.C.L., Mutucumarana, R.K. and Andrew, M.S., 2017. Effect of marination method and holding time on physicochemical and sensory characteristics of broiler meat. *The Journal of Agricultural Sciences*, 12(3), 172-184.
- [12] Girish, P.S., Nath, L., Thomas, R. and Alam, T., 2018. Development of shelf stable ready-to-eat pork curry using retort processing technology. *Journal of Packaging Technology and Research*, 2(1), 61-66.
- [13] Devadason, I.P., Anjaneyulu, A.S.R., Mendiritta, S.K. and Murthy, T.R.K., 2014. Quality and shelf life of buffalo meat blocks processed in retort pouches. *Journal of Food Science and Technology*, 51(12), 3991-3997.
- [14] Rajan, S., Kulkarni, V.V. and Chandirasekaran, V., 2014. Preparation and storage stability of retort processed Chettinad chicken. *Journal of Food Science and Technology*, 51(1), 173-177.
- [15] Rajkumar, V., Dushyanthan, K. and Das, A.K., 2010. Retort pouch processing of Chettinad style goat meat curry-a heritage meat product. *Journal of Food Science and Technology*, 47(4), 372-379.

- [16] Muhlisin, M., Kim, D.S., Song, Y.R., Cho, Y.J., Kim, C.J., An, B.K., Kang, C.W. and Lee, S.K., 2013. Effect of cooking time and storage temperature on the quality of home-made retort pouch packed *Chuncheon Dakgalbi*. *Korean Journal for Food Science of Animal Resources*, 33(6), 737-743.
- [17] Cichero, J.A.Y., 2016. Adjustment of food textural properties for elderly patients. *Journal of Texture Studies*, 47(4), 277-283.
- [18] Klehm, B.J., King, D.A., Dilger, A.C., Shackelford, S.D. and Boler, D.D., 2018. Effect of packaging type during postmortem aging and degree of doneness on pork chop sensory traits of loins selected to vary in color and marbling. *Journal of Animal Science*, 96(5), 1736-1744.
- [19] Spitler, S. and Yoakam, L.R., 2014. *1,001 Delicious Soups and Stews: From Elegant Classics to Hearty One-pot Meals*. Chicago: Agate Publishing, Inc.
- [20] Stumbo, C.R., 1973, *Thermobacteriology in Food Processing*. 2<sup>nd</sup> ed. New York: Academic Press.
- [21] AOAC., 2000. *Official Methods of Analysis*. 17<sup>th</sup> ed. Gaithersburg: AOAC International.
- [22] Majumdar, R.K., Roy, D. and Saha, A., 2017. Textural and sensory characteristics of retort-processed freshwater prawn (*Macrobrachium rosenbergii*) in curry medium. *International Journal of Food Properties*, 20(11), 2487-2498.
- [23] Meilgaard, M., Civille, G.V. and Car, B.T., 2007. *Sensory Evaluation Techniques*. Boca Raton: CRC Press.
- [24] U.S. Food and Drug Administration (USFDA), 2007. *Bacteriological Analytical Manual*. [Online] Available at: <https://www.fda.gov/food/laboratory-methods-food/bacteriological-analytical-manual-bam>
- [25] Salfinger, Y. and Tortorello, M.L., 2015. *Compendium of Methods for the Microbiological Examination of Foods*. Washington: American Public Health Association.
- [26] Petracci, M., Bianchi, M., Mudalal, S. and Cavani, C., 2013. Functional ingredients for poultry meat products. *Trends in Food Science and Technology*, 33(1), 27-39.
- [27] Xiong, Y.L., 2012. Nonmeat ingredients and additives. In: Y.H. Hui, ed. *Handbook of Meat and Meat Processing*. Boca Raton: CRC Press, pp. 573-587.
- [28] Kaewthong, P. and Wattanachant, S., 2018. Optimizing the electrical conductivity of marinade solution for water-holding capacity of broiler breast meat. *Poultry Science*, 97(2), 701-708.
- [29] Sen, R.A., Naveena, B.M., Muthukumar, M., Babji, Y. and Murthy, T.R.K., 2005. Effect of chilling, polyphosphate and bicarbonate on quality characteristics of broiler breast meat. *British Poultry Science*, 46(4), 451-456.
- [30] Mudalal, S., Petracci, M., Tappi, S., Rocculi, P. and Cavani, C., 2014. Comparison between the quality traits of phosphate and bicarbonate-marinated chicken breast fillets cooked under different heat treatments. *Food and Nutrition Sciences*, 5(1), 35-44.
- [31] Santos, V.M.O., Caldara, F.R., Seno, L.O., Feijo, G.L.D., Almeida Paz, I.C.L., Garcia, R.G., Naas, I.A. and Altemio, A.D.C., 2012. Marinade with alkaline solutions for the improvement of pork quality. *Pesquisa Agropecuária Brasileira*, 47(11), 1655-1662.
- [32] Pathare, P.B. and Roskilly, A.P., 2016. Quality and Energy Evaluation in Meat Cooking. *Food Engineering Reviews*, 8(4), 435-447.
- [33] Jiang, Q., Han, J., Gao, P., Yu, L., Xu, Y. and Xia, W., 2018. Effect of heating temperature and duration on the texture and protein composition of Bighead Carp (*Aristichthys nobilis*) muscle. *International Journal of Food Properties*, 21(1), 2110-2120.

## Fourier Regression and ARIMAX Model for Forecasting Monthong Durian Price Index

Kanittha Yimnak<sup>1\*</sup> and Rungsarit Intaramo<sup>2</sup>

<sup>1</sup>Department of Applied Statistics, Faculty of Science and Technology,  
Rajamangala University of Technology Thanyaburi, Thailand

<sup>2</sup>Department of Mathematics, Faculty of Science, Thaksin University, Thailand

Received: 29 May 2020, Revised: 17 February 2021, Accepted: 6 April 2021

### Abstract

The purposes of this study were to create models for forecasting the Monthong durian price index at the farm and to compare the forecasting efficiency of ARIMAX model (Autoregressive Integrated Moving Average with Exogenous Variable model) and Fourier Regression model. The data set was collected monthly between January 2014 and December 2020 (a total of 84 months). Production index and China consumer confidence were used as explanatory variables. The efficiency of both methods was compared by Mean Absolute Percentage Error (MAPE). From the result, we found that the ARIMAX (1,1,1) and Fourier regression models were both suitable for forecasting the Monthong durian price index. However, the MAPE value obtained from the ARIMAX model was 3.365 times higher than that obtained from Fourier regression model, suggesting that the Fourier regression model is more efficient.

**Keywords:** Monthong durian price index; China consumer confidence; Fourier regression; ARIMAX model  
DOI 10.14456/cast.2021.57

### 1. Introduction

Durian is an important economic fruit of Thailand, especially Monthong durian. By around a decade ago, durian exports had been increased quickly. China has the greatest demand for durian [1] because it is a famous fruit in China. This increasing demand gave farmers the motivation to expand durian cultivation. The Office of Agricultural Economics in Thailand reported that durian production increased to 1,017,097 tons in year 2019 [2]. Monthong durian, a famous species that is grown in the eastern region of Thailand, has been increasingly cultivated because it has a good taste and attracts high prices in the market. Modelling for forecasting the Monthong durian price provides information that can help agricultural authorities and related parties to assist farmers. There are many factors (or exogenous variables) expected to affect the Monthong durian price index at the farm and these types of factors were used to construct the models such as the production index (PI) and China consumer confidence (CCC). PI and CCC are collected from the Office of Agricultural Economics, Thailand [3] and the National Bureau of Statistics of China [4], respectively. According

---

\*Correspondence author: Tel.: +66 86-4182542  
E-mail: kanittha\_y@rmutt.ac.th

to the market mechanism, excessive production affects the product prices, and the production index was chosen for constructing the model. Moreover, China consumer confidence is used as an explanatory variable because durian is a popular fruit in China. There are many methods for forecasting time series. The most popular method is Box Jenkins method using ARIMA model (Autoregressive Integrated Moving Average model). This modelling method is taken into the consideration of the correlation or the behavior of the data in the past for forecasting future data [5]. In addition, sometimes time series data may be affected by other factors (exogenous variable) that can influence the accuracy of the forecast value. Therefore, models for forecasting time series data have been developed based on other factors called ARIMAX model (Autoregressive Integrated Moving Average with Exogenous Variable model) [5, 6].

Regression model, one of the choices, is purposed to compare the efficacy of modelling. It is used for studying the correlation between independent variables and a dependent variable. There are three approaches for regression modelling such as parametric, semiparametric and nonparametric regression. The parametric regression model has rigorous assumption. A data set that does not correspond to the assumptions causes lower model performance [7]. On the other hand, there are no assumptions in the nonparametric regression model. For an unknown form of regression function (or a function curve), there are many functions proposed such as spline kernel, wavelet, local polynomial and Fourier. In this study, we used Fourier regression approach, proposed by Bilodea [8] for nonparametric and semiparametric cases. It is used for modelling because it can recognize datasets that have trigonometric pervading in the sine and cosine cases [7]. In addition, the dataset of the Monthong durian price index corresponds to Fourier approach. Fourier biresponse series was developed to estimate the nonparametric regression model by Semiati [9], and then Fourier series was applied for semiparametric regression [10].

## 2. Methodology

### 2.1 ARIMAX model

The ARIMAX model was presented by Tiao and Box [11]. This model was developed from the ARIMA model. The ARIMAX (p,d,q,r) model [6] can be written as:

$$(1 - B)^d (1 - \phi_1 B - \phi_2 B^2 - \dots - \phi_p B^p) Y_t = \theta_0 + (1 - \theta_1 B - \theta_2 B^2 - \dots - \theta_q B^q) \varepsilon_t + \sum_{i=1}^r \alpha_i X_{it}, \quad (1)$$

Where  $B$  is the backward shift operator.

$\phi_1, \dots, \phi_p$  are the parameters of the autoregressive part of model,

$\theta_0, \theta_1, \dots, \theta_q$  are the parameters of the moving average part,

$d$  is a number of times of order differencing,

$\nabla^d = (1 - B)^d$ ,

$(1 - \theta_1 B - \theta_2 B^2 - \dots - \theta_q B^q)$  is a moving average polynomial with order  $q$ ,

$(1 - \phi_1 B - \phi_2 B^2 - \dots - \phi_p B^p)$  is an autoregressive polynomial with order  $p$ ,

$\varepsilon_t$  are error terms,

$X_t$  is the value of the independent variable  $X$  at time  $t$ .

The steps for constructing the ARIMAX model [12] are presented as follows:

1) Test the stationary of the dependent series by correlogram of  $r_k$  and  $r_{kk}$  that are shown in equations (2) and (3) [6], respectively. The nonstationary respond series can be transformed by  $1^{st}, 2^{nd}, \dots, n^{th}$  differencing steps.

$$r_k = \frac{\sum_{t=1}^{n-k} (Y_t - \bar{Y})(Y_{t+k} - \bar{Y})}{\sum_{t=1}^n (Y_t - \bar{Y})^2} , \quad (2)$$

$$r_{kk} = \begin{cases} r_1 \\ \frac{r_k - \sum_{j=1}^{k-1} r_{k-1,j} r_{k-j}}{1 - \sum_{j=1}^k r_{k-1} r_j} \end{cases} , \quad (3)$$

2) Determine the order of the parameters  $p$  and  $q$  by considering the sample autocorrelation function (SACF) and the sample partial autocorrelation function (SPACF).

3) Estimate the coefficients using least square method (or maximum likelihood method) and test the significance along with the residual series.

4) Operate the same process to the input series as was done for the respond series.

5) Assign the structure of the ARIMAX model by approximating the cross-correlation coefficient between the response series and the input series to set the structure of the ARIMAX model.

6) Verify that the model coincides with the attributes of the time series data by creating diagnostic analysis. The suitability tests of the model are considered as follows:

6.1) The mean absolute percentage error (MAPE) and the square root of the mean square error (RMSE) with the smallest values as in the equations (4a) and (4b)

$$MAPE = \frac{1}{n} \sum_{t=1}^n \frac{|y_t - \hat{y}_t|}{y_t} \times 100 , \quad (4a)$$

$$RMSE = \sqrt{\frac{1}{n} \sum_{t=1}^n (y_t - \hat{y}_t)^2} , \quad (4b)$$

where  $y_t$  is the actual value at time  $t$  ,  $\hat{y}_t$  is the forecast value at the time  $t$  and  $n$  is the number of observations.

6.2)  $R^2$  is as follows:

$$R^2 = 1 - \frac{\frac{1}{n} \sum_{t=1}^n (y_t - \hat{y}_t)^2}{\frac{1}{n} (y_t - \bar{y})^2} \quad (5)$$

6.3) Box and Ljung or Q-statistic for testing the suitability of the model is as follows:

$$Q_m = n(n+2) \sum_{j=1}^m \left\{ \frac{r_k^2(e_t)}{(n-k)} \right\} , \quad (6)$$

where  $e_t$  is the forecasting error at time  $t$ ,

$n$  is the number of observations,

$m$  is the number of lags being tested.

The calculated  $Q$  value is the Chi-square distribution and has the degree of freedom equal to  $m - n$ . Under the null hypothesis, it can be said that the model does not have autocorrelation (or the term of estimated residual has a white noise appearance).

## 2.2 Fourier regression

Multiple regression is an analysis of the correlation between independent variables ( $x_{ji}; i = 1, 2, \dots, n, j = 1, 2, \dots, p$ ) and dependent variable ( $y_i; i = 1, 2, \dots, n$ ) as follows:

$$y_i = \beta_0 + \beta_1 x_{1i} + \beta_2 x_{2i} + \dots + \beta_j x_{ji} + \varepsilon_i \quad (7)$$

Where  $\varepsilon$  is the residual of the model. The residual  $\varepsilon \sim N(0, \sigma^2)$  is not reciprocally correlated. Parameter estimation can be solved by ordinary least square (OLS) method or maximum likelihood estimation (MLE) method [13]. The equation (7) can be written in matrix form as:

$$\mathbf{Y} = \mathbf{X}\boldsymbol{\beta} + \boldsymbol{\varepsilon} \quad (8)$$

where

$$Y = \begin{bmatrix} y_1 \\ y_2 \\ \vdots \\ y_n \end{bmatrix}_{n \times 1}; X = \begin{bmatrix} 1 & x_{11} & x_{12} & \dots & x_{1p} \\ 1 & x_{21} & x_{22} & \dots & x_{2p} \\ \vdots & \vdots & \vdots & \ddots & \vdots \\ 1 & x_{n1} & x_{n2} & \dots & x_{np} \end{bmatrix}_{n \times (p+1)}; \boldsymbol{\beta} = \begin{bmatrix} \beta_0 \\ \beta_1 \\ \vdots \\ \beta_p \end{bmatrix}_{(p+1) \times 1}; \boldsymbol{\varepsilon} = \begin{bmatrix} \varepsilon_1 \\ \varepsilon_2 \\ \vdots \\ \varepsilon_n \end{bmatrix}_{n \times 1}$$

For the nonparametric regression method, the curve shape which is presumed to be put within a certain functional shape, is used for constructing the correlation model for dependent and independent variables [14]. The Fourier regression model is as follows:

$$y_i = \eta(x_i) + \varepsilon_i \quad (9)$$

where  $\eta(x_i)$  that is the unknown shape is the regression curve. Moreover, it is presumed to be sleek on function space and  $x_i$  is explanatory variable. A trigonometric polynomial function, having a degree of flexibility to attune to the dataset, is a Fourier series as follows:

$$f(x) = \frac{1}{2} \alpha_0 + \gamma x + \sum_{k=1}^k \alpha_k \cos kx. \quad (10)$$

The equation (7) can be transformed as:

$$\mathbf{y} = \mathbf{f}(\mathbf{x}) + \boldsymbol{\varepsilon},$$

where

$f(x) = [f(x_{11}) \ f(x_{12}) \ \dots \ f(x_{1n}) \ f(x_{21}) \ f(x_{22}) \ \dots \ f(x_{2n}) \ \dots \ f(x_{p1}) \ f(x_{p2}) \ \dots \ f(x_{pn})]^T$ , and  $f(x_{ji})$ , curvilinear function can be solved by equation (11).

$$f(x) = \frac{1}{2} \alpha_0 + \gamma_j x_{ji} + (\alpha_{j1} \cos x_{ji} + \alpha_{j2} \cos 2x_{ji} + \dots + \alpha_{jk} \cos kx_{ji}) \quad (11)$$

Let  $\mathbf{f}(\mathbf{x}) = \mathbf{A}\boldsymbol{\theta}$ ,

$\mathbf{A} =$

$$\begin{bmatrix} 1 & x_{11} & \cos x_{11} & \cos 2x_{11} & \dots & \cos Kx_{11} & x_{21} & \cos x_{21} & \cos 2x_{21} & \dots & \cos Kx_{21} & \dots & x_{p1} & \cos x_{p1} & \cos 2x_{p1} & \dots & \cos Kx_{p1} \\ 1 & x_{12} & \cos x_{12} & \cos 2x_{12} & \dots & \cos Kx_{12} & x_{22} & \cos x_{22} & \cos 2x_{22} & \dots & \cos Kx_{22} & \dots & x_{p2} & \cos x_{p2} & \cos 2x_{p2} & \dots & \cos Kx_{p2} \\ \vdots & \vdots & \vdots & \vdots & \ddots & \vdots & \vdots & \vdots & \vdots & \ddots & \vdots & \ddots & \vdots & \vdots & \vdots & \ddots & \vdots \\ 1 & x_{1n} & \cos x_{1n} & \cos 2x_{1n} & \dots & \cos Kx_{1n} & x_{2n} & \cos x_{2n} & \cos 2x_{2n} & \dots & \cos Kx_{2n} & \dots & x_{pn} & \cos x_{pn} & \cos 2x_{pn} & \dots & \cos Kx_{pn} \end{bmatrix}_{n \times (p(K+1)+1)}$$

$$\theta = [\emptyset \ \gamma_1 \ \alpha_{11} \ \alpha_{12} \ \dots \ \alpha_{1K} \ \gamma_2 \ \alpha_{21} \ \alpha_{22} \ \dots \ \alpha_{2K} \ \dots \ \alpha_{1K} \ \gamma_p \ \alpha_{p1} \ \alpha_{p2} \ \dots \ \alpha_{pK}]^T_{1 \times (p(K+1)+1)}$$

where  $\emptyset = \frac{n}{2}\alpha_0$  and  $\alpha_0$  are constant. The OLS method is used to estimate nonparametric regression.  $\psi(\theta) = \varepsilon^T \varepsilon$  and  $\hat{\theta} = (A^T A)^{-1} A^T y$  are the estimations of nonparametric regression by the Fourier series [7]. Appropriate  $K$  values tend to be large. The most suitable  $K$  value indicates a better fit model.

### 3. Results and Discussion

The models of the ARIMAX and Fourier regression for forecasting Monthong durian price index are discussed as follows.

#### 3.1 ARIMAX model for forecasting the Monthong durian price index

Figure 1 represents the correlogram of the Monthong durian price index as being white noise or the residuals is the normal distribution. The probable orders of autoregressive and moving average ( $p$  and  $q$ ), which considered the values of ACF and PACF that are out of the 95% confidence range, are shown in Table 1. The suitable model for forecasting the Monthong durian price index was ARIMAX (1,1,1) due to having low errors and the highest stationary  $R^2$ . Considering the  $Q$ -statistics, the probability is greater than the significance level of 0.05, indicating that the error of the model has a normal distribution which means that it has a mean value of zero and constant variance.

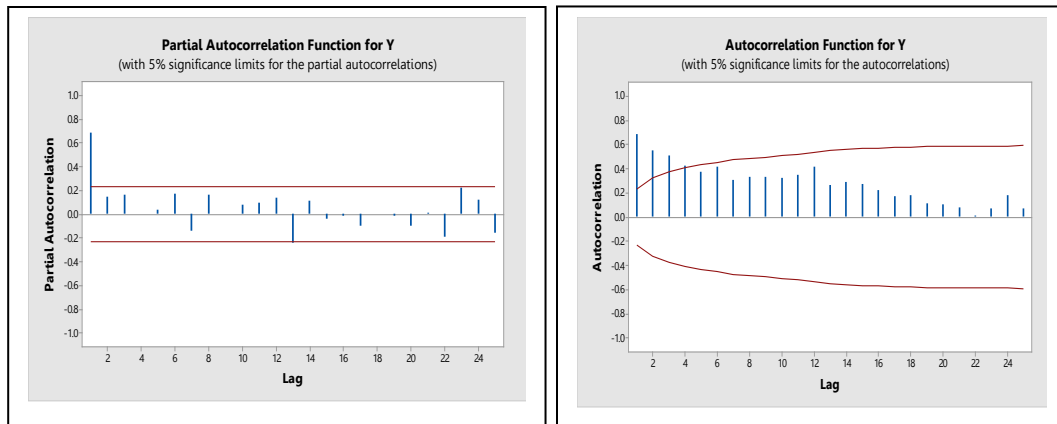


Figure 1. The correlogram of the Monthong durian price index

**Table 1.** ARIMAX parameter estimation

Model	Variable	Coefficient	t-statistic	p-value	R <sup>2</sup>	RMSE	MAPE	Q-statistic	p-value
ARIMAX (1,0,1)	AR(1)	.823	9.712	.000	0.705	77.884	14.879	23.055	0.112
	MA(1)	.125	.839	.404					
	$x_1$	-.298	-2.951	.004					
	$x_2$	3.330	9.313	.000					
ARIMAX (2,0,1)	AR(1)	1.552	7.372	.000	0.667	76.377	12.758	26.520	0.033
	AR(2)	-.557	-2.860	.005					
	MA(1)	.896	5.480	.000					
	$x_1$	-.275	-2.503	.014					
	$x_2$	3.103	2.338	.022					
ARIMAX (1,0,2)	AR(1)	.782	6.804	.000	0.650	78.340	14.929	22.406	0.098
	MA(1)	.074	.445	.658					
	MA(2)	-.079	-.527	.600					
	$x_1$	-.325	-2.996	.004					
	$x_2$	3.356	9.851	.000					
ARIMAX (1,1,0)	AR(1)	-0.295	-2.759	0.007	0.657	76.650	15.881	26.713	0.062
	$x_1$	-0.270	-4.276	0.000					
	$x_2$	0.318	3.665	0.000					
ARIIMAX (0,1,1)	MA(1)	.620	6.413	.000	0.687	73.217	15.881	20.360	.256
	$x_1$	-.200	-4.256	.000					
	$x_2$	.247	4.361	.000					
<b>ARIMAX (1,1,1)</b>	<b>AR(1)</b>	<b>.342</b>	<b>2.050</b>	<b>.044</b>	<b>0.705</b>	<b>71.491</b>	<b>15.148</b>	<b>19.710</b>	<b>0.234</b>
	<b>MA(1)</b>	<b>.908</b>	<b>6.685</b>	<b>.000</b>					
	<b><math>x_1</math></b>	<b>-.121</b>	<b>-1.979</b>	<b>.051</b>					
	<b><math>x_2</math></b>	<b>.159</b>	<b>2.279</b>	<b>.025</b>					

### 3.2 Fourier regression for forecasting the Monthong durian price index

Table 2 shows the MAPE and R<sup>2</sup> values when K=5, 10, 15, 20, 25, 30, 35, and 40, respectively. The optimum K value is K=40 as it has the lowest MAPE and the highest R<sup>2</sup>. Figure 2 shows the line of actual data and the line of the forecast of the Monthong durian price index by the Fourier regression method when K=10, 30, and 40, respectively. The forecast line with K=40 and the actual data line coincide closely.

**Table 2.** The values of K, MAPE and R<sup>2</sup> when K = 5,10,15,20,25,30,35 and 40

K	MAPE	R <sup>2</sup>	K	MAPE	R <sup>2</sup>
5	21.3369	0.5484	25	16.9538	0.7718
10	20.6831	0.6054	30	14.0312	0.8472
15	18.9405	0.6649	35	10.0862	0.9045
20	17.6595	0.7108	<b>40</b>	<b>4.5010</b>	<b>0.9776</b>

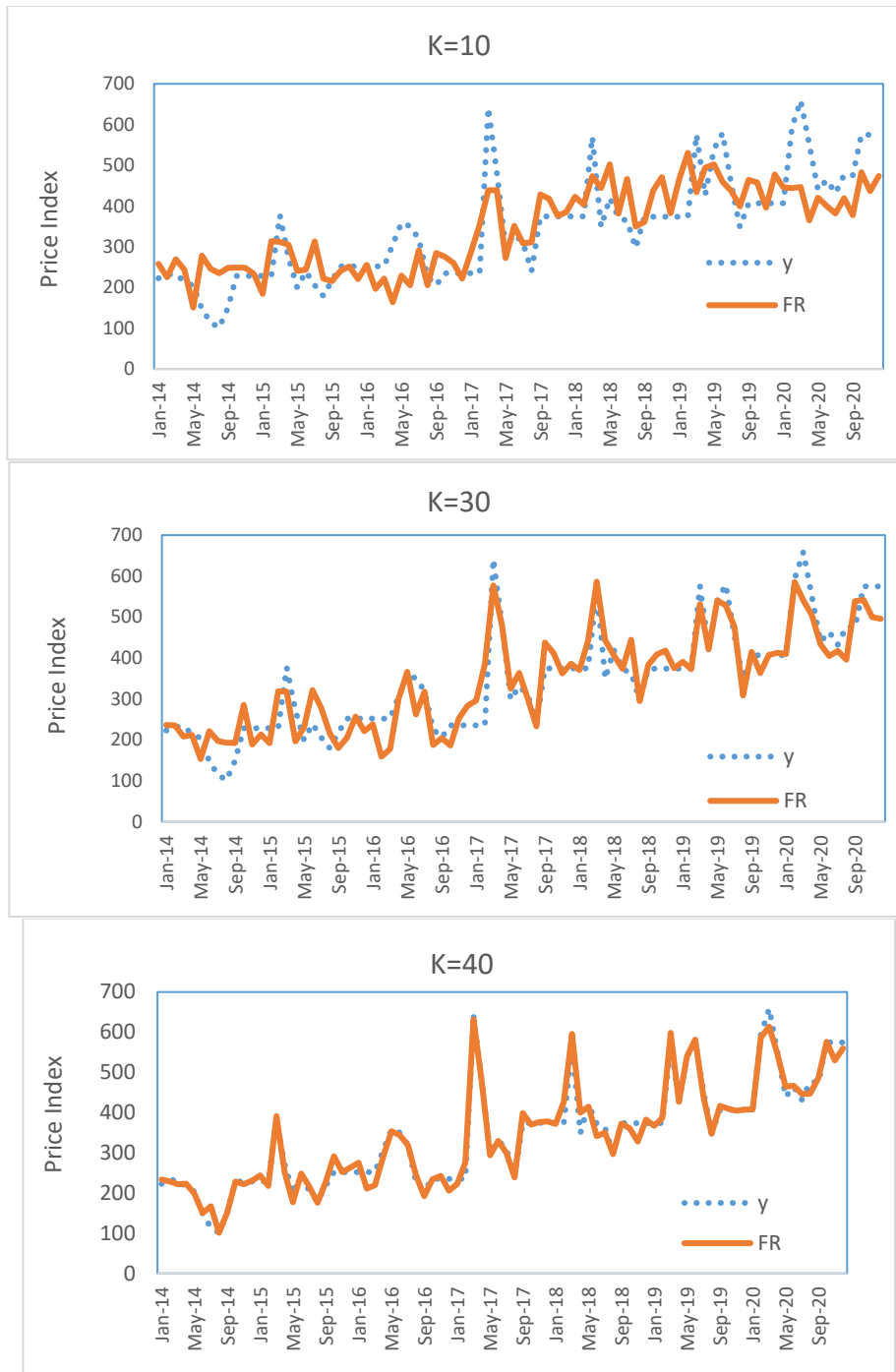


**Figure 2.** Graphs showing the comparison between the actual values (y) and the forecasted values using the Fourier regression (FR) when  $K=10, 30,$  and  $40$

Table 3 reveals the comparison of the MAPE between ARIMAX model and Fourier regression model and the line graphs of both models were coincided with the actual values (as can be seen in Figure 3). Although the ARIMAX model and Fourier regression model are the effective models for forecasting Monthong durian price index, the MAPE using ARIMAX model was 3.365 times more than Fourier regression model. Therefore, Fourier regression model is more accurate than ARIMAX model. However, Fourier regression model, nonparametric regression, used many parameters to fit the model.

**Table 3.** The comparison of MAPE between ARIMAX and Fourier regression models

Model	MAPE	Comparison ratio
ARIMAX	15.148	3.365 :1
Fourier Regression	4.5010	

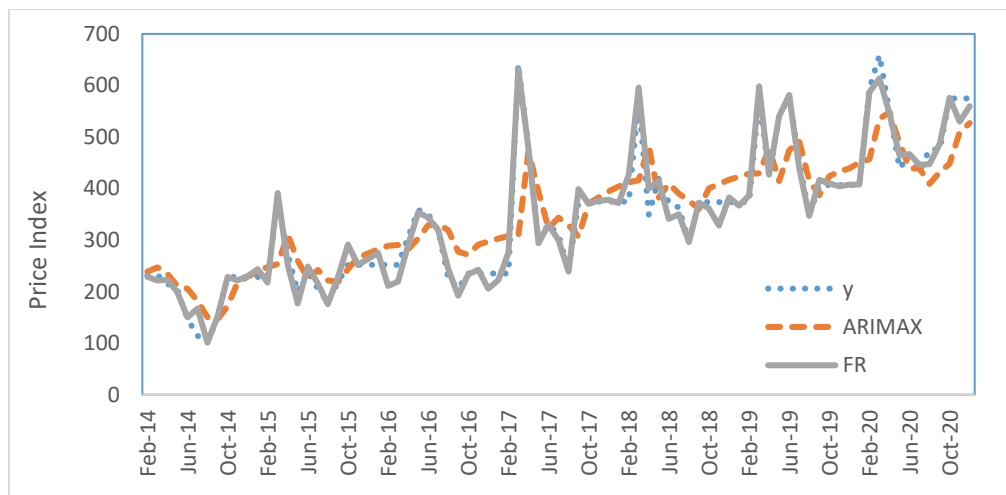


**Figure 3.** Graphs showing the actual values (y), the forecasted values of ARIMAX model (ARIMAX) and Fourier regression model (FR)

#### 4. Conclusions

This paper presents the comparison of the forecasting model efficiency between ARIMAX model and Fourier regression model for forecasting Monthong durian price index using the data set between January 2014 and December 2020. Production index and China consumer confidence were explanatory variables. The results show that both models have the performance for forecasting Monthong durian price index. Nevertheless, Fourier regression model provides the lower errors.

#### References

- [1] Isvilanonda, S., 2019. *The Situation of the World Production and Consumption of Durian and Thai Exports of Durian, Document Assembled in the Forum "Look at the future of Thai Export Durian Market"*. [online] Available at: <https://www.slideshare.net/somporn isvilanonda/durian-production-and-consumption-and-thailand-export-70619>

- [2] Office of Agricultural Economics, 2020. *Agricultural Production Index*. [online] Available at: [http://www.oae.go.th/assets/portals/1/fileups/aeocdata/files/Table1\\_th\\_agriPriceIndex\\_02\\_64.XLS](http://www.oae.go.th/assets/portals/1/fileups/aeocdata/files/Table1_th_agriPriceIndex_02_64.XLS)
- [3] Office of Agricultural Economics, 2020. *Agricultural Price Index*. [online] Available at: [http://www.oae.go.th/assets/portals/1/fileups/aeocdata/files/Table2\\_th\\_agriPriceIndex\\_02\\_64.XLS](http://www.oae.go.th/assets/portals/1/fileups/aeocdata/files/Table2_th_agriPriceIndex_02_64.XLS)
- [4] National Bureau of Statistics of China, 2020. *China Consumer Confidence*. [online] Available at: <https://tradingeconomics.com/china/consumer-confidence>
- [5] Dhakonlayodhin, B. and Areepong, Y., 2018. A comparison of forecasting models of stock price using ARIMA and ARIMAX models. *Huachiew Chalermprakiet Science and Technology Journal*, 4(1), 44-55.
- [6] Anggraeni, W., Vinarti, R. and Kurniawati, Y., 2015. Performance comparisons between Arima and Arimax method in moslem kids clothes demand forecasting: Case study. *Procedia Computer Science*, 72, 630-637.
- [7] Prahutama, A., Suparti and Utami, T.W., 2018. Modelling fourier regression for time series data- a case study: modelling inflation in foods sector in Indonesia. *Journal of Physics: Conference Series*, 974, 012067, <https://doi.org/10.1088/1742-6596/974/1/012067>
- [8] Bilodeau, M., 1992. Fourier Smoother and Additive Models. *The Canadian Journal of Statistics*, 3, 257-259.
- [9] Semiati, R., 2010. *Fourier Birespon Series Nonparametric Regression*. Thesis. ITS, Surabaya.
- [10] Asrini, L.J., 2012. Fourier series parametric regression. *Proceedings of the National Seminar FMIPA Universitas Negeri Surabaya*, 24 November 2012, Surabaya, Indonesia, pp. 77-80.
- [11] Tiao, G.C. and Box, G.E.P., 1981. Modelling multiple time series with applications. *Journal of the American Statistical Association*, 76(376), 802-816.
- [12] Yang, M., Xie, J., Mao, P., Wang, C. and Ye, Z., 2017. Application of the ARIMAX model on forecasting freeway traffic flow. *17<sup>th</sup> COTA International Conference of Transportation Professionals*, 7-9 July 2017, Shanghai, China.
- [13] Drapper, N.R and Smith, H., 1992. *Applied Regression Analysis*. 2<sup>nd</sup> ed. New York: Marcel Dekker.
- [14] Eubank, R.L., 1988. *Spline Smoothing and Nonparametric Regression*. New York: Marcel Dekker.

## Two-sample Location Tests under Violation of the Normality and Variance Homogeneity Assumptions

Mongkol Leelaphaiboon<sup>1</sup> and Bumrungsak Phuenaree<sup>2\*</sup>

<sup>1</sup>Department of Applied Mathematics and Statistics, Faculty of Sciences and Liberal Arts, Rajamangala University of Technology Isan, Nakhonratchasima, Thailand

<sup>2</sup>Department of Mathematics, Faculty of Science, Burapha University, Chonburi, Thailand

Received: 26 November 2020, Revised: 15 March 2021, Accepted: 8 April 2021

### Abstract

In this research, the performance of four test statistics, the independent  $t$ -test, Welch's  $t$ -test, the Mann-Whitney test and the permutation test, were compared under combined violations of normality and homogeneity of variance. In a simulation study, we generated data from symmetric and asymmetric distributions. The results showed that all methods displayed reliable results in terms of protecting type I error rates at the nominal level, except for the Mann-Whitney test which provides an inflation of type I error rates. Considering the power of the tests for symmetric distributions with the homogeneity of variances, the independent  $t$ -test is the best test when the sample data are drawn from normal and uniform distributions, while the Mann-Whitney test is the most powerful for the logistic and Laplace distributions. With symmetric distributions in heterogeneity of variance cases, the permutation test is the most powerful test. For gamma distribution, the permutation test is the best test. In addition, this test is also the best option for the low degree of skewness for Log-normal distribution.

**Keywords:** permutation test; Welch's  $t$ -test; Mann-Whitney test; statistical power; type I error  
DOI 10.14456/cast.2021.58

### 1. Introduction

Two sample  $t$ -test is one of the most frequently used approach in statistics. This method is a test of equality of two means. There are three conditions: a) normality assumption b) homogeneity of variances and c) independence of samples, that need to be examined before using this test. The independent  $t$ -test is derived under an equal variance situation. If two samples have an unequal variance, Welch's  $t$ -test is generally preferred.

Both independent  $t$ -test and Welch's  $t$ -test are robust tests when the first two assumptions were violated. However, there is no guarantee that  $t$ -test is the most powerful [1] and in this case, the other methods that non-parametric alternative approach should be performed. Mann-Whitney test is one of the most commonly used non-parametric statistical test for two samples. This test can

---

\*Corresponding author: E-mail: bumrungsak@buu.ac.th

be used when the distributions are unknown; in other words, there is no normality assumption. Therefore, non-parametric tests are also called distribution free.

One of the non-parametric statistics that can be used to compute the sampling distribution for all test statistics is the permutation test. The permutation test does not need any assumptions. It gives a simple way to find the sampling distribution for all test statistics. If the null hypothesis is true, any observations from one group can be permuted to the other. The permutation test can be applied to many parametric statistics. In order to examine this test, the sampling distribution of the difference in means of two groups is considered in this work.

In some fields of research, especially in medical work and psychological data, the assumptions of normality and homogeneity of variance are often violated [1, 2]. Thus, the main purpose of this work is to compare the performance of four test statistics: the independent  $t$ -test, Welch's  $t$ -test, the Mann-Whitney test and the permutation test in order to figure out the best testing procedure. The non-normal data used in this study are symmetric and asymmetric distributions with varying degrees of standard deviation ratios.

## 2. Materials and Methods

This research studies four methods; the independent  $t$ -test, Welch's  $t$ -test, Mann-Whitney test and the permutation test, all of which can be used to compare location parameters in two populations. Consider two groups A and B. Let  $X_1, X_2, \dots, X_n$  be the observations of A, and  $Y_1, Y_2, \dots, Y_n$  be the observations of B. The details of each test are as follows.

### 2.1 Independent $t$ -test

The independent two sample  $t$ -test is always used to compare two means when the population variances are equal. This test can be calculated as follows [2];

$$t = \frac{\bar{X} - \bar{Y}}{\sqrt{S_p^2 \left( \frac{1}{n_X} + \frac{1}{n_Y} \right)}} \sim t_{n_X + n_Y - 2} \quad (1)$$

$$S_p^2 = \frac{(n_X - 1)S_X^2 + (n_Y - 1)S_Y^2}{n_X + n_Y - 2}$$

where  $\bar{X}$  and  $\bar{Y}$  are the sample means,  $S_X^2$  and  $S_Y^2$  are the sample variances, and  $n_X$  and  $n_Y$  are the sample sizes.

### 2.2 Welch's $t$ -test

The Welch's  $t$ -test is used to compare two means in the case of unequal variances [2]. This test is computed using the formula below:

$$W = \frac{\bar{X} - \bar{Y}}{\sqrt{\frac{S_X^2}{n_X} + \frac{S_Y^2}{n_Y}}} \sim t_\nu \quad (2)$$

where  $\bar{X}$  and  $\bar{Y}$  are the sample means,  $S_X^2$  and  $S_Y^2$  are the sample variances, and  $n_X$  and  $n_Y$  are the sample sizes.

The degree of freedom ( $\nu$ ) is given by [2]

$$\nu = \left( \frac{S_X^2}{n_X} + \frac{S_Y^2}{n_Y} \right)^2 \left( \frac{S_X^4}{n_X^3 - n_X^2} + \frac{S_Y^4}{n_Y^3 - n_Y^2} \right)^{-1} \quad (3)$$

### 2.3 Mann-Whitney test

The Mann-Whitney test (MW) is a nonparametric test that is used when the two samples are not drawn from the normal distribution [3]. This test involves calculating

$$MW = \min(U_X, U_Y) \quad (4)$$

$$U_X = n_X n_Y + n_X(n_X + 1) / 2 - R_X$$

$$U_Y = n_X n_Y + n_Y(n_Y + 1) / 2 - R_Y$$

where  $n_X$  and  $n_Y$  are the sample sizes of the first and the second groups respectively, and  $R_X$  and  $R_Y$  are the sum of the ranks in samples X and Y.

When the observations are large enough, the statistic  $MW$  is approximately normal distributed with mean  $n_X n_Y / 2$  and variance  $n_X n_Y (n_X + n_Y + 1) / 12$ . The test statistic becomes

$$z = \left( MW - \frac{n_X n_Y}{2} \right) \left( \sqrt{\frac{n_X n_Y (n_X + n_Y + 1)}{12}} \right)^{-1} \quad (5)$$

### 2.4 Permutation test

Suppose that  $X_1, X_2, \dots, X_{n_X}$  and  $Y_1, Y_2, \dots, Y_{n_Y}$  are  $n_X + n_Y = N$  random samples from the first and the second groups, respectively. Considering  $N$  samples for this study, the  $n_X$  are randomly assigned to the first group, whereas the remaining  $N - n_X$  will be assigned to the other group. There are  $\binom{N}{n_X}$  possible randomizations. Then computed the difference in means,  $D = \bar{X} - \bar{Y}$  for each of these randomizations [4]. The p-value can be calculated as

$$p\text{-value} = P(|D_i| \geq |D^*|) = \frac{\sum_{i=1}^{\binom{N}{n_X}} I(|D_i| \geq |D^*|)}{\binom{N}{n_X}} \quad (6)$$

where  $D_i$  difference in means for  $i$  th randomization and  $D^*$  is the difference in means of the observations. But if the samples are large, for example, if there are 10 observations in each sample,

then over 184,000 randomizations are possible;  $\binom{20}{10} = 184,756$ . It is not easy to obtain all permutations in a short run-time computer program, so the p-value can be estimated with the Monte Carlo sampling from the permutation distribution [4]. The approximate p-value is

$$\hat{p} = \frac{1 + \sum_{i=1}^B I(|D_i| \geq |D^*|)}{B + 1} \quad (7)$$

where  $B$  is permutation replications.

### 2.5 Simulation Study

This section provides simulation case studies for the type I error rates and the test powers of four statistics; the independent  $t$ -test (T), Welch's  $t$ -test (WT), the Mann-Whitney test (MW) and the permutation test (PER). The data were generated under six sampling distributions; normal, uniform, logistic, Laplace, gamma and lognormal distributions with balance sample sizes;  $n = 10, 15, 20, 25, 30, 50$  and  $100$ .

In order to examine the power of the test, two sets of the difference in parameters ( $\Delta$ ) were considered. The first set was  $\{0, 1, 2\}$ ; location parameters for symmetric data, and the second set was  $\{0, 0.25, 0.50, 0.75\}$ ; shape and scale parameters for skewed data. The effect of unequal variances for symmetric distributions were considered by defining the standard deviation ratios. These values were 1.0, 1.5, 2.0 and 2.5. The coefficients of skewness for gamma and lognormal distributions were 1 and 2. The summary of all distribution simulation cases are shown in Tables 1 and 2.

In this study, the Monte Carlo technique was performed using R version 3.4.1 [5]. The simulation and permutation trials were 10,000 and 2,000 respectively. The results for type I error rates and test powers are shown in Tables 3 -13.

**Table 1.** Summary of symmetric distribution simulation cases

Sampling distribution	Normal, Uniform, Logistic, Laplace
Difference in location parameters (means)	$\Delta = 0, 1, 2$
Standard deviation ratios	1.0, 1.5, 2.0, 2.5
Method	T, WT, MW, PER
Equal sample sizes	10, 15, 20, 25, 30, 50, 100
Significance level	0.05

**Table 2.** Summary of skew distribution simulation cases

Sampling distribution	Gamma, Lognormal
Coefficient of skewness	1, 2
Difference in parameters	$\Delta = 0, 0.25, 0.50, 0.75$
Gamma ( $\alpha, \beta$ ) *	Group 1; Gamma ( $\alpha, \beta$ )
$\beta = 1$	Group 2; Gamma ( $\alpha, \beta + \Delta$ )
Lognormal ( $\mu, \sigma^2$ ) **	Group 1; Lognormal ( $\mu, \sigma^2$ )
$\mu = 1$	Group 2; Lognormal ( $\mu + \Delta, \sigma^2$ )
Method	WT, MW, PER
▪ Equal sample sizes	10, 15, 20, 25, 30, 50, 100
▪ Significance level	0.05

\* Gamma ( $\alpha, \beta$ );  $\alpha$  and  $\beta$  are shape and scale parameters respectively.

\*\* Lognormal ( $\mu, \sigma^2$ );  $\mu$  and  $\sigma^2$  are location and shape parameters respectively.

\*\*\*Both shape parameters;  $\alpha$  and  $\sigma^2$ , are defined as the coefficients of skewness.

### 3. Results and Discussion

For each studied situation, two criteria were used to examine the efficiency tests. The first criterion was the type I error rates ( $\hat{\alpha}$ ), which should be close to the significance level of 0.05. The criterion of robustness was established on the Cochran's limit, that is  $0.04 \leq \hat{\alpha} \leq 0.06$  for this work [6]. If the type I error rates are in this interval, it can be assumed that the rates are sufficiently close to the nominal level.

The second criterion was the power of the test. The methods that have the highest power are considered as the best among all the methods.

#### 3.1 Type I error rates

In Tables 3, 4 and 7, it can be seen that type I error rates fell well within the range of Cochran's criteria. This implies that the rates for all test statistics are maintained near the nominal level regardless of the distribution shapes and sample sizes. In other words, they provide appropriate control of the type I error probability.

As seen in Tables 5 and 6, the type I error rates of the Mann-Whitney test increased when the variance ratio became larger. In other words, the Mann-Whitney test provides the inflation of type I error [7]. This type of results reveals the problem of this test. If the samples are selected randomly from two populations with the same means but with different variances, the type I error rates are far from the significance level in many cases. It shows the problem of lack of robustness of this test. In other words, the Mann-Whitney test is sensitive to population differences [8, 9]. Therefore, the Mann-Whitney test is not investigated in terms of the power values in these situations.

### 3.2 Power of the test

#### 3.2.1 Symmetric Distribution in homogeneity of variance cases

Table 8 illustrates the power values of all tests for normal and uniform distributions. It can be clearly seen that all cases of the independent *t*-test have the highest power values. Moreover, the powers of all test are the same when the mean difference is 2 ( $\Delta = 2$ ) and the sample sizes are greater than 15.

The details of the comparative study for logistic and Laplace distributions are shown in Table 9. The power of Mann-Whitney test is the highest when the mean difference is 1. However, all tests are powerful when the mean difference is 2 ( $\Delta = 2$ ) and the sample sizes are greater than 20.

With the heterogeneity of variance in Tables 10 and 11, almost all cases of the permutation test have the highest power values. However, both tests are powerful when the sample sizes become large.

**Table 3.** Type I error rates for normal and logistic distributions in homogeneity of variance cases

n	Normal			Logistic		
	T	MW	PER	T	MW	PER
10	0.0491	0.0465	0.0514	0.0484	0.0430	0.0489
15	0.0527	0.0470	0.0518	0.0486	0.0469	0.0494
20	0.0485	0.0485	0.0483	0.0476	0.0462	0.0479
25	0.0519	0.0483	0.0508	0.0498	0.0482	0.0501
30	0.0495	0.0494	0.0494	0.0511	0.0491	0.0504
50	0.0466	0.0483	0.0467	0.0517	0.0484	0.0503
100	0.0535	0.0545	0.0534	0.0507	0.0479	0.0511

**Table 4.** Type I error rates for uniform and Laplace distributions in homogeneity of variance cases

n	Uniform			Laplace		
	T	MW	PER	T	MW	PER
10	0.0536	0.0430	0.0524	0.0461	0.0414	0.0499
15	0.0494	0.0424	0.0487	0.0525	0.0508	0.0540
20	0.0503	0.0486	0.0493	0.0499	0.0491	0.0504
25	0.0496	0.0495	0.0497	0.0510	0.0513	0.0528
30	0.0526	0.0524	0.0521	0.0528	0.0532	0.0553
50	0.0485	0.0488	0.0489	0.0476	0.0513	0.0480
100	0.0484	0.0486	0.0480	0.0492	0.0511	0.0488

**Table 5.** Type I error rates for normal and logistic distributions in heterogeneity of variance cases

$\frac{\sigma_2}{\sigma_1}$	n	Normal			Logistic		
		WT	MW	PER	WT	MW	PER
1.5	10	0.0497	0.0445	0.0520	0.0450	0.0454	0.0497
	15	0.0506	0.0516	0.0528	0.0494	0.0477	0.0518
	20	0.0496	0.0511	0.0516	0.0441	0.0513	0.0458
	25	0.0507	0.0535	0.0511	0.0515	0.0531	0.0521
	30	0.0512	0.0540	0.0521	0.0503	0.0530	0.0533
	50	0.0449	0.0449	0.0453	0.0507	0.0524	0.0513
	100	0.0534	0.0557	0.0532	0.0498	0.0533	0.0511
2.0	10	0.0457	0.0475	0.0501	0.0452	0.0466	0.0526
	15	0.0442	0.0484	0.0479	0.0439	0.0460	0.0503
	20	0.0464	0.0571	0.0490	0.0496	0.0598	0.0531
	25	0.0516	0.0585	0.0540	0.0500	0.0574	0.0538
	30	0.0493	0.0590	0.0508	0.0467	0.0582	0.0500
	50	0.0524	0.0585	0.0529	0.0473	0.0578	0.0490
	100	0.0471	0.0577	0.0473	0.0525	0.0601	0.0517
2.5	10	0.0483	0.0568	0.0562	0.0555	0.0561	0.0576
	15	0.0515	0.0581	0.0560	0.0482	0.0567	0.0569
	20	0.0482	0.0611	0.0527	0.0486	0.0498	0.0510
	25	0.0510	0.0638	0.0543	0.0501	0.0664	0.0545
	30	0.0480	0.0620	0.0504	0.0486	0.0598	0.0517
	50	0.0510	0.0633	0.0534	0.0486	0.0616	0.0503
	100	0.0493	0.0627	0.0497	0.0513	0.0638	0.0518

**Table 6.** Type I error rates for uniform and Laplace distributions in heterogeneity of variance cases

$\frac{\sigma_2}{\sigma_1}$	n	Uniform			Laplace		
		WT	MW	PER	WT	MW	PER
1.5	10	0.0514	0.0491	0.0517	0.0414	0.0418	0.0486
	15	0.0502	0.0516	0.0511	0.0480	0.0477	0.0526
	20	0.0504	0.0562	0.0506	0.0478	0.0514	0.0526
	25	0.0561	0.0614	0.0560	0.0471	0.0515	0.0499
	30	0.0498	0.0559	0.0502	0.0488	0.0509	0.0501
	50	0.0529	0.0595	0.0532	0.0488	0.0528	0.0504
	100	0.0494	0.0558	0.0499	0.0457	0.0470	0.0455
2.0	10	0.0540	0.0566	0.0557	0.0401	0.0466	0.0515
	15	0.0540	0.0630	0.0580	0.0449	0.0502	0.0517
	20	0.0563	0.0633	0.0555	0.0481	0.0542	0.0525
	25	0.0453	0.0586	0.0468	0.0488	0.0572	0.0533
	30	0.0518	0.0647	0.0526	0.0488	0.0515	0.0514
	50	0.0491	0.0644	0.0491	0.0452	0.0546	0.0483
	100	0.0458	0.0615	0.0464	0.0487	0.0548	0.0503
2.5	10	0.0554	0.0610	0.0597	0.0469	0.0484	0.0528
	15	0.0535	0.0672	0.0578	0.0457	0.0510	0.0560
	20	0.0517	0.0682	0.0547	0.0482	0.0580	0.0545
	25	0.0496	0.0699	0.0525	0.0490	0.0572	0.0541
	30	0.0502	0.0707	0.0533	0.0452	0.0563	0.0509
	50	0.0529	0.0700	0.0543	0.0472	0.0615	0.0496
	100	0.0500	0.0706	0.0500	0.0513	0.0589	0.0526

**Table 7.** Type I error rates for skewed distribution

Skewness	n	Gamma			Lognormal		
		WT	MW	PER	WT	MW	PER
1	10	0.0445	0.0427	0.0510	0.0492	0.0461	0.054
	15	0.0496	0.0466	0.0533	0.0471	0.0441	0.0493
	20	0.0480	0.0471	0.0500	0.0531	0.0527	0.0541
	25	0.0468	0.0478	0.0478	0.0522	0.0489	0.0523
	30	0.0506	0.0525	0.0518	0.0510	0.0512	0.0519
	50	0.0483	0.0483	0.0494	0.0518	0.0509	0.0520
	100	0.0536	0.0513	0.0544	0.0501	0.0510	0.0493
2	10	0.0405	0.0459	0.0497	0.0407	0.0434	0.0509
	15	0.0426	0.0445	0.0501	0.0439	0.0447	0.0504
	20	0.0451	0.0517	0.0505	0.0461	0.0497	0.0520
	25	0.0478	0.0509	0.0507	0.0452	0.0481	0.0483
	30	0.0465	0.0462	0.0502	0.0464	0.0489	0.0494
	50	0.0465	0.0501	0.0486	0.0513	0.0502	0.0524
	100	0.0490	0.0516	0.0497	0.0478	0.0503	0.0487

**Table 8.** Power values for normal and uniform distributions in homogeneity of variance cases

n	$\Delta = 1$					
	Normal			Uniform		
	T	MW	PER	T	MW	PER
10	0.5645*	0.5126	0.5633	0.5381*	0.4632	0.5365
15	0.7553*	0.7171	0.7543	0.7502*	0.6675	0.7487
20	0.8646*	0.8440	0.8639	0.8721*	0.8080	0.8711
25	0.9334*	0.9211	0.9327	0.9397*	0.8869	0.9379
30	0.9686*	0.9602	0.9684	0.9714*	0.9402	0.9701
50	0.9979*	0.9973	0.9979*	0.9991*	0.9947	0.9989
100	1.0000*	1.0000*	1.0000*	1.0000*	1.0000*	1.0000*
n	$\Delta = 2$					
	Normal			Uniform		
	T	MW	PER	T	MW	PER
10	0.9884*	0.9805	0.9881	0.9933*	0.9712	0.9930
15	0.9992*	0.9991	0.9992*	1.0000*	0.9975	1.0000*
20	1.0000*	1.0000*	1.0000*	1.0000*	1.0000*	1.0000*
25	1.0000*	1.0000*	1.0000*	1.0000*	1.0000*	1.0000*
30	1.0000*	1.0000*	1.0000*	1.0000*	1.0000*	1.0000*
50	1.0000*	1.0000*	1.0000*	1.0000*	1.0000*	1.0000*
100	1.0000*	1.0000*	1.0000*	1.0000*	1.0000*	1.0000*

\* Tests with the highest power value

**Table 9.** Power values for logistic and Laplace distributions in homogeneity of variance cases

n	$\Delta = 1$					
	Logistic			Laplace		
	T	MW	PER	T	MW	PER
10	0.5722	0.5545*	0.5743	0.5892	0.6216*	0.5942
15	0.7542	0.7572*	0.7537	0.7588	0.8213*	0.7609
20	0.8672	0.8837*	0.8670	0.8661	0.9283*	0.8661
25	0.9319	0.9453*	0.9320	0.9272	0.9714*	0.9286
30	0.9699	0.9774*	0.9702	0.9605	0.9900*	0.9610
50	0.9977	0.9992*	0.9977	0.9979	0.9997*	0.9977
100	1.0000*	1.0000*	1.0000*	1.0000*	1.0000*	1.0000*
n	$\Delta = 2$					
	Logistic			Laplace		
	T	MW	PER	T	MW	PER
10	0.9834*	0.9817	0.9834*	0.9751	0.9785*	0.9752
15	0.9988	0.9995*	0.9988	0.9982	0.9987*	0.9983
20	1.0000*	0.9999	1.0000*	0.9996	1.0000*	0.9996
25	1.0000*	1.0000*	1.0000*	1.0000*	1.0000*	1.0000*
30	1.0000*	1.0000*	1.0000*	1.0000*	1.0000*	1.0000*
50	1.0000*	1.0000*	1.0000*	1.0000*	1.0000*	1.0000*
100	1.0000*	1.0000*	1.0000*	1.0000*	1.0000*	1.0000*

\* Tests with the highest power value

**Table 10.** Power values for symmetric distribution in heterogeneity of variance cases with  $\Delta = 1$

$\sigma_2$	Normal		Logistic		Uniform		Laplace		
$\sigma_1$	n	WT	PER	WT	PER	WT	PER	WT	PER
1.5	10	0.3831	0.3949*	0.3889	0.4036*	0.3503	0.3541*	0.4177	0.4385*
	15	0.5426	0.5475*	0.5440	0.5518*	0.5171	0.5187*	0.5696	0.5815*
	20	0.6727	0.6754*	0.6733	0.6777*	0.6644	0.6655*	0.6872	0.6961*
	25	0.7729	0.7742*	0.7717	0.7742*	0.7680	0.7684*	0.7757	0.7833*
	30	0.8414	0.8430*	0.8496	0.8511*	0.8477	0.8490*	0.8395	0.8417*
	50	0.9720	0.9722*	0.9687	0.9692*	0.9762	0.9765*	0.9712	0.9713*
	100	0.9996*	0.9996*	0.9998*	0.9997	0.9999*	0.9999*	0.9999*	0.9999*
2.0	10	0.2615	0.2783*	0.2721	0.2933*	0.2336	0.2447*	0.2968	0.3269*
	15	0.3700	0.3857*	0.3939	0.4068*	0.3616	0.3716*	0.4234	0.4400*
	20	0.4824	0.4940*	0.5044	0.5156*	0.4812	0.4902*	0.5248	0.5378*
	25	0.5887	0.5963*	0.5921	0.5995*	0.5724	0.5792*	0.6042	0.6144*
	30	0.6657	0.6704*	0.6771	0.6840*	0.6531	0.6556*	0.6803	0.6898*
	50	0.8711	0.8727*	0.8807	0.8827*	0.8824	0.8848*	0.8761	0.8800*
	100	0.9934*	0.9934*	0.9937	0.9940*	0.9940	0.9943*	0.9913	0.9918*

**Table 10.** (cont.)

$\sigma_2$		Normal		Logistic		Uniform		Laplace	
$\sigma_1$	n	WT	PER	WT	PER	WT	PER	WT	PER
2.5	10	0.1900	0.2118*	0.1128	0.1399*	0.1747	0.1918*	0.2257	0.2536*
	15	0.2790	0.2966*	0.1515	0.1729*	0.2581	0.2705*	0.3059	0.3277*
	20	0.3636	0.3784*	0.1853	0.2006*	0.3490	0.3596*	0.3883	0.4067*
	25	0.4403	0.4507*	0.2232	0.2378*	0.4201	0.4303*	0.4711	0.4884*
	30	0.5095	0.5197*	0.2597	0.2711*	0.4977	0.5039*	0.5245	0.5365*
	50	0.7389	0.7405*	0.7395	0.7445*	0.7364	0.7411*	0.7425	0.7476*
	100	0.9583	0.9588*	0.9587	0.9588*	0.9576	0.9587*	0.9544	0.9549*

\* Tests with the highest power value

**Table 11.** Power values for symmetric distribution in heterogeneity of variance cases with  $\Delta = 2$

$\sigma_2$		Normal		Logistic		Uniform		Laplace	
$\sigma_1$	n	WT	PER	WT	PER	WT	PER	WT	PER
1.5	10	0.9056	0.9119*	0.9040	0.9115*	0.9186	0.9207*	0.8876	0.8954*
	15	0.9843	0.9852*	0.9760	0.9770*	0.9896	0.9895*	0.9753	0.9770*
	20	0.9977	0.9980*	0.9966	0.9969*	0.9991	0.9992*	0.9932	0.9934*
	25	0.9999*	0.9999*	0.9994*	0.9992	0.9999*	0.9999*	0.9989	0.9990*
	30	1.0000*	1.0000*	0.9999*	0.9999*	1.0000*	1.0000*	0.9997	0.9998*
	50	1.0000*	1.0000*	1.0000*	1.0000*	1.0000*	1.0000*	1.0000*	1.0000*
	100	1.0000*	1.0000*	1.0000*	1.0000*	1.0000*	1.0000*	1.0000*	1.0000*
2.0	10	0.7377	0.7577*	0.7528	0.7736*	0.7366	0.7530*	0.7615	0.7855*
	15	0.9120	0.9180*	0.9032	0.9118*	0.9201	0.9240*	0.8949	0.9020*
	20	0.9734	0.9748*	0.9670	0.9697*	0.9763	0.9774*	0.9573	0.9615*
	25	0.9906	0.9911*	0.9878	0.9889*	0.9947*	0.9947*	0.9844	0.9862*
	30	0.9978	0.9979*	0.9964	0.9967*	0.9987*	0.9987*	0.9963	0.9967*
	50	1.0000*	1.0000*	1.0000*	1.0000*	1.0000*	1.0000*	0.9999*	0.9999*
	100	1.0000*	1.0000*	1.0000*	1.0000*	1.0000*	1.0000*	1.0000*	1.0000*
2.5	10	0.5711	0.6054*	0.3026	0.3477*	0.5534	0.5802*	0.6183	0.6566*
	15	0.7789	0.7966*	0.4462	0.4780*	0.7695	0.7816*	0.7911	0.8090*
	20	0.8929	0.9001*	0.5546	0.5787*	0.8921	0.8973*	0.8849	0.8939*
	25	0.9454	0.9483*	0.6573	0.6739*	0.9522	0.9540*	0.9378	0.9432*
	30	0.9781	0.9790*	0.7409	0.7527*	0.9790	0.9797*	0.9699	0.9716*
	50	0.9990	0.9991*	0.9989*	0.9988	0.9997*	0.9997*	0.9989*	0.9989*
	100	1.0000*	1.0000*	1.0000*	1.0000*	1.0000*	1.0000*	1.0000*	1.0000*

\* Tests with the highest power value

### 3.2.2 Skew distribution

Considering the skew distribution with coefficient of skewness varying; 1 and 2, the permutation test behaves better than the other two when both samples come from gamma distributions (Table 12).

Table 13 shows the power values of all tests for lognormal data. The permutation test gives the highest power when the coefficients of skewness are 1. However, the test power of all test statistics reaches to 1 when the sample sizes are greater than 10 with the high difference in location parameters. For high degree of skewness, the permutation test gives the best results when the sample sizes are 10. But, the Mann-Whitney test becomes the best test when the sample sizes are at least 15.

**Table 12.** Power values for Gamma distribution

$\Delta$	n	Skewness =1			Skewness =2		
		WT	MW	PER	WT	MW	PER
0.25	10	0.1352	0.1279	0.1484*	0.0563	0.0636	0.0731*
	15	0.2012	0.1833	0.2108*	0.0764	0.0753	0.0882*
	20	0.2650	0.2463	0.2721*	0.0931	0.0863	0.1012*
	25	0.3345	0.3103	0.3348*	0.1095	0.1020	0.1173*
	30	0.3905	0.3627	0.3954*	0.1198	0.1131	0.1281*
	50	0.5999	0.5591	0.6013*	0.1859	0.1601	0.1907*
	100	0.8853*	0.8448	0.8853*	0.3426	0.2768	0.3434*
0.5	10	0.3679	0.3365	0.3922*	0.0964	0.1020	0.1288*
	15	0.5494	0.5056	0.5634*	0.1483	0.1418	0.1750*
	20	0.6874	0.6449	0.6954*	0.2040	0.1867	0.2239*
	25	0.7927	0.7471	0.7957*	0.2582	0.2249	0.2724*
	30	0.8630	0.8287	0.8644*	0.3147	0.2698	0.3268*
	50	0.9778	0.9645	0.9780*	0.4972	0.4125	0.5042*
	100	1.0000*	0.9999	1.0000*	0.8085	0.6867	0.8103*
0.75	10	0.6099	0.5798	0.6459*	0.1479	0.1537	0.1970*
	15	0.8103	0.7698	0.8205*	0.2525	0.2340	0.2879*
	20	0.9242	0.9012	0.9277*	0.3554	0.3109	0.3841*
	25	0.9686	0.9520	0.9692*	0.4469	0.3861	0.4694*
	30	0.9884	0.9803	0.9887*	0.5368	0.4522	0.5530*
	50	1.0000*	0.9998	1.0000*	0.7659	0.6560	0.7719*
	100	1.0000*	1.0000*	1.0000*	0.9733	0.9179	0.9737*

\* Tests with the highest power value

**Table 13.** Power values for Log-normal distribution

$\Delta$	n	Skewness =1			Skewness =2		
		WT	MW	PER	WT	MW	PER
0.25	10	0.3694	0.3575	0.3872*	0.1275	0.1365	0.1541*
	15	0.5300	0.5168	0.5392*	0.1933	0.2048	0.2123*
	20	0.6664	0.6606	0.6725*	0.2574	0.2821*	0.2720
	25	0.7682	0.7601	0.7696*	0.3012	0.3262*	0.3109
	30	0.8361	0.8377*	0.8369	0.3611	0.3948*	0.3684
	50	0.9710*	0.9696	0.9709	0.5577	0.5911*	0.5620
	100	0.9997*	0.9996	0.9997*	0.8431	0.8801	0.8440
0.5	10	0.9012	0.8915	0.9104*	0.4110	0.4406	0.4642*
	15	0.9825	0.9800	0.9834*	0.6009	0.6309*	0.6307
	20	0.9973	0.9968	0.9977*	0.7279	0.7714*	0.7451
	25	0.9996*	0.9996*	0.9996*	0.8244	0.8612*	0.8337
	30	1.0000*	1.0000*	1.0000*	0.8917	0.9198*	0.8918
	50	1.0000*	1.0000*	1.0000*	0.9874	0.9932*	0.9880
	100	1.0000*	1.0000*	1.0000*	0.9998	1.0000*	0.9998
0.75	10	0.9980	0.9979	0.9984*	0.7345	0.7825	0.7922*
	15	1.0000*	1.0000*	1.0000*	0.9076	0.9248*	0.9246
	20	1.0000*	1.0000*	1.0000*	0.9698	0.9805*	0.9743
	25	1.0000*	1.0000*	1.0000*	0.9908	0.9963*	0.9918
	30	1.0000*	1.0000*	1.0000*	0.9979	0.9993*	0.9983
	50	1.0000*	1.0000*	1.0000*	1.0000*	1.0000*	1.0000*
	100	1.0000*	1.0000*	1.0000*	1.0000*	1.0000*	1.0000*

\* Tests with the highest power value

#### 4. Conclusions

Based on the numerical studies from the previous section, increasing sample size is found in this study to improve the test power for all testing procedures, but the standard deviation ratios seem to have the different kinds of impact. In other words, the power values drop when the standard deviation ratios increase. Moreover, the power values of low skewness are greater than those of high skewness.

The results for the homogeneity of variance demonstrate that the independent *t*-test is a better test than the other two when the sample data are drawn from the normal and uniform distributions, while the Mann-Whitney test is the most powerful for the logistic and Laplace distributions. However, all tests perform well when the mean differences and the sample sizes become large.

With the symmetric distribution in heterogeneity of variance cases, the permutation test is more powerful than the Welch *t*-test. Moreover, both tests reach the same power values when the sample sizes become large. However, the Mann-Whitney test is not appropriate because the concept of this test is to test that two samples drawn from the same distribution; same means and same variances.

Instead of considering the difference in means, we consider the difference in parameters for skew distribution; the scale and shape parameters. So, the Mann-Whitney test can be examined in this case. For the gamma distribution, the permutation test is the best test. In addition, this test is also the best option in the case of low degree of skewness for log-normal distribution.

In conclusion, the concepts of all test are different. The Welch's  $t$ -test and the permutation test should be used to compare the central tendency of two populations, whereas the Mann-Whitney test should always be used to investigate two populations that are identical distribution. Of course, researchers should adopt the procedure that corresponds best with the objectives of their research design.

## References

- [1] Boneau, C.A., 1960. The effects of violations of assumptions underlying the  $t$  test. *Psychological Bulletin*, 57(1), 49-64.
- [2] Fagerland, M.W. and Sandvik L., 2009. Performance of five two-sample location tests for skewed distributions with unequal variances. *Contemporary Clinical Trials*, 30, 490-496.
- [3] Nadim, N., 2008. The Mann-Whitney  $U$ : a test for assessing whether two independent samples come from the same distribution. *Tutorials in Quantitative Methods for Psychology*, 4(1), 13-20.
- [4] Ernst, M.D., 2004. Permutation methods: a basis for exact inference. *Statistical Science*, 19(4), 676-685.
- [5] R Development Core Team, 2019. *R: A Language and Environment for Statistical Computing*. Vienna: R Foundation for Statistical Computing.
- [6] Hatchavanich, D., 2014. A comparison of type I error and power of Bartlett's test, Levene's test and O'Brien's test for homogeneity of variance test. *Southeast-Asian Journal of Sciences*, 3(2), 181-194.
- [7] Kasuya, E., 2001. Mann-Whitney  $U$  test when variances are unequal. *Animal Behaviour*, 61, 1247-1249.
- [8] Stonehouse, J.M. and Forrester, G.J., 1998. Robustness of the  $t$  and  $U$  tests under combined assumption violations. *Journal of Applied Statistics*, 25(1), 63-74.
- [9] Fagerland, M.W., 2012.  $t$ -tests, non-parametric tests, and large studies-a paradox of statistical practice? *BMC Medical Research Methodology*, 12, 78, <https://doi.org/10.1186/1471-2288-12-78>.

## Gold Recovery from Copper-Gold Tailings by Ammoniacal Thiosulphate Leaching

Kamolwich Income<sup>1\*</sup>, Sirinat Boonpo<sup>2</sup>, Thidarat Kruatian<sup>2</sup>, Ponlayuth Sooksamiti<sup>1</sup> and Sukjit Kungwankunakorn<sup>2</sup>

<sup>1</sup>Department of Primary Industries and Mines, Ministry of Industry, Bangkok, Thailand

<sup>2</sup>Department of Chemistry, Faculty of Science, Chiang Mai University, Chiang Mai, Thailand

Received: 14 October 2020, Revised: 11 February 2021, Accepted: 12 April 2021

### Abstract

Ammoniacal thiosulphate leaching is a safer method to apply for gold leaching because it does not involve the use of cyanide. It has been found to be a better method than other leaching methods. It is non-toxic and environment-friendly for gold extraction. In this study, the method was developed especially for gold leaching from copper-gold tailings samples. Various factors such as copper(II) sulphate concentration, ammonium thiosulphate concentration, pH, solid-liquid ratio, temperature and rotation speed were studied to determine optimum conditions for leaching. It was found that the most suitable condition were 0.07 M copper(II) sulphate, 0.5 M ammonium thiosulphate, pH = 10, solid-liquid ratio = 1:10, room temperature (30 °C), rotation speed = 400 rpm and 5 h leaching time. Flame atomic absorption spectrometry was used to analyse the concentration of gold after the leaching process was performed. The performance of ammoniacal thiosulphate leaching method was evaluated by standard material No. ST 279. It was found that the precision of ammoniacal thiosulphate leaching method considered from relative standard deviation value was 2.28%. The accuracy which was considered from the recovery value was 97.63%. The detection limit of gold by flame atomic absorption spectrometry was 0.006 mg/l. The ammoniacal thiosulphate leaching method with optimum condition was applied for gold extraction from copper-gold tailings from northeastern part of Thailand. The results indicated that gold concentration from the ammoniacal thiosulphate leaching method was in the range of 65.52-89.50 g/t. Recovery by the ammoniacal thiosulphate leaching method was greater than 90% as was confirmed by the fire assay standard method.

**Keywords:** ammoniacal thiosulphate leaching; atomic absorption spectrometry; copper-gold tailings; fire assay; gold

DOI 10.14456/cast.2021.59

---

\*Corresponding author: Tel.: (+66) 53221385 Fax: (+66) 53225184  
E-mail: Kamolwich\_in@hotmail.com

## 1. Introduction

Gold holds a prestigious and highly special position in the periodic table when compared to other metals. For many centuries, it has been recognized as the most “noble” of metals due to its resistance towards most corrosive forces. It also has been known as King of the Metals because of its economic value. Gold is sophisticated, robust and mechanically malleable. It, furthermore, has beautiful color and sparkling appearance. It has long been considered as a useful and ideal material for culture and art, as well as for coin currency and jewelry. In more recent times, gold metal has become an important material for the electricity and electronics industry because of its high electrical and thermal conductivity [1]. It is not generally thought to be a homologue of the other two coinage metals in the periodic table, copper and silver as it possesses totally different oxidation states, oxidation potentials, coordination numbers and coordination geometries [2-4]. The atomic number of gold is  $Z = 79$ . Gold has only one stable isotope, which has an atomic mass of 197 [5]. The freezing and boiling points of gold are  $1064^{\circ}\text{C}$  and  $3081^{\circ}\text{C}$ , respectively. The density of pure gold is  $19300\text{ kg/m}^3$  in spite of the fact that the density of native gold typically is  $15000\text{ kg/m}^3$ . Gold is inert under the conditions of ambient pressure and temperature. Consequently, there are very few naturally occurring compounds of metal. Gold has a metallic luster. Its color is distinctively golden or deep yellow; however, it may be light yellow or orange/yellow with high contents of silver and copper, respectively. Pure gold is an excellent electrical and thermal conductor [6].

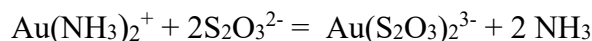
Gold is present in small amount in clays, pyrite and it is generally found in copper, silver, bismuth, zinc, lead, tellurium and antimony ores [7]. Copper-gold tailings involves the removal of gold which contains in copper ores and iron ores during the floatation process of gold mining. Content of gold in copper ores is related to the copper content. Copper ores with a high percentage of copper generally present a high percentage of gold. In general, copper ores contain gold between 2 and 30 g/t. A high amount of gold, in the range of 10- 30 g/t, is usually found in copper ores that contain 10-15% of copper. Other components in ores are iron and rocks. The leaching of gold is very interesting for study owing to the high value of gold although it is contained in small amount in copper ores. Previous studies focused on the cyanide leaching method, which was used for leaching of gold in a variety of samples [7-11].

In the cyanidation method, copper and iron must be removed before the leaching process as the metals can also react with cyanide, which interferes with gold leaching. Cyanide is toxic to human health and aquatic life even at low concentrations [12]. Exposure to cyanide leads to various thyrotoxic and neuropathic conditions in humans [13], and thus the concentration of cyanide in water is limited to 0.2 mg/l by WHO [14]. Moreover, the difficulty of gold leaching, cost of gold extraction and process time of this method have made it of value to investigate other methods of gold extraction from tailings [15].

The process of ammoniacal thiosulphate leaching is based on the removing of gold out of gold bearing ores without toxic cyanide as a reagent. The ammoniacal thiosulphate leaching method has many advantages when compared with cyanidation method. It offers lower toxicity and greater efficiency for treatment of gold deposits associated with preg-robbing ores. During the leaching process of gold by the ammoniacal thiosulphate method, the chemical reactions involved are dissolution, oxidation and complexation. The chemistry of the ammoniacal thiosulfate system for extraction of gold involves the relationship of three major components which are thiosulfate, ammonia and copper. Gold is stabilized by thiosulfate, whilst copper and ammonia speed up the leaching reaction [16-18]. Generally, when a mild oxidant such as oxygen appears in the reaction, gold dissolves slowly in alkaline solution of thiosulphate. The alkaline solution functions to prevent the decomposition at low pH of thiosulphate. The dissolution reaction [19] can be written as:



The dissolution of gold in thiosulfate is blocked under conditions of a lack of ammonia by the coating of sulfur on the gold surface that is the cause of decomposition of thiosulfate. This problem is prevented by ammonia because ammonia is absorbed on the surfaces of gold over thiosulfate. Hence, gold is transferred into the solution in the form of amine complex [20]. Then, it is replaced by thiosulfate as presented below.



However, the main role of ammonia in thiosulfate system is to stabilize the oxidant (copper) by forming copper (II) amine complexes which speed up the dissolution of gold as shown below [21].



The presence of ammonia hinders the dissolution of iron oxides, silica, silicates, and carbonates, which are the most common gangue minerals found in gold bearing ores. An oxidant is needed to oxidize metallic gold to gold(I) in the thiosulphate system, and it is shown in the solution as copper(II) ions. Various oxidants including oxygen, hydrogen peroxide, ferric ion, ozone, and formamidine disulfide, were used in previous studies [22]. Gold in the form of an anionic aurocomplex was dissolved by ammonium thiosulphate, which is stable over a wide range of pH and Eh values. The dissolution reaction for gold can be written as:



To understand the chemical reactions during the leaching process, the Eh-pH equilibrium was investigated in previous studies. The studies reported the involvement of Eh and pH in the predominant species of gold in the system in which  $[\text{Au}(\text{S}_2\text{O}_3)_2]^{3-}$  and  $[\text{Au}(\text{NH}_3)_2]^+$  were concerned. Moreover, the pH values were significantly changed by changes in the thiosulfate or ammonia concentration that had an effect on the presence of gold species. At conditions above pH of 9, the predominant species of gold in the system was  $[\text{Au}(\text{S}_2\text{O}_3)_2]^{3-}$  (a higher stability) rather than  $[\text{Au}(\text{NH}_3)_2]^+$  [23, 24]. The dissolution of gold was also significantly influenced by the pH because of the occurrence of different ratios of  $\text{NH}_3/\text{NH}_4^+$  that related to the stability zone of  $\text{Cu}(\text{NH}_3)_4^{2+}$  [25]. Besides, there was a report about the effect of the reagent concentration on gold leaching. At low concentrations of reagent, the copper ammonium complex is stable in narrow pH region and at high concentrations of reagent, the copper ammonium complex is stable in a broader pH range [17]. From the above data, it can be concluded that the efficiency of gold leaching by ammoniacal thiosulfate system significantly depends on many factors. Therefore, the optimal conditions should be investigated in order to enhance the efficiency of extraction.

This study has focused on the extraction of gold from copper-gold tailings by the ammoniacal thiosulphate leaching method on laboratory scale, a method that is safer to use for gold extraction because it takes place without cyanide. The optimum conditions for gold extraction by the ammoniacal thiosulphate leaching method for copper-gold tailings sample were studied specifically. The recoveries of gold by the ammoniacal thiosulphate leaching were confirmed with results of the recoveries from the fire assay standard method. The result of this study indicate that the developed ammoniacal thiosulphate leaching method is efficient to be applied for gold extraction from copper-gold tailing samples.

## 2. Materials and Methods

### 2.1 Apparatus and reagents

A Varian SpectrAA 220FS atomic absorption spectrometer from Varian (Varian, Australia) was used for Au measurement. These conditions are given in Table 1. Powder X-ray diffraction pattern of sample was obtained from 5 to 55 in  $2\theta$  by X-ray diffractometer (XRD) with cobalt  $K\alpha$  radiation (BTX II Benchtop XRD, Olympus). A Jones riffle sampler from Tyler (USA) and roll crusher from Retsch GmbH (Germany) were used for sample preparation. A crucible furnace was used for sample fusion.

**Table 1.** Measurement conditions for AAS

Parameters	Conditions
Wavelength (nm)	242.4
Slit width (nm)	1.0
Fuel	Acetylene
Oxidant	Air
Flame stoichiometry	Oxidizing

The copper-gold tailing samples that were used in both fire assay and ammoniacal thiosulfate method were obtained from gold mining process at the Phutubfa gold mine in Wangsaphung district, Loei province, Thailand. The copper concentrate, standard material No. ST 279 (Au = 7.18 g/t), was obtained from Gannet, Australia and was used to evaluate the efficiency of gold leaching by ammoniacal thiosulfate method. Ammonium thiosulphate was obtained from Merck, Germany. Copper sulphate pentahydrate was from Fluka, USA. The 1000  $\mu\text{g/ml}$  of Au standard solution was obtained from BDH Chemicals, England. Working standard solutions were prepared by appropriate dilution of the stock standard solution. All other reagents were of analytical-reagent grade (E. Merck, Darmstadt, Germany) and all solutions were prepared with deionized water.

### 2.2 Preparation of copper-gold tailing samples

For the sampling of copper-gold tailing samples, systematic random sampling was applied for this study. Approximately 2-2.5 kg in total of sample was collected from 4 different points of depth of the big bag containing copper-gold tailings using a grain solid sample probe. Then, the sample amount was reduced by two sampling processes, cone and quartering, as well as sample division to 600 g. After that, the copper-gold tailing samples were set by using a Jones Riffle sampler and dried at 104°C for 2 h. The dried samples were then ground by roll crushers. Finally, the ground samples were sieved into the size fraction of 150  $\mu\text{m}$  [26] and stored in sample bottles.

### 2.3 Analysis of mineralogical species in copper-gold tailings by X-ray diffraction technique

Copper-gold tailings samples were packed into sample cells before the samples were analyzed. X-ray diffractometry was performed on a BTX II X-ray diffraction analyzer equipped with a cobalt

anode. The conditions of operation are shown in Table 2. The results were identified based on X Powder (search-match program) and the database of International Center for Diffraction Data (ICDD).

**Table 2.** X-ray diffraction instrument settings and analytical conditions

Parameters	Conditions
Voltage (kV)	30.5
Start $2\theta$ (degree)	5
Step size (degree)	0.05
Divergence slit (degree)	1
Current (mA)	0.35
Stop $2\theta$ (degree)	55
Time/step (second)	10
Anti-scattering slit (degree)	1

## 2.4 Determination of gold by fire assay standard method

Five grams of the copper-gold tailing samples were placed in a plastic bag with 50 g PbO and about 36.5 g of a flux containing 20 g  $\text{Na}_2\text{CO}_3$ , 10 g  $\text{Na}_2\text{B}_4\text{O}_7 \cdot 10\text{H}_2\text{O}$ , 5 g  $\text{SiO}_2$  and 1.5 g flour. After combining, the plastic bag with mixed components was put into a fire clay crucible. Then, Ag as silver foil was added. The crucible was brought into a preheated furnace and fused at  $1100^\circ\text{C}$  for 1 h. The molten contents were then poured into an iron mold to cool. Pb regulus containing the analyses was separated from slag and cleaned by hammering and brushing. Magnesite cupels were preheated in a furnace at  $950^\circ\text{C}$ . After that, Pb regulus was put on a cupel which was allow to remain in the furnace until all oxidized lead had been absorbed by the cupel. A dofe was taken out of each cupel after cooling, hammered flat to speed up dissolution, and then transferred into a 10 ml porcelain crucible. The dofe bead was parted with  $\text{HNO}_3$  (1:7 %v/v) and  $\text{HNO}_3$  (3:1 %v/v) to eliminate silver and other impurities from the gold. The gold was washed with  $\text{NH}_4\text{OH}$  (1:9 %v/v) and dissolved with 5 ml of aqua regia in 50 ml beaker. After the gold had dissolved, the volume of the solution was made up to 50 ml with diluted HCl. After that, the prepared solution was analyzed by atomic absorption spectrometer, using the Varian SpectrAA 220FS instrument with an air-acetylene flame, to determine Au concentration. This experiment was repeated three times [27].

## 2.5 Evaluating performance of the ammoniacal thiosulphate leaching

The analysis of standard material No. ST 279 was carried out ten times to evaluate the precision of ammoniacal thiosulphate leaching method. The relative standard deviation was calculated. The analysis of standard material No. ST 279 was performed ten times to evaluate the accuracy of the ammoniacal thiosulphate leaching method. The results were calculated as the percentage of recovery. Limit of detection (LOD) of flame atomic absorption spectrometer instrument for determination of gold was determined by analysis of blank samples ten times. LOD was calculated using 3SD.

## 2.6 Extraction of gold in copper-gold tailings by ammoniacal thiosulphate leaching

To prepare the leaching solution, the dissolution of the appropriate chemicals in deionized water to the required concentration was conducted. A weighed amount of ammonium thiosulphate was dissolved in water. Then, the accurate volume of a solution of copper(II) sulphate in aqueous ammonia was added. Finally, the pH of the solution was adjusted by applying aqueous ammonia [25]. Each experiment was conducted in a 250 ml Erlenmeyer flask which contained copper-gold tailings mixed with the ammoniacal thiosulphate, which was then placed on a magnetic stirrer as shown in Figure 1. The solid particles were kept in suspension through the use of a mechanical stirrer. During a total retention time of 5 h, samples were taken continually at fixed intervals. The gold concentration in the leaching solutions was analyzed by flame atomic absorption spectrometry. The experiment was repeated three times.

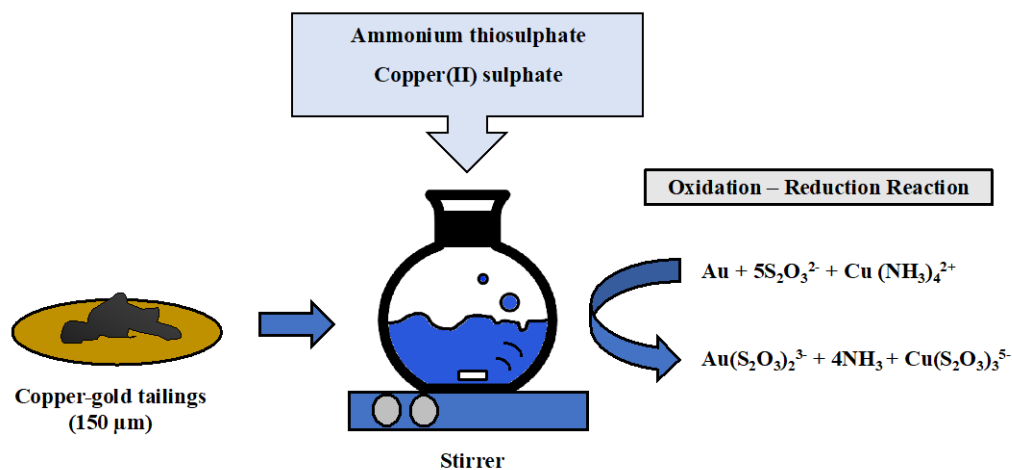


**Figure 1.** The ammoniacal thiosulphate leaching of gold in copper-gold tailings

## 3. Results and Discussion

### 3.1 Mineralogical species in copper-gold tailings by X-ray diffraction

The X-ray diffraction results of TK54-01 copper-gold tailings sample, which contained 82.04 g/t of gold (Analysis with fire assay standard method), presented the spectral patterns of chalcopyrite ( $\text{CuFeS}_2$ ), pyrite ( $\text{FeS}_2$ ), pyrrhotite ( $\text{Fe}_{1-x}\text{S}$ ,  $x = 0-0.2$ ) and quartz ( $\text{SiO}_2$ ) as shown in Figure 2. The results indicated that copper-gold tailings were composed of chalcopyrite, pyrite, pyrrhotite and quartz.

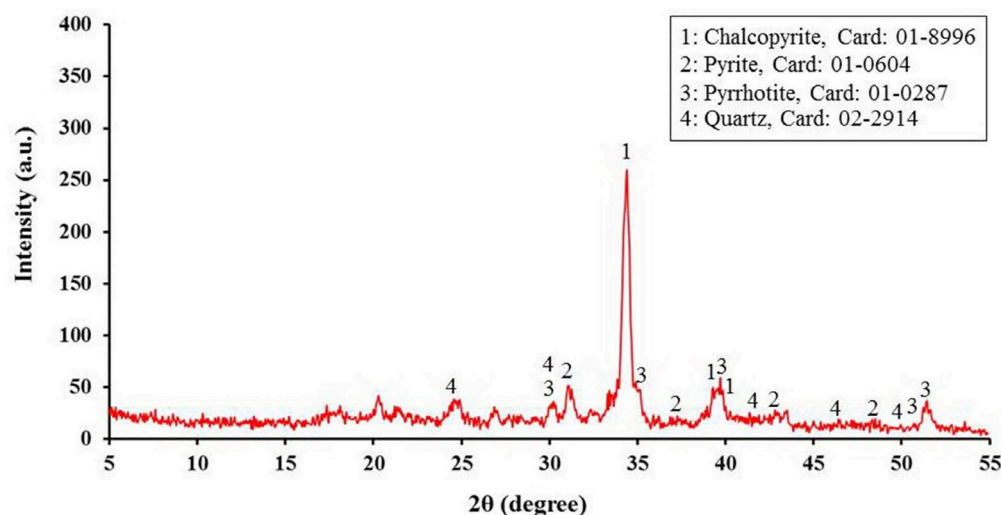


**Figure 2.** X-ray diffraction pattern of copper-gold tailings sample (TK54-01)

### 3.2 Evaluating performance of the ammoniacal thiosulphate leaching

The precision of the ammoniacal thiosulphate leaching method was studied by analysis of standard material No. ST 279 ten times. The results showed that the precision with replicative analyses, expressed as the relative standard deviation (%RSD), was found to be 2.28% which was less than 5%. This indicated that the ammoniacal thiosulphate leaching method provided good repeatability for gold under optimum conditions. The accuracy was evaluated by analysis of standard material No. ST 279 ten times. The results were in a good agreement with certified values. The recovery value was found to be 97.63%, which was higher than 95%. Hence, the ammoniacal thiosulphate leaching method is accurate. The flame atomic absorption spectrometric system programmatically generated the calibration curve. It was plotted and shown absorbance versus gold concentration. The linear range of the calibration curve was in the range of 2-10 mg/l. The calibration equation was  $y = 0.036x + 0.0028$ , and  $R^2$  was 0.9995. Sensitivity, defined as slope of regression line, was 0.036 ppm. Limit of detection (LOD) was defined as concentration corresponding to 3SD of ten blank signals. Limit of detection of gold in flame atomic absorption spectrometry was found to be 0.006 mg/l.

### 3.3 Optimization of gold extraction conditions by ammoniacal thiosulphate leaching

The gold extraction method was developed using ammoniacal thiosulphate leaching and gold was determined by flame atomic absorption spectrometry. The experimental parameters were analyzed three times. The optimum parameter of ammoniacal thiosulphate leaching for gold extraction was very important to study. Several factors relevant to leaching efficiency were studied and optimized. Analytical factors, copper(II) sulphate concentration, ammonium thiosulphate concentration, pH, solid-liquid ratio, temperature and rotation speed on gold leaching were investigated for quantitative recovery of gold.

### 3.3.1 Effect of copper(II) sulphate concentration on gold leaching

The influence of Copper(II) sulphate on gold leaching was studied. The results are shown in Figure 3. Copper(II) sulphate concentration was varied from 0.01-0.09 M. Constant experimental conditions were 0.5 M ammonium thiosulphate, pH = 10, solid-liquid ratio = 1:10, room temperature (30°C) and rotation speed = 400 rpm. As shown in Figure 3, increasing copper(II) sulphate concentration up to 0.07 M shifted gold concentration-time curves to higher values ( $66.68 \pm 2.73$  g/t). However, above the aforementioned concentration, gold leaching recoveries plummeted to lower values. The major reason was that increasing  $\text{Cu}^{2+}$  ion concentration decreased the stability region of the  $\text{Cu}(\text{NH}_3)_4^{2+}$  complex. The process led to a broadened stability region of solid copper compounds including,  $\text{Cu}_2\text{O}$ ,  $\text{CuO}$ ,  $\text{Cu}_2\text{S}$  and  $\text{CuS}$ . Thus, an increment of copper ion concentration led to formation of solid copper compounds by having higher consumption of thiosulphate as a result of changing Eh-pH equilibrium of the system [28].

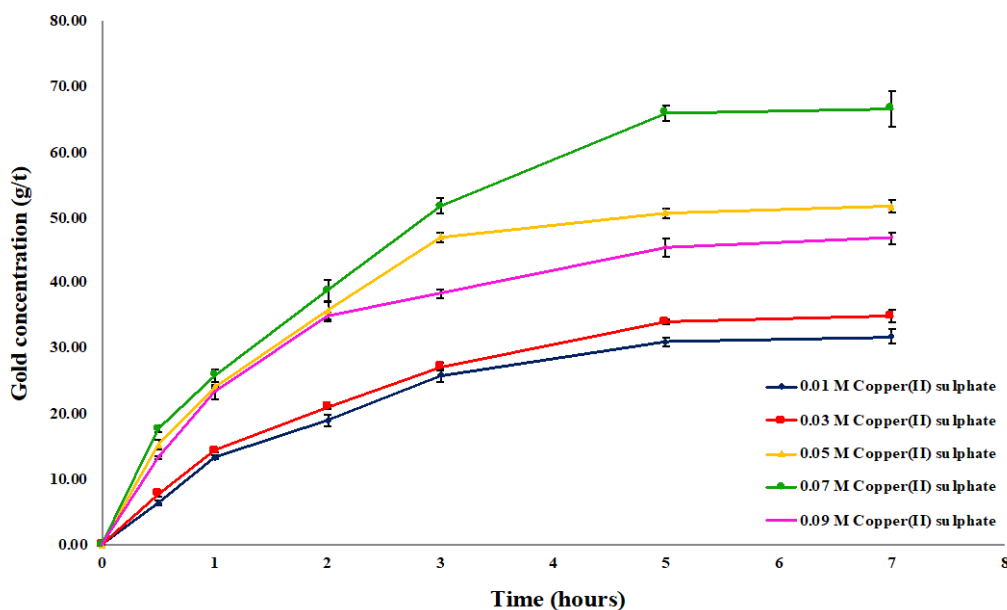
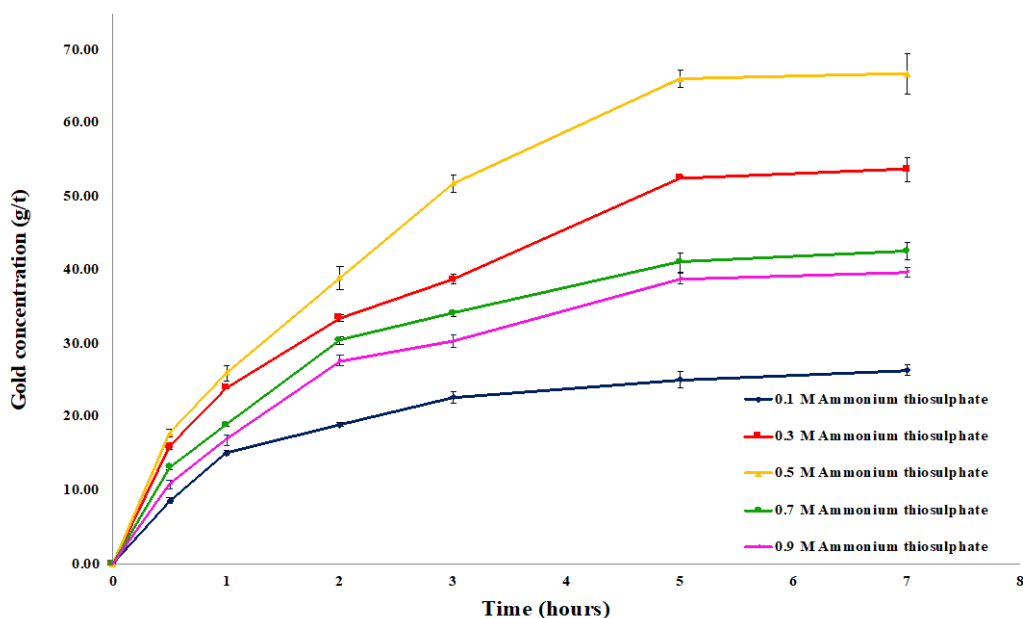


Figure 3. Effect of copper(II) sulphate concentration on gold leaching

### 3.3.2 Effect of ammonium thiosulphate concentration on gold leaching

Ammonium thiosulphate influence on gold leaching was examined. The results are shown in Figure 4. Ammonium thiosulphate concentration was varied from 0.1-0.9 M whilst the constant experimental conditions were 0.07 M copper (II) sulphate, pH = 10, solid-liquid ratio = 1:10, room temperature (30°C) and rotation speed = 400 rpm. Recovery of gold was enhanced by increasing ammonium thiosulphate concentration up to 0.5 M ( $66.68 \pm 2.73$  g/t) as shown in Figure 4, but a negligible effect on gold dissolution was obtained at higher ammonium thiosulphate concentrations. Increasing concentration of ammonium thiosulphate is attributable to a wider stability region of  $\text{Cu}(\text{S}_2\text{O}_3)_3^{5-}$  complex because the change of thiosulfate or ammonia concentration has an effect in the pH values which influence the occurring of gold species in the



**Figure 4.** Effect of ammonium thiosulphate concentration on gold leaching

system as explained in Eh-pH diagram in the previous study [23]. This result revealed that the stability region of  $\text{Cu}(\text{NH}_3)_4^{2+}$  complex in leach solution continuously decreased. In all cases, the rate of gold leaching increased slowly after 5 h of reaction [25].

### 3.3.3 Effect of pH on gold leaching

The previous studied reported that pH affected the predominant species of gold in the ammoniacal thiosulphate system. At different pH, different ratio of  $[\text{Au}(\text{S}_2\text{O}_3)_2]^{3-}$  and  $[\text{Au}(\text{NH}_3)_2]^+$  are present in the system, and these have an effect on the leaching of gold. Moreover, the occurrence of  $\text{Cu}(\text{NH}_3)_4^{2+}$ , which is an oxidant in the system, needs suitable pH condition [23]. Therefore, this parameter should be investigated. The influence of pH on gold leaching was scrutinized, and the outcomes are illustrated in Figure 5. In these experiments, pH was varied from 9-11 while constant experimental conditions were 0.07 M copper (II) sulphate, 0.5 M ammonium thiosulphate, solid-liquid ratio = 1:10, room temperature (30°C) and rotation speed = 400 rpm. The results indicated that pH of 10 shifted gold concentration-time curves to the highest values. This pH value was considered the most suitable condition in this study. Gold concentration decreased when pH was above pH 10. High pH values reduced the thermodynamic stability region of  $\text{Cu}(\text{S}_2\text{O}_3)_3^{5-}$  and  $\text{Cu}(\text{NH}_3)_4^{2+}$ . Hence, this process resulted in lower gold leaching recoveries because the thermodynamic stability regions of solid copper species such as CuO and  $\text{Cu}_2\text{O}$  were widened [29]. Additionally, copper appeared in solid  $(\text{NH}_4)_5\text{Cu}(\text{S}_2\text{O}_3)_3$  form. The solid reduced the oxidant activity of copper tetraammine complex and covered the surface of mineral, hindering thiosulphate attack [28].

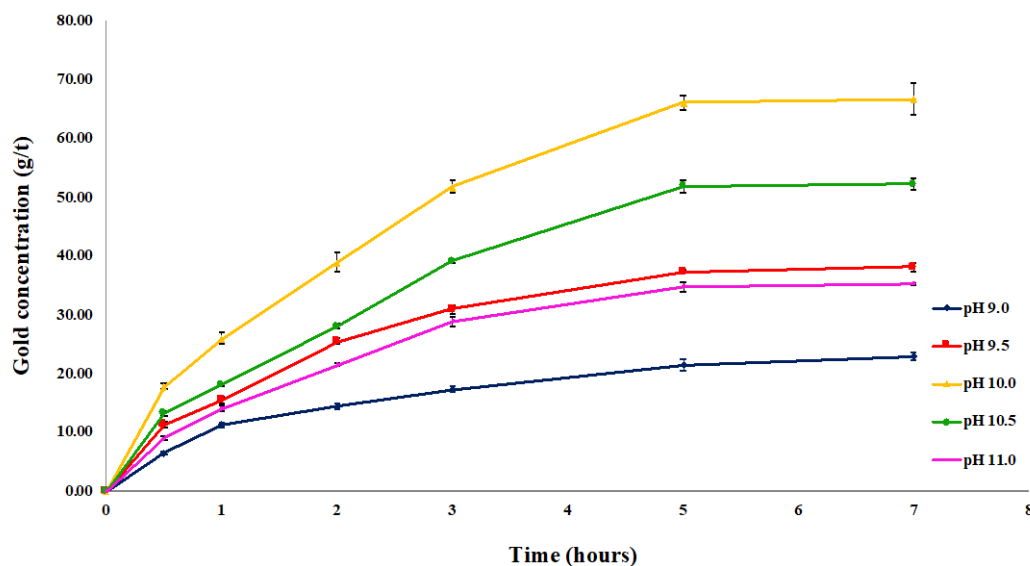


**Figure 5.** Effect of pH on gold leaching

### 3.3.4 Effect of solid-liquid ratio on gold leaching

The influence of solid-liquid ratio on gold leaching was investigated and the results are shown in Figure 6. The solid-liquid ratio is the ratio of copper-gold tailings to leach solution. Solid-liquid ratios (1:20, 1:10, 1:5, 3:10 and 2:5) were considered. Constant experimental conditions were 0.07 M copper (II) sulphate, 0.5 M ammonium thiosulphate, pH = 10, room temperature (30 °C) and rotation speed = 400 rpm. As illustrated in Figure 6, the solid-liquid ratios of 1:10 and 1:20 provided the highest gold concentrations. However, higher solid-liquid ratios above 1:10 led to lower gold concentration. The following two factors may have contributed to the decreasing of gold concentration. First, at higher solid-liquid ratio, leach solution concentration may not have been high enough to leach copper-gold tailings effectively; second, at high solid-liquid ratios, crowding of particles occurred resulting in more reduced contact with solution than particle-particle contact, thereby reducing leaching [30]. The solid-liquid ratios of 1:10 and 1:20 were shown to have similar leaching efficiency. Finally, only 1:10 ratio was selected to be used because of its better leaching solution than that of 1:20 ratio.

### 3.3.5 Effect of temperature on gold leaching

The influence of temperature on gold leaching was investigated and the results are shown in Figure 7. Temperature was varied from room temperature (30°C) to 70°C while the constant experimental conditions were 0.07 M copper(II) sulphate, 0.5 M ammonium thiosulphate, pH = 10, solid-liquid ratio = 1:10 and rotation speed = 400 rpm. As shown in Figure 7, insignificant differences of gold recovery with temperature between 30 and 70°C were observed. A previous report indicated that the temperature had an important role in the reaction rate of gold as it was involved in the chemical reaction speed [31]. However, that research was done over a short period of time (5 min) for leaching. In this study, a long period of time (5 h) was operated to get a high leaching efficiency, which was the purpose of this study. The reason why the increase of

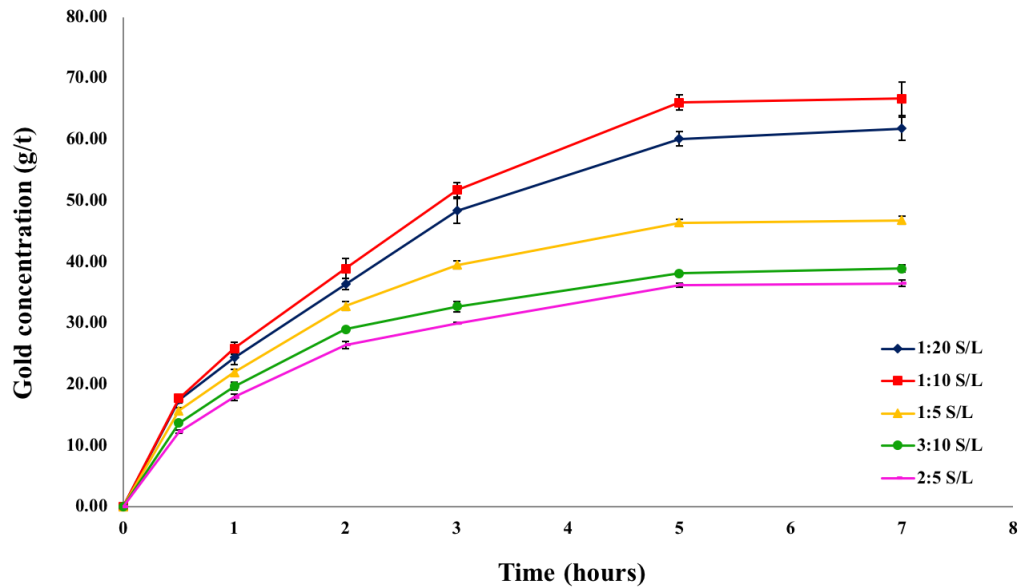


Figure 6. Effect of solid-liquid ratio on gold leaching

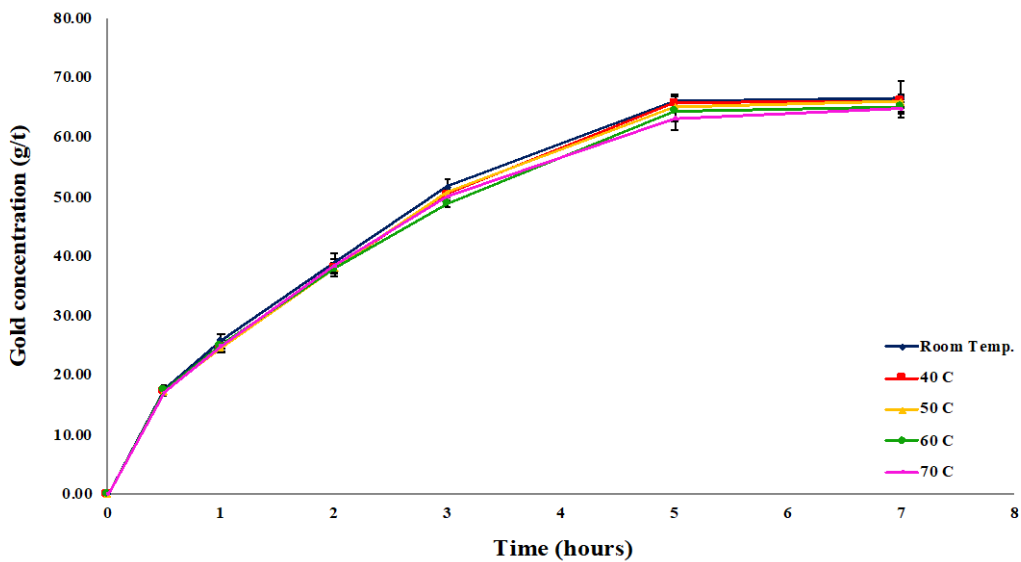


Figure 7. Effect of temperature on gold leaching

temperature did not have much effect on gold leaching recovery might be due to the use of a long period of time (5 h). This long leaching time was enough to compete for the reaction of gold leaching at 30-70°C. Hence, room temperature (30°C) was considered to be optimum for gold leaching by this method.

### 3.3.6 Effect of rotation speed on gold leaching

The influence of rotation speed on gold leaching was investigated and the results are shown in Figure 8. Rotation speed was varied from 300-700 rpm, while the constant experimental conditions were 0.07 M copper (II) sulphate, 0.5 M ammonium thiosulphate, pH = 10, solid-liquid ratio = 1:10 and room temperature (30°C). It is evident from Figure 8 that gold leaching increased with an increment of rpm from 300-400 rpm; however, beyond 400 rpm, the leaching of gold was decreased. It can be explicitly seen that speeds of rotation beyond 400 rpm caused turbulence that induced small fluctuations in pH and Eh values in the system which may have an impact on leaching performance as described by Rath *et al.* [30].

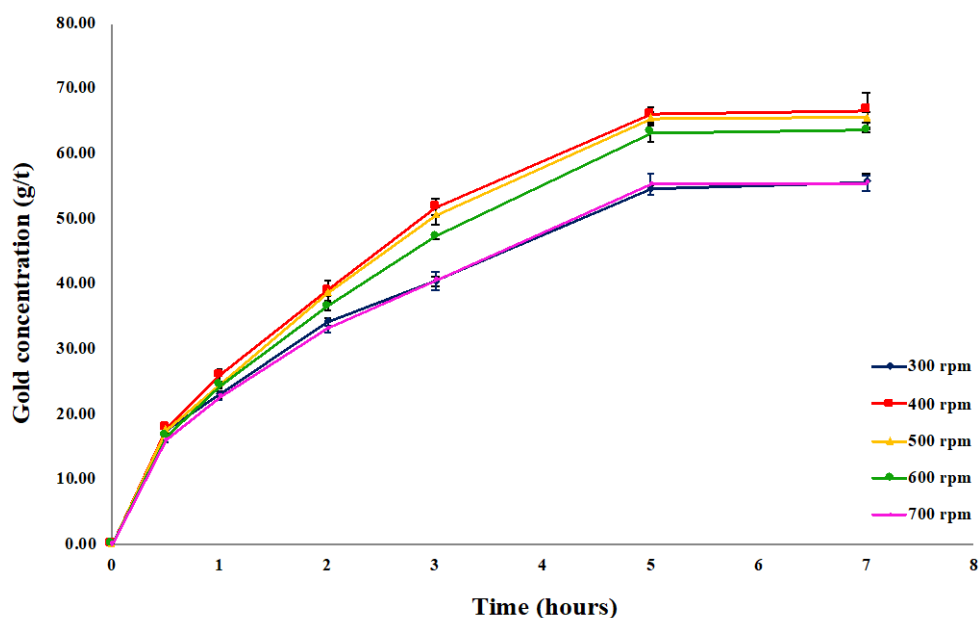


Figure 8. Effect of rotation speed on gold leaching

### 3.4 Determination of gold in copper-gold tailing samples by fire assay standard method

Copper-gold tailings samples were collected from the Phutubfa gold mine in Wang Saphung district, Loei province, Thailand. Samples were preconcentrated following the proposed method. Then, the analyte in solution samples was detected by flame atomic absorption spectrometry. This experiment was performed in triplicate for each sample. The results in Table 3 show that the concentrations of gold in studied copper-gold tailings samples were in the range of 71.93-92.46 g/t. Precision was considered from relative standard deviation values ( $n = 8$ ). It was found that relative standard deviation values of less than 5% were considered satisfactory.

### 3.5 Extraction of gold in copper-gold tailing samples by ammoniacal thiosulphate leaching

The optimized method was applied to determine the gold in copper-gold tailing samples. Samples were analyzed for gold by the ammoniacal thiosulphate leaching method three times. The results in Table 3 indicate that the concentrations of gold in copper-gold tailing samples were between 65.52-89.50 g/t. Precision was considered from relative standard deviation values ( $n = 8$ ). It was found that relative standard deviation values of less than 5% were considerably satisfactory.

**Table 3.** Comparison of ammoniacal thiosulphate leaching method with fire assay standard method

Sample	Au concentration (g/t)				% Recovery Au
	Fire assay*	%RSD	Ammoniacal thiosulphate leaching*	%RSD	
TK54-01	82.04±1.10	1.29	80.05±1.51	1.89	97.57
TK54-02	84.32±1.12	1.33	80.67±1.92	2.38	95.67
TK54-03	92.46±1.43	1.55	89.50±2.43	2.72	96.80
TK54-04	80.69±0.91	1.13	77.06±2.51	3.26	95.50
TK54-05	78.16±0.82	1.05	71.84±2.59	3.61	91.91
TK54-06	72.06±2.52	3.50	65.52±1.96	2.99	90.92
TK55-01	89.87±1.73	1.93	81.42±1.28	1.57	90.60
TK55-02	75.63±1.40	1.85	70.56±1.49	2.11	93.30
TK55-03	86.95±0.97	1.12	82.21±2.19	2.66	94.55
TK55-04	71.93±1.58	2.20	68.33±2.76	4.04	95.00
TK55-05	76.01±0.57	0.75	71.69±2.60	3.63	94.32
TK55-06	74.54±1.32	1.77	70.62±1.34	1.90	94.74

\*N=3

### 3.6 Evaluation of gold recovery by ammoniacal thiosulphate leaching with the result from fire assay standard method

The recovery of gold from this method was analyzed to evaluate the efficiency of gold extraction in copper-gold tailings by ammoniacal thiosulfate leaching. Flame atomic absorption spectrometry is a common technique for detecting gold at low concentration. This technique has high sensitivity, selectivity and much less interference. The gold recoveries of each sample by ammoniacal thiosulfate leaching method and fire assay standard method were investigated and compared. The results are shown in Table 3. If fire assay standard method results were assumed to represent 100% recovery of gold, we obtained recoveries greater than 90% for all samples by

ammoniacal thiosulphate leaching method. A good agreement was obtained from acceptable percent recovery. These results confirmed the validity of our proposed method. This study showed that ammoniacal thiosulphate leaching method to be an alternative extraction method as it provided good recoveries for gold extraction from copper-gold tailings.

#### 4. Conclusions

In this study, the most suitable conditions for gold leaching using the ammoniacal thiosulphate leaching were obtained at 0.07 M copper(II) sulphate, 0.5 M ammonium thiosulphate, pH 10, solid-liquid ratio = 1:10, room temperature (30°C), rotation speed = 400 rpm, and about 5 h of leaching. The precision of ammoniacal thiosulphate leaching method was considered from %RSD values. It was found to be 2.28% which was less than 5%, the maximum value of acceptable relative standard deviation. This indicated that ammoniacal thiosulphate leaching method provided good repeatability for gold under the optimum conditions. Accuracy was considered from the results in comparison with true values of standard material No. ST 279. The achieved results were consistent with certified values. Recovery value was equal to 97.63% which was higher than 95%, the minimum value of acceptable percentage recovery. The detection limit of gold in flame atomic absorption spectrometry, which is defined as the concentration corresponding to 3SD of ten blank signals, was found to be 0.006 mg/l. The ammoniacal thiosulphate leaching method and fire assay standard method were performed for gold determination. From the results, if fire assay standard method results were assumed to represent 100% recovery of gold, we should obtain recoveries greater than 90% for all samples by the ammoniacal thiosulphate leaching method. A good agreement was obtained with the acceptable percent recovery. Therefore, this study shows that the ammoniacal thiosulphate leaching method is an alternative to the standard method of fire assay. It gives good recoveries for gold in copper-gold tailings. According to results from the study, optimum conditions may enhance gold leaching. Furthermore, this method can be applied in the mine industry because of its environment-friendly aspects.

#### 5. Acknowledgements

The department of Primary Industries and Mines, Ministry of Industry is gratefully acknowledged. We would also like to thank the Department of Chemistry, Faculty of Science, Chiang Mai University for the research support.

#### References

- [1] Schmidbaur, H., 1999. *Gold-Progress in Chemistry, Biochemistry and Technology*. Chichester: John Wiley&Sons.
- [2] Puddephatt, R.J., 1978. *The Chemistry of Gold*. Amsterdam: Elsevier.
- [3] Rapsom, W.S. and Groenewald, T., 1978. *Gold Usage*. London: Academic Press.
- [4] Schmidbaur, H., 1990. The fascinating implications of new results in gold chemistry. *Gold Bulletin*, 23(1), 11-21.
- [5] Schmidbaur, H., Cronje, S., Djordjevic, B. and Schuster, O., 2005. Understanding gold chemistry through relativity. *Chemical Physics*, 311(1-2), 151-161.

- [6] Marsden, J.O. and House, C.I., 2006. *The Chemistry of Gold Extraction*. 2<sup>nd</sup> ed. Littleton: Society for Mining, Metallurgy, and Exploration, Inc. (SME).
- [7] Petrovic, N., Budelan, D., Cokic, S. and Nestic, B., 2001. The determination of the content of gold and silver in geological samples. *Journal of the Serbian Chemical Society*, 66(1), 45-52.
- [8] Estay, H., Carvajal, P., Gonzalez, K., Yanez, H., Bustos, W., Castro, S. and Arriagada, F., 2013. Cyanide leaching of copper-gold-silver ores. *5<sup>th</sup> International Seminar on Process Hydrometallurgy*, Santiago, Chile, July 10-12, 2013, 153-160.
- [9] Oraby, E., Esksteen, J. and Tanda, B., 2017. Gold and copper leaching from gold-copper ores and concentrates using a synergistic lixiviant mixture of glycine and cyanide. *Hydrometallurgy*, 169, 339-345.
- [10] Neelameggham, N.R., Alam, S., Oosterhof, H., Jha, A., Dreisinger, D. and Wang, S., 2015. *Rare Metal Technology 2015*. Cham.: Springer.
- [11] Anderson, C., 2012. Fundamentals of the analysis of gold, silver and platinum group metals. *Proceedings of 36<sup>th</sup> International Precious Metals Institute; a Sure Bet-World Economics Affect Precious Metals*, Las Vegas, U.S.A., 2012, 190-216.
- [12] Kwaansa-Ansah, E.E., Amenofe, L.P., Armah, E.K. and Opoku, F., 2017. Human health risk assessment of cyanide levels in water and tuber crops from Kenyasi, a mining community in the Brong Ahafo Region of Ghana. *International Journal of Food Contamination*, 4(16), <https://doi.org/10.1186/s40550-017-0061-y>
- [13] Dube, P.N. and Hosetti, B.B., 2010. Behavior surveillance and oxygen consumption in the freshwater fish *Labeo rohita* (Hamilton) exposed to sodium cyanide. *Biotechnology in Animal Husbandry*, 26(1-2), 91-103
- [14] Wilson, J., 1983. Cyanide in human disease: A review of clinical and laboratory evidence. *Fundamental and Applied Toxicology*, 3(5), 397-399.
- [15] Medina, D. and Anderson, C.G., 2020. A review of the cyanidation treatment of copper-gold ores and concentrates. *Metals*, 10(7), 897, <https://doi.org/10.3390/met10070897>
- [16] Societe Generale de Surveillance, 2008. *Thiosulphate Leaching - an Alternative to Cyanidation in Gold Processing*. [online]. Available at: <https://www.sgs.com/-/media/global/documents/flyers-and-leaflets/sgs-min-wa018-thiosulphate-leaching-alternative-to-cyanide-in-gold-processing-en-11.pdf>
- [17] Aylmore, M.G. and Muri, D.M. 2001. Thiosulphate leaching of gold - a review. *Minerals Engineering*, 14, 135-174.
- [18] Zhang, H.M. and Senanyake, G., 2016. A review of ammoniacal thiosulfate leaching of gold: An update useful for further research in non-cyanide gold lixivants. *Mineral Processing and Extractive Metallurgy Review*, 37(6), 385-411.
- [19] White, H.A., 1905. The solubility of gold in thiosulfates and thiocyanates. *Journal of the Chemical Metallurgical and Mining Society of South Africa*, 5, 109-111.
- [20] Chen, J., Deng, T., Zhu, G. and Zhao, J., 1996. Leaching and recovery of gold in thiosulfate based system – a research summary at ICM. *Transactions of Indian Institute of Metallurgy*, 49(6), 841-849.
- [21] Ter-Arakelyan, K.A., Bagdasaryan, K.A., Oganyan, A.G., Mkrtchyan, R.T. and Babayan, G.G., 1984. On technological expediency of sodium thiosulphate usage for gold extraction from raw material. *Izv. VUZ Tsvetn. Metallurgy*, 5, 72-76
- [22] Hiskey J.B., 1981. Thiourea as a lixiviant for gold and silver – leaching, recovery and economics. *Proceeding of the 100<sup>th</sup> AIME Meeting*, Chicago, USA, 22-26 February 1981, 83-91.
- [23] Hancock, R.D., Finkelstein, N.P. and Evers, A., 1974. Linear free energy relationships in aqueous complex formation reactions of the d<sub>10</sub> metals ions, *Journal of Inorganic Nuclear Chemistry*, 36(11), 2539-2543.

- [24] Wan, R.Y. and Brierley, J.A., 1997. Thiosulfate leaching following bio-oxidation pretreatment for gold recovery from refractory carbonaceous-sulfidic ore. *Mining Engineering*, 49(8), 76-80.
- [25] Navarro, P., Vargas, C., Villarroel, A. and Alguacil, F.J., 2002. On the use of ammoniacal/ammonium thiosulphate for gold extraction from a concentrate. *Hydrometallurgy*, 65(1), 37-42.
- [26] American Society for Testing and Materials, 2005. *Standard Test Method for Fire Assay Determination of Gold in Copper Concentrates by Gravimetry: Annual book of ASTM E 1805-02*, West Conshohocken: ASTM International.
- [27] Australian Standard, 1991. *Methods for the Analysis of Copper, Lead, Zinc, Gold and Silver Ores: Part 1 Determination of Gold (Fire Assay-Flame AAS Method)*, NSW: Standards Australia.
- [28] Arslan, F. and Sayiner, B., 2007. Extraction of gold and silver from Turkish gold ore by ammoniacal thiosulphate leaching. *Mineral Processing and Extractive Metallurgy Review*, 29(1), 68-82.
- [29] Abbruzzese, C., Fornari, P., Massidda, R., Veglio, F. and Ubaldini, S., 1995. Thiosulphate leaching for gold hydrometallurgy. *Hydrometallurgy*, 39(1-3), 265-276.
- [30] Rath, R.K., Hiroyoshi, N., Tsunekawa, M. and Hirajima, T., 2003. Ammoniacal thiosulphate leaching of gold ore. *The European Journal of Mineral Processing and Environmental Protection*, 3(3), 344-352.
- [31] Hung, H.V., Hai, H.T., Nga, N.T., Lee, J.-C. and Jeong, J., 2011. Study on effect of temperature on gold leaching from electronic scraps using thiosulphate with copper(II) catalyst in ammonia media. *Journal of Science & Technology*, 82A, 37-41.

## Influence of Solvent Temperature and Type on Naphthalene Solubility for Tar Removal in a Dual Fluidized Bed Biomass Gasification Process

Pimnara Tonpakdee<sup>1</sup>, Janjira Hongrapipat<sup>2</sup>, Vilailuck Siriwongrungron<sup>1\*</sup>, Reinhard Rauch<sup>3</sup>, Shusheng Pang<sup>4</sup>, Jullapong Thaveesri<sup>5</sup>, Michael Messner<sup>2</sup>, Matthias Kuba<sup>6,7</sup> and Hermann Hofbauer<sup>7</sup>

<sup>1</sup>College of Advanced Manufacturing Innovation, King Mongkut's Institute of Technology Ladkrabang, Bangkok, Thailand

<sup>2</sup>Güssing Renewable Energy (Thailand) Co., Ltd., Bangkok, Thailand

<sup>3</sup>Engler-Bunte-Institute, Karlsruhe Institute of Technology, Karlsruhe, Germany

<sup>4</sup>Department of Chemical and Process Engineering, University of Canterbury, Christchurch, New Zealand

<sup>5</sup>Ministry of Industry, Bangkok, Thailand

<sup>6</sup>Bioenergy2020+ GmbH, Wienerstraße 49, 7540 Güssing, Austria

<sup>7</sup>Institute of Chemical, Environmental and Bioscience Engineering, TU Wien, Vienna, Austria

Received: 19 October 2020, Revised: 9 April 2021, Accepted: 22 April 2021

### Abstract

Tar condensation is a cause of blockage in downstream application of the gasification process. An oil scrubber is considered as an effective method for tar removal. In this research, the naphthalene solubility in different local Thai oils and water was investigated in a laboratory-scale test-rig. The solubility value was conducted at 30, 50, 70, and 80°C. Biodiesels investigated were rapeseed methyl ester (RME) and two different palm methyl esters (PME 1 and PME 2). Furthermore, vegetable oils including sunflower oil, rice bran oil, crude palm oil, and refined palm oil were examined. The results showed that higher temperature enhanced naphthalene solubility in all types of investigated oils. Biodiesel has the highest value of naphthalene solubility. All scrubbing oils have similar naphthalene solubility trends at the temperature range of 50-80°C in the order of RME > PME 1 > PME 2 > diesel > sunflower oil > refined palm oil > rice bran oil > crude palm oil. Based on these experimental investigations, PME 1 has a naphthalene solubility value similar to RME. Therefore, PME 1 has been selected to be tested as scrubbing solvent in the 1 MW<sub>el</sub> prototype dual fluidized gasifier located in Nong Bua district, Nakhon Sawan province, Thailand.

**Keywords:** tar removal; oil scrubber; solvent scrubbing; naphthalene; dual fluidized bed biomass gasification

DOI.14456/cast.2021.60

---

\*Corresponding author: E-mail: vilailuck.si@kmitl.ac.th  
Tel.: 02-329-8264 ext. 2182

## 1. Introduction

Biomass gasification transforms biomass and solid carbonaceous fuel into a gaseous secondary energy carrier. When using steam as gasifying agent, reforming reactions occur inside the gasification reactor. The so-called product gas from the gasification process contains primarily hydrogen, carbon monoxide, carbon dioxide, methane, and C<sub>2</sub>-C<sub>4</sub> hydrocarbons [1]. The product gas has a high heating value of 10-18 MJ/Nm<sup>3</sup> compared to air gasification (4-7 MJ/Nm<sup>3</sup>) and thus can be further used for efficient generation of electricity, chemicals, and liquid fuels [2, 3]. However, there are undesired components in the product gas, mainly a mixture of high molecular weight hydrocarbons, defined as tar, and traces of ammonia, hydrogen sulfide, and hydrogen chloride [4-6].

Tar is an organic complex mixture of hydrocarbons that can be condensed, such as aromatics and polyaromatic hydrocarbons [7]. The tar composition and concentration depend on the type of biomass and operating conditions [7, 8]. "Tar is divided into five classes based on molecular weight, which are (1) GC-undetectable, (2) heterocyclic aromatics, (3) light aromatic (1 ring), (4) light polycyclic aromatic hydrocarbon (PAH) compounds (2 - 3 rings), and (5) heavy PAH compounds (4 - 7 rings)" [7, 8]. Tars in the product gas condense when the temperature of the product gas decreases. The class 5 tar components condense at higher temperatures even at low concentrations. The tar classes 2 and 4, heterocyclic aromatics and light PAHs, condense at around 0-125°C even at very low concentrations [8]. Tar condensation causes blocking in the downstream equipment. This is a major problem in biomass gasification and therefore tars must be removed to obtain a reliable operation [9].

There are many tar removal techniques. Yet, physical tar removal is widely used in the downstream cleaning process because it is easy to control and requires low energy [10-13]. Physical tar removal processes can be classified into two systems, which are dry systems such as cyclones and filters, and wet systems such as spray towers and packed column scrubbers. For scrubbers, the scrubbing solvent plays an important role for the design and tar removal efficiency. Water scrubbing has been reported as a common technique [14]. Nevertheless, the main disadvantage of the water scrubber is the low solubility of tar compounds. This is because water belongs to the hydrophilic (polar) group, but the main tar components (PAHs) belong to the hydrophobic (non-polar) group. So, only a few kinds of tar components can dissolve in water [15, 16]. This means that water is not a suitable solvent to remove tar in the product gas [17]. Besides water scrubbing, oil scrubbing is an interesting option because oil belongs to the hydrophobic group, which is the same as tar [18-20].

It was reported that the tar solubility in oil was much higher than in water. Phuphuakrat *et al.* [16] found that a water scrubber could remove only 31.8% of gravimetric tar. The removal efficiencies of tar compounds in each type of oil absorbents were observed to be in the following descending order: diesel fuel > vegetable oil > biodiesel fuel > engine oil > water [16]. The authors recommended that vegetable oil and biodiesel were interesting and were suitable solvents for tar removal [16]. Ahmad and Zainal [21] showed 22% and 75% total tar removal efficiency when water and waste palm cooking oil collected from restaurants were used as scrubbing solvent, respectively. Moreover, temperature is a primary parameter that affects tar solubility in the solvent [21]. In the work of Nakamura *et al.* [22], the tar removal performance of bio-oil as a scrubbing solvent at different temperatures was investigated. The result showed that the tar removal efficiency was 63.8, 73.3, and 54.3% at 40, 50, and 60°C, respectively.

Biodiesel, namely rapeseed methyl ester (RME), has been used for tar removal in commercial dual fluidized bed (DFB) steam gasification processes in Europe [23]. In Thailand, the 1 MW<sub>el</sub> prototype DFB steam gasification process, engineered and constructed by Gussing Renewable Energy Company, is the first plant in Asia [24]. It is a pioneering and innovative DFB

gasifier that can be fuelled with various types of biomass and waste [24]. This DFB gasifier power plant is located at Nong Bua district in Nakhon Sawan province.

One of major operating costs of this DFB gasifier is from the use of imported RME in the tar removal process. Substituting the imported RME with a locally supplied solvent as the tar scrubbing solvent was an objective. Therefore, it was decided to investigate the tar solubility of different local oils in Thailand in a laboratory scale test-rig. Based on previous gas chromatography-mass spectrometry (GC-MS) analysis of used RME after scrubber and other studies, it was observed that naphthalene was present as a component of high content in the product gas from the DFB gasifier [25, 26].

The aim of this research work was to find a feasible local Thai oil to substitute for the imported biodiesel that is currently used in the tar scrubbing system of the prototype commercial-scale DFB gasification process located in Thailand. Naphthalene was used as a tar model compound. Its solubility in various types of local Thai oils and water at various temperatures was studied.

## **2. Materials and experimental setup**

### **2.1 Materials**

#### **2.1.1 Tar model compound**

Naphthalene was employed in this study as a representative of total tar due to its high content in the product gas from the DFB steam biomass gasifier. Naphthalene is classified as a class 4 type of tar, and it is condensable at low temperature and at very low concentration [8]. The purity of naphthalene used was 99%, and it was purchased from Sigma-Aldrich Inc.

#### **2.1.2 Scrubbing solvents**

The solvents used in this research are divided into two types, namely the hydrophilic (polar) group and hydrophobic (non-polar) group. Water is the only representative solvent of the hydrophilic group. For hydrophobic group, there are three kinds of oil, i.e. (1) methyl ester or biodiesel, (2) vegetable oils (sunflower oil, rice bran oil, crude palm oil, and refined palm oil), and (3) diesel. All of the scrubbing solvents, except RME, were purchased locally in Thailand.

The RME used in this current research was imported from Germany and had the same specification as that used in the prototype commercial-scale DFB gasification process in Thailand and the commercial DFB gasifier power plant in Austria. Two palm methyl esters (PME), namely PME 1 and PME 2, were purchased locally in Thailand.

Solvent properties were also experimentally determined in this research. The densities of the oils were determined using the Archimedes' principle. The viscosities of oils were measured by Brookfield DVIII Ultra. A Gas Chromatograph-Mass Spectrometer (GC-MS) was used to analyze the components of oil. In the GC-MS analysis, oils were diluted at 100:1 in hexane except for diesel, which was diluted at 100:1 in acetone. Sample volume of 0.2  $\mu\text{l}$  was injected into HP-5 Column. Helium was used as carrier gas at the flow rate of 0.9 ml/min. The oven temperature was started from 40°C until the temperature reached 250°C.

### **2.2 Experimental set up and analysis**

Figure 1 displays the experimental set up for the investigation of the naphthalene solubility in various solvents. The effect of the temperature was studied by varying solvent temperature at 30,

50, 70, and 80°C. These temperatures are in the operating ranges of the scrubber in the commercial DFB biomass gasification process.

In the experiment, scrubbing solvent of 20 ml was heated in a water bath to the desired temperature. The temperature of the solvent (T1) was controlled steadily by a thermostat of the water bath temperature (T2). Naphthalene was slowly added to the solvent at the same rate for all experiments. The temperatures of the solvents were kept constant through the controlling of the water bath temperature. The mixing of naphthalene in solvent was performed by a magnetic stirrer with the same constant speed of 750 rpm for all scrubbing solvents. The total time consumed for a complete test of a single solvent at a particular temperature was between 3 and 5 h, and tests were done in triplicate.

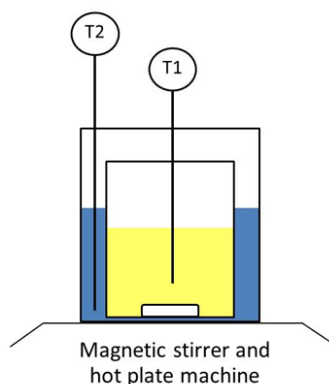


**Figure 1.** Experimental set up for tar solubility study

The solubility value of naphthalene was calculated using equation (1). The amount of naphthalene was visually determined when first crystals appeared at constant solvent temperature.

$$\text{Solubility value} = \frac{\text{Amount of tar (g)}}{\text{Volume of solvent (l)}} \quad (1)$$

### 3. Results and Discussion

#### 3.1 Effect of solvent temperature on naphthalene solubility

The average value of naphthalene solubility was calculated from three repetitive test values for each set of conditions, i.e. solvent type and temperature. The average value of naphthalene solubility (g naphthalene/l solvent) is presented in Figure 2. The percentage of naphthalene solubility standard deviation for all conditions does not exceed  $\pm 5\%$ .

Figure 2 shows the dependency of naphthalene solubility with temperature and type of the scrubbing solvent. All scrubbing solvents showed a similar trend with increasing the temperature. When the temperature of the scrubbing solvent was increased, the naphthalene solubility increased. The solubility of naphthalene slightly increased at low temperatures from 30°C to 50°C but significantly increased at high temperatures from 50°C to 80°C.

When naphthalene was added into the scrubbing solvent, the temperature of scrubbing solvent decreased, as observed during the experiments. According to thermodynamics principles known as Le Chatelier's principle, the solubility of naphthalene is an endothermic dissolution process. Therefore, increasing the temperature of a solvent leads to an increase in naphthalene

solubility. The increasing rate of the naphthalene solubility is related to its melting point. The melting point of naphthalene influences the solubility. The naphthalene solubility was significantly increased from 50°C to 80°C because the temperature was getting closer to the melting point of naphthalene, which was at 80-82°C [27].

### 3.2 Effect of solvent type on naphthalene solubility

As shown in Figure 2, the solubility of naphthalene in the solvents can be ranked in the order of biodiesel > diesel > vegetable oil > water. The biodiesel group showed the highest naphthalene solubility and among the three biodiesels tested, it was found that RME and PME 1 had competitive

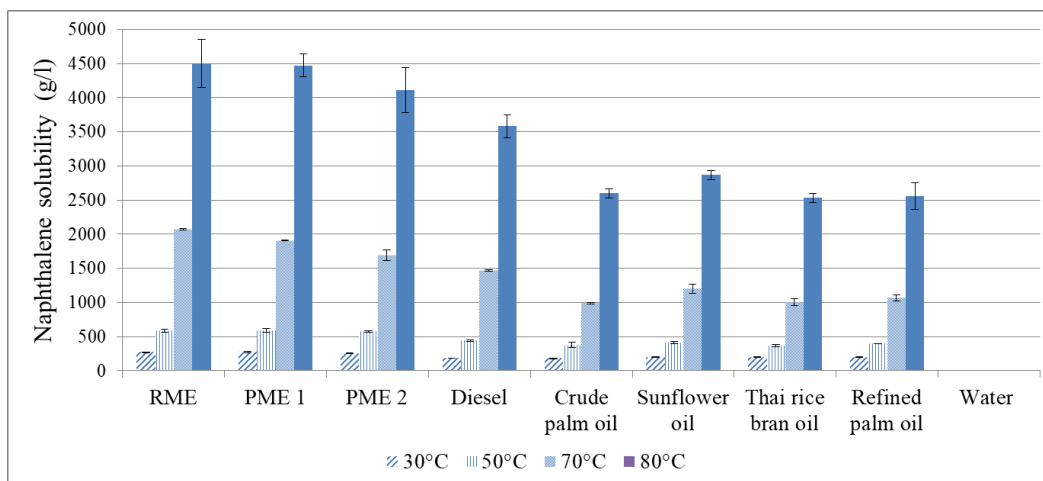


**Figure 2.** Naphthalene solubility in various scrubbing solvents at different temperatures

solubility values of  $271.23 \pm 6.65$  and  $271.00 \pm 8.05$  g/l at 30°C,  $582.55 \pm 23.60$  and  $586.90 \pm 26.45$  g/l at 50°C,  $2070.77 \pm 9.08$  and  $1906.30 \pm 3.15$  g/l at 70°C, and  $4499.00 \pm 349.33$  and  $4468.18 \pm 166.17$  g/l at 80°C, respectively. At 70°C, RME has slightly more tar solubility than PME 1. For PME 2, it showed competitive solubility values at the solvent temperatures of 30°C to 50°C, but showed a lower solubility than RME and PME 1 at the solvent temperatures of 50°C to 80°C.

All scrubbing solvents had similar naphthalene solubility trends for 50-80°C as RME > PME 1 > PME 2 > diesel > sunflower oil > refined palm oil. The naphthalene solubility of Thai rice bran oil and crude palm oil were slightly different. Except at 30°C, diesel showed higher naphthalene solubility than sunflower oil, refined palm oil, and rice bran oil.

The properties of solvent affect the solubility value. The diffusion process is related to the viscosity of solvent. A lower viscosity solvent has a higher diffusion coefficient, and hence a higher dissolution rate than a higher viscosity solvent [15, 16]. A high dissolution rate often means high solubility. The viscosities of the solvents are presented in Tables 1 and 2. Biodiesel showed approximately 10 times lower viscosity than vegetable oil, and thus naphthalene solubility in biodiesel was noticeably higher than in vegetable oil. It means that naphthalene is absorbed in biodiesel more than in other oils at the same temperature. Comparing diesel with biodiesel, although diesel shows approximately 1.47 cP lower viscosity than biodiesel, naphthalene solubility in diesel is lower than biodiesel.

**Table 1.** Properties of biodiesel

Properties	Unit	RME	PME 1	PME 2
Density at 30°C	g/cm <sup>3</sup>	0.8817	0.8758	0.8755
Viscosity at 30°C	cP	4.93	4.97	4.94
Ester content	wt %	98.00	98.80	98.80
- Saturated ester	wt %	7.19	50.59	64.39
- Unsaturated ester	wt %	90.81	48.20	34.37
Methanol	wt %	0.02	0.017	0.041
Water content	% (m/m)	0.0185	0.023	0.029
Cloud point	°C	-4	14	19
Flash point	°C	-	>170	155

**Table 2.** Properties of diesel and vegetable oil

Properties	Unit	Diesel	Sunflower oil	Refined palm oil	Thai rice bran oil	Crude palm oil
Density at 30°C	g/cm <sup>3</sup>	0.8380	0.9259	0.9273	0.9362	0.8373
Viscosity at 30°C	cP	3.46	40.06	52.90	53.87	1072.67
Ester content	wt %	21.895	97.762	92.259	91.399	96.892
Alkanes	wt %	68.673	-	-	-	-
Aromatic	wt %	9.435	-	-	-	-
Alcohol	wt %	-	2.238	7.130	2.682	3.107
Organic acid	wt %	-	-	-	5.920	-
Aldehyde	wt %	-	-	0.611	-	-

In addition, interactions between solute and solvent also influence the naphthalene solubility. These interactions are; solute-solute interaction, solvent-solvent interaction, and solute-solvent interaction. In this research, solute-solvent interaction is focused since this study tested only one solute in various solvent types. Diesel and biodiesel have straight-chain alkanes but the alkane chain length of diesel is shorter than that of biodiesel. With the increase in alkane chain length, the solubility of naphthalene also increases. Naphthalene dissolves in diesel through the bonding of London dispersion forces, which are the weakest intermolecular forces [28]. On the contrary, naphthalene dissolves in biodiesel through the bonding of the dipole-induced dipole forces, which are stronger than London dispersion forces [29]. Strong intermolecular bonding interaction of solute-solvent leads to high dissolution of solute in a solvent. Therefore, naphthalene can be dissolved in biodiesel more than diesel [28-30].

### 3.2.1 Naphthalene solubility in biodiesel

According to Table 1, RME, PME1 and PME2 show insignificantly different viscosities and ester contents. Methanol belongs to the alcohol group, which is classified as polar substance. Thus, naphthalene can better dissolve in RME, PME1 and PME2, respectively. In addition, RME, PME1 and PME2 have different amounts of saturated esters and unsaturated esters. The degree of unsaturated ester content also influences the naphthalene solubility. Saturated ester such as palmitic acid (C16:0) has no carbon double bonds whereas unsaturated esters such as oleic acid (C18:1) and linoleic acid (C18:2) have double carbon bonds. The aromatic tar solubility increases with increasing unsaturated ester content. Saturated esters are straighter-chained hydrocarbon molecules than unsaturated esters. This means that saturated esters have a solvent structure that is more closely packed [29]. An increment of unsaturated ester attributes to an increase of freedom of movement in solvent structure [29]. This allows aromatic tar molecules to bond with unsaturated esters more easily than saturated esters [29]. As illustrated in Figure 3, RME has the highest unsaturated ester (mainly oleic acid and linoleic acid) followed by PME1 and PME2. Therefore, RME has the highest naphthalene solubility while PME2 has the lowest naphthalene solubility.

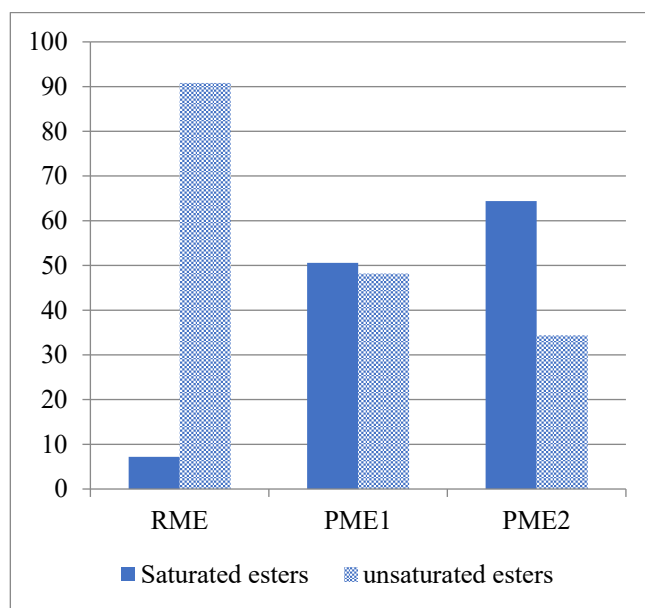


**Figure 3.** Percentage of saturated esters and unsaturated esters of biodiesel

### 3.2.2 Naphthalene solubility in vegetable oil

The properties of vegetable oils that affect naphthalene solubility are summarized in Table 2. The vegetable oils with higher viscosity have lower dissolution rate, and hence lower naphthalene solubility [15, 16]. Sunflower oil has the lowest viscosity. Thus, sunflower oil has the highest naphthalene solubility. Thai rice bran oil and crude palm oil have the lowest naphthalene solubility.

The composition of each vegetable oil also influences the naphthalene solubility. Among the main composition of vegetable oil are ester groups. When rating the polarity of functional groups from highest to lowest, they are in the following order: amide > organic acid > alcohol > aldehyde > ketone > amine > ester > ether > alkane. According to the solubility principle, a non-polar solute

(naphthalene) is likely to dissolve in non-polar solvents. Sunflower oil shows the lowest polar substance (alcohol content). Thus, naphthalene solubility in sunflower oil presents the highest value. Furthermore, organic acid is a strong polar compound that is present in Thai rice bran oil. Thus, naphthalene solubility in refined palm oil is higher than in Thai rice bran oil. Naphthalene solubility in Thai rice bran oil and crude palm oil is lowest due to the high viscosity of crude palm oil and highly polar substances of Thai rice bran oil.

### 3.2.3 Naphthalene solubility in water

When using water as an absorbing solvent, it was found that naphthalene was insoluble in water at all temperatures because naphthalene is a cyclic aromatic compound and is non-polar whereas water belongs to a hydrophilic polar group [8]. So, a water scrubber is not an appropriate device for the removal of naphthalene from the product gas, but it can be used for some classes of tar such as phenol [16].

### 3.3 Implementation of naphthalene solubility in a tar removal process

From the results discussed above, PME1 was chosen as a substitute of RME for tar removal in the 1 MW<sub>el</sub> prototype dual fluidized gasification in Nong Bua district, Nakhon Sawan province, Thailand. The tar concentrations in the producer gas when using the imported RME and PME1 were 93±59 and 86±28 mg/Nm<sup>3</sup>, respectively. The tar concentration with the substituted local PME1 scrubbing solvent was considered to be comparable with the imported RME. The cost of the local PME as the scrubbing solvent for the tar removal process was approximately 25% lower than that of the imported RME.

## 4. Conclusions

The solubility of naphthalene in different solvents, locally available in Thailand, was investigated. For all the temperatures between 30 and 80°C, naphthalene solubility in biodiesel was the highest; hence it was predicted to be the best among all other tested solvents for tar removal. Based on these experimental results, PME1 showed a similar naphthalene solubility to RME. Thus, PME1 was selected to be tested as a scrubbing solvent in the Thailand 1 MW<sub>el</sub> prototype DFB gasifier at Nong Bua district in Nakhon Sawan province, Thailand. The tar concentration was found to be comparable between RME and PME1, but the cost of PME1 was lower by approximately 25%.

In addition, more research work in the laboratory will be conducted to investigate other tar compounds mostly generated in the biomass DFB gasifier process such as anthracene, pyrene, fluoranthene, and biphenyl.

## 5. Acknowledgements

The authors gratefully appreciate the financial support of this research work from the College of Advanced Manufacturing Innovation (AMI), King Mongkut's Institute of Technology Ladkrabang (KMITL) Grant No. 2559-02-10-002.

## References

- [1] Sutton, D., Kelleher, B. and Ross, J.R.H., 2001. Review of literature on catalysts for biomass gasification. *Fuel Processing Technology*, 73(3), 155-173.
- [2] Thornley, P., Gilbert, P., Shackley, S. and Hammond, J., 2015. Maximizing the greenhouse gas reductions from biomass: The role of life cycle assessment. *Biomass and Bioenergy*, 81, 35-43.
- [3] Basu, P., 2010. *Biomass Gasification and Pyrolysis*. Boston: Academic Press.
- [4] Bridgwater, A.V., 1995. The technical and economic feasibility of biomass gasification for power generation. *Fuel*, 74(5), 631-653.
- [5] Kienberger, T., Zuber, C., Novosel, K., Baumhagl, C. and Karl, J., 2013. Desulfurization and in situ tar reduction within catalytic methanation of biogenous synthesis gas. *Fuel*, 107, 102-112.
- [6] Benedikt, F., Kuba, M., Schmid, J.C., Müller, S. and Hofbauer, H., 2019. Assessment of correlations between tar and product gas composition in dual fluidized bed steam gasification for online tar prediction. *Applied Energy*, 238, 1138-1149.
- [7] Milne, T.A., Evans, R.J. and Abatzoglou, N., 1998. *Biomass Gasifier "Tars" : Their Nature, Formation, and Conversion*. [online] Available at: <https://core.ac.uk/download/pdf/206771461.pdf>.
- [8] Li, C. and Suzuki, K., 2009. Tar property, analysis, reforming mechanism and model for biomass gasification—An overview. *Renewable and Sustainable Energy Reviews*, 13(3), 594-604.
- [9] Asadullah, M., 2014. Biomass gasification gas cleaning for downstream applications: A comparative critical review. *Renewable and Sustainable Energy Reviews*, 40, 118-132.
- [10] Devi, L., Ptasinski, K. and Janssen, F.J.J.G., 2003. A review of the primary measures for the tar elimination in biomass gasification processes. *Biomass and bioenergy*, 24(2), 125-140.
- [11] Phuphuakrat, T., Namioka, T. and Yoshikawa, K., 2010. Tar removal from biomass pyrolysis gas in two-step function of decomposition and adsorption. *Applied energy*, 87(7), 2203-2211.
- [12] Chen, H.J., Wu, J., Wang, X.Y., Zhu, Y.Z., Yang, L., Wu, H., Chen, Z.Q., Zhang, C. and Wan, L., 2016. Simulated biomass tar removal mechanism and performance by a Quench coupled with Absorption Technology. *Fuel processing technology*, 146, 90-98.
- [13] Paethanom, A., Nakahara, S., Kobayashi, M., Prawisudha, P. and Yoshikawa, K., 2012. Performance of tar removal by absorption and adsorption for biomass gasification. *Fuel processing technology*, 104, 144-154.
- [14] Bhoi, P.R., Huhnke, R.L., Singarapu, K., Kumar, A. and Payton, M.E., 2015. Solubility enhancement of producer gas tar compounds in water using sodium dodecyl sulfate as a surfactant. *Fuel processing technology*, 133, 75-79.
- [15] Ozturk, B. and Yilmaz, D., 2006. Absorptive Removal of Volatile Organic Compounds from Flue Gas Streams. *Process Safety and Environmental Protection*, 84(5), 391-398.
- [16] Phuphuakrat, T., Namioka, T. and Yoshikawa, K., 2011. Absorptive removal of biomass tar using water and oily materials. *Bioresour Technology*, 102(2), 543-549.
- [17] Balas, M., Lisy, M., Skala, Z. and Pospisil, J. (2014). Wet scrubber for cleaning of syngas from biomass gasification. *Development and Chemistry, Advances in Environmental Sciences*, Santorini Island, July 17-21, 2014, 195-201.
- [18] Bhoi, P.R., Huhnke, R.L., Kumar, A., Payton, M.E., Patil, K.N. and Whiteley, J.R., 2015. Vegetable oil as a solvent for removing producer gas tar compounds. *Fuel processing technology*, 133, 97-104.

- [19] Unyaphan, S., Tarnpradab, T., Takahashi, F. and Yoshikawa, K., 2017. Improvement of tar removal performance of oil scrubber by producing syngas microbubbles. *Applied Energy*, 205, 802-812.
- [20] Unyaphan, S., Tarnpradab, T., Takahashi, F. and Yoshikawa, K., 2017. An investigation of low cost and effective tar removal techniques by venturi scrubber producing syngas microbubbles and absorbent regeneration for biomass gasification. *Energy Procedia*, 105, 406-412.
- [21] Ahmad, N.A. and Zainal, Z.A., 2016. Performance and chemical composition of waste palm cooking oil as scrubbing medium for tar removal from biomass producer gas. *Journal of Natural Gas Science and Engineering*, 32, 256-261.
- [22] Nakamura, S., Unyaphan, S., Yoshikawa, K., Kitano, S., Kimura, S., Shimizu, H. and Taira, K., 2015. Tar removal performance of bio-oil scrubber for biomass gasification. *Biofuels*, 5(6), 597-606.
- [23] Hofbauer, H., Reinhard, R., Bosch, K., Koch, R. and Christian, A., 2002. Biomass CHP Plant Güssing – A Success Story. *Expert Meeting, Pyrolysis and Gasification of Biomass and Waste 2002*, Strasbourg, France, January 01, 2002, 527-536.
- [24] Hongrapipat, J., Messner, M., Henrich, C., Koch, M., Nanning, L., Rauch, R. and Hofbauer, H., 2015. 1 MWel Prototype Dual Fluidised Bed Gasifier Fuelled with Renewable Energy Resources by Gussing Renewable Energy. *Renewable Energy World Asia Conference 2015*, Bangkok, Thailand, September 01, 2015.
- [25] Kirnbauer, F., Wilk, V., Kitzler, H., Kern, S. and Hofbauer, H., 2012. The positive effects of bed material coating on tar reduction in a dual fluidized bed gasifier. *Fuel*, 95, 553-562.
- [26] Kuba, M. and Hofbauer, H., 2018. Experimental parametric study on product gas and tar composition in dual fluid bed gasification of woody biomass. *Biomass and Bioenergy*, 115, 35-44.
- [27] Tyrer, D., 1912. The Theory of Solubility. *Journal of Physical Chemistry*, 16(1), 69-85.
- [28] Michel, L. and Joussot-Dubien, J. 1973. New evidence for oriented interaction between normal alkanes and aromatic molecules from spectral solvent shifts. *Chemical Physics*, 2(2), 245-248.
- [29] Muzenda, E., 2014. Aromatic compounds and ester polymeric solvents interactions. *International Journal of Chemical, Environmental and Biological Sciences (IJCEBS)*, 2(2), 113-117.
- [30] Scheepers, J. J., Muzenda, E. and Belaid, M. 2012. Influence of structure on fatty acid ester-alkane interactions. *International Conference on Chemical Engineering and its Application (ICCEA'2012)*, Bangkok Thailand, September 8-9, 2012, 93-102.

## Effects of Ethylthiosulfanylate and Chromium (VI) on the State of Glutathione Antioxidant System and Oxidative Stress Marker Content in Rat Kidneys

Bohdan Kotyk\* and Ruslana Iskra

Department of Biochemistry Adaptation and Ontogenesis of Animals, Institute of Animal Biology of NAAS, Lviv, Ukraine

Received: 9 August 2020, Revised: 24 April 2021, Accepted: 13 May 2021

### Abstract

Hexavalent chromium (Cr(VI)) is a heavy metal and powerful toxicant with strong oxidative properties. Antioxidant defense system plays a key role in the processes of elimination and prevention of the negative effects of Cr(VI)-induced oxidative stress in biological systems. Prolonged action of Cr(VI)-induced oxidative stress leads to dysfunction of the antioxidant defense system and as a result provokes cell apoptosis. Ethylthiosulfanylate is synthetic sulfur-containing organic compound that belongs to the class of thiosulfonates. Structurally, thiosulfonates are synthetic analogues of natural organosulfur biologically active substances obtained from garlic, onion, cauliflower and broccoli. Thiosulfonates have antioxidant properties and activate the processes of reactive oxygen species (ROS) utilization. Therefore, the aim of this study was to examine the effect of ethylthiosulfanylate as a synthetic analogue of natural biologically active substances on the state of glutathione antioxidant system and oxidative stress marker content in the kidneys of rats under the condition of Cr(VI)-induced oxidative stress. Our results report that 14 days of ethylthiosulfanylate pretreatment (100 mg/kg body weight) caused attenuation of the intensity of Cr(VI)-induced lipid and protein peroxidation processes ( $P < 0.05$ ). Moreover, previous impact of ethylthiosulfanylate prevented depletion of the total reduced glutathione (GSH) pool after 14 days of potassium dichromate action in kidneys of rats ( $P < 0.05$ ). The present study indicates that ethylthiosulfanylate had antioxidant properties and partially inhibited Cr(VI)-induced oxidative damage in kidneys of rats. The obtained results may become a part of the background for the creation of effective methods of prevention and correction of the antioxidant and pro-oxidant states in kidneys affected by the action of Cr(VI)-induced oxidative stress.

**Keywords:** rats; antioxidant system; kidneys; oxidative stress; ethylthiosulfanylate; hexavalent chromium

DOI 10.14456/cast.2021.61

---

\*Corresponding author: Tel.: (+38) 09341 79385

E-mail: kicyniabo@gmail.com

## 1. Introduction

Chromium is a silver-gray, lustrous metal that can be in eleven different oxidation states from – IV to + VI. The most common and persistent forms of chromium are Cr(III) and Cr(VI) [1]. Cr(III) is an important trace element for humans and animals and is widely distributed in nature in the form of chromium-containing compounds. Hexavalent Cr(VI) is a heavy metal with high toxicity, carcinogenicity, and mutagenicity, and it causes oxidative stress in the cells of living organisms [2]. Cr(VI) occurs in nature as chromium-containing compounds present in ultramafic rocks or in its ionic form in water. The main sources of hexavalent chromium compounds are anthropogenic activity and industry. Hexavalent chromium compounds are used for industrial purposes in the processes of leather tanning and wood preservatives and finds use in the production of textiles, stainless steel, refractory materials, anti-corrosion coatings, pigments for paints and plastics [1]. Hexavalent chromium is a powerful toxicant and has strong oxidative properties. Reduction of hexavalent chromium to its trivalent form generates a large number of hydroxyl radicals, superoxide anions, hydrogen peroxide, thiol radicals, and chromium salts and as a result activates the peroxidation processes of biomolecules [1]. The kidneys are very sensitive to Cr(VI)-induced oxidative stress. Intraperitoneal action of potassium dichromate at a dose of 20 mg/kg body weight causes a decrease of GSH content and an increase of lipid peroxidation process in rat kidneys [3]. Potassium dichromate exposure at a dose of 15 mg/kg body weight leads to an increase in serum creatinine and urea content, as well as an increase in malondialdehyde (MDA) concentration, myeloperoxidase activity and tumor necrosis factor content in rat kidney tissue. A similar dose of potassium dichromate causes a decrease in melatonin content and damage to renal tubules, and leads to negative histopathological changes in the kidneys of rats [2].

The antioxidant defense system plays a key role in the processes of elimination, prevention and mitigation of the negative effects of Cr(VI)-induced oxidative stress in biological systems [1, 4]. However, the prolonged and intense action of Cr(VI)-induced oxidative stress leads to depletion of antioxidant defense system enzymes and as a result provokes cell apoptosis [5, 6]. In recent years, an urgent task for scientists has been to find compounds with antioxidant properties that have the ability to prevent Cr(VI)-induced depletion of the antioxidant defense system. Biologically active substances with antioxidant, detoxifying and cytoprotective properties can effectively perform the elimination and prevention of the negative effects of Cr(VI)-induced oxidative stress [2, 3]. Vitamin E and atorvastatin pretreatment decreases the intensity of MDA and nitric oxide formation, reduces superoxide dismutase (SOD) activity in rat kidneys, and attenuates the intensity of rat serum creatinine and urea elevation under the action of potassium dichromate oxidative stress [2]. Pycnogenol attenuates the increase of thiobarbituric acid reactive substances (TBARS), MDA, carbonyl group of proteins (CP), and prevents depletion of GSH content and catalase (CAT) activity in rat kidneys under the condition of  $K_2Cr_2O_7$  toxicity [7]. The literature also reports that carvedilol and extra virgin olive oil can effectively ameliorate potassium dichromate toxicity due to a decrease of TBARS level and through the restoration of GSH content and the enzymatic activity of glutathione peroxidase (GP), glutathione S-transferase (GST), SOD, and CAT in rat kidneys [8]. The antioxidant activity of ascorbic acid protects rat brain against  $K_2Cr_2O_7$ -induced peroxidation processes, GSH content depletion and glutathione reductase (GR) activity suppression [9].

Ethylthiosulfanylate is synthetic sulfur-containing organic compound. The ethylthiosulfanylate molecule has the structure  $RSO_2SR'$  in which R is an aniline residue and R' is an alkyl residue ( $-C_2H_5$ ) [10]. Ethylthiosulfanylate belongs to the class of thiosulfonates ( $RSO_2SR'$ ), which are synthetic analogues of organosulfur biologically active substances obtained from garlic, onion, cauliflower and broccoli. Thiosulfonates have antioxidant properties and activate the processes of detoxification and ROS and free radical utilization [11]. Thiosulfonates perform the processes of Nrf2-induced activation of the *nqo1* and *gstp1* gene promoters, which control the

activity of more than 200 genes responsible for the activation of antioxidant defense system enzymes and free radical scavenging [12]. Thiotaaurine (2-aminoethane thiosulfonate), which belongs to the class of thiosulfonates, prevents increase in TBARS level and GSH content depletion in the blood plasma and liver of rats under the action of acetaminophen-induced oxidative stress. The thiotaaurine thiosulfonate molecule has the structure  $RSO_2SR'$  in which R is an aminoethane residue and R' is a hydrogen atom (-H) [13].

Organosulfur natural analogues of thiosulfonates obtained from garlic extracts activate the mechanisms of hydroxyl radical scavenging and suppression of superoxide anion generation processes [14]. Allicin is one of the main organosulfur components of garlic extracts. Molecules of allicin regulate the activity of nuclear transcription factor (Nrf2), which is responsible for the antioxidant defense system gene expression. Allicin-induced stimulation of Nrf2 leads to the activation of enzymes such as SOD, glutathione GP, GST, NAD(P)H: quinone oxidoreductase 1 (NQO1), gamma-glutamylcysteine synthetase ( $\gamma$ -GCS), hemoxidase (HO)-1 and to the inhibition of Ang II-induced oxidative stress pathways [15, 16].

Thus, nowadays there is enough information describing the effects of thiosulfonates and their natural analogues on the state of the pro/antioxidant system of animals. However, there is little known about the antioxidant properties of thiosulfonates under the condition of heavy metals-induced oxidative stress in the tissues of animals. Due to the important role of thiosulfonates and their natural analogues in maintaining the antioxidant status in living organisms, the purpose of our studies was to investigate the effect of ethylthiosulfanylate as a synthetic analogue of natural biologically active substances on the state of glutathione antioxidant system and oxidative stress marker content in the kidneys of rats under the condition of Cr(VI)-induced oxidative stress.

## 2. Materials and Methods

### 2.1 Experimental design

The research was conducted in the vivarium of the Institute of Animal Biology of NAAS on white male Wistar laboratory rats (130-140 g), which were randomly divided into 7 groups with 5 animals per group. Animals of all groups were fed with standard compound feed for laboratory rats with free access to drinking water and feed.

Group I (intact control): were injected daily intraperitoneally with 150  $\mu$ l of physiological saline solution for 7 days.

Group III/Group IV: received potassium dichromate ( $K_2Cr_2O_7$ ) intraperitoneally at a dose 2.5 mg Cr(VI)/kg body weight per day for 7 days/14 days.

Group II: were injected daily intragastrally with 1000  $\mu$ l of oil for 14 days («Oleina» oil, traditional: refined, deodorized, frozen; Producer of PJSC with II «DOEP»; certified according to State Standard of Ukraine 4492: 2017 and complies with ISO 14024) and then immediately after that injected daily intraperitoneally with 150  $\mu$ l of physiological saline solution for 7 days.

Group V: were injected daily intragastrally with an oil solution of ethylthiosulfanylate at a dose of 100 mg/kg body weight for 14 days and then immediately after that were injected daily intraperitoneally with 150  $\mu$ l of physiological saline solution for 7 days.

Group VI/Group VII: received intragastrally an oil solution of ethylthiosulfanylate at a dose 100 mg/kg body weight daily for 14 days and then immediately after that received  $K_2Cr_2O_7$  intraperitoneally daily at a dose of 2.5 mg Cr(VI)/kg body weight per day for 7 days/14 days.

All procedures were made to minimize animal suffering following the guidelines of European Convention "For the Protection of Vertebrate Animals Used for Experimental and Other Scientific Purposes" (Strasbourg, 1986) and "Common Ethical Principles for Animal Experiments"

(Ukraine, 2001). Permission to conduct research was obtained from the Committee on Bioethics of Institute of Animal Biology NAAS of Lviv (Protocol № 80). The effects of newly synthesized ethyl 4-aminobenzenethiosulfonate compound were studied on the rat body synthesized at the Department of Technology of Biologically Active Compounds, Pharmacy and Biotechnology of National University "Lviv Polytechnic" according to the protocol described in detail in Lubenets *et al.* [10, 17].

After decapitation of the animals, which occurred under thiopental anesthesia, the kidneys were collected. All procedures on kidneys were performed at 4°C. The research material was the kidney homogenates of rats, which were prepared on 0.05 M Tris-HCl buffer with pH 7.4 in the ratio 1 g of tissue and 9 ml of buffer (1:9, weight/volume) and then centrifuged for 15 min at 1000 g. After centrifugation, obtained supernatants were analyzed for GSH content, peroxidation product level, and antioxidant enzyme activity.

### 2.1.1 Groups of animals

The groups of animals were compared according to the following scheme (Figure 1). Group I was an intact control in relation to experimental groups III and IV, each of which did not receive an oil solution. Group II was a control in relation to experimental groups V, VI and VII, each of which received an oil solution. We recorded the percentage (%) change in indicators for III and IV experimental groups relative to the group I (intact control). We recorded also the % change in indicators for V, VI and VII experimental groups relative to group II (oil control). At the final stage, we analyzed % change in indicators of III/IV experimental groups relative to the group I (intact control) and compared it with % change in indicators of VI/VII experimental groups relative to the group II (oil control).

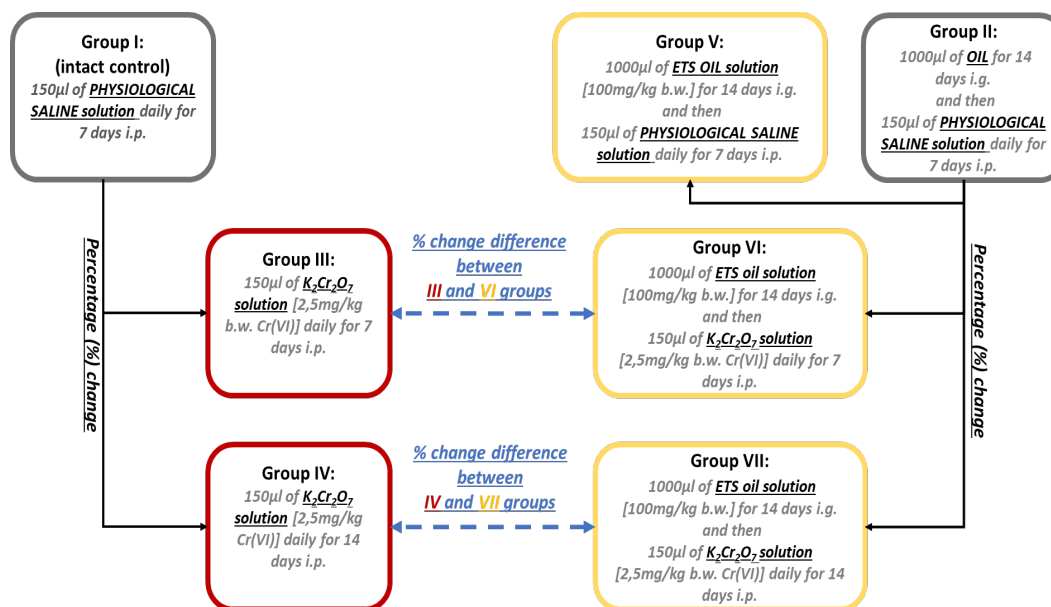


**Figure 1.** Groups of animals

ETS (ethylthiosulfanylate), i.p. (intraperitoneally), i.g. (intra-gastrally), b.w. (body weight)

## **2.2 Processing**

### **2.2.1 Concentration of LHP**

The content of LHP (lipid hydroperoxides) was determined according to the principle of precipitation of proteins with trichloroacetic acid solution and lipid extraction by ethanol action [18]. This method is based on the spectrophotometrically measurement of the level of colored product that forms the interaction of the experimental extracts (ethanol extracts of lipids) with ammonium thiocyanate. The absorption was measured spectrophotometrically at  $\lambda$  480 nm. The concentration of LHP was determined by the difference between values of control and experimental samples and was expressed as SU/g tissue.

### **2.2.2 Concentration of TBARS**

The content of TBARS (thiobarbituric acid reactive substances) in homogenates was determined by color reaction of MDA with thiobarbituric acid (TBA) [18]. The reaction was conducted at high temperature in an acidic environment. The level of colored product (colored complex of one MDA and two TBA molecules) was measured spectrophotometrically at  $\lambda$  535 nm and  $\lambda$  580 nm, and the values were expressed as nmol MDA/g tissue.

### **2.2.3 Concentration of CP**

The content of CP (carbonyl group of proteins) was determined by the interaction of the carbonyl groups of amino acids with 2,4-dinitrophenylhydrazine (DNPH) with the formation of 2,4-dinitrophenylhydrazones [18]. The absorption was measured spectrophotometrically at  $\lambda$  370 nm and the values were expressed in nmol CP/mg protein.

### **2.2.4 Activity of GP**

GP (glutathione peroxidase, EC 1.11.1.9) activity was established by the rate of oxidation of GSH before and after incubation with tertiary butyl hydroperoxide [18]. The intensity of GSH oxidation was determined by the formation of colored product (dinitrophenyl anion) during the interaction of 5,5-dityiobis-2-nitrobenzoic acid (DTNBA) with SH-groups. The absorption was measured spectrophotometrically at  $\lambda$  412 nm. The activity of GP was expressed in nmol GSH/min. $\times$ mg protein.

### **2.2.5 Activity of GR**

GR (glutathione reductase, EC 1.6.4.2) activity was determined in the reaction medium which consisted of 2.5 ml of 0.15 M phosphate buffer (pH 7.4), 0.2 ml of oxidized glutathione (7.5 mM), 0.1 ml of tissue homogenate and 0.1 ml of NADPH (1.2 mM). The enzyme activity was determined spectrophotometrically at  $\lambda$  340 nm for 1 min at 37°C. The GR activity was calculated using the molar absorption ratio for NADPH at the wavelength of 340 nm and expressed in  $\mu$ mol NADPH/min. $\times$ mg protein. The intensity of reaction depends on the tempo of extinction decrease. The principle of this method is based on determining the rate of glutathione reduction in the presence of NADPH [18].

### 2.2.6 Concentration of GSH

The content of GSH (reduced glutathione) in kidney homogenates was determined according to the principle of measurement of the level of formation of colored product – thionitrophenyl anion as described by Rosalovsky *et al.* [19]. The thionitrophenyl anion formation process is based on the interaction between DTNBA and SH-groups of GSH molecules. The absorption was measured spectrophotometrically at  $\lambda$  412 nm. The content of GSH was expressed in mmol GSH/g tissue.

### 2.2.7 Protein concentration

The concentration of total protein in the tissue homogenates was measured by the Lowry method [20] using "Simko LTD" kits (Ukraine, Lviv). The measurements of all absorbance values were performed on a spectrophotometer "Unico" 1205 (USA).

### 2.3 Statistical analysis

Statistical evaluation of the results was performed using mean values (M)  $\pm$  standard error (S.E.M), and the variances between groups were tested for significance using one-way ANOVA, followed by Tukey-Kramer test. The differences were statistically significant at  $P < 0.05$ . All calculations were performed using Microsoft Excel software.

## 3. Results and Discussion

### 3.1 Oxidative stress markers

Our results reported that Cr(VI) administration caused an increase in oxidative stress marker levels in rat kidney tissue (Table 1). The content of LHP in the kidneys of animals of III (Cr(VI) 7 days) and IV (Cr(VI) 14 days) experimental groups was significantly increased in comparison with group I (control) by 48 and 57%, respectively. The level of kidney CP under the action of Cr(VI) was significantly elevated by 62% (group III) and 97% (group IV) compared to the group I. We also observed a significantly higher concentration of TBARS in rat kidneys of groups III (Cr(VI) 7 days) and IV (Cr(VI) 14 days) compared to the group I by 15 and 23%, respectively. The content of LHP and CP was significantly elevated in the rat kidney tissue of groups III (Cr(VI) 7 days) and IV (Cr(VI) 14 days) compared to the group II by 48 and 57% (LHP) and 93% (CP), respectively. Transition metals and especially Cr(VI) are catalysts in the processes of oxidative destruction of biological macromolecules. A wide range of ROS (hydroxyl radical, superoxide anion, hydrogen peroxide) are generated during the Cr(VI) reduction to Cr(V), Cr(IV) and Cr(III). The result of ROS generation is an increase of peroxidation processes of lipids and proteins in the kidney tissue. Cr(VI)-induced activation of peroxidation processes causes the formation of oxidative stress products, such as LHP, TBARS and CP [3, 7].

Administration of ethylthiosulfanylolate during the 14 days caused decrease of the LHP level in the kidney tissue of rats of group V relative to the group II by 9%. Ethylthiosulfanylolate pretreatment by the next action of Cr(VI) led to significant increase of LHP content in the rat kidneys of VI and VII experimental groups compared with the group II by 9 and 22%, respectively. However, the increase of LHP content in the rat kidneys of groups VI (9%) and VII (22%) relative to the group II was by 39 and 35% lower than the percentage increase of LHP concentration in the kidneys of animals of groups III (48%) and IV (57%) compared to the group I.

**Table 1.** The content of indicators of oxidative stress in kidneys of rats (M±S.E.M., n=5)

Group s of animal s	I – Control	II – Oil	III – Cr 7 days	IV – Cr 14 days	V – Ethylth.	VI – Ethylth. + Cr 7 days	VII – Ethylth. + Cr 14 days
LHP. SU/g tissue	0.23±0.0 04	0.23±0.03* **	0.34±0.02* **	0.36±0.005* **	0.21±0.01* **,#	0.25±0.01* **,#	0.28±0.01* **,#
TBAR S. nmol/g tissue	6.29±0.3 1	6.27±0.13* *	7.22±0.58* *	7.76±0.16**	5.71±0.25* *	5.94±0.73* *	6.01±0.05* *
CP. nmol/m g prot.	0.39±0.0 9	0.40±0.03* **	0.63±0.08* **	0.77±0.07** *	0.42±0.03* **,#	0.43±0.01* **,#	0.56±0.05* **,#

Note: Significant difference of II, III, IV, V, VI, VII groups compared to the group I (control) is: \*\*-\*\*\* (P < 0.01 – P < 0.001); significant difference of V, VI, VII groups compared to the group II is: # (P < 0.05).

After 14 days of ethylthiosulfanylolate exposure, CP content was not changed in the kidneys of rats of group V compared to the group II. The level of CP by previous influence of ethylthiosulfanylolate and the next action of  $K_2Cr_2O_7$  was statistically elevated in the kidneys of rats of groups VI and VII in comparison with group II by 8 and 40%, respectively. However, the increase of CP content in the rat kidneys of groups VI (8%) and VII (40%) relative to the group II was by 54 and 57% lower than the percentage increase of CP concentration in the kidneys of animals of groups III (62%) and IV (97%) compared to the group I. The level of LHP and CP was significantly decreased in the rat kidneys of group VI (Ethylth. + Cr(VI) 7 days) compared to the group III (Cr(VI) 7 days) by 26 and 32%, respectively. Significant decrease of LHP and CP concentration was also observed in the kidneys of animals of group VII (Ethylth. + Cr(VI) 14 days) compared to the group IV (Cr(VI) 14 days) by 22, and 27%, respectively.

This may indicate that ethylthiosulfanylolate has antioxidant properties. It is known that polysulfides are secondary antioxidants (peroxide scavengers), which are involved in the mechanisms of reduction of lipid hydroperoxides to alcohols by inhibition of the chain reactions of autoxidation. Organosulfur polysulfides have the ability to transform first into sulfoxides and then into sulfenic acid during the processes of lipid hydroperoxide reduction. Sulfenic acid is capable of interacting with lipid hydroperoxides and decomposing them by dehydration [21, 22]. According to the literature, polysulfides and organosulfur compounds have the ability to transform into other sulfur-containing molecules and thiols, such as GSH molecules. [23, 24]. In turn, GSH molecules play an important role in non-enzymatic pathway of hydrogen peroxide scavenging and inhibition of the processes of LHP and CP formation [25].

Therefore, Cr(VI)-induced oxidative stress arises after intraperitoneal potassium dichromate injections and leads to increase of the content of LHP, TBARS and CP (groups III and IV) in rat kidney tissue. Previous intragastric exposure of ethylthiosulfanylolate partially inhibits the processes of lipid and protein peroxidation and suppressed the intensity of the formation of LHP and CP in the kidney tissue of animals (groups VI and VII) under the action of Cr(VI).

### 3.2 Glutathione antioxidant system

The action of Cr(VI) at 7 (groups III) and 14 days (groups IV) led to a significant increase of GP activity in the kidneys of animals compared to the control (group I) by 128 and 43%, respectively (Table 2). The literature data report that Cr(VI) activates the processes of hydrogen peroxide and hydroxyl radical formation, which in turn stimulates lipid peroxidation processes [3, 7]. Kotyzova *et al.* [26] suggest that the increase of LHP level and hydrogen peroxide content from Cr(VI)-induced oxidative stress leads to GP activation in the kidneys of rats. However, GR activity after Cr(VI) exposure in the rat kidneys of III (Cr(VI) 7 days) and IV (Cr(VI) 14 days) experimental groups was significantly decreased compared to the group I by 37 and 41%, respectively. The GSH content after 7 days of potassium dichromate administration was statistically higher by 7% in the kidney tissue of animals of group III in comparison with the group I. This may indicate that the accumulation of cellular GSH in rat kidneys reduces the concentration of ROS and LHP under the condition of Cr(VI) induced oxidative stress after 7 days of  $K_2Cr_2O_7$  injection [27]. However, after 14 days of potassium dichromate administration, the level of GSH was statistically lower by 23% in the rat kidneys of group IV in comparison with group I. GSH content was also significantly lower in the kidneys of animals of III and IV groups compared to the group II by 30 and 50%, respectively.

The literature data report that GSH plays a key role in a non-enzymatic process of Cr(VI) reduction to Cr(V) and Cr(IV). The reduction of Cr(VI) by GSH generates GS-Cr(V)/Cr(VI) complexes, which can subsequently be transformed into solids. Utilization of GSH by Cr(VI) reduction may be the reason for the GSH content depletion [1]. The processes of ROS neutralization also cause an active decrease in the level of the GSH molecules [8, 28]. The pathway of new GSH molecules biosynthesis is ATP-dependent [29], and ATP deficiency may cause a decrease in the GSH content in cells [30]. Heavy metal-induced oxidative stress leads to dysfunction of the mitochondrial respiratory chain and as a result inhibition of the processes of mitochondrial ATP synthesis [25]. GR catalyzes the process of GSH recovery in the presence of NADPH. Cr(VI) toxicity leads to decrease in the content of NADPH [1], and this could be the reason for the decrease in the efficiency of the reduction process of GSSG to GSH [31, 32]. GR induces the enzymatic process of NADPH-dependent Cr(VI) reduction to Cr(V) [1]. Cr(VI) action leads to NADPH oxidase (NOX) activation and as a result provokes the more intensive use of NADPH molecules with NOX participation [32]. The reason for the GR depletion under the action of  $K_2Cr_2O_7$  may be the disruption of GR enzymatic activity during Cr(VI) reduction and Cr-induced depletion of the GSH pool and NADPH content [9]. Prolonged Cr(VI)-induced loading of GR enzymatic activity may cause depletion of the corresponding enzyme activity. GR induces the enzymatic pathway of Cr(VI) reduction to Cr(V) in the presence of NADPH. The products of Cr(VI) reduction are NADPH-Cr(V) complexes, which can also be transformed into solids [1]. Mehany *et al.* [2] suggest that potassium dichromate exposure inhibits the activity of many antioxidant enzymes. Cr(VI) is able to bind to the SH group of the active site of the enzyme. Cr(VI) action leads to displace of cofactors-metals from the active site and disrupts the activity of antioxidant enzymes and this may be the reason of GR activity depletion under the action of Cr(VI)-induced oxidative stress.

After ethylthiosulfanylate pretreatment for 14 days, the GSH level was significantly increased by 36% in the kidneys of animals of group V compared to group II. The previous impact of ethylthiosulfanylate on the next action of Cr(VI) for 7 and 14 days also led to significant increase of GSH content in the rat kidneys of VI and VII experimental groups relative to group II by 39 and 38%, respectively. The GSH content was significantly higher in the kidneys of animals of group VI (Ethylth. + Cr(VI) 7 days) compared to the group III (Cr(VI) 7 days) and in the rat kidney tissue of group VII (Ethylth. + Cr(VI) 14 days) compared to the group IV (Cr(VI) 14 days) by 100 and 176%, respectively.

**Table 2.** Indicators of glutathione antioxidant system in kidneys of rats (M±S.E.M., n=5)

Groups of animals	I- Contro l	II-Oil	III-Cr7 days	IV-Cr14 days	V- Ethylth.	VI- Ethylth.+ Cr7 days	VII- Ethylth.+ Cr14 days
GP. nmol/min.× mg prot.	52.6±1. 27	48.02±2.69 ***	120.05±9.59 ***	75.36±1.07 ***	65.68±9.92 ***	91.77±16.82 ***	66.08±15.21 ***
GR. μmol/min.× mg prot.	3.13±0. 39	3.19±0.42* *	1.96±0.09**	1.87±0.28* *	3.05±0.32* *	2.78±0.21**	2.12±0.27**
GSH. mmol/g tissue	0.43±0. 06	0.66±0.07* **	0.46±0.11** *	0.33±0.02* **	0.9±0.05** *,#	0.92±0.09** *,#	0.91±0.07** *,#

Note: the statistically significant difference II, III, IV, V, VI, VII groups compared to the group I (control) is: \*\*-\*\*\* (P < 0.01 – P < 0.001); the statistically significant difference V, VI, VII groups compared to the group II is: # (P < 0.05).

Thiosulfonates are responsible for the Nrf2-dependent activation of antioxidant defense gene expression that encodes  $\gamma$ -GCS and glutathione synthetase (GS) [15, 16, 29]. The main function of these enzymes is carrying out the processes of GSH molecule biosynthesis. At first stage,  $\gamma$ -GCS induces the synthesis of gamma-glutamylcysteine from L-glutamate and cysteine. Then, GS catalyzes the second stage of GSH molecule biosynthesis from gamma-glutamylcysteine. These two steps are ATP-dependent and play an important role in maintaining the pool of cellular GSH. During biochemical processes, thiosulfonates have the ability to transform into other sulfur-containing compounds, which can be further used as materials for the synthesis of GSH molecules [33].

Therefore, Cr(VI)-induced oxidative stress represents a high load on the glutathione defense system activity and induces an intense activation of GP (III and IV groups), depletion of GR resource (III and IV groups) and decrease of GSH content (group IV) in the rat kidney tissue. The effect of ethylthiosulfanylate without Cr(VI) action, on the contrary, leads to the accumulation of renal GSH (group V). Ethylthiosulfanylate pretreatment partially offsets the negative effect of K<sub>2</sub>Cr<sub>2</sub>O<sub>7</sub>-induced oxidative stress and prevents the depletion of the GSH pool in the kidneys of animals (groups VI and VII) under the action of Cr(VI).

#### 4. Conclusions

It is known that biologically active substances with antioxidant properties (atorvastatin, pycnogenol, carvedilol, extra virgin olive oil, ascorbic acid, vitamin E) have the ability to ameliorate Cr(VI)-induced toxicity. Even though there has been little known about the antioxidant properties of thiosulfonates, there is enough information describing the protective properties of thiosulfonates against Cr(VI) toxicity in tissues of animal organism. Our results indicate that ethylthiosulfanylate pretreatment may be effective in correcting Cr(VI)-induced oxidative stress. We assume that further studies of the antioxidant properties of ethylthiosulfanylate are important for the better understanding of the role of thiosulfonates in the mechanisms of prevention of heavy metals-induced oxidative stress.

In general, the obtained results report that potassium dichromate causes Cr(VI)-induced oxidative stress and leads to disbalance of glutathione antioxidant defense system mechanisms. Pretreatment with ethylthiosulfanylate partially eliminates the negative effects of Cr(VI)-induced oxidative stress, attenuates the intensity of peroxidation processes and prevents depletion of GSH content under the condition of Cr(VI)-induced oxidative stress. Ethylthiosulfanylate administration also leads to accumulation of the total GSH pool in rat kidneys.

We hypothesize that a possible mechanism for preventing Cr(IV) toxicity may be related to ethylthiosulfanylate-induced GSH accumulation in rat kidneys. GSH accumulation is very important under the condition of Cr(VI)-induced oxidative stress. GSH molecules initiate the reduction of toxic Cr(VI) compounds to a non-toxic form – Cr(III). GSH molecules are also involved in the enzymatic reduction of LHP and non-enzymatic neutralization of ROS. Therefore, it can be assumed that the ethylthiosulfanylate-induced accumulation of GSH may contribute to inhibition of peroxidation processes, suppression of ROS formation, and stimulation of Cr(VI) reduction processes under the condition of  $K_2Cr_2O_7$  toxicity. We hypothesize also that a possible mechanism for preventing Cr(IV)-induced oxidative stress may be related to ethylthiosulfanylate-induced decreasing in the intensity of lipid peroxidation processes in rat kidneys. Literature data report that thiosulfonates are able to react directly with free radicals. Organosulfur compounds and polysulfides are involved in the processes of LHP reduction and decomposition. It is possible that the above antioxidant properties of organosulfur compounds can be used to explain the possible mechanisms for the prevention of Cr(VI)-induced oxidative stress with the participation of ethylthiosulfanylate.

In the following studies, we plan to determine the additional indicators needed to better understand the antioxidant properties of ethylthiosulfanylate. In particular, we plan to investigate the effect of ethylthiosulfanylate on the enzymatic activity of  $\gamma$ -GCS (gamma-glutamylcysteine synthetase), GS (glutathione synthetase), GST (glutathione S-transferase), SOD and CAT. We are also interested in the measuring of  $H_2O_2$  concentration and level of Cr(VI) accumulation in rat tissues. Furthermore, we plan also to combine the action of ethylthiosulfanylate with other effective protectors against Cr(VI) toxicity. It is known that vitamin E has a positive antioxidant effect and reduces the intensity of Cr(VI)-induced oxidative damage. Perhaps the combined effect of ethylthiosulfanylate with vitamin E will increase the effectiveness of counteraction of Cr(VI)-induced oxidative stress.

Our results indicate that ethylthiosulfanylate pretreatment partially stabilized Cr(VI)-induced disturbance in the mechanisms of the antioxidant defense system action in rat kidneys. Moreover, the results of our study may become a part of the background for creation of effective methods of prevention and correction of the antioxidant and pro-oxidant states in kidneys affected by the action of Cr(VI)-induced oxidative stress.

## References

- [1] Saha, R., Nandi, R. and Saha, B., 2011. Sources and toxicity of hexavalent chromium. *Journal of Coordination Chemistry*, 64(10), 1782-1806.
- [2] Mehany, H.A., Abo-youssef, A.M., Ahmed, L.A., El-Shaimaa, A. and El-Latif, H.A.A., 2013. Protective effect of vitamin E and atorvastatin against potassium dichromate-induced nephrotoxicity in rats. *Beni-Suef University Journal of Basic and Applied Sciences*, 2(2), 96-102.
- [3] Boşgelmez, I.I. and Güvendik, G., 2004. Effects of taurine on oxidative stress parameters and chromium levels altered by acute hexavalent chromium exposure in mice kidney tissue. *Biological Trace Element Research*, 102(1-3), 209-225.

- [4] Atmaca, G., 2004. Antioxidant effects of sulfur-containing amino acids. *Yonsei Medical Journal*, 45(5), 776-788.
- [5] Asatiani, N., Kartvelishvili, T., Abuladze, M., Asanishvili, L. and Sapojnikova, N., 2011. Chromium (VI) can activate and impair antioxidant defense system. *Biological Trace Element Research*, 142, 388-397.
- [6] Stanley, J.A., Sivakumar, K.K., Nithy, T.K., Arosh, J.A., Hoyer, P.B., Burghardt, R.C. and Banu, S.K., 2013. Postnatal exposure to chromium through mother's milk accelerates follicular atresia in F1 offspring through increased oxidative stress and depletion of antioxidant enzymes. *Free Radical Biology and Medicine*, 61, 179-196.
- [7] Parveen, K., Khan, M.R. and Siddiqui, W.A., 2009. Pycnogenol® prevents potassium dichromate ( $K_2Cr_2O_7$ )-induced oxidative damage and nephrotoxicity in rats. *Chemico-Biological Interactions*, 181(3), 343-350.
- [8] Sahu, B.D., Koneru, M., Bijargi, S.R., Kota, A. and Sistla, R., 2014. Chromium-induced nephrotoxicity and ameliorative effect of carvedilol in rats: Involvement of oxidative stress, apoptosis and inflammation. *Chemico-Biological Interactions*, 223, 69-79.
- [9] Zeid, E.H.A., Hussein, M.M.A. and Ali, H., 2018. Ascorbic acid protects male rat brain from oral potassium dichromate-induced oxidative DNA damage and apoptotic changes: the expression patterns of caspase-3, P 53, Bax, and Bcl-2 genes. *Environmental Science and Pollution Research*, 25(13), 13056-13066.
- [10] Lubenets, V., Havryliak, V., Pylypets, A. and Nakonechna, A., 2018. Changes in the spectrum of proteins and phospholipids in tissues of rats exposed to thiosulfonates. *Regulatory Mechanisms in Biosystems*, 9(4), 495-500.
- [11] Zenkov, N.K., Menshchikova, E.B., Kandalintseva, N.V., Oleynik, A.S., Prosenko, A.E., Gusachenko, O.N., Shklyayeva, O.A., Vavilin, V.A. and Lyakhovich, V.V., 2007. Antioxidant and antiinflammatory activity of new water-soluble sulfur-containing phenolic compounds. *Biochemistry (Moscow)*, 72(6), 644-651.
- [12] Vavilin, V.A., Shintyapina, A.B., Safronova, O.G., Antontseva, E.V., Mordvinov, V.A., Nikishina, M.V., Kandalintseva, N.V., Prosenko, A.E. and Lyakhovich, V.V., 2014. Position of an active thiosulfonate group in new phenolic antioxidants is critical for ARE-mediated induction of GSTP1 and NQO1. *Journal of Pharmaceutical Sciences and Research*, 6(4), 178-183.
- [13] Acharya, M. and Lau-Cam, C.A., 2013. Comparative evaluation of the effects of taurine and thiotaurine on alterations of the cellular redox status and activities of antioxidant and glutathione-related enzymes by acetaminophen in the rat. *Advances in Experimental Medicine and Biology*, 776, 199-215.
- [14] Chung, L.Y., 2006. The antioxidant properties of garlic compounds: allyl cysteine, alliin, allicin, and allyl disulfide. *Journal of Medicinal Food*, 9(2), 205-213.
- [15] Li, X.-H., Li, C.-Y., Lu, J.-M., Tian, R.-B. and Wei, J., 2012. Allicin ameliorates cognitive deficits ageing-induced learning and memory deficits through enhancing of Nrf2 antioxidant signaling pathways. *Neuroscience Letters*, 514(1), 46-50.
- [16] Li, X.-H., Li, C.-Y., Xiang, Z.-G., Hu, J.-J., Lu, J.-M., Tian, R.-B. and Jia, W., 2012. Allicin ameliorates cardiac hypertrophy and fibrosis through enhancing of Nrf2 antioxidant signaling pathways. *Cardiovascular Drugs and Therapy*, 26(6), 457-465.
- [17] Lubenets, V., Karpenko, O., Ponomarenko, M., Zahoriy, G., Krychkovska, A. and Novikov, V., 2013. Development of new antimicrobial compositions of thiosulfonate structure. *Chemistry & Chemical Technology*, 7(2), 119-124.
- [18] Vlizlo, V.V., Fedoruk, R.S., Ratych, I.B., Vishchur, O.I., Sharan, M.M., Vudmaska, I.V., Fedorovych, Y.I., Ostapiv, D.D., Stapai, P.V., Buchko, O.M., Hunchak, A.V., Salyha, Y.T., Stefanyshyn, O.M., Hevkan, I.I., Lesyk, Y.V., Simonov, M.R., Nevostruieva, I.V., Khomyn, M.M., Smolianinov, K.B., Havryliak, V.V., Kolisnyk, H.V., Petrukh, I.M., Broda, N.A.,

- Luchka, I.V., Kovalchuk, I.I., Kropyvka, S.Y., Paraniak, N.M., Tkachuk, V.M., Khrabko, M.I., Shtapenko, O.V., Dzen, Y.O., Maksymovych, I.Y., Fedorovych, V.V., Yuskiv, L.L., Dolaichuk, O.P., Ivanytska, L.A., Sirko, Y.M., Kystsiv, V.O., Zahrebelnyi, O.V., Simonov, R.P., Stoianovska, H.M., Kyryliv, B.Y., Kuziv, M.I., Maior, K.Y., Kuzmina, N.V., Talokha, N.I., Lisna, B.B., Klymyshyn, D.O., Chokan, T.V., Kaminska, M.V., Kozak, M.R., Oliinyk, A.V., Holova, N.V., Dubinskyi, V.V., Iskra, R.Y., Ravis, Y.F., Tsepko, N.L., Kyshko, V.I., Oleksiuk, N.P., Denys, H.H., Slyvchuk, Y.I. and Martyn, Y.V., 2012. *Laboratory Methods of Investigation in Biology, Stockbreeding and Veterinary*. 2<sup>nd</sup> ed. Lviv: Spolom.
- [19] Rosalovsky, V.P., Grabovska, S.V. and Salyha, Y.T., 2015 Changes in glutathione system and lipid peroxidation in rat blood during the first hour after chlorpyrifos exposure. *The Ukrainian Biochemical Journal*, 87(5), 124-132.
- [20] Lowry, O.H., Rosebrough, N.J., Farr, A.L. and Randall, R.J., 1951. Protein measurement with the Folin phenol reagent. *The Journal of Biological Chemistry*, 193(1), 265-275.
- [21] Soleimani, M., Dehabadi, L., Wilson, L.D. and Tabil, L.G., 2018. Antioxidants classification and applications in lubricants. In: D. Johnson, ed. *Lubrication-Tribology, Lubricants and Additives*. Saskatoon: Intech Open, pp. 23-42.
- [22] Chauvin, J.R., Griesser, M. and Pratt, D.A., 2019. The antioxidant activity of polysulfides: it's radical! *Chemical Science*, 10, 4999-5010.
- [23] Yaremkevych, O., Polischuk, I., Mandzynets, S., Bura, M., Sanagurskyi, D., Lubenec, V. and Novikov, V., 2011. Analysis of variance of influence of thiosulphonic acid derivatives on the Na<sup>+</sup>, K<sup>+</sup>-ATP-ase activity of loach embryos in vitro. *Visnyk of the Lviv University, Series Biology*, 57, 38-46.
- [24] Pylypets, A.Z., Iskra, R.Y., Havryliak, V.V., Nakonechna, A.V., Novikov, V.P. and Lubenets, V.I., 2017. Effects of thiosulfonates on the lipid composition of rat tissues. *The Ukrainian Biochemical Journal*, 89, 56-62.
- [25] Reyes, J.L., Molina-Jijón, E., Rodríguez-Muñoz, R., Bautista-García, P., Debray-García, Y. and Namorado, M., 2013. Tight junction proteins and oxidative stress in heavy metals-induced nephrotoxicity. *BioMed Research International*, 2013, <https://doi.org/10.1155/2013/730789>
- [26] Kotyzova, D., Hodkova, A., Bludovska, M. and Eybl, V., 2015. Effect of chromium (VI) exposure on antioxidant defense status and trace element homeostasis in acute experiment in rat. *Toxicology and Industrial Health*, 31(11), 1044-1050.
- [27] Geetha, S., Sai Ram, M., Mongia, S., Singh, V., Ilavazhagan, G. and Sawhney, R., 2003. Evaluation of antioxidant activity of leaf extract of Seabuckthorn (*Hippophae rhamnoides* L.) on chromium(VI) induced oxidative stress in albino rats. *Journal of Ethnopharmacology*, 87(2-3), 247-251.
- [28] Saber, T.M., Farag, M.R. and Cooper, R.G., 2015. Ameliorative effect of extra virgin olive oil on hexavalent chromium-induced nephrotoxicity and genotoxicity in rats. *Revue de Médecine Vétérinaire*, 166(1-2), 11-19.
- [29] Franklina, C.C., Backosa, D.S., Moharb, I., Whiteb, C.C., Formanc, H. J. and Kavanagh, T.J., 2009. Structure, function, and post-translational regulation of the catalytic and modifier subunits of glutamate cysteine ligase. *Molecular Aspects of Medicine*, 30(1-2), 86-98.
- [30] Schütt, F., Aretz, S., Auffarth, G.U. and Kopitz, J., 2012. Moderately reduced ATP levels promote oxidative stress and debilitate autophagic and phagocytic capacities in human RPE cells. *Investigative Ophthalmology & Visual Science*, 53(9), 5354-5361.
- [31] Kurata, M., Suzuki, M. and Agar, N.S., 2000. Glutathione regeneration in mammalian erythrocytes. *Comparative Haematology International*, 10, 59-67.
- [32] Pratheeshkumar, P., Son, Y.O., Divya, S.P., Roy, R.V., Hitron, J.A., Wang, L., Kim, D., Dai, J., Asha, P., Zhang, Z., Wang, Y. and Shi, X., 2014. Luteolin inhibits Cr(VI)-induced malignant cell transformation of human lung epithelial cells by targeting ROS mediated multiple cell signaling pathways. *Toxicology and Applied Pharmacology*, 281(2), 230-241.

- [33] Mampuys, P., McElroy, C.R., Clark, J.H., Orru, R.V.A. and Maes, B.U.W., 2020. Thiosulfonates as emerging reactants: Synthesis and applications. *Advanced Synthesis and Catalysis*, 362(1), 3-64.

## **An Assessment of Privacy Concerns on Personal Health Information: Thailand Case Study**

Charnsak Srisawatsakul and Waransanang Boontarig\*

Faculty of Computer Science, Ubon Ratchathani Rajabhat University,  
Ubon Ratchathani, Thailand

Received: 21 January 2021, Revised: 2 April 2021, Accepted: 6 May 2021

### **Abstract**

One of the most important industries that transforms into digital infrastructure is healthcare. Most healthcare organizations worldwide collect and process personal health information digitally. Personal health information is considered highly sensitive information. Hence, the increased collection of health information has raised concerns throughout society regarding potential privacy issues. Therefore, previous research paid attention to the study of privacy of health information in several contexts. In Thailand, Thai people are becoming more aware of privacy concerns than ever before. The reason is that the personal data protection act will become effective in May 2021. Hence, this study aims to understand the privacy concerns and behavioral intention to reveal Thais' personal health information. In this paper, we applied the Internet Users' Information Privacy Concerns model to the health information context. We collected data using an online questionnaire. The population consisted of Thai people who shared personal health information with the healthcare industry. The participants in this research were selected by the accidental sampling method. There were 84 participants in Thailand who were employed in the hypotheses testing using the linear regression equations. This study shows that personal health information collection and awareness directly influence personal health information privacy concerns. Furthermore, trusting belief is a factor that affects people's behavioral intention to share health information. The findings should help the healthcare industry to better understand the patients, so that they will offer their information willingly.

**Keywords:** GDPR; health information; IUIPC; PDPA; privacy concern; privacy  
DOI 10.14456/cast.2021.62

### **1. Introduction**

Over the past decade, privacy concerns of personal information have been increasing around the world. The large-scale breach of personal information is the main reason that has accelerated the debate on how much personal information should be accessible by other entities, either private or government organizations. Organizations that store and process personal data need to be concerned about their privacy policies, and this is required by law in various parts of the world. The European

---

\*Corresponding author: Tel.: (+66) 061-0509991  
E-mail: waransanang.s@ubru.ac.th

Union (EU) employed the General Data Protection Regulation (GDPR) for the protection of personal data across European countries [1, 2]. The aim of GDPR was to protect personal data and ensure that it was processed securely. In Thailand, the government announced a new privacy law, which was the Personal Data Protection Act (PDPA) [3]. The government published PDPA in the Government Gazette on 27 May 2019. However, there is a grace period of 2 years before all of the act becomes effective. It has a similar purpose to GDPR, which is to protect the privacy of personal data.

Personal health information refers to medical histories, laboratory results, demographic information, mental and physical health conditions, insurance information, and any form of information that a healthcare professional collects to identify an individual and determine appropriate care [4]. It is considered one of the most sensitive forms of information, according to GDPR [5] and PDPA [3]. Furthermore, the healthcare industry has adopted numerous information technologies to digitize patients' health information, such as EMR (Electronic Medical Record). To date, the volume of personal health information collected in electronic form has continued to increase at exponential rates. Therefore, the privacy of personal health information is a vital concern of the industry.

Throughout the past decade, personal information privacy has become an increasingly interesting topic among researchers worldwide. However, there is still a lag of research on privacy concerns of personal health information in Thailand. Moreover, Thais are less concerned with the confidentiality and privacy of their information [6]. Hence, this prospective study investigates Thai people's privacy concerns in the personal health information context. This study's empirical research approach was adapted from the Internet Users' Information Privacy Concerns (IUIPC)[7].

## 2. Materials and Methods

### 2.1 Privacy

Nowadays, the GDPR defines the privacy of data as “empowering your users to make their own decisions about who can process their data and for what purpose” Personal data relating to the inherited or acquired genetic characteristics of a natural person which give unique information about the physiology or the health of that natural person and which result, in particular, from an analysis of a biological sample from the natural person in question. However, privacy can be interpreted differently in various circumstances. Previous researchers have described it as dynamic, elastic, and multidimensional in the perception that it varies with life experience [8]. Solove [9] suggested that privacy can be classified as “(1) the right to be let alone; (2) limited access to the self; (3) secrecy; (4) control of personal information; (5) personhood; and (6) intimacy”. Likewise, Margulis [10] believes that the psychological concept subsumes a wide variety of privacy meanings. Privacy in the previous literature often focuses on how to control, protect, and preserve personal information [11]. Bennett [12] predicted that privacy could be used as a commodity in the information market economy, and his prediction has become true.

Thailand's Personal Data Protection act focuses on collecting, processing, disclosure, protection, and the rights of the data subjects. A violation of the PDPA could lead to a penalty of three million Thai baht [3] for the organizations. Therefore, the PDPA has raised Thai people's attention toward concerns about privacy of personal data.

In this study, we do not define privacy as any constitutional or legal concept [11]. However, this study's privacy refers to the belief and the reaction to the inside and outside stimuli. There are three categories of individuals' privacy concerns based on their level [13]. Firstly, the unconcerned privacy group. This group shows no privacy concerns at all. Secondly, those willing to disclose

personal data, and thus have less privacy in exchange for the benefit they will get. Lastly, privacy absolutists refer to a group of people who have serious concerns about their privacy.

## 2.2 Personal health information

The GDPR considered health information as “genetic data,” which means: “Personal data relating to the inherited or acquired genetic characteristics of a natural person which give unique information about the physiology or the health of that natural person and which result, in particular, from an analysis of a biological sample from the natural person in question” [1].

Most patients voluntarily reveal their health information to receive treatment from a healthcare specialist. Examples of personal health information are demographic, allergies, symptoms, diagnoses, prescriptions, medical histories, encounter summaries, etc. Therefore, the health industry is now quickly disturbed by health information technology. That technology helps the health industry save costs, increase efficiency, improve services, and protect personal health information. One of the most famous examples of health information technology is Electronic Medical Record. The information stored in the EMR of a patient may be exposed to many individuals in the treatment processes, such as doctors, physicians, nurses, pharmacists, and technicians. Moreover, outsiders such as insurance companies and patient employers may also need to access those medical records from time to time. Therefore, the access to and storage and processing of personal health information requires the explicit adapting of inclusive policies.

## 2.3 Internet users' information privacy concerns

Malhotra *et al.* [7] developed a construct for reflecting an individual's view toward the concern of information privacy on the internet. The construct is called Internet Users' Information Privacy Concerns (IUIPC). It contains ten-items for self-assessment questions. However, the author suggested that it should be used along with fifteen items of the CFIP (Concern for Information Privacy) scale to measure an individual's privacy concerns. Malhotra *et al.* [7] also suggested that the IUIPC should be used in the general privacy context with appropriate rewording to make the items relate to a specific context. For example, the word “online” in the questions could be eliminated so the construct can be used in the offline context [14].

Previous research applied the IUIPC to study privacy concerns in a different context. Kusyanti *et al.* [15] studied teenager's information privacy concerns on Facebook in Indonesia using the IUIPC. The result showed that the users were concerned about losing control of personal information but still had the intention of using Facebook. Sipior *et al.* [16] revalidated the method and construction of the IUIPC. The results suggested that the IUIPC construct was still applicable when applied in mobile advertising [14]. The researchers also added perceived ubiquity as an extended factor to the IUIPC. Pape *et al.* [17] re-applied the IUIPC in Japan and compared the results with results from the USA [7]. The results suggested that the IUIPC was still valid and reliable. However, trusting beliefs and risk beliefs showed some results that were contrary to those of the original IUIPC.

In the healthcare context, Angst and Agarwal [18] studied the individuals' behavioral intentions and privacy in order to digitize the medical information to the EHR. They applied the CFIP with 366 subjects. The results suggested that the appropriate message framing could increase the positive attitude toward the EHR for people in the high privacy concern group.

In conclusion, this study investigates Thai people's behavioral intentions and concerns about sharing personal health information. We employed the constructs of IUIPC with rewording into the context of personal health information for our research model.

## 2.4 Research model and hypothesis

According to the literature reviewed in the previous section, the research model is shown in Figure 1. The dependent variable is the behavioral intention toward sharing health information (BI). It was predicted by Trusting Beliefs (TB) and Risk Beliefs (RB) which are independent variables. Collection (CL), Control (CR), and Awareness (AW) are independent variables used to predict the Personal Health Information Privacy Concern (PHIPC) as the dependent variable. PHIPC also acts as an independent variable to predict the Trusting Beliefs and Risk Beliefs. The definition and hypothesis of each factor are shown below.

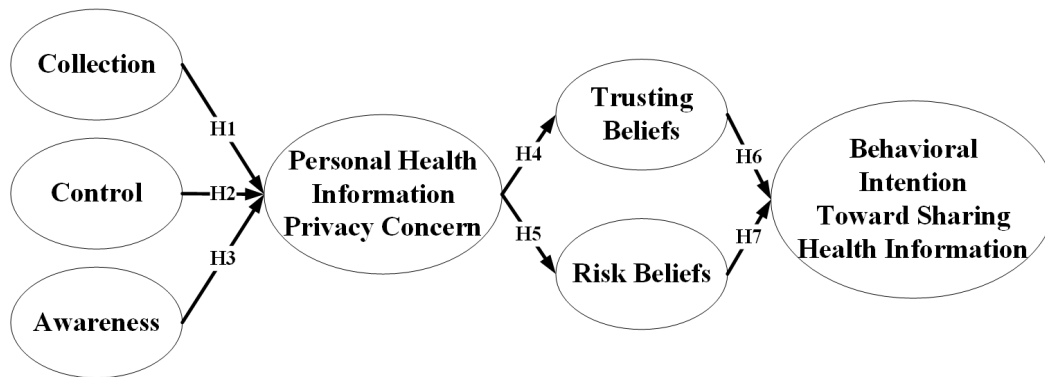


Figure 1. Research model of the study

### 2.4.1 Collection

The collection of personal data is the beginning of information privacy concerns [7]. In this context, the collection of personal health information can be defined as “the degree to which a person is concerned about the amount of personal health data possessed by others relative to the value of benefits received” [7].

In other words, individuals would offer personal health data in return for benefits such as disease diagnosis and treatment. They may refuse to release their health data if they expect negative consequences.

**H1:** The collection of personal health data will positively affect personal health information privacy concerns.

### 2.4.2 Control

Nowadays, the GDPR requires that the data subjects have the right to control their data. The controls include obtaining consent, right of access and right of data portability, rights of rectification and erasure, right to restriction of processing and right to object, identification of data processors, and compliance of the data transfer outside the European Union [19]. The patients take high risks in revealing their health information to the health sector or third parties. Hence, control over personal health information could affect the privacy concerns of personal health information.

**H2:** The control of personal health data will positively affect personal health information privacy concerns.

### 2.4.3 Awareness

Awareness is the patient's understanding and concern for the data processors or an organization's privacy policies and practices that process their personal health information.

**H3:** The awareness of the data controller and data processor's privacy policy will positively affect personal health information privacy concerns.

### 2.4.4 Personal health information privacy concerns

Campbell [20] defined information privacy concerns as “an individual’s subjective views of fairness within the context of information privacy.” In this study, information privacy is the context of personal health information shared with other people or organizations.

### 2.4.5 Trusting and risk beliefs

Trusting beliefs are defined as “the degree to which people believe a firm is dependable in protecting consumers’ personal information.” Risk beliefs refer to the expectation that a high potential for loss is associated with the release of personal information to the firm [7]. Trusting and risk beliefs are the original factors in the IUIPC model. They can be used to explain how an individual reveals their personal information. Therefore, more privacy concerns may not have much effect on trusting and risk beliefs. In this context, we proposed that personal health information privacy concerns will affect trusting and risk beliefs. Moreover, trusting and risk could be the factors that affect the behavioral intention toward the release of personal health information to the healthcare sector.

**H4:** Personal health information privacy concerns will negatively affect trusting beliefs.

**H5:** Personal health information privacy concerns will positively affect risk beliefs.

**H6:** The trusting beliefs will positively affect behavioral intention to use the health information system.

**H7:** The risk beliefs will negatively affect behavioral intention to use the health information system.

## 2.5 Collection of data

In this study, the population of the research consists of Thai people who have experience sharing personal health information with healthcare services. Nevertheless, the total number of populations is unknown. The sample of this research was done by the accidental sampling method. Data were collected using a self-administered online questionnaire. Each of the constructs was measured with a 7-point Likert scale. The questionnaire was online for a three-week period. The URL of the questionnaire was sent to the participants via E-mail and social media services, including Facebook and Line. In the questionnaire, we explained the meaning of privacy concerns of personal health information and the control of personal health information. It was divided into two parts; the first part elicited information on demographic information and the second part was designed to test the hypothesis using the constructs from IUIPC. The collected data were recorded as a Microsoft Excel spreadsheet for data screening. The Statistical Package for Social Science (SPSS) program was used to analyze the effect between dependent and independent variables.

### 3. Results and Discussion

This section explains the results of the statistical analysis, including validity and reliability analysis, and multicollinearity analysis. Lastly, to test the hypotheses, four linear regression equations were used to predict the dependent variables.

#### 3.1 Demographic variables

The total number of responses to this questionnaire was 125. Of these, 84 participants completed the questionnaire after data screening. Hence, those 84 datasets were used for empirical analysis. Table 1 shows the demographic information of the participants.

**Table 1.** Demographic information of the participants

Variables	Frequency	Percentage
<b>Gender</b>		
Male	27	32.1
Female	57	67.9
<b>Total</b>	84	100
<b>Age</b>		
18-25	29	34.5
26-33	9	10.7
34-42	25	29.8
More than 42	21	25
<b>Total</b>	84	100

#### 3.2 Validity and reliability analysis of the constructs

The questionnaire was analyzed using the Index of Item Objectives Congruence (IOC) to confirm the validity. It was sent to 3 experts to give the points for each item. The result showed that the IOC value was more than 0.5. Therefore, the questionnaire met the criterion of validity. Furthermore, the questionnaire was also tested for reliability using Cronbach's alpha coefficient [21]. The Cronbach's alpha coefficient greater than 0.70 should be considered as a good and reliable questionnaire. The Cronbach's alpha value for each variable of the questionnaire is shown in Table 2. The Cronbach's alpha coefficient values range from 0.668-0.922 is considered highly reliable [22]. Hence, the validity and reliability requirements of the constructs were satisfied.

**Table 2.** The Cronbach's alpha coefficient

Factor	Number of questions	Cronbach's alpha coefficient
Trusting Beliefs	3	0.895
Risk Beliefs	3	0.794
Personal Health Information Privacy Concern	3	0.824
Collection	4	0.922
Control	3	0.668
Awareness	3	0.862

### 3.3 Multicollinearity analysis

The multicollinearity analysis started by examining the correlation between variables, which was done by Pearson’s product-moment correlation coefficient. It was used to assess the strength and direction of relationships between the variables. The result of Pearson’s correlation coefficient analysis from this study is shown in Table 3. It shows that some variables significantly correlated with each other. Pearson’s correlation coefficient's highest value was 0.680 at the correlation between the behavioral intention to share health information and trusting beliefs. However, Pearson’s correlation coefficient should be less than 0.8 to prevent multicollinearity. Hence, there was no issue with correlation between variables in our dataset.

**Table 3.** Correlation matrix of Pearson's correlation coefficient

	BI	TB	RB	CL	CR	AW	PHIPC
BI	1	.680**	.058	-.037	.130	.436**	.139
TB	.680**	1	.126	-.082	.156	.383**	.175
RB	.058	.126	1	.647**	.410**	.181	.514**
CL	-.037	-.082	.647**	1	.546**	.179	.598**
CR	.130	.156	.410**	.546**	1	.571**	.497**
AW	.436**	.383**	.181	.179	.571**	1	.340**
PHIPC	.139	.175	.514**	.598**	.497**	.340**	1

\* Correlation is significant at the 0.01 level (2-tailed).

Furthermore, the constructs were analyzed to find the tolerance and Variance Inflation Factor (VIF) of variables to further confirm that there was no issue with multicollinearity. The results of those analyses are shown in Table 4. The lowest tolerance value was 0.471, and the VIF was 1.016. The highest tolerance value was 0.984, and the VIF was 2.125. The cut-off value of tolerance must not be less than 0.10, and VIF must not be more than 5 [23]. Therefore, these results confirmed that there was no multicollinearity detected between independent variables.

**Table 4.** Tolerance and variance inflation factor of variables

Multiple Linear Regression Model	Variables		Tolerance	Variance Inflation Factor (VIF)
	Dependent Variable	Independent Variable		
1	PHIPC	CL	0.965	1.033
		CR	0.471	2.125
		AW	0.968	1.033
2	BI	TB	0.984	1.016
		RB	0.984	1.016

### 3.4 Hypotheses testing results using multiple linear regression

#### 3.4.1 Assumption testing

The collected data were tested for linearity, normality, and homoscedasticity, all of which are required for the linear regression model to be valid and reliable [24]. The normality of the data was also not violated in this study. From the graph of the normal P-P plot of standardized residuals

(Figures 2-5, left side), we can see that most of the values go along with the diagonal line in systematic order. However, model 2 (Figure 3) and model 5 (Figure 5) show some dots that depart from the diagonal line. Nevertheless, the residuals still have the pattern moving along the diagonal line. Moreover, Pallant [25] suggests that a normality assumption's violation should not be a big issue when the sample size is larger than 40. Thus, the testing of normality was satisfied.

It is usually a good way to test for linearity and homoscedasticity using the scatterplot between the regression standardized residuals and regression standardized predicted value [26]. The scatterplots of four regression models are shown in Figures 2 to 5 (right side). Homoscedasticity means that the variance of the residuals is constant. Therefore, as the predicted values increase (along the X-axis), the residuals' variation should be approximately similar. Therefore, our scatterplots suggest that the regression standardized residual values were in the range of -3.3 to 3.3, meaning no outlier, and the assumption of homoscedasticity was justified.

Field [27] suggested that the linearity issue can be investigated from the scatterplot by examining the curve in this graph. The chances are that the data have broken the assumption of linearity. This study's scatterplots show that most residuals are randomly and evenly distributed throughout the zero standard residual value line. Hence, the linearity assumption is consistent. In conclusion, this study's data met the assumptions of homoscedasticity of variance and linearity and can be used for the regression equations.

### 3.4.2 Regression Variate Results

A multiple linear regression equation was calculated to predict personal health information privacy concerns. Table 5 shows the results of the calculation. The regression equation is significant ( $F(2,81) = 28.490, p < 0.001$ ). The  $R^2$  of this model is 0.413. It could predict 41 percent of the variance of PHIPC. The prediction equation for PHIPC is equal to  $2.008 + 0.426 (CL) + 0.122 (CR) + 0.272 (AW)$  where all independent variables are measured on the 7-point Likert scale. Health information privacy concerns increased by 0.426 for one unit increase in collection and 0.272 for awareness. Collection and awareness are significant predictors of personal health information privacy concerns. The control was not significant.

There are two simple linear regression models to determine the prediction of trusting beliefs and risk beliefs. The personal health information privacy concern was used as a predictor. The results are shown in Table 6. The first model, personal health information privacy concern, is non-significant when predicting trusting beliefs. However, the regression equation is significant in the second model ( $F(1,82) = 29.398, p < 0.001$ ). The  $R^2$  of this model is 0.264. It could predict 26 percent of the variance of risk beliefs. The prediction equation of risk beliefs is equal to  $1.469 + 0.554 (RB)$ . The concern of privacy in personal health information increases by 0.554 for each point of risk beliefs.

Behavioral intention toward sharing health information was predicted by the trusting beliefs and risk beliefs using a multiple linear regression model. The results of those analyses are shown in Table 7. A significant regression equation was found only with the trusting beliefs variable ( $F(1,81) = 70.689, p < 0.001$ ). The risk beliefs factor was found to be not significant for predicting behavioral intention toward sharing health information. The  $R^2$  of this model was 0.463. It could predict 46 percent of the variance of behavioral intention toward sharing health information. The result predicted that behavioral intention toward sharing health information was equal to  $-4.117 + 0.763 (TB) + (-0.032) (RB)$ . The behavioral intention toward sharing health information increased by 0.763 for each point of trusting beliefs.

The risk beliefs factor is also predicted by trusting beliefs. However, the trusting beliefs factor was found to be not significant for predicting risk beliefs.

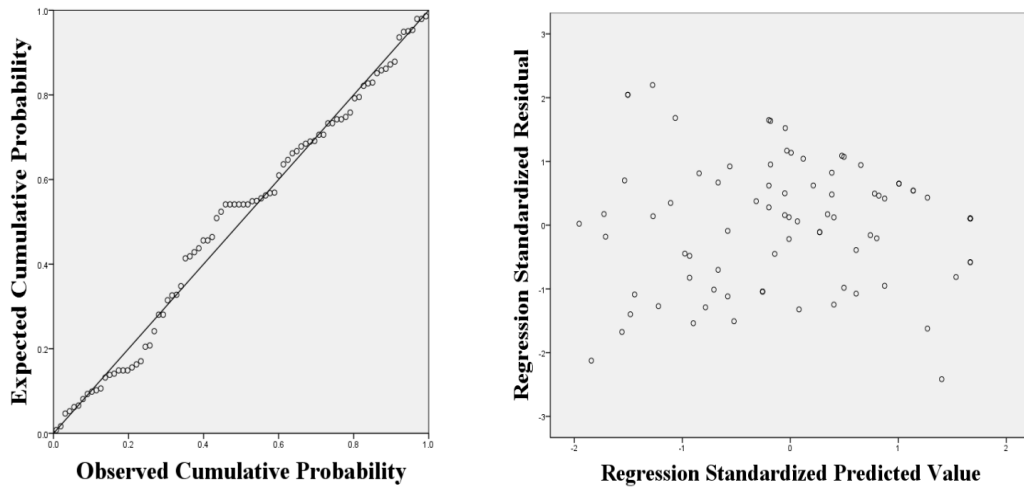


**Figure 2.** Model 1 normal p-p plot of regression standardized residual (left) and scatter plot (right). Dependent variable: PHIPC

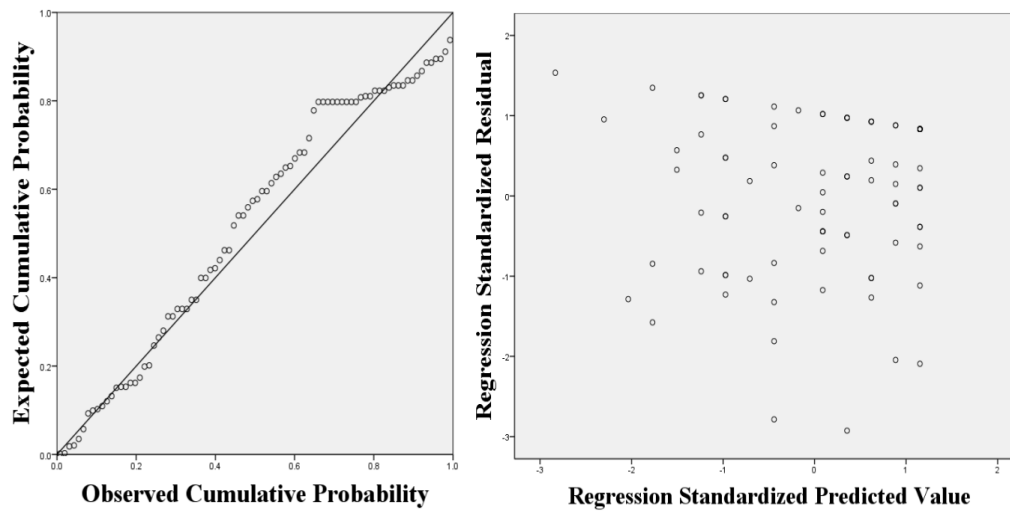


**Figure 3.** Model 2 normal p-p plot of regression standardized residual (left) and scatter plot (right). Dependent variable: TB

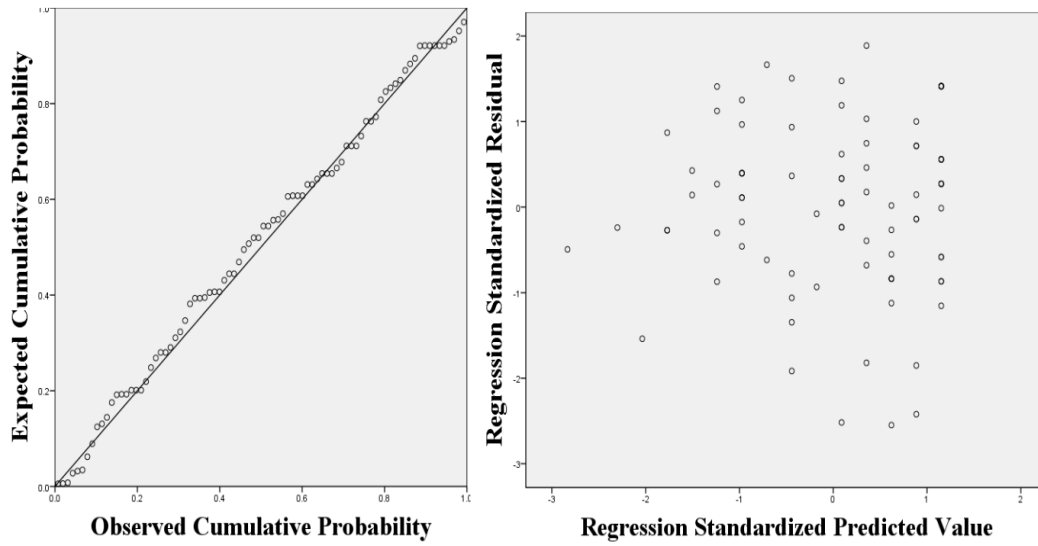


**Figure 4.** Model 3 normal p-p plot of regression standardized residual (left) and scatter plot (right). Dependent variable: RB

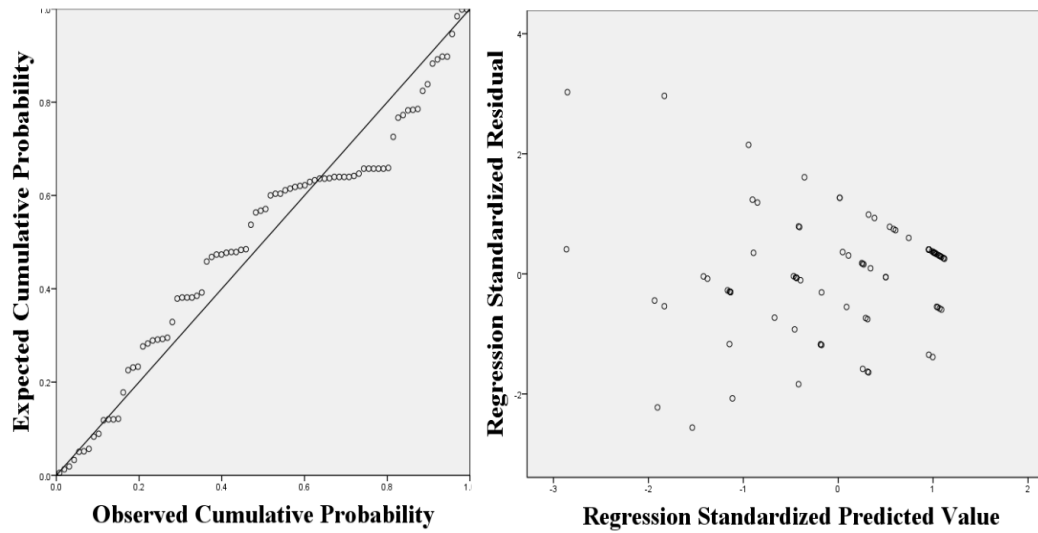


**Figure 5.** Model 4 normal p-p plot of regression standardized residual (left) and scatter plot (right). Dependent variable: BI

**Table 5.** Multiple linear regression with the collection, control, and awareness to predict personal health information privacy concerns

Independent Variables	Unstandardized Coefficients		Standardized Coefficients	t	p-value	Collinearity Statistics	
	B	Std. Error	Beta			Tolerance	VIF
(Constant)	2.008	.629		3.194	.002		
Collection	.426	.067	.555	6.409	<0.001	.968	1.033
Control	.122 <sup>c</sup>	.983	.328	.109	.471	2.125	.471
Awareness	.272	.098	.240	2.774	<0.001	.968	1.033

\*Dependent variable: Personal health information privacy concern

**Table 6.** Simple linear regression models with personal health information privacy concerns to predict trusting beliefs and risk beliefs

Model	Dependent Variable	Independent Variables	Unstandardized Coefficients		Standardized Coefficients	t	p-value.
			B	Std. Error	Beta		
1	Trusting Beliefs	(Constant)	4.516	.681		6.631	<0.001
		PHIPC	.192	.120	.175	1.606	.112
2	Risk Beliefs	(Constant)	1.469	.582		2.525	.014
		PHIPC	.554	.102	.514	5.421	<0.001

Dependent variable: Trusting Beliefs and Risk Beliefs

**Table 7.** Multiple linear regression with trusting beliefs and risk beliefs to predict behavioral intention toward sharing health information

Independent Variables	Unstandardized Coefficients		Standardized Coefficients	t	p-value	Collinearity Statistics	
	B	Std. Error	Beta			Tolerance	VIF
(Constant)	-4.117	.634		-6.495	<0.001		
Trusting Beliefs	.763	.092	.684	8.339	<0.001	.984	1.016
Risk Beliefs	-.032	.093	-.029	-.348	.729	.984	1.016

Dependent variable: Behavioral intention toward sharing health information

This study set out to assess the personal health information privacy concerns of people in Thailand. Furthermore, the second aim of this study was to investigate the factors affecting behavioral intention to share health information. The proposed research model was adapted from UIIPC [7]. We proposed and quantitatively evaluated seven hypotheses to investigate the research questions. A total of four regression analyses was used to test the hypotheses. The findings of this study are summarized as shown in Figure 6.

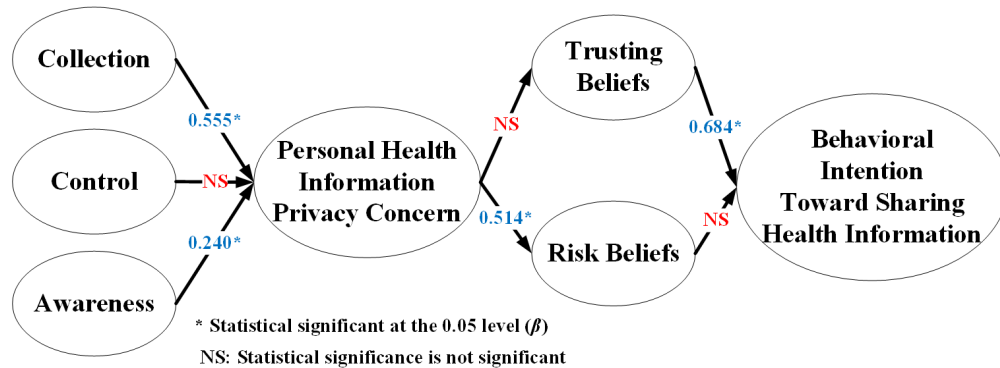


**Figure 6.** Results of the research model

The results showed that personal health information privacy concerns were significantly predicted by collection ( $\beta=0.555$ ,  $p<0.001$ ) and awareness ( $\beta=0.240$ ,  $p<0.001$ ). Nevertheless, the control of health information was not statistically significant when predicting personal health information privacy concerns.

Personal health information privacy concerns were significantly positively predicted by risk beliefs ( $\beta=0.514$ ,  $p<0.001$ ). On the other hand, they were negatively predicted by trusting beliefs. However, previous research suggested that personal health information privacy concerns negatively related to trusting beliefs as per our hypothesis [16]. What surprising is that trusting beliefs is the only independent variable that significantly predicts behavioral intention toward sharing health information ( $\beta=0.684$ ,  $p<0.001$ ). Therefore, the study rejected hypotheses H2, H4, and H7. On the contrary, we accepted hypotheses H1, H3, H5, and H6.

One of the more significant findings to emerge from this study is that participants will have more concerns about personal health information privacy if they have no control over the collection of personal health information. For example, if they need to provide more personal information than the doctor needs or information that seems unrelated to the disease, they will have raised their concern. These results are consistent with Malhotra *et al.* [7], Sipior *et al.* [16], and Pape *et al.* [17]. Furthermore, the awareness of how the healthcare organization processes their personal health information also affects the privacy concerns. Personal health information privacy concerns also have a positive effect on risk beliefs. If the participants are more concerned about the unclear privacy policy, they will have an increased expectation of the risks concerning their data. Surprisingly, the degree to which participants believe in protecting personal health information from the healthcare provider positively affects the behavioral intention to share health information. In accordance with the present results, previous studies have demonstrated that trusting beliefs were found to be a predictor of the user's intention to provide information [7, 16, 17], a finding that supported our results.

The PDPA will be effective in May 2021, raising awareness of Thai people's privacy concerns. The findings of this study have several important implications for supporting the PDPA. The results should facilitate compliance with the PDPA and increase intention to share personal health information at the same time. For example, a healthcare sector should transparently make public their privacy policy that complies with Thailand's PDPA. This suggestion is based on this study's results that the trusting beliefs factor is strongly affected by the behavioral intention to share health information. Third parties that request health information, such as an insurance companies or medical laboratories, also need to demonstrate a transparent privacy policy to increase patient information collection, awareness, and trust.

#### 4. Conclusions

In conclusion, Thai people raised privacy concerns for their personal health information based on the perception of collection of their information and awareness of the privacy policies. Thus, the healthcare industry must clarify how patients' health information will be collected, stored, and processed. Additionally, those clarifications should be available publicly to the patients. This will increase the patients' trusting beliefs, so they will be more ready to voluntarily reveal their health information. The small sample size may somewhat limit these findings. However, this study's findings will act as indicators for our planned future research into privacy concerns. An additional uncontrolled factor is the possibility that some of the participants still do not fully understand just what information privacy is about. Therefore, the interview method should be considered for future research. In addition, this research has thrown up many questions in need of further investigation. Further research should also focus on the factors that could accelerate the right level of privacy concerns in healthcare. Moreover, privacy concerns in other industries should be investigated.

#### 5. Acknowledgments

The authors would like to express their gratitude to Univ.-Prof. Dipl.-Ing. Dr. Gerald Quirchmayr at the University of Vienna for his valuable recommendations on the research topic.

#### References

- [1] European Union, 2019. *Complete Guide to GDPR Compliance*. [online] Available at: <https://gdpr.eu/>
- [2] EUR-Lex, 2019. *Regulation (EU) 2016/679 of the European Parliament and of the Council*. [online] Available at: <https://eur-lex.europa.eu/legalcontent/EN/TXT/HTML/>
- [3] Thai Government, 2019. *Personal Data Protection Act*. [online] Available at: <https://drive.google.com/open?id=1MzGNi3kdDPA0E52n8bDybeuDNkIM8xJe>.
- [4] HIQA, 2017. *Privacy Impact Assessment Toolkit for Health and Social Care*. [e-book] Dublin: Health Information and Quality Authority.
- [5] WP29, 2016. *Article 29 - Data Protection Working Party*. [Online] Available at: [https://ec.europa.eu/newsroom/document.cfm?doc\\_id=44137](https://ec.europa.eu/newsroom/document.cfm?doc_id=44137).
- [6] Theera-ampornpunt, N., 2009. *Medical Informatics: A Look from USA to Thailand*. [Online]. Available at: [https://scholar.google.co.th/scholar?hl=th&as\\_sdt=0%2C5&q=Medical+Informatics%E2%80%AF%3A+A+Look+from+USA+to+Thailand&btnG=](https://scholar.google.co.th/scholar?hl=th&as_sdt=0%2C5&q=Medical+Informatics%E2%80%AF%3A+A+Look+from+USA+to+Thailand&btnG=)
- [7] Malhotra, N.K., Kim, S.S. and Agarwal, J., 2004. Internet users' information privacy concerns (IUIPC): The construct, the scale, and a causal model. *Information Systems Research*, 15(4), 336-355.
- [8] Altman, I., 1977. Privacy regulation: Culturally universal or culturally specific? *Journal of Social Issues*, 33(3), 66-84.
- [9] Solove, D.J., 2002. Conceptualizing privacy. *California Law Review*, 90(4), 1087-1155.
- [10] Margulis, S.T., 1977. Conceptions of privacy: Current status and next steps. *Journal of Social Issues*, 33(3), 5-21.
- [11] Margulis, S.T., 2003. Privacy as a social issue and behavioral concept. *Journal of Social Issues*, 59(2), 243-261.
- [12] Bennett, C.J., 1995. *The Political Economy of Privacy: A Review of the Literature*. University of Victoria, Department of Political Science, Victoria.

- [13] Westin, A.F., 2003. Social and political dimensions of privacy. *Journal of Social Issues*, 59(2), 431-453.
- [14] Okazaki, S., Molina, F.J. and Hirose, M., 2012. Mobile advertising avoidance: exploring the role of ubiquity. *Electronic Markets*, 22(3), 169-183.
- [15] Kusyanti, A., Puspitasari, D.R., Catherina, H.P.A. and Sari, Y.A.L., 2017. Information privacy concerns on teens as Facebook users in Indonesia. *Procedia Computer Science*, 124, 632-638.
- [16] Sipior, J.C., Ward, B.T. and Connolly, R., 2013. Empirically assessing the continued applicability of the IUIPC construct. *Journal of Enterprise Information Management*. 26(6), 661-678.
- [17] Pape, S., Ivan, A., Harborth, D., Nakamura, T., Kiyomoto, S., Takasaki, H. and Rannenber, K., 2020. Re-evaluating internet users' information privacy concerns: the case in Japan. *AIS Transactions on Replication Research*, 6(18), 1-18.
- [18] Angst, C.M. and Agarwal, R., 2009. Adoption of electronic health records in the presence of privacy concerns: The elaboration likelihood model and individual persuasion. *MIS Quarterly*, 33(2), 339-370.
- [19] Commission Nationale de l'Informatique et des Libertés, 2018. *Privacy Impact Assessment (PIA) Methodology*. [online] Available at: <https://www.cnil.fr/en/privacy-impact-assessment-pia>
- [20] Campbell, A.J., 1997. Relationship marketing in consumer markets: A comparison of managerial and consumer attitudes about information privacy. *Journal of Direct Marketing*, 11(3), 44-57.
- [21] Santos, J.R.A., 1999. Cronbach's alpha: A tool for assessing the reliability of scales. *Journal of extension*, 37(2), 1-5.
- [22] Nunnally, J.C., 1994. *Psychometric theory 3E*. New Delhi: Tata McGraw-hill Education.
- [23] Hair, J.F., Anderson, R.E., Tatham, R.L. and Black, W.C., 1998. *Multivariate Data Analysis*. 5<sup>th</sup> ed. Upper Saddle River: Prentice Hall.
- [24] Tabachnick, B.G. and Fidell, L.S., 2007. *Using Multivariate Statistics*. Boston: Pearson.
- [25] Pallant, J., 2020. *SPSS Survival Manual: A Step-by-Step Guide to Data Analysis using IBM SPSS*. 7<sup>th</sup> ed. Milton: Routledge.
- [26] Allen, P.J. and Bennett, K., 2007. *SPSS for the Health and Behavioural Sciences*. South Melbourne: Thomson Learning.
- [27] Field, A., 2009. *Discovering Statistics Using SPSS*. 3rd ed. London: SAGE Publications Ltd.

Review article

## **A Review of COVID-19: Nature of the Virus and Impact of Lockdown on Air Pollution over India and the World**

N.V. Krishna Prasad<sup>1\*</sup>, P. Sasikala<sup>2</sup>, S. Ramesh<sup>1</sup>, M.S.S.R.K.N. Sarma<sup>1</sup>,  
Thomaskutty Mathew<sup>1</sup>, T. Anil Babu<sup>1</sup> and N. Madhavi<sup>3</sup>

<sup>1</sup>Department of Physics, GSS, GITAM Deemed to be University, Bengaluru, India

<sup>2</sup>Department of Mathematics, GSS, GITAM Deemed to be University, Bengaluru, India

<sup>3</sup>Department of Statistics, Government College (Autonomous), Rajhamundry, India

Received: 5 September 2020, Revised: 9 February 2021, Accepted: 24 February 2021

### **Abstract**

A new infection was reported on 31<sup>st</sup> December, 2019 from the city of Wuhan (China) to WHO. It was later named COVID-19 disease and was declared pandemic on 11<sup>th</sup> March, 2020. Estimates predicted that forty to sixty percent of world population would be affected by this virus. This virus has created an immeasurable crisis in the entire world economically, socially as well as environmentally with adverse effect on health. Worldwide lockdowns have been implemented to curtail virus transmission. Lockdown starting and ending dates have varied depending on the country. These lockdowns have had significant impact on air quality due to sudden reduction in vehicular traffic as well as shutdown of industries. It was reported that thirty percent reduction in air pollution was experienced by Wuhan city due to the lockdown. Many research publications have reported the impact of air pollution on human health for the last few decades. However, for the first time, forced lockdown created a chance to review the air pollution in various cities. In this review, we present some of the published results related to the nature of virus and impact of lockdown on air pollution over India and the world.

**Keywords:** COVID-19; lockdown; air pollution  
DOI 10.14456/cast.2021.63

### **1. Introduction**

Huanan Seafood market, a wet market in Wuhan city of China was the origin of an unknown respiratory disease that was identified in December 2019 and named COVID-19. It was reported that this disease had infected the entire world [1-3] and WHO declared it a pandemic on 11<sup>th</sup> of March 2020 [4]. This type of virus was reported for the first time and is characterized by cough, cold, running nose, fever, body aches and sore throat. Since no vaccine is available right now, wearing masks, social/physical distancing and continuous sanitization is being followed to avoid

---

\*Corresponding author: Tel.: 91-8971199913

E-mail: drnvkprasad@gmail.com

the spreading of virus [5]. As per the data of WHO Corona Virus Disease (COVID-19) Dashboard, World Health Organization confirmed cases of 20.71 millions, recovered cases of 12.58 million and death cases of 0.74 million on 6<sup>th</sup> August of 2020 throughout the world [4]. The current scenario of lockdown has shown huge impact on air pollution of cities which are urbanized due to almost zero traffic and shut down in industries. This unpredicted situation has brought a change in the local environment which needs to be monitored. In this regard studies related to air quality and its impact on human health have come into the lime light. Emission of air pollutants and particulate matter have been a major contributor to respiratory diseases. As per the data of WHO in 2018 [4], death rate due to respiratory diseases by particulate matter (PM) concentration was reported to be 700 million per year. Nearly ninety percent of world's population was reported to live in areas with poor air quality [6] with 4.2 million premature deaths being recorded worldwide [7]. Controlling of virus transmission started with implementation of lockdown that stimulated improvement in air quality. This lockdown which was made mandatory by all governments is of prime interest in analysing environmental data and may lead to interesting results if any.

## 2. Nature of COVID-19

This previous unknown respiratory disease named COVID-19 is caused by SARS-Cov-2 virus which was reported for first time, and which is highly contagious in nature. The reason for rapid spread of the disease has not yet been confirmed [8]. Two other corona virus diseases, Severe Acute Respiratory Syndrome (SARS) and Middle East Respiratory Syndrome (MERS) were reported in 2003 and 2012, respectively [2]. The death rate of COVID-19 is five times less than SARS virus, which might have originated in bats and got transmitted to humans via some intermediate animals. The COVID-19 virus has a better organism sequence identity compared to the SARS and MERS corona viruses [9]. It is reported that the organic compounds that combine to form proteins of this virus differ from other corona viruses based on S-protein [10]. This virus may be treated as another form of SARS and MERS viruses [11]. Mode of action of corona virus involves closeness, penetration, biosynthesis, and formation followed by release. It was reported that on binding to host cells, the virus enters the cells via penetration and RNA enters the nucleus for reproduction. After biosynthesis of viral proteins, viral particles are formed and released by lysis [12]. The symptoms of corona virus infection appear in an individual after an incubation period of about 5.2 days. The gap between onset and death of the infected patients ranges between 6 to 41 days, a period of time that varies depending on the age of the person. The severity of this infection ranges from mild to no symptoms (30%) to severe symptoms (10%) and critical symptoms (5%) cases [1]. Another report confirmed the incubation period to be 5.1 days [13]. This virus can damage central nervous system [11]. Patients with a track record of pre-existing conditions that include surgeries, hypertension, heart disease and so on, are more prone to death [14]. Consumption of alcohol and smoking leads to adverse effects [12]. Diabetes triggers severity of COVID-19 infection and mortality, and diabetic patients are more prone to death when compared to sufferers of other diseases [15]. Reports also indicated that virus transmission from mother to baby was possible [16]. It was reported that children of age between 10 to 19 years were less vulnerable to infection. The percentage of infected children who developed asymptomatic, mild, moderate and severe conditions were reported to be 4.4%, 50.9%, 38.8% and 5.9%, respectively, where as 18.5% of adults developed severe disease [12].

### 3. Impact of Lockdown on Air Pollution in India

India imposed a nationwide lockdown from 24<sup>th</sup> March to 3<sup>rd</sup> May 2020. The strict lockdown during this period definitely reduced air pollution in all cities throughout the country; however, this was not a permanent solution in controlling air pollution problems. Literature published in 2020 that reported air pollution data during lockdown period. Analysis of different pollutants between 16<sup>th</sup> March to 14<sup>th</sup> April of 2017, 2018, 2019 and 2020 for 22 cities that included Bhopal and Dewas (Central India), Patna, Jorapokhar, Brajrajnagar, Kolkata, Gaya (East India), Amritsar, Faridabad, Agra, Jodhpur, Delhi, Varanasi, Kanpur (North India), Chennai, Thiruvanthapuram, Bengaluru, Amravati (South India), Mumbai, Ahmedabad, Pune, and Nagpur (West India), were reported. Hourly concentrations of NO<sub>2</sub>, O<sub>3</sub>, SO<sub>2</sub>, CO, NO<sub>x</sub>, PM<sub>10</sub>, and PM<sub>2.5</sub> along with temperature, relative humidity, wind direction and wind speed obtained from the official Pollution Control Board of India website [17], were analysed. Decreases in PM<sub>10</sub> (31%), PM<sub>2.5</sub> (43%), CO (10%), NO<sub>2</sub> (18%), increase in ozone by 17% and negligible change in SO<sub>2</sub> during lockdown period in comparison with previous years for all the cities mentioned above, were reported. Air Quality Index (AQI) was reported to be lower by 44%, 33%, 29%, 15% and 32% in North, South, East, Central and Western India, respectively [18]. Table 1 shows the decline in Air Quality Index (AQI) in India during lockdown.

**Table 1.** Percentage decrease in AQI in India during COVID-19 lockdown [18]

Location	% Decrease of AQI
Northern India	44
Southern India	33
Eastern India	29
Central India	15
Western India	32

Analysis of in-situ measured ambient air quality for Delhi, Hyderabad, Chennai, Mumbai and Kolkata between 2015 to 2020 indicated substantial reductions in PM<sub>2.5</sub> concentration of 41%-53% (Delhi), 26%-54% (Hyderabad), 19%-43% (Chennai), 10%-39% (Mumbai), and 24%-36% (Kolkata) [19]. It is a known fact that cities with high volumes of traffic record high values of PM<sub>2.5</sub> concentration. Studies related to the impact of lockdown on air pollutants and aerosol concentration in analysing pre-monsoon cloud-to-ground and inter-cloud lightning activity reported a reduction of more than 40% in these pollutants due to lockdown which reduced the lightning activity around Kolkata [20]. Air quality data of PM<sub>2.5</sub>, PM<sub>10</sub>, NO<sub>2</sub>, SO<sub>2</sub>, CO, NH<sub>3</sub>, and O<sub>3</sub> from 34 monitoring stations spread over most polluted capital city, Delhi, were analysed. The results demonstrated a remarkable improvement with 50% reduction in PM<sub>10</sub> and PM<sub>2.5</sub> levels compared to pre-lockdown phase, while other pollutants showed a reduction of CO by 30.35% and NO<sub>2</sub> by 52.68%. Air quality improved by 40% to 50% with four days after commencement of lockdown. Reductions in National Air Quality Index (NAQI) were found to be 49%, 37%, 31%, 43%, and 54% in the Eastern, Western, Northern, Southern and Central parts of Delhi, respectively [21].

### 4. Impact of Lockdown on Air Pollution around the World

As per WHO [22], yearly mean concentration of air quality should not exceed 10 mg/m<sup>3</sup>. Meteosim [23] reported that Delhi, the capital of India, was the most polluted capital with yearly mean of 113.5 mg/m<sup>3</sup> PM<sub>2.5</sub> concentration for the year 2018 [23]. It was reported that 27% of the

capitals of Asian countries had a tendency of decreasing PM<sub>2.5</sub> concentration, excepted Tokyo (Japan), Kathmandu (Nepal), Jakarta (Indonesia) and Singapore which showed an increasing trend. The highest weekly averages of 183mg/m<sup>3</sup> and 140mg/m<sup>3</sup> PM<sub>2.5</sub> for Dhaka (Bangladesh) and Delhi (India) with 24% and 40% reductions during lockdown week were reported. At the same time seventeen European capitals recorded a decrease of PM<sub>2.5</sub> concentration by 23% on average while Bogota (Colombia), one of the four capitals in American continent analysed, exhibited the highest PM<sub>2.5</sub> reduction (57%) [24]. Moreover, it was reported that CO<sub>2</sub> emissions reduced by 25% in Asian country such as China, and by 6% worldwide [25]. Comparison between annual deaths due to NO<sub>2</sub> emissions with that of deaths due to COVID-19 indicated that home isolation during Covid pandemic was an appropriate decision [26]. Compilation of information from NASA and ESA reported that home isolation benefited North America, China and Europe environmentally on a temporary basis [27]. A regression model was developed with thirty-five variables from socioeconomic to environmental that were related to the disease in first three months of the outbreak in the USA [28]. Reports indicate that 78% of 4443 deaths occurred in a single day on 19<sup>th</sup> March, 2020 in Europe, were from five highly contaminated areas and indicated long term exposure to particulate pollutants acted as a major contributor to corona virus mortality in the entire world [29]. Significant reduction in CO and NO<sub>2</sub> levels in Rio de Janeiro (Brazil) were reported. They also reported reduction in PM<sub>10</sub> and increase in ozone (attributed to increase in NMHC/NO<sub>x</sub> ratios) in all locations of study during first partial lockdown [30]. Hourly air pollution for fine particulate matter, ozone, oxides of nitrogen and nitrogen dioxide was measured in the air monitoring network of Ontario (Canada) for 2020 as well as for previous five years and reported. This report indicated no significant reduction in fine particulate matter with reduction in ozone concentration at twelve of the thirty-two monitors compared to the previous years. Nitrogen oxide and nitrogen dioxide show the lowest concentrations at 22 of 29 monitors. However, they observed no variation in fine particulate matter from historic values [31]. Studies related to temperature effect on COVID-19 for Canada using daily meteorological data with statistical model along with 77,700 plus cases between January to May 2020 indicated no dependence of virus on ambient temperature [32]. The impact of traffic reduction and reduced industrial emissions on air quality during lockdown in China was reported. AQI and concentrations of six pollutants (O<sub>3</sub>, CO, NO<sub>2</sub>, SO<sub>2</sub>, PM<sub>2.5</sub> and PM<sub>10</sub>) during COVID-19 control period in northern China were studied. The improvement in air quality because of reduced emissions from transport and secondary industrial sector was observed. Reduction in CO, NO<sub>2</sub>, SO<sub>2</sub> and PM<sub>2.5</sub> concentrations, with increase in O<sub>3</sub> was reported. However, these reductions could not eliminate air pollution completely [33]. The correlation between the extent of increased diffusion, capacity of causing virus and surface air pollution in Milan (Italy) was investigated. Daily average concentrations of PM<sub>2.5</sub>, PM<sub>10</sub>, Relative Humidity, Temperature, PBL Height, Wind Speed and Atmospheric Pressure between January-April 2020 were collected and analysed. It was reported that increase in confirmed COVID-19 cases was due to the high level of urban air pollution, instead of indoor transmission or direct human-to-human contact [34]. The occurrence of severe air pollution in North China in spite of reduced activity due to COVID-19 was analysed. It indicated that the benefits of reduced emission were masked by adverse meteorology and severe air pollution, factors that could not be avoided [35]. A report on impact of COVID-19 virus on ultra-fine particles was first of its kind which reported the impact of virus on air pollution related to traffic for a US city. The data were collected five weeks before and ten weeks after lockdown and showed significant decrease in ultra fine particles by 4% to 29%, PM<sub>2.5</sub> (33%), NO (33%), NO<sub>2</sub> (29%), NO<sub>x</sub> (30%) and CO (17%) [36]. Table 2 displays the % decrease in particulate matter concentration and air pollutants during lock down in the U.S city during lockdown.

**Table 2.** Percentage decrease in particulate matter concentration and air pollutants during lock down in a U.S city [36]

Parameter	% Decrease
PM <sub>2.5</sub>	33
NO	33
NO <sub>2</sub>	29
NO <sub>x</sub>	30
CO	17

The decline in PM<sub>2.5</sub> concentration in major cities around the world including Mumbai and Delhi (India), Shanghai and Beijing (China), Rome (Italy), Zaragoza (Spain), Dubai (UAE), New York and Los Angeles (USA) during COVID-19 lockdown was reported [37]. Investigation of change in source contributions, chemical composition and local transport of PM<sub>2.5</sub> particles during lockdown was done and compared with 2019 for the city of Wuhan which indicated a decrease of PM<sub>2.5</sub> concentration with 92% emission reduction [38]. An analysis of air quality based on NO<sub>2</sub> during lock down in two big cities, Madrid and Barcelona, Spain, showed reductions in NO<sub>2</sub> concentration by 62% and 50%, respectively [39]. The dependence of PM concentration on Relative Humidity was also reported in a detailed manner [40].

## 5. Conclusions

In this review paper, we explored some of the results published very recently after the COVID- 19 outbreak. The idea was to bring all the results related to lockdown impact on air pollution around the globe into a single entity. From the review of available literature, it is very clear that almost 90% of cities all over the world experienced an improvement in air pollution due to forced lockdown. Even though this is a good sign or indication in terms of improved air quality which acts as major contributor to respiratory diseases, this cannot be adopted on continuous basis when keeping the socioeconomic conditions of human beings into consideration. This lockdown may be helpful for this year's monsoon to give adequate rainfall due to drastic reduction in air pollution as we have seen in the above results. However, this also depends on various local factors. Many reports indicated that increase of air pollution prevents rainfall. However, an alternative in reducing air pollution may be investigated on permanent basis. This restricted lockdown may be implemented as policy decision keeping the existence of mankind in terms of good health and other factors.

## 6. Acknowledgements

The authors deeply acknowledge Central Pollution Control Board for providing valuable data through their official website.

## References

- [1] Madabhavi, I., Sarkar, M. and Kadakol, N., 2020. COVID-19: a review. *Monaldi Archives for Chest Disease*, 90(2), 1298, <https://doi.org/10.4081/monaldi.2020.1298>

- [2] Chatterjee, P., Nagi, N, Agarwal, A, Das, B. and Banerjee, S., 2020. The 2019 novel coronavirus disease (COVID-19) pandemic: A review of the current evidence. *Indian Journal of Medical Research*, 151(2), 147-159.
- [3] Jiang, F., Deng, L., Zhang, L., Cai, Y., Cheung, C.W. and Xia, Z., 2020. Review of the clinical characteristics of coronavirus disease 2019 (COVID-19). *Journal of General Internal Medicine*, 35(5), 1545-1549.
- [4] World Health Organization, 2018. *Ambient (Outdoor) Air Pollution*. [Online] Available at: [https://www.who.int/news-room/fact-sheets/detail/ambient-\(outdoor\)-air-quality-and-health](https://www.who.int/news-room/fact-sheets/detail/ambient-(outdoor)-air-quality-and-health)
- [5] Padhi, A., Kumar, S., Gupta, E. and Saxena, S.K., 2020. Laboratory diagnosis of novel coronavirus disease 2019 (COVID-19) infection. In: S. Saxena, ed. *Coronavirus Disease 2019 (COVID-19). Medical Virology: From Pathogenesis to Disease Control*. Singapore: Springer, pp. 95-107.
- [6] Ng, C.F.S., Hashizume, M., Obase, Y., Doi, M., Tamura, K., Tomari, S., Kawano, T., Fukushima, C., Matsuse, H., Chung, Y., Kim, Y., Kunimitsu, K., Kohno, S. and Mukae, H., 2019. Associations of chemical composition and sources of PM<sub>2.5</sub> with lung function of severe asthmatic adults in a low air pollution environment of urban Nagasaki, Japan. *Environmental Pollution*, 252, 599-606.
- [7] Cohen, A.J., Brauer, M., Burnett, R., Anderson, H.R., Frostad, J., Estep, K., Balakrishnan, K., Brunekreef, B., Dandona, L., Dandona, R., Feigin, V., Freedman, G., Hubbell, B., Jobling, A., Kan, H., Knibbs, L., Liu, Y., Martin, R., Morawska, L., Pope, C.A., Shin, H., Straif, K., Shaddick, G., Thomas, M., van Dingenen, R., van Donkelaar, A., Vos, T., Murray, C.J.L. and Forouzanfar, M.H., 2017. Estimates and 25-year trends of the global burden of disease attributable to ambient air pollution: an analysis of data from the global burden of diseases study 2015. *Lancet*, 389, 1907-1918.
- [8] Wang, L., Wang, Y., Ye, D. and Liu, Q., 2020. Review of the 2019 novel coronavirus (SARS-CoV-2) based on current evidence. *International Journal of Antimicrobial Agents*, 55(6), 105948, <https://doi.org/10.1016/j.ijantimicag.2020.105948>
- [9] Singhal, T., 2020. A review of coronavirus disease-2019 (COVID-19). *The Indian Journal of Pediatrics*, 87 (4), 281-286.
- [10] Kannan, S., Ali, P.S.S., Sheeza, A. and Hemalatha, K., 2020. COVID-19 (novel coronavirus 2019)–recent trends, SARS, *European Review for Medical and Pharmacological Sciences*, 24(4), 2006-2011.
- [11] Ahmad, I. and Rathore, F.A., 2020. Neurological manifestations and complications of COVID-19: A literature review. *Journal of Clinical Neuroscience*, 77, 8-12.
- [12] Yuki, K., Fujiogi, M. and Koutsogiannaki, S., 2020. COVID-19 pathophysiology: A review. *Clinical Immunology*, 215, 108427, <https://doi.org/10.1016/j.clim.2020.108427>
- [13] Lauer, S.A., Kyra, H.G., Qifang, B., Jones, F.K., Zheng, Q., Meredith, H.R., Azman, A.S., Reich, N.G. and Lessler, J., 2020. The incubation period of coronavirus disease 2019 (COVID-19) from publicly reported confirmed cases: estimation and application. *Annals of Internal Medicine*, 172(9), 577-582.
- [14] Adhikari, S.P., Meng, S., Wu, Y.J., Mao, Y.P., Ye, R.X., Wang, Q.Z., Sun, C., Sylvia, S., Rozelle, S., Raat, H. and Zhou, H., 2020. Epidemiology, causes, clinical manifestation and diagnosis, prevention and control of coronavirus disease (COVID-19) during the early outbreak period: a scoping review. *Infectious Diseases of Poverty*, 9(1), 1-12.
- [15] Abdi, A., Jalilian, M., Sarbarzeh, P.A. and Vlaisavljevic, Z., 2020. Diabetes and COVID-19: A systematic review on the current evidences. *Diabetes Research and Clinical Practice*, 166, 108347, <https://doi.org/10.1016/j.diabres.2020.108347>
- [16] Alzamora, M. C., Paredes, T., Caceres, D., Webb, C.M., Valdez, L.M. and Rosa, M.L., 2020. Severe COVID-19 during pregnancy and possible vertical transmission. *American Journal of Perinatology*, 37(8), 861-865.

- [17] Central Pollution Control Board, Ministry of Environment, Forest and Climate Change, Government of India, 2020. *Air Quality*. [Online] Available at <https://cpcb.nic.in/index.php>
- [18] Sharma, S., Zhang, M., Anshika, Gao, J., Zhang, H. and Kota, S.H., 2020. Effect of restricted emissions during COVID-19 on air quality in India. *Science of the Total Environment*, 728, 138878, <https://doi.org/10.1016/j.scitotenv.2020.138878>
- [19] Kumar, P., Hama, S., Omidvarborna, H., Sharma, A. Sahani, J., Abhijith, K.V., Debele, S.E., Zavala-Reyes, J.C., Barwise, Y. and Tiwari, A., 2020. Temporary reduction in fine particulate matter due to ‘anthropogenic emissions switch-off’ during COVID-19 lockdown in Indian cities. *Sustainable Cities and Society*, 62, 102382, <https://doi.org/10.1016/j.scs.2020.102382>
- [20] Chowdhuri, I., Pal, S.C., Saha, A., Chakraborty, R., Ghosh, M. and Roy, P., 2020. Significant decrease of lightning activities during COVID-19 lockdown period over Kolkata megacity in India. *Science of the Total Environment*, 747, 141321, <https://doi.org/10.1016/j.scitotenv.2020.141321>
- [21] Mahato, S., Pal, S. and Ghosh, K.G., 2020. Effect of lockdown amid COVID-19 pandemic on air quality of the megacity Delhi, India. *Science of the Total Environment*, 730, 139086, <https://doi.org/10.1016/j.scitotenv.2020.139086>
- [22] WHO, 2020. *Coronavirus Disease (COVID-19) Pandemic*. [Online] Available at: <https://www.who.int/>
- [23] Meteosim, 2019. *World Most Polluted Cities*. [Online] Available at: <https://www.meteosim.com/en/world-most-polluted-cities/>
- [24] Rodríguez-Urrego, D. and Rodríguez-Urrego, L., 2020. Air quality during the COVID-19: PM<sub>2.5</sub> analysis in the 50 most polluted capital cities in the world. *Environmental Pollution*, 266, 115042, <https://doi.org/10.1016/j.envpol.2020.115042>
- [25] Hanaoka, T. and Masui, T., 2020. Exploring effective short-lived climate pollutant mitigation scenarios by considering synergies and trade-offs of combinations of air pollutant measures and low carbon measures towards the level of the 2°C target in Asia. *Environmental Pollution*, 261, 113650, <https://doi.org/10.1016/j.envpol.2019.113650>
- [26] Dutheil, F., Baker, J.S. and Navel, V., 2020. COVID-19 as a factor influencing air pollution? *Environmental Pollution*, 263, 114466, <https://doi.org/10.1016/j.envpol.2020.114466>
- [27] Muhammad, S., Long, X. and Salman, M., 2020. COVID-19 pandemic and environmental pollution: A blessing in disguise? *Science of the Total Environment*, 728, 138820, <https://doi.org/10.1016/j.scitotenv.2020.138820>
- [28] Mollalo, A., Vahedi, B. and Rivera, K.M., 2020. GIS-based spatial modeling of COVID-19 incidence rate in the continental United States. *Science of the Total Environment*, 728, 138884, <https://doi.org/10.1016/j.scitotenv.2020.138884>
- [29] Ogen, Y., 2020. Assessing nitrogen dioxide (NO<sub>2</sub>) levels as a contributing factor to coronavirus (COVID-19) fatality. *Science of the Total Environment*, 726, 138605, <https://doi.org/10.1016/j.scitotenv.2020.138605>
- [30] Siciliano B., Dantas, G., Silva, C.M. and Arbilla, G., 2020. Increased ozone levels during the COVID-19 lockdown: Analysis for the city of Rio de Janeiro, Brazil. *Science of the Total Environment*, 737, 139765, <https://doi.org/10.1016/j.scitotenv.2020.139765>
- [31] Adams, M.D., 2020. Air pollution in Ontario, Canada during the COVID-19 state of emergency. *Science of the Total Environment*, 742, 140516, <https://doi.org/10.1016/j.scitotenv.2020.140516>
- [32] To, T., Zhang, K., Maguire, B., Terebessy, E., Fong, I., Parikh, S. and Zhu, J., 2021. Correlation of ambient temperature and COVID-19 incidence in Canada. *Science of the Total Environment*, 750, 141484, <https://doi.org/10.1016/j.scitotenv.2020.141484>
- [33] Wang, Y., Yuan, Y., Wang, Q., Liu, C., Zhi, Q. and Cao, J., 2020. Changes in air quality related to the control of coronavirus in China: Implications for traffic and industrial emissions. *Science of the Total Environment*, 731, 139133, <https://doi.org/10.1016/j.scitotenv.2020.139133>

- [34] Zoran, M.A., Savastru, R.S., Savastru, D.M. and Tautan, M.N., 2020. Assessing the relationship between surface levels of PM<sub>2.5</sub> and PM<sub>10</sub> particulate matter impact on COVID-19 in Milan, Italy. *Science of the Total Environment*, 738, 139825, <https://doi.org/10.1016/j.scitotenv.2020.139825>
- [35] Wang, P., Chen, K., Zhu, S., Wang, P. and Zhang, H., 2020. Severe air pollution events not avoided by reduced anthropogenic activities during COVID-19 outbreak. *Resources, Conservation and Recycling*, 158, 104814, <https://doi.org/10.1016/j.resconrec.2020.104814>
- [36] Xiang, J., Austin, E., Gould, T., Larson, T., Shirai, J, Liu, Y., Marshall, J. and Seto, E., 2020. Impacts of the COVID-19 responses on traffic-related air pollution in a Northwestern US city. *Science of the Total Environment*, 747, 141325, <https://doi.org/10.1016/j.scitotenv.2020.141325>
- [37] Chauhan, A. and Singh, R.P., 2020. Decline in PM<sub>2.5</sub> concentrations over major cities around the world associated with COVID-19. *Environmental Research*, 187, 109634, <https://doi.org/10.1016/j.envres.2020.109634>
- [38] Zheng, H., Kong, S., Chen, N., Yan, Y., Liu, D., Zhu, B., Xu, K., Cao, W., Ding, Q., Lan, B., Zhang, Z., Zheng, M., Fan, Z., Cheng, Y., Zheng, S., Yao, L., Bai, Y., Zhao, T. and Qi, S., 2020. Significant changes in the chemical compositions and sources of PM<sub>2.5</sub> in Wuhan since the city lockdown as COVID-19. *Science of the Total Environment*, 739, 140000, <https://doi.org/10.1016/j.scitotenv.2020.140000>
- [39] Baldasano, J.M., 2020. COVID-19 lockdown effects on air quality by NO<sub>2</sub> in the cities of Barcelona and Madrid (Spain). *Science of the Total Environment*, 741, 140353, <https://doi.org/10.1016/j.scitotenv.2020.140353>
- [40] Lou, C., Liu, H., Li, Y., Peng, Y., Wang, J. and Dai, L., 2017. Relationships of relative humidity with PM<sub>2.5</sub> and PM<sub>10</sub> in the Yangtze River Delta, China. *Environmental Monitoring and Assessment*, 189(11), 582, <https://doi.org/10.1007/s10661-017-6281-z>

## Instructions for Authors

Current Applied Science and Technology journal contains research reports, articles concerning development work, reviews of the literature and research activities. The objectives are to publish and promote research contributions and innovative work in fields associated with applied science and technology. An electronic journal is provided on the website (<https://www.tci-thaijo.org/index.php/cast/index>). The editors reserve the right to require revision of the submitted manuscript as a condition for final acceptance.

The institute and the editorial board claim no responsibility for the contents or views expressed by the authors of individual articles. Copying is allowed provided that acknowledgement is made. All articles submitted for publication will be assessed by a group of distinguished.

### **Ethics:**

The journal is committed to maintaining the high level of integrity in the content published and has a Conflict of Interest policy in place. The journal uses plagiarism detection software to screen the submissions. If plagiarism is found, the COPE guidelines on plagiarism will be followed. For more details, please see [https://www.tci-thaijo.org/index.php/cast/navigationMenu/view/Publication\\_Ethics](https://www.tci-thaijo.org/index.php/cast/navigationMenu/view/Publication_Ethics).

### **Page Charge: Free**

### **Submission of Manuscripts:**

Manuscripts must be written in English and submitted online. Manuscripts are to be reviewed (double blinded) by at least 3 referees specializing in relevant fields. Revised manuscripts have to be sent online.

**All manuscripts should be submitted to:** <https://www.tci-thaijo.org/index.php/cast/index>

### **Contact:**

**Editor of Current Applied Science and Technology**  
**King Mongkut's Institute of Technology Ladkrabang**  
**1 Soi Chalongkrung 1, Ladkrabang District,**  
**Bangkok 10520, Thailand**  
**Tel: 662-329-8136**  
**Fax: 662-329-8221**  
**Email: [cast@kmitl.ac.th](mailto:cast@kmitl.ac.th)**

### **Manuscript Preparation Guide:**

**General:** Manuscripts must be typewritten using *Microsoft Word for Windows*, single-spaced with margin set-up (in page set up menu) as follows (see also the document template):

Top Margin	1.5"	Bottom Margin	1.5"
Left Margin	1.5"	Right Margin	1.5"

Good quality printouts using A4 paper size are required. Format should be a single column. Times New Roman font type is required. Font sizes for various text functions are as follows:

<b>Text functions</b>	<b>Size *</b>	<b>Typeface</b>
Title	14 (CT)	Bold
Author and co-authors	11 (CT)	Normal
Address for correspondence	11 (CT)	Normal
Abstract and main text	10 (LJ)	Normal
Section heading and number including “Abstract”, “Acknowledgement”, “References”	12 (CT)	Bold
Subsection heading and number	11 (LJ)	Bold

\* CT = Center Text, LJ = Left Justified.

The corresponding author should be noted (included a Fax number and E-mail address) and indicated with an asterisk. Full postal addresses must be given for all co-authors, keyed to names (if required) by superscripted Arabic numbers.

**Paper Length:** Should not normally exceed 10 pages including figures and tables  
**Spelling:** American English  
**Abstract:** Should not exceed 250 words  
**Keywords:** Should not exceed 8 keywords  
**Text:** Authors are requested to use the following order when typing:-  
*All research reports (Full Length or Short Reports):* Title, Authors, Affiliations, Abstract, Keywords, Introduction (in reserch papers this must be confined to relevant matters, and must not be a general review of cognate literature), Materials and Methods, Results and Discussion, Conclusions, Acknowledgements, References.

*Reviews and Discussion Papers* will be considered in any format appropriate to the purposes of the authors, although adherence to the general guidelines described above is encouraged.

**Line Art Figures:** Figures can be drawn using several packages such as Win Draw®, Auto CAD®, Corel Draw®, VISIO® etc.

**Photographs:** Actual size photographs are acceptable. However, they can also be put into a text stream using a good-resolution scanner. All photographs must be clear when printed in monochrome.

**Graphs:** Several packages available today can produce attractive and professional graph presentation. Some also provide curve-fitting function, which can be useful. However, two-dimensional bar charts are preferred. All graphs must be clear in monochrome printing.  
Equations and complex expressions: Math CAD®, Math Writer® and Equation Editor® (included in Microsoft Word®) are acceptable for presentation of this type of material.

**Citations:** Citations in the text should be denoted by numbers between square brackets (i.e. [1, 2], [1-3], [1, 3-8]...) *in the order of first appearance in the text.*

**References:** References should be numbered to correspond with the text citations. References must be arranged as follows:

### **Books**

Author's surname(s), Initials., Year. *Title of Book*. Edition. (only include this if not the first edition)  
Place of publication: Publisher.

*Example:*

- [1] Einstein, A. 2019. *Relativity. The Special and the General Theory*. Ghaziabad: Samaira Book Publishers.

### **Chapters of edited books**

Chapter author's surname(s), Initials., Year of book. Title of chapter. In: Book editor(s) initials. surnames, ed. or eds. *Title of Book*. Place of publication: Publisher, Chapter number or first and last page numbers.

*Example:*

- [2] Smith, J.E., 2006. Public perception of biotechnology. In: C. Ratledge and B. Kristiansen, eds. *Basic Biotechnology*. Cambridge: Cambridge University Press, pp. 3-24.

### **E-books**

Author's surname(s), Initials., Year, *Title of Book*. [e-book] Place of publication: Publisher. Available through: include e-book source/database, web address or URL.

*Example:*

- [3] Willey, J., Sherwood, L. and Woolverton, C.J., eds. 2013. *Prescott's Microbiology*. 9<sup>th</sup> ed. [e-book] New York: McGraw-Hill. Available through: Libribook website < www.libribook.com >

### **Journal articles**

Author's surname(s), Initials., Year. Title of article. *Full Title of Journal*, Volume number (Issue number), Page numbers.

*Example:*

- [4] Ross, A. B., Junyapoon, S., Jones, J.M., Williams, A. and Bartle, K.D., 2005. A study of different soots using pyrolysis– GC– MS and comparison with solvent extractable material. *Journal of Analytical and Applied Pyrolysis*, 74(1-2), 494-501.

### **In case of online journal articles without page number:**

Author's surname(s), Initials., Year. Title of article. *Full Title of Journal*, Volume number (Issue number), DOI-based link.

*Example:*

- [5] Tanasupawat, S., Phongsopitanun, W., Suwanborirux, K., Ohkuma, M. and Kudo, T. 2016. *Streptomyces actinomycinicus* sp. nov., isolated from soil of a peat swamp forest. *International Journal of Systematic and Evolutionary Microbiology*, 66(1), <https://doi.org/10.1099/ijsem.0.000716>.

### **Proceedings**

Author's surname(s), Initials., Year. Title of article. *Full Title of Proceedings*, Place of Conference, Date, page numbers.

*Example:*

- [6] Thanaboripat, D., Ruangrattanametee, V. and Srikitkademwat, K., 2010. Control of growth and aflatoxin production of aflatoxin producing fungi in corn by salts. *Proceedings of the 8<sup>th</sup> International Symposium on Biocontrol and Biotechnology*, Pattaya, Thailand, October 4-6, 2010, pp. 283-289.

### **Patent**

Inventor surname(s), Initial(s), Assignee, Year. *Title*. Place. Patent number (status, if an application).

*Example:*

- [7] Leonard, Y., Super Sports Limited, 2008. *Tin Can Manufacture and Method of Sealing*. Canada. Pat. 12,789, 675.

**Dissertation**

Author's surname, Year of publication. *Title of Dissertation*. Level. Official name of University, Country.

*Example:*

- [8] Sukcharoen, O., 2017. *Inhibitory Effect of Plant Essential Oils on Growth and Aflatoxin Production by Aspergillus flavus IMI 242684 and Aspergillus parasiticus IMI 283883*. Ph.D. King Mongkut's Institute of Technology Ladkrabang, Thailand.

**Websites**

Authorship or Source, Year. *Title of Document*. [online] Available at: include web site address/URL (Uniform Resource Locator).

*Example:*

- [9] NHS Evidence, 2003. *National Library of Guidelines*. [online] Available at: <http://www.library.nhs.uk/guidelines>.

**Acknowledgements:** These should be as brief as possible.

**Proofs:**

Proofs will be sent to the corresponding author and *must* be returned as soon as possible. Corrections should be restricted to typesetting errors.

**Copyright:**

The author(s) transfer(s) the copyright of the article to Current Applied Science and Technology effective if and when the article is accepted for publication.

**Page Numbering:**

All pages must be sequentially numbered, preferably by using the automatic page numbering function on your computer.

**Copyright Material:**

It is the authors' responsibility to obtain written permission from the copyright holder (usually the book or journal publisher) to use copyright material, and to send a copy of this consent with the manuscript. This consent is not normally denied but it is an international legal requirement that it be obtained.

**Note:**

Please note that authors are urged to check their proofs carefully before returning, since the inclusion of late corrections cannot be guaranteed.

Author(s) are responsible for ensuring that the submitted manuscript fully meets the requirements specified in the above Instructions. Manuscripts which fail to do so will be returned unedited to the Author(s) for correction in accordance with the above requirements, before they can be submitted to the processes of Referee evaluation.

1.5"

TEMPLATE

**Enter title here (14 PT type size, Title Case, Bold, Centered)**

Author Information entered here:

Name (in full)

Affiliation

City

Country

(11 pt type size, upper and lower case, centered under the title)

**How to Use This Document Template**

Insert the information in your document in place of the text here. For the body of your document, use Times New Roman 10 pt. Font, upper and lower case, double-spaced. Allow an extra half space above a line containing superscripts and/or below a line containing subscripts. The whole text should be left-justified. The headings should be 12 pt size, uppercase, bold and centered.

1.5"

**Abstract (12pt)**

1.5"

Maximum 250 words here. (10 pt)

.....  
.....  
.....  
.....  
.....

**Keywords:** (10 pt)

Maximum of 8 words

**1. Introduction (12 pt)**

Clearly explain the nature of the problem, previous work, purpose, and contribution of the paper (10 pt).

.....  
.....  
.....  
.....  
.....

\*Corresponding author: Tel.: ..... Fax: .....

E-mail: .....

## 2. Materials and Methods (12 pt)

.....  
.....  
.....  
.....

## 3. Results and Discussion (12 pt)

.....  
.....

## 4. Conclusions (12 pt)

Clearly indicate advantages, limitations and possible applications (10 pt).

.....  
.....

## 5. Acknowledgements (12 pt)

A brief acknowledgement section may be included here (10 pt).

.....  
.....

## References (12 pt)

References must be numbered in the order cited in the manuscript and indicated in the text by a number in square brackets (e.g. [1, 2]) (10 pt).

Example of References must be arranged as follows:

- [1] Barker, R. Kirk, J. and Munday, R.J., 1988. *Narrative Analysis*. 3rd ed. Bloomington: Indiana University Press.
- [2] Samson, C., 1970. Problems of information studies in history. In: S. Stone, ed. *Humanities Information Research*. Sheffield: CRUS, pp. 44-68.
- [3] Carlsen, J. and Charters, S., 2007. *Global Wine Tourism*. [e-book] Wallingford: CABI Pub. Available through: Anglia Ruskin University Library website <[www.libweb.anglia.ac.uk](http://www.libweb.anglia.ac.uk)>.
- [4] Ross, A.B., Junyapoon, S., Jones, J.M., Williams, A. and Bartle, K.D., 2005. A study of different soots using pyrolysis–GC–MS and comparison with solvent extractable material. *Journal of Analytical and Applied Pyrolysis*, 74(1-2), 494-501.
- [5] Thanaboripat, D., Ruangrattanametee, V. and Srikitkademwat, K., 2010. Control of growth and aflatoxin production of aflatoxin producing fungi in corn by salts. *Proceeding of the 8<sup>th</sup> International Symposium on Biocontrol and Biotechnology*, Pattaya, Thailand, October 4-6, 2010, 283-289.

- [6] Leonard, Y., Super Sports Limited., 2008. *Tin Can Manufacture and Method of Sealing*. Canada. Pat. 12,789, 675.
- [7] Richmond, J., 2005. *Customer Expectations in the World of Electronic Banking: a Case Study of the Bank of Britain*. Ph.D. Anglia Ruskin University.
- [8] NHS Evidence, 2003. *National Library of Guidelines*. [online] Available at: <http://www.library.nhs.uk/guidelines>

**Note:**

Tables and Graphs: Minimum of 10 pt type size, all captions should be upper and lower case, centered. Each table and figure must be on a separate page (or pages if required), **and must be embedded in the text**.

Illustrations and Photographs: Halftones, minimum of 10 pt type size, bold, captions should be in upper and lower case, centered. Images must be computer-designed with clearly visibility.

## **Contact**

**Editor of Current Applied Science and Technology  
King Mongkut's Institute of Technology Ladkrabang  
1 Soi Chalongkrung 1, Ladkrabang District  
Bangkok 10520, Thailand  
Tel: 662-329-8136 Fax: 662-329-8221  
E-mail: [cast@kmitl.ac.th](mailto:cast@kmitl.ac.th)  
Website: <https://www.tci-thaijo.org/index.php/cast/index>**

**KING MONGKUT'S INSTITUTE OF TECHNOLOGY LADKRABANG**

**1 Soi Chalongkrung 1, Ladkrabang District Bangkok 10520, Thailand**

**Tel: 662-329-8136 Fax: 662-329-8221**

**E-mail: [cast@kmitl.ac.th](mailto:cast@kmitl.ac.th)**

**Website: <https://www.tci-thaijo.org/index.php/cast/index>**